Client:

DG Rijkswaterstaat,

Rijksinstituut voor Kust en Zee | RIKZ

Modelling of Sand Transport in DELFT3D-ONLINE

Report

November 2003

WL | delft hydraulics

Client:

DG Rijkswaterstaat,

Rijksinstituut voor Kust en Zee | RIKZ

Modelling of Sand Transport in DELFT3D-ONLINE

L.C. van Rijn and D.J.R. Walstra

Report

November 2003

wl | delft hydraulics

WL | delft hydraulics

CLIENT: **DG Rijkswaterstaat; Rijks-Instituut voor Kust en Zee**

TITLE: **Modelling of sand transport in DELFT3D**

RIKZ of Rijkswaterstaat and Delft Hydraulics are working together (VOP) on the development/improvement and verification/validation of morphological models within the framework K2005*Coastal Nourishment of Rijkswaterstaat (see Report Z2478 of Delft Hydraulics and Website //VOP.wldelft.nl).
The present study (within the VOP-programme) is focussed on the following subjects:

1. Improvement and application of the engineering sand transport formulations;
   - derivation of bed roughness predictor;
   - verification of oscillatory bed load and suspended load transport model;
   - analysis of sand transport in deep water (effect of angle between current and wave direction on transport process);
   - application of improved model for computation of net sand transport rate in deep water (20 m) using wave, wind and tidal current data from previous studies;
2. Improvement of DELFT3D-ONLINE model with recently developed formulations;
   - implementation of new bed roughness predictor;
   - implementation of TR2000-approximation functions;
   - harmonisation of DELFT-MOR and DELFT-ONLINE computercode and input routines;
   - application of the improved model to laboratory testcase (Basin experiment; Benchmarking Testcase 1 of SANDPIT project);
3. Detailed application of the DELFT3D-ONLINE model to existing nourishment cases (Egmond, Delfland).

The activities under 1. and 2. are described in this report. Activity 3 will be described seperately.
Chapter 2: Description of sand transport formulations as used in DELFT3D model
Chapter 3: Improvement and validation of engineering sand transport formulations; derivation of bed roughness predictor; verification of bed-load transport; verification of oscillatory suspended load transport; effect of near-bed wave-induced streaming on bed load and suspended load transport.
Chapter 4: Application and verification of various transport and morphological models.

REFERENCES: **Contract RKZ 1331**
K2005*Suppleren

VER.	ORIGINATOR		DATE	REMARKS	REVIEW		APPROVED BY	
	L.C. van Rijn		**November 2003**		**D. Roelvink**		**T. Schilperoort**	
	D.J.R. Walstra							

PROJECT IDENTIFICATION:	**Z3624**
KEYWORDS:	Sand transport and Morphology

CONTENTS:	TEXT PAGES	**126**	TABLES	**36**	FIGURES	**45**	APPENDICES	**3**

STATUS: ☐ PRELIMINARY ☐ DRAFT ☒ FINAL

Contents

1

1 Introduction..1–1

2 Sand transport formulations in DELFT3D model..2–1

2.1 Introduction..2–1

2.2 Model description 2–4

2.2.1 Hydrodynamics...2–4

2.2.1.1 Boundary Conditions 2–8

2.2.1.2 Solution Procedure...2–8

2.2.2 Waves...2–10

2.2.2.1 General..2–10

2.2.2.2 Wave Effects 2–10

2.2.3 Sediment dynamics and bed level evolution..............................2–11

2.2.3.1 3-Dimensional advection-diffusion equation for current-related suspended transport 2–12

2.2.3.2 Suspended sediment size and sediment settling velocity...........2–13

2.2.3.3 Sediment mixing and dispersion...2–14

2.2.3.4 Reference concentration 2–17

2.2.4 Bed load transport..2–22

2.2.5 Wave-related suspended transport 2–24

2.2.6 Approximation formulas for current-related suspended transport 2–25

2.2.7 Numerical aspects...2–26

3 Improvement and validation of engineering sand transport formulations ...3—1

3.1 Derivation of bed roughness predictor...3—1

3.1.1 Approach ....3—1

3.1.2 Bed form characteristics in oscillatory flows ....3—2

3.1.3 Bed form characteristics in combined oscillatory and weak, steady flows ....3—6

3.1.4 Summary..3—9

3.1.5 Analysis of measured bed-roughness values ....3—10

3.1.6 Derivation of bed roughness predictor.....................................3—15

3.2 Verification of bed-load transport...3—19

3.2.1 Approach and formulations ....3—19

3.2.2 Bed load transport in tidal flow: Puget Sound, Washington, USA, 1964 ....3—22

3.2.3 Bed load transport in tidal flow: Salmon bank, Washington, USA, 1968 ....3—22

3.2.4 Bed-load transport in tidal flow: ridge south of IJ-channel, North Sea (1994)...3—23

3.2.5 Bed-load transport in coastal conditions (steady and oscillatory flow): Skerries bank, Start Bay, UK, 1979 ....3—24

3.2.6 Bed-load transport in coastal conditions: Sable Island bank, the Scotian Shelf, Canada (1999) ....3—25

3.2.7 Bed-load transport in coastal conditions: Spratt Sand, Teignmouth, South-west coast of England (2001)....................3—27

3.2.8 Bed-load and suspended load transport data from new experiments (within Sandpit-project) in wave tunnel..............3—29

3.2.9 Bed-load transport from new experiments (within Sandpit-Project) at field site Noordwijk of North Sea ....3—36

3.2.10 Conclusions of bed load verification results............................3—37

3.3 Verification of oscillatory suspended load transport.............................3—38

3.3.1 Approach and formulations ....3—38

3.3.2 Data from large-scale Deltaflume..3—39

3.3.3 Data from Egmond field site..3—43

3.4 Effect of near-bed wave-induced streaming on bed load and suspended load transport ....3—44

3.4.1 Introduction....................3—44

3.4.2 Lagrangian and Eulerian streaming velocities in near-bed region....................3—44

3.4.3 Modelling of Eulerian streaming in DELFT3D....................3—59

3.4.4 Sand transport associated with wave-induced streaming in the near-bed region....................3—60

3.4.5 Sensitivity computation results related to streaming velocity and bed roughness....................3—61

4 Application and Verification of TRANSPOR2000 in deep water conditions 4—1

4.1 Introduction....................4—1

4.2 Effect of various parameters on sand transport in deep water....................4—1

4.2.1 Introduction....................4—1

4.2.2 Results....................4—2

4.2.3 Conclusions....................4—3

4.3 Net sand transport rates....................4—3

4.3.1 Introduction....................4—3

4.3.2 Method....................4—4

4.3.2.1 Forcing....................4—4

4.3.2.2 Coefficients....................4—4

4.3.2.3 Model....................4—5

4.3.3 Results....................4—5

4.3.3.1 Base case....................4—5

4.3.3.2 Sensitivity runs....................4—7

4.3.3.3 Sensitivity runs (continued)....................4—12

4.3.4 Conclusions....................4—14

4.4 DELFT3D validation runs....................4—15

4.4.1 Introduction....................4—15

4.4.2 Description of Havinga experiment....................4—15

4.4.3 Modelling Approach ....4—16

4.4.4 Discussion on results ....4—18

5 Summary and conclusions...5—1

5.1 Sand transport formulations in DELFT3D model ....5—1

5.2 Ripples and bed roughness ....5—1

5.3 Verification of bed load transport model ....5—2

5.4 Verification of oscillatory suspended load transport model.....................5—3

5.5 Effect of near-bed wave-induced streaming on bed load transport and suspended load transport...5—4

5.6 Application of engineering sand transport formulations in deep water ...5—5

5.7 Recommendations..5—6

6 References...6—1

A Wave height and wind velocity data..A—1

B The percentage of occurrence of wave data....................................B—1

C Current velocities and water levels..C—1

1 Introduction

RIKZ of Rijkswaterstaat and Delft Hydraulics are working together on the development/improvement, verification/validation and evaluation of morphodynamic models within the framework K2005 of Rijkswaterstaat (see Report Z2478 of Delft Hydraulics and Website http://vop.wldelft.nl) and within the SANDPIT-project (website: http://sandpit.wldelft.nl).

Much effort has been put in recent years at:

- improving the basic sand transport formulations using theoretical and empirical information, which has resulted in a detailed, time-dependent sand transport model (POINT-SAND) for the sheet flow regime and a more pragmatic, engineering sand transport model (TRANSPOR2000); and,
- implementing this knowledge in morphodynamic models (UNIBEST, SUTRENCH, DELFT-MOR and DELFT3D-ONLINE).

Most of these basic formulations (bed-load transport, oscillatory suspended transport, reference concentration and near bed mixing due to waves) have, however, not been tested rigorously using field data sets including combined current and wave conditions. Similarly, the transport formulations recently implemented in the morphodynamic model DELFT3D-ONLINE have not been tested properly. Furthermore, a basic problem of sand transport modelling is the specification of bed roughness related to the generation and degeneration of bed forms in the lower and upper regimes (ripples, mega-ripples, plane bed). Ideally, the bed roughness should be predicted by the model for given flow, wave and sediment conditions.

The present study (Project 3 of the VOP-programme based on Contract RKZ 1331 of Rijkswaterstaat plus additional budgets from NCK and Basic Research of Delft Hydraulics) is aimed at addressing these topics, as follows:

- Improvement and application of the engineering sand transport formulations;
  - derivation of bed roughness predictor;
  - verification of oscillatory bed load and suspended load transport model;
  - analysis of sand transport in deep water (effect of angle between current and wave direction on transport process);
  - application of improved model for computation of net sand transport rate in deep water (20 m) using wave, wind and tidal current data from previous studies;
- Improvement of DELFT3D-ONLINE model with recently developed formulations;
  - implementation of new bed roughness predictor;
  - implementation of TR2000-approximation functions;
  - harmonisation of DELFT-MOR and DELFT-ONLINE computer code and input routines;
  - application of the improved model to laboratory testcase (Basin experiment; Benchmarking Testcase 1 of SANDPIT project);
- Detailed application of the DELFT3D-ONLINE model to existing nourishment cases (Egmond, Delfland).

The activities under 1. and 2. (performed by L.C. van Rijn, D.J.R. Walstra and T. van Kessel of WL | Delft Hydraulics in cooperation with M. Boers and J. de Ronde of RIKZ of Rijkswaterstaat) are described in this report.

Chapter 2 addresses the central focus point of the study: the DELFT-ONLINE model. The formulations (including the newly derived bed roughness predictor) implemented in this 3D-model are described in detail.

Chapter 3 addresses the derivation of the bed roughness predictor and the validation of the bed load transport and oscillatory suspended transport using data from field surveys and from the large-scale Delta flume. The problems of the reference concentration and near-bed wave-induced mixing are not yet considered as field data information is lacking. This will be a topic for future studies (VOP and SANDPIT, 2004).

Chapter 4 addresses various applications of the new formulations using the UNIBEST, SUTRENCH and DELFT-ONLINE models, as follows:

- Application of DELFT-ONLINE on BM Testcase 1 (bed level development of trench in laboratory experiment);
- Sand transport in deep water; effect of wave-current angle on transport rate using SUTRENCH-model;
- Net yearly-averaged sand transport rates at 20 m depth of the JARKUS-profile 76 (Noordwijk location) using UNIBEST-model

The activities related to the modelling of existing shoreface nourishments will be reported separately in 2004.

Conclusions and recommendations for future research developments are given in Chapter 5.

2 Sand transport formulations in DELFT3D model

2.1 Introduction

Section 2.1 of this chapter gives a detailed description of the implemented processes in DELFT3D-ONLINE. Sub-sections 2.2.1 and 2.2.2 present overviews of the hydrodynamics of currents and waves (largely taken from **Lesser et al., 2003**). Sub-Section 2.2.3 describes the sediment transport formulations based on TR2000 for non-cohesive sediment following **Van Rijn (1993, 2000 and 2002)** which have been implemented in DELFT3D-ONLINE as part of the present study. Similar formulations are available in the UNIBEST, SUTRENCH and DELFT3D-MOR models.

Besides the TR2000 approach, the DELFT3D-ONLINE and DELFT-MOR offer a number of extra sediment transport relations for non-cohesive sediment. The basic differences between DELFT-MOR and DELFT-ONLINE models are summarised below:

- **DELFT3D-MOR:**
  - Can only operate in 2DH mode.
  - OFFLINE coupling between hydrodynamic and transport/bottom modules which implies:
    - the various models are run separately, for the data communication between the models a so-called communication file is used,
    - morphological calculations are usually based on tide-averaged transports,
    - upscaling of the morphological development is achieved by updating the flow data with a so-called continuity correction (constant discharge trough cells),
    - as the bottom module operates separately from the other models, the time step for the morphological development is independent from the flow time step (it is possible to use an automated time stepping mechanism based on a courant criterion).
- **DELFT3D-ONLINE:**
  - Can operate in 2DH and in 3D mode.
  - ONLINE coupling between hydrodynamic and transport/bottom modules which implies:
    - the flow, transport and bottom updating are now merged into one ONLINE-model, only the wave model is executed separately (data communication between online model and waves model is again based on the communication file),
    - transport and bottom updating is now performed at every flow time step,
    - upscaling of the morphological development is achieved by upscaling the bottom developments during each time step by means of a so-called morphological scaling factor, MSF (e.g. with MSF=100, a morphological prediction based on a tidal cycle of 12.5 hours would be approx. 52 days).
    - value of morphological scaling factor has to be prescribed by the user and should depend on the variability of the area of interest, dynamic areas require a

lower MSF value whereas for more stable environments the MSF can be increased (typical range is 10 and 1000 for dynamic and stable areas respectively).

An overview of the basic formulations that can be applied in these models, is given in Tables 2.1.1A,B and 2.1.2.

Type of model	Spatial dimension	Transport approach
UNIBEST	**1D**	***Bed load transport*** Equilibrium transport based on intra-wave approach of TR2000 ***Wave-related suspended transport*** Equilibrium transport based on method of TR2000 ***Current-related suspended transport*** 1) Computation of concentration profile based on method of TR2000 (local equilibrium; adjustment effect is neglected) 2) Reference concentration at bed derived from TR2000 ***Bed roughness*** specified by user
SUTRENCH	**2DV**	***Bed load transport*** Equilibrium transport based on intra-wave approach of TR2000 ***Wave-related suspended transport*** Equilibrium transport based on method of TR2000 ***Current-related suspended transport*** 1) Computation of concentration profile based numerical solution of advection-diffusion equation; mixing based on TR2000 2) Reference concentration at bed derived from TR2000 ***Bed roughness*** specified by user

Table 2.1.1A *Sand transport approaches in UNIBEST and SUTRENCH models*

Type of model	Spatial dimension	Transport approach
DELFT-MOR	**2DH**	***Bed load transport*** Various equilibrium formulations (See Table 2.1.2) ***Wave-related suspended transport*** Not modelled ***Current-related suspended transport*** 1) Depth-averaged sand concentration derived from equilibrium sand transport formulation (see Table 2.1.2) plus adjustment factor based on method of Galappatti 2) Available equilibrium suspended transport formulations (see Table 2.1.2) without adjustment of transport ***Bed roughness*** specified by user
DELFT-ONLINE	2DH	***Bed load transport*** a) Equilibrium transport based on approximation function of TR2000 b) Other equilibrium formulations (See Table 2.1.2) ***Wave-related suspended transport*** Equilibrium transport based on approximation method of TR2000 ***Current-related suspended transport*** 1) Depth-averaged sand concentration derived from equilibrium sand transport formulation plus adjustment factor based on method of Galappatti 2) Equilibrium suspended transport formulations (no adjustment): a)TR2000 (detailed formulations) b)TR2000 (approximation functions) c) Other formulations; see Table 2.1.2 ***Bed roughness*** a) specified by user b) roughness predictor
DELFT-ONLINE	3D and 2DV	***Bed load transport*** a) Equilibrium transport based on approximation function of TR2000 b) Other equilibrium formulations (See Table 2.1.2) ***Wave-related suspended transport*** Equilibrium transport based on approximation method of TR2000 ***Current-related suspended transport*** 1) Concentration derived from advection-diffusion equation 2) Reference concentration derived from a) TR2000 b) Other formulations (Table 2.1.2); ref concentration is calculated backwards from equilibrium suspended transport using computed velocity profiles and mixing coefficient ***Bed roughness*** a) specified by user b) roughness predictor

Table 2.1.1B *Sand transport approaches in DELFT-MOR and DELFT3D-ONLINE model*

Formula	Transport modes	Waves	IFORM
Engelund-Hansen (1967)	Total transport	No	1
Meyer-Peter-Muller (1948)	Bed load transport	No	2
Swanby (Ackers-White, 1973)	Total transport	No	3
General formula	Total transport	No	4
Bijker (1971)	Bed load + suspended	Yes	5
Van Rijn (1984)	Bed load + suspended	No	7
Soulsby / Van Rijn	Bed load + suspended	Yes	11
Soulsby	Bed load + suspended	Yes	12
Van Rijn (TR2000)	Bed load + suspended	Yes	0
Van Rijn (TR1993)	Bed load + suspended	Yes	-1
Van Rijn (TR2000 Approximated, see Section 2.2.6)	Bed load + suspended	Yes	-2

Remarks: Application of a total transport formulation implies that total load transport is treated as bed-load transport; suspended load transport is assumed to be zero.

Table 2.1.2 *Sand transport formulations in DELFT-MOR and DELFT3D-ONLINE*

2.2 Model description

2.2.1 Hydrodynamics

The DELFT3D-FLOW module solves the unsteady shallow-water equations in two (depth-averaged) or three dimensions. The system of equations consists of the horizontal momentum equations, the continuity equation, the transport equation, and a turbulence closure model. The vertical momentum equation is reduced to the hydrostatic pressure relation as vertical accelerations are assumed to be small compared to gravitational acceleration and are not taken into account. This makes the DELFT3D-FLOW model suitable for predicting the flow in shallow seas, coastal areas, estuaries, lagoons, rivers, and lakes. It aims to model flow phenomena of which the horizontal length and time scales are significantly larger than the vertical scales.

The user may choose whether to solve the hydrodynamic equations on a Cartesian rectangular, orthogonal curvilinear (boundary fitted), or spherical grid. In three-dimensional simulations a boundary fitted (σ-coordinate) approach is used for the vertical grid direction. For the sake of clarity the equations are presented in their Cartesian rectangular form only.

<u>Vertical σ-coordinate system</u>

The vertical σ-coordinate is scaled as $(-1 \leq \sigma \leq 0)$

$$\sigma = \frac{z-\zeta}{\zeta + d} \qquad (2.2.1)$$

The flow domain of a 3D shallow water model consists of a number of layers. In a σ-coordinate system, the layer interfaces are chosen following planes of constant σ. Thus, the number of layers is constant over the horizontal computational area. For each layer a set of coupled conservation equations is solved. The partial derivatives in the original Cartesian coordinate system are expressed in σ-coordinates by use of the chain rule. This introduces additional terms (**Stelling and Van Kester, 1994**).

Generalised Lagrangian mean (GLM) reference frame

In simulations including waves the hydrodynamic equations are written and solved in a GLM reference frame (**Andrews and McIntyre, 1978; Groeneweg and Klopman, 1998; and Groeneweg 1999**). In GLM formulation the 2DH and 3D flow equations are very similar to the standard Eulerian equations, however, the wave-induced driving forces averaged over the wave period are more accurately expressed. The relationship between the GLM velocity and the Eulerian velocity is given by:

$$\begin{aligned} U &= u + u_s \\ V &= v + v_s \end{aligned} \tag{2.2.2}$$

where U and V are GLM velocity components, u and v are Eulerian velocity components, and u_s and v_s are the Stokes' drift components. For details and verification results we refer to **Walstra et al. (2000)**.

Hydrostatic pressure assumption

Under the so-called "shallow water assumption" the vertical momentum equation reduces to the hydrostatic pressure equation. Under this assumption vertical acceleration due to buoyancy effects or sudden variations in the bottom topography is not taken into account. The resulting expression is:

$$\frac{\partial P}{\partial \sigma} = -\rho g h \tag{2.2.3}$$

Horizontal momentum equations

The horizontal momentum equations are

$$\begin{aligned} &\frac{\partial U}{\partial t} + U\frac{\partial U}{\partial x} + v\frac{\partial U}{\partial y} + \frac{\omega}{h}\frac{\partial U}{\partial \sigma} - fV = -\frac{1}{\rho_0}P_x + F_x + M_x + \frac{1}{h^2}\frac{\partial}{\partial \sigma}\left(\nu_V \frac{\partial u}{\partial \sigma}\right) \\ &\frac{\partial V}{\partial t} + U\frac{\partial V}{\partial x} + V\frac{\partial V}{\partial y} + \frac{\omega}{h}\frac{\partial V}{\partial \sigma} - fU = -\frac{1}{\rho_0}P_y + F_y + M_y + \frac{1}{h^2}\frac{\partial}{\partial \sigma}\left(\nu_V \frac{\partial v}{\partial \sigma}\right) \end{aligned} \tag{2.2.4}$$

in which the horizontal pressure terms, P_x and P_y, are given by (Boussinesq approximations)

$$\frac{1}{\rho_0}P_x = g\frac{\partial\zeta}{\partial x} + g\frac{h}{\rho_0}\int_{\sigma}^{0}\left(\frac{\partial\rho}{\partial x} + \frac{\partial\sigma'}{\partial x}\frac{\partial\rho}{\partial\sigma'}\right)d\sigma'$$

$$\frac{1}{\rho_0}P_y = g\frac{\partial\zeta}{\partial y} + g\frac{h}{\rho_0}\int_{\sigma}^{0}\left(\frac{\partial\rho}{\partial y} + \frac{\partial\sigma'}{\partial y}\frac{\partial\rho}{\partial\sigma'}\right)d\sigma' \tag{2.2.5}$$

The horizontal Reynold's stresses, F_x and F_y, are determined using the eddy viscosity concept (e.g. **Rodi, 1984**). For large scale simulations (when shear stresses along closed boundaries may be neglected) the forces F_x and F_y reduce to the simplified formulations

$$F_x = \nu_H\left(\frac{\partial^2 U}{\partial x^2} + \frac{\partial^2 U}{\partial y^2}\right) \qquad F_y = \nu_H\left(\frac{\partial^2 V}{\partial x^2} + \frac{\partial^2 V}{\partial y^2}\right) \tag{2.2.6}$$

in which the gradients are taken along σ-planes. In Eq. (2.2.4) M_x and M_y represent the contributions due to external sources or sinks of momentum (external forces by hydraulic structures, discharge or withdrawal of water, wave stresses, etc.).

Continuity equation

The depth-averaged continuity equation is given by

$$\frac{\partial\zeta}{\partial t} + \frac{\partial\left[h\bar{U}\right]}{\partial x} + \frac{\partial\left[h\bar{V}\right]}{\partial y} = S \tag{2.2.7}$$

in which S represents the contributions per unit area due to the discharge or withdrawal of water, evaporation, and precipitation.

Transport equation

The advection-diffusion equation reads

$$\frac{\partial[hc]}{\partial t} + \frac{\partial[hUc]}{\partial x} + \frac{\partial[hVc]}{\partial y} + \frac{\partial(\omega c)}{\partial\sigma} =$$
$$h\left[\frac{\partial}{\partial x}\left(D_H\frac{\partial c}{\partial x}\right) + \frac{\partial}{\partial y}\left(D_H\frac{\partial c}{\partial y}\right)\right] + \frac{1}{h}\frac{\partial}{\partial\sigma}\left[D_V\frac{\partial c}{\partial\sigma}\right] + hS \tag{2.2.8}$$

in which S represents source and sink terms per unit area.

In order to solve these equations the horizontal and vertical viscosity (ν_H and ν_V) and diffusivity (D_H and D_V) need to be prescribed. In DELFT3D-FLOW the horizontal viscosity and diffusivity are assumed to be a superposition of three parts: 1) molecular viscosity, 2) "3D turbulence", and 3) "2D turbulence". The molecular viscosity of the fluid (water) is a constant value $O(10^{-6})$. In a 3D simulation "3D turbulence" is computed by the selected turbulence closure model (see the turbulence closure model section below). "2D turbulence" is a measure of the horizontal mixing that is not resolved by advection on the horizontal computational grid. 2D turbulence values may either be specified by the user as a constant or space-varying parameter, or can be computed using a sub-grid model for horizontal large eddy simulation (HLES). The HLES model available in DELFT3D-FLOW is based on theoretical considerations presented by **Uittenbogaard (1998)** and is fully discussed by **Van Vossen (2000)**.

For use in the transport equation, the vertical eddy diffusivity is scaled from the vertical eddy viscosity according to

$$D_V = \frac{\nu_V}{\sigma_c} \tag{2.2.9}$$

in which σ_c is the Prandtl-Schmidt number given by

$$\sigma_c = \sigma_{c0} F_\sigma(Ri) \tag{2.2.10}$$

where σ_{c0} is purely a function of the substance being transported. In the case of the algebraic turbulence model, $F_\sigma(Ri)$ is a damping function that depends on the amount of density stratification present via the gradient Richardson's number (**Simonin et al., 1989**). The damping function, $F_\sigma(Ri)$, is set equal to 1.0 if the $k-\varepsilon$ turbulence model is used, as the buoyancy term in the $k-\varepsilon$ model automatically accounts for turbulence-damping effects caused by vertical density gradients.

We note that the vertical eddy diffusivity used for calculating the transport of "sand" sediment constituents may, under some circumstances, vary somewhat from that given by Eq. (2.2.9) above. The diffusion coefficient used for sand sediment is described in more detail in Section 2.2.3.

<u>Turbulence closure models</u>
Several turbulence closure models are implemented in DELFT3D-FLOW. All models are based on the so-called "eddy viscosity" concept (**Kolmogorov, 1942; Prandtl, 1945**). The eddy viscosity in the models has the following form

$$\nu_V = c'_\mu L \sqrt{k} \tag{2.2.11}$$

in which c'_μ is a constant determined by calibration, L is the mixing length, and k is the turbulent kinetic energy.

Two types of turbulence closure models are available in DELFT3D-FLOW. The first is the "algebraic" turbulence closure model that uses algebraic/analytical formulas to determine k and L and therefore the vertical eddy viscosity. The second is the $k-\varepsilon$ turbulence closure model in which both the turbulent energy k and the dissipation ε are produced by production terms representing shear stresses at the bed, surface, and in the flow. The "concentrations" of k and ε in every grid cell are then calculated by transport equations. The mixing length L is determined from ε and k according to

$$L = c_D \frac{k\sqrt{k}}{\varepsilon} \tag{2.2.12}$$

in which c_D is another calibration constant.

2.2.1.1 Boundary Conditions

In order to solve the systems of equations, the following boundary conditions are required:

Bed and free surface boundary conditions
In the σ-coordinate system the bed and the free surface correspond with σ-planes. Therefore the vertical velocities at these boundaries are simply

$$\omega(-1) = 0 \quad and \quad \omega(0) = 0 \tag{2.2.13}$$

Friction is applied at the bed as follows:

$$\frac{\nu_V}{h}\frac{\partial u}{\partial \sigma}\bigg|_{\sigma=-1} = \frac{\tau_{bx}}{\rho} \qquad \frac{\nu_V}{h}\frac{\partial v}{\partial \sigma}\bigg|_{\sigma=-1} = \frac{\tau_{by}}{\rho} \tag{2.2.14}$$

where τ_{bx} and τ_{by} are bed shear stress components that include the effects of wave-current interaction.

Friction due to wind stress at the water surface may be included in a similar manner. For the transport boundary conditions the vertical diffusive fluxes through the free surface and bed are set to zero.

Lateral boundary conditions
Along closed boundaries the velocity component perpendicular to the closed boundary is set to zero (a free-slip condition). At open boundaries one of the following types of boundary conditions must be specified: water level, velocity (in the direction normal to the boundary), discharge, or Riemann (weakly reflective boundary condition, **Verboom and Slob, 1984**). Additionally, in the case of 3D models, the user must prescribe the use of either a uniform or logarithmic velocity profile at inflow boundaries.

For the transport boundary conditions we assume that the horizontal transport of dissolved substances is dominated by advection. This means that at an open inflow boundary a boundary condition is needed. During outflow the concentration must be free. DELFT3D-FLOW allows the user to prescribe the concentration at every σ–layer using a time series. For sand sediment fractions the local equilibrium sediment concentration profile may be used.

2.2.1.2 Solution Procedure

DELFT3D-FLOW is a numerical model based on finite differences. To discretise the 3D shallow water equations in space, the model area is covered by a rectangular, curvilinear, or spherical grid. It is assumed that the grid is orthogonal and well-structured. The variables are arranged in a pattern called the Arakawa C-grid (a staggered grid). In this arrangement the water level points (pressure points) are defined in the centre of a (continuity) cell; the velocity components are perpendicular to the grid cell faces where they are situated.

Hydrodynamics

An alternating direction implicit (ADI) method is used to solve the continuity and horizontal momentum equations (**Leendertse 1987**). The advantage of the ADI method is that the implicitly integrated water levels and velocities are coupled along grid lines, leading to systems of equations with a small bandwidth. **Stelling (1983)** extended the ADI method of Leendertse with a special approach for the horizontal advection terms. This approach splits the third-order upwind finite-difference scheme for the first derivative into two second-order consistent discretisations, a central discretisation and an upwind discretisation, which are successively used in both stages of the ADI-scheme. The scheme is denoted as a "cyclic method" (**Stelling and Leendertse, 1991**). This leads to a method that is computationally efficient, at least second-order accurate, and stable at Courant numbers of up to approximately 10. The diffusion tensor is redefined in the σ-coordinate system assuming that the horizontal length scale is much larger than the water depth (**Mellor and Blumberg, 1985**) and that the flow is of boundary-layer type.

The vertical velocity, ω, in the σ-coordinate system is computed from the continuity equation,

$$\frac{\partial \omega}{\partial \sigma}=-\frac{\partial \zeta}{\partial t}-\frac{\partial [hU]}{\partial x}-\frac{\partial [hV]}{\partial y} \tag{2.2.15}$$

by integrating in the vertical from the bed to a level σ. At the surface the effects of precipitation and evaporation are taken into account. The vertical velocity, ω, is defined at the iso-σ-surfaces. ω is the vertical velocity relative to the moving σ-plane and may be interpreted as the velocity associated with up- or down-welling motions. The vertical velocities in the Cartesian coordinate system can be expressed in the horizontal velocities, water depths, water levels, and vertical coordinate velocities according to:

$$w=\omega+U\left(\sigma\frac{\partial h}{\partial x}+\frac{\partial \zeta}{\partial x}\right)+V\left(\sigma\frac{\partial h}{\partial y}+\frac{\partial \zeta}{\partial y}\right)+\left(\sigma\frac{\partial h}{\partial t}+\frac{\partial \zeta}{\partial t}\right) \tag{2.2.16}$$

Transport

The transport equation is formulated in a conservative form (finite-volume approximation) and is also solved using the so-called "cyclic method" (**Stelling and Leendertse, 1991**). For steep bottom slopes in combination with vertical stratification, horizontal diffusion along σ-planes introduces artificial vertical diffusion (**Huang and Spaulding, 1996**). DELFT3D-FLOW includes an algorithm to approximate the horizontal diffusion along z-planes in a σ-coordinate framework (**Stelling and Van Kester, 1994**). In addition, a horizontal Forester filter (**Forester, 1979**) based on diffusion along σ-planes is applied to remove any negative concentration values that may occur. The Forester filter is mass conserving and does not inflict significant amplitude losses in sharply peaked solutions.

2.2.2 Waves

2.2.2.1 General

Wave effects can also be included in a DELFT3D-FLOW simulation by running the separate DELFT3D-WAVE module. A call to the DELFT3D-WAVE module must be made prior to running the FLOW module. This will result in a communication file being stored which contains the results of the wave simulation (RMS wave height, peak spectral period, wave direction, mass fluxes, etc) on the same computational grid as is used by the FLOW module. The FLOW module can then read the wave results and include them in flow calculations. Wave simulations may be performed using the 2nd generation wave model HISWA (**Holthuijsen et al., 1989**) or the 3rd generation SWAN model (**Holthuijsen et al., 1993**). A significant practical advantage of using the SWAN model is that it can run on the same curvilinear grids as are commonly used for DELFT3D-FLOW calculations; this significantly reduces the effort required to prepare combined WAVE and FLOW simulations.

In situations where the water level, bathymetry, or flow velocity field change significantly during a FLOW simulation, it is often desirable to call the WAVE module more than once. The computed wave field can thereby be updated accounting for the changing water depths and flow velocities. This functionality is possible by way of the MORSYS steering module that can make alternating calls to the WAVE and FLOW modules. At each call to the WAVE module the latest bed elevations, water elevations and, if desired, current velocities are transferred from FLOW.

2.2.2.2 Wave Effects

In coastal seas wave action may influence morphology for a number of reasons. The following processes are presently accounted for in DELFT3D-FLOW.

1. Wave forcing due to breaking (by radiation stress gradients) is modelled as a shear stress at the water surface (**Svendsen, 1985; Stive and Wind, 1986**). This radiation stress gradient is modelled using the simplified expression of **Dingemans et al. (1987)**, where contributions other than those related to the dissipation of wave energy are neglected. This expression is as follows,

$$\vec{M} = \frac{D}{\omega}\vec{k} \tag{2.2.17}$$

   in which $\vec{M}$ = Forcing due to radiation stress gradients (N/m^2), D = Dissipation due to wave breaking (W/m^2), ω = Angular wave frequency (rad/s), and $\vec{k}$ = Wave number vector (rad/m).
2. The effect of the enhanced bed shear stress on the flow simulation is accounted for by following the parameterisations of **Soulsby et al. (1993)**. Of the several models available, the simulations presented in this report use the wave-current interaction model of **Fredsøe (1984)**.
3. The wave-induced mass flux is included and is adjusted for the vertically non-uniform Stokes drift (**Walstra et al., 2000**).

4. The additional turbulence production due to dissipation in the bottom wave boundary layer and due to wave white capping and breaking at the surface is included as extra production terms in the $k-\varepsilon$ turbulence closure model (**Walstra et al., 2000**).
5. Streaming (a wave-induced current in the bottom boundary layer directed in the direction of wave propagation) is modelled as an additional shear stress acting across the thickness of the bottom wave boundary layer (**Walstra et al., 2000**).

Processes 3, 4, and 5 have only recently been included in DELFT3D-FLOW and are essential if the (wave-averaged) effect of waves on the flow is to be correctly represented in 3D simulations. This is especially important for the accurate modelling of sediment transport in a near-shore coastal zone.

2.2.3 Sediment dynamics and bed level evolution

For the transport of non-cohesive sediment, **Van Rijn's (1993 and 2000)** approach is followed by default. The user can also specify a number of other transport formulations (see Table 2.1.2) The transport relations are a mix of Van Rijn's original TRANSPOR1993 model, its successor TRANSPOR2000 (TR2000) and approximation formulations (**Van Rijn, 2002**). In all these formulations Van Rijn distinguishes between bed load and suspended load which both have a wave-related and current-related contribution:

$$
\begin{aligned}
S_s &= S_{s,c} + S_{s,w} \\
S_b &= S_{b,c} + S_{b,w}
\end{aligned}
\tag{2.2.18}
$$

in which S_s is the suspended transport, S_b the bed load transport, $S_{s,c}$ and $S_{s,w}$ the respective current-related and wave-related suspended transports, $S_{b,c}$ and $S_{b,w}$ the respective current-related and wave-related bed load transports. The transport gradients in x- and y-direction are being used in the sediment continuity equation to determine the bed level changes, as follows:

$$
\frac{\partial z_b}{\partial t} + \frac{\partial\left(S_{b,x} + S_{s,x}\right)}{\partial x} + \frac{\partial\left(S_{b,y} + S_{s,y}\right)}{\partial y} = 0
\tag{2.2.19}
$$

with:
$S_{b,x} = S_{b,c,x} + S_{b,w,x}$ being the bed-load transport in x-direction (u-velocity direction),
$S_{b,y} = S_{b,c,y} + S_{b,w,y}$ being the bed-load transport in y-direction (v-velocity direction),
$S_{s,x} = S_{s,c,x} + S_{s,w,x}$ being the suspended load transport in x-direction (u-velocity direction),
$S_{s,y} = S_{s,c,y} + S_{s,w,y}$ being the suspended load transport in y-direction (v-velocity direction), and $S_{b,c}$ and $S_{b,w}$ are the current-related and wave-related bed load transports, $S_{s,c}$ and $S_{s,w}$ are the current-related and wave-related suspended load transports (in x and y directions).

The bed-load transport contributions are based on a quasi-steady approach, which implies that the bed-load transport is assumed to respond almost instantaneously to orbital velocities within the wave cycle and to the prevailing current-velocity. Similarly, the wave-related suspended load transport contribution is assumed to respond almost instantaneously to the orbital velocities. These transport contributions ($S_{b,c}$, $S_{b,w}$ and $S_{s,w}$) can be formulated in

terms of time-averaged (over the wave period) parameters resulting in relatively simple transport expressions.
The current-related suspended load transport is based on the variation of the suspended sand concentration field due to the effects of currents and waves. Using a 2DH-approach, the sand concentration field is described in terms of the depth-averaged equilibrium sand concentration derived from equilibrium transport formulations and an adjustment factor based on the (numerical) method of Galappatti. Using a 3D-approach, the sand concentration field is based on the numerical solution of the 3D advection-diffusion equation (see Sub-Section 2.2.3.1).

In the present upgraded version of DELFT3D the following modifications have been implemented:
1) suspended transport from TRANSPOR2000 (**Van Rijn, 2000**) in stead of TRANSPOR93,
2) bed load transport based on new approximation formulations (**Van Rijn, 2002**).

The upgrade of TRANSPOR1993 to TRANSPOR2000 is primarily related to modifications in the formulations of the suspended transport parameters. Below a summary of the modifications is given:
1 Modification of the thickness of the effective near-bed sediment mixing layer (δ_s), see Eq. (2.2.27).
2 The expressions for the parametric mixing coefficients have also been modified ($\varepsilon_{s,w,max}$, $\varepsilon_{s,w,bed}$), see Eq. (2.2.26).
3 The wave related efficiency factor (μ_w), see Eq. (2.2.49).

2.2.3.1 3-Dimensional advection-diffusion equation for current-related suspended transport

Three-dimensional transport of suspended sediment is calculated by solving the three-dimensional advection-diffusion (mass-balance) equation for the suspended sediment:

$$\begin{aligned}&\frac{\partial c^{(\ell)}}{\partial t}+\frac{\partial uc^{(\ell)}}{\partial x}+\frac{\partial vc^{(\ell)}}{\partial y}+\frac{\partial\left(w-w_s^{(\ell)}\right)c^{(\ell)}}{\partial z}+\\&\quad-\frac{\partial}{\partial x}\left(\varepsilon_{s,x}^{(\ell)}\frac{\partial c^{(\ell)}}{\partial x}\right)-\frac{\partial}{\partial y}\left(\varepsilon_{s,y}^{(\ell)}\frac{\partial c^{(\ell)}}{\partial y}\right)-\frac{\partial}{\partial z}\left(\varepsilon_{s,z}^{(\ell)}\frac{\partial c^{(\ell)}}{\partial z}\right)=0,\end{aligned} \tag{2.2.20}$$

where:

$c^{(\ell)}$	mass concentration of sediment fraction (ℓ) [kg/m^3],
u, v and w	flow velocity components [m/s],
$\varepsilon_{s,x}^{(\ell)}, \varepsilon_{s,y s,y}^{(\ell)}$ and $\varepsilon_{s,z}^{(\ell)}$	eddy diffusivities of sediment fraction (ℓ) [m^2/s],
$w_s^{(\ell)}$	sediment settling velocity of sediment fraction (ℓ); hindered settling effects are taken into account [m/s].

The local flow velocities and eddy diffusivities are based on the results of the hydrodynamic computations. Computationally, the three-dimensional transport of sediment is computed in exactly the same way as the transport of any other conservative constituent, such as salinity, heat, and constituents. There are, however, a number of important differences between sediment and other constituents. For example, the exchange of sediment between the bed and the flow, and the settling velocity of sediment under the action of gravity. These additional processes for sediment are obviously of critical importance. Other processes such as the effect that sediment has on the local mixture density, and hence on turbulence damping, can also be taken into account. In addition, if a net flux of sediment from the bed to the flow, or vice versa, occurs then the resulting change in the bathymetry should influence subsequent hydrodynamic calculations. The formulation of several of these processes are sediment-type specific, this especially applies for sand and mud.

Based on the computed sand concentration field, the current-related suspended transport rates in x- and y-directions are computed as:

$$\begin{aligned} S_{s,c,x} &= \int_a^h \left(uc - \varepsilon_{s,x} \frac{\partial c}{\partial x} \right) dz \\ S_{s,c,y} &= \int_a^h \left(vc - \varepsilon_{s,y} \frac{\partial c}{\partial y} \right) dz \end{aligned} \tag{2.2.21}$$

2.2.3.2 Suspended sediment size and sediment settling velocity

The settling velocity of a non-cohesive ("sand") sediment fraction is computed following the method of **Van Rijn (1993)**. The formulation used depends on the diameter of the sediment in suspension:

$$\begin{aligned} w_{s,0}^{(\ell)} &= \frac{(s^{(\ell)}-1)g\, d^{(\ell)2}}{18\upsilon}, & 65\ \mu m < d \leq\ 100\,\mu m \\ w_{s,0}^{(\ell)} &= \frac{10\nu}{d}\left[\left(1+\frac{0.01(s^{(\ell)}-1)g\, d^{(\ell)3}}{\upsilon^2}\right)^{0.5} - 1\right], & 100\ \ \mu m < d \leq 1000\,\mu m \\ w_{s,0}^{(\ell)} &= 1.1\left[(s^{(\ell)}-1)g\, d^{(\ell)}\right]^{0.5}, & 1000\,\mu m < d \end{aligned} \tag{2.2.22}$$

where:

$s^{(\ell)}$	relative density of sediment fraction (ℓ).
$d^{(\ell)}$	representative diameter of sediment fraction (ℓ).
υ	kinematic viscosity coefficient of water [m^2/s].

If only one sediment fraction is used, the representative diameter of the suspended sediment can be determined based on two options via the user-defined properties SEDDIA (d_{50} of bed material) and IOPSUS (options for determining d_s is determined based on the mobility parameter, M, see Eq. (2.2.57), as follows:

1) a suspended sediment diameter based in the following expression:

$$
\begin{aligned}
d_s &= \min\left[0.5 d_{50,} \left(1+0.0008\left(\frac{d_{50}}{d_{10}}-1\right)(\psi-250)\right)d_{50}\right] && \mathit{for}\,\psi < 250 \\
d_s &= d_{50} && \mathit{for}\,\psi \geq 250
\end{aligned}
\tag{2.2.23}
$$

for ψ see Eq. (2.2.38),

2) d_s=*FACDSS* d_{50}; based on a multiplication of the user-defined properties SEDDIA (d_{50} of bed material) and FACDSS (see also remark)

Remark:
In the case of non-uniform bed material **Van Rijn (1993)** concluded that, on the basis of measurements, d_s is in the range of 60% to 100% of d_{50} of the bed material. If the bed material is very widely graded (well sorted) consideration should be given to using several sediment fractions to model its behaviour more accurately.

2.2.3.3 Sediment mixing and dispersion

DELFT3D-FLOW supports four turbulence closure models:

- Constant coefficient.
- Algebraic eddy viscosity closure model.
- $k-L$ turbulence closure model.
- $k-\varepsilon$ turbulence closure model.

The first is a simple constant value which is specified by the user. A constant eddy viscosity will lead to parabolic vertical velocity profiles (laminar flow). The other three turbulence closure models are based on the eddy viscosity concept of **Kolmogorov (1942)** and **Prandtl (1945)** and offer zero, first, and second order closures for the turbulent kinetic energy (k) and for the mixing length (L). All three of the more advanced turbulence closure models take into account the effect that a vertical density gradient has on damping the amount of vertical turbulent mixing.

The output of a turbulence closure model is the eddy viscosity at each layer interface; from this the vertical sediment mixing coefficient is calculated using the following expressions:

Using the algebraic or k-L turbulence model
Without waves
If the algebraic or k-L turbulence model is selected and waves are inactive then the vertical mixing coefficient for sediment is computed from the vertical fluid mixing coefficient calculated by the selected turbulence closure model. For non-cohesive sediment the fluid mixing coefficient is multiplied by Van Rijn's 'beta factor' which is intended to describe the different diffusivity of a fluid 'particle' and a sand grain. Expressed mathematically:

$$\varepsilon_s^{(\ell)} = \beta\,\varepsilon_f\,, \tag{2.2.24}$$

where:

$\varepsilon_s^{(\ell)}$ vertical sediment mixing coefficient for sediment fraction (ℓ).

β Van Rijn's 'beta' factor for the sediment fraction.

ε_f vertical fluid mixing coefficient calculated by the selected turbulence closure model.

Including waves
If waves are included in a simulation using the algebraic or k-L turbulence closure model then the sediment mixing coefficient for non-cohesive sediment fractions is calculated entirely separately from the turbulence closure model, using expressions given by **Van Rijn (1993)** for both the current-related and wave-related vertical turbulent mixing of sediment.

The current-related mixing is calculated using the 'parabolic-constant' distribution recommended by Van Rijn:

$$\begin{aligned}
\varepsilon_{s,c}^{(\ell)} &= \kappa \beta u_{*,c}\, z(1 - z/h), && \text{when } z < 0.5h, \\
\varepsilon_{s,c}^{(\ell)} &= 0.25 \kappa \beta u_{*,c}\, h, && \text{when } z \geq 0.5h,
\end{aligned} \tag{2.2.25}$$

where:

$\varepsilon_{s,c}^{(\ell)}$ vertical sediment mixing coefficient due to currents (for this sediment fraction).

$u_{*,c}$ current-related bed shear velocity.

In the lower half of the water column this expression should produce similar turbulent mixing values to those produced by the algebraic turbulence closure model. The turbulent mixing in the upper half of the water column is generally of little importance to the transport of 'sand' sediment fractions as sediment concentrations in the upper half of the water column are low.

The wave- related mixing is calculated following **Van Rijn (1993, 2000)**. In this case Van Rijn recommends a step type distribution over the vertical, with a linear transition between the two steps, see Figure 2.1.1.

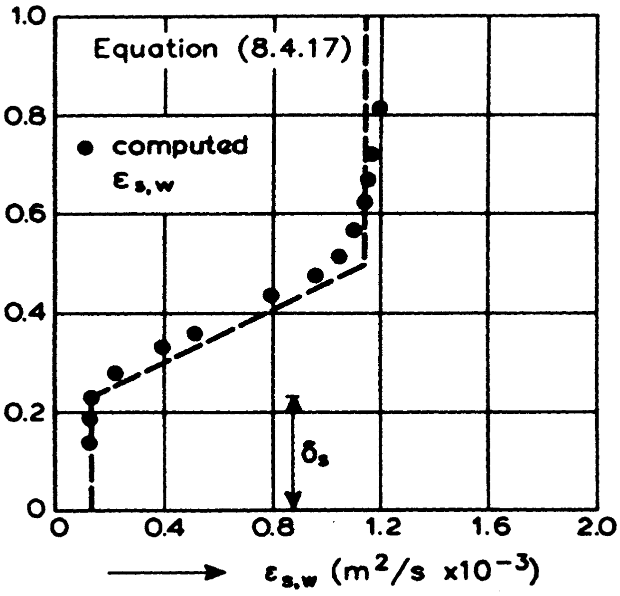

Figure 2.2.1 *Sediment mixing coefficient (Van Rijn 1993).*

The expressions used to set this distribution are:

$$\varepsilon_{s,w}^{(\ell)} = \varepsilon_{s,bed}^{(\ell)} = 0.018\beta_w \delta_s^{(\ell)} \hat{U}_\delta, \qquad \text{when} \qquad z \leq \delta_s^{(\ell)},$$

$$\varepsilon_{s,w}^{(\ell)} = \varepsilon_{s,\max}^{(\ell)} = \frac{0.035\gamma_{br} h H_s}{T_p}, \qquad \text{when} \qquad z \geq 0.5h, \tag{2.2.26}$$

$$\varepsilon_{s,w}^{(\ell)} = \varepsilon_{s,bed}^{(\ell)} + \left(\varepsilon_{s,\max}^{(\ell)} - \varepsilon_{s,bed}^{(\ell)}\right)\left[\frac{z-\delta_s^{(\ell)}}{0.5h-\delta_s^{(\ell)}}\right], \qquad \text{when} \quad \delta_s^{(\ell)} < z < 0.5h,$$

where $\delta_s^{(\ell)}$ (the thickness of the near-bed sediment mixing layer) is estimated using Van Rijn's formulation, given by:

$$\delta_s^{(\ell)} = \min\left[0.5, \max\left\{0.1, \max\left(5\gamma_{br}\delta_w, 10\gamma_{br}k_{s,w}\right)\right\}\right] \tag{2.2.27}$$

where:

δ_w thickness of the wave boundary layer:

$$\delta_w = 0.072\hat{A}_\delta\left(\frac{\hat{A}_\delta}{k_{s,w}}\right)^{0.25} \tag{2.2.28}$$

γ_{br} empirical coefficient related to wave breaking:

$$\gamma_{br} = 1 + \left(\frac{H_s}{h} - 0.4\right)^{0.5} \quad \text{and } \gamma_{br} = 1 \text{ for } \frac{H_s}{h} \leq 0.4 \tag{2.2.29}$$

$k_{s,w}$ wave-related bed roughness (as calculated for suspended sediment transport).

The total vertical sediment mixing coefficient according to Van Rijn is based on the sum of the squares:

$$\varepsilon_s^{(\ell)} = \sqrt{\varepsilon_{s,c}^{(\ell)2} + \varepsilon_{s,w}^{(\ell)2}}\ , \tag{2.2.30}$$

where ε_s is the vertical sediment diffusion coefficient used in the suspended sediment transport calculations for this sediment fraction.

Using the $k-\varepsilon$ turbulence model
In the case of the $k-\varepsilon$ turbulence closure model the vertical sediment mixing coefficient can be calculated directly from the vertical fluid mixing coefficient calculated by the turbulence closure model, using the following expression:

$$\varepsilon_s^{(\ell)} = \beta_{cw}^{(\ell)}\,\varepsilon_f\,, \tag{2.2.31}$$

where:

$\varepsilon_s^{(\ell)}$ vertical sediment mixing coefficient of sediment fraction (ℓ).

$\beta_{cw}^{(\ell)}$ the effective Van Rijn's 'beta' factor of sediment fraction (ℓ). It consists of a wave and current related contribution:

$$\beta_{cw}{}^{(\ell)} = 1 + 2\left[\frac{w_s^{(\ell)}}{u_{*,cw}}\right]^2. \tag{2.2.32}$$

$u_{*,cw}$ combined wave and current-related shear velocity

ε_f vertical fluid mixing coefficient calculated by the $k-\varepsilon$ turbulence closure model

This implies that the value of $\beta_{cw}{}^{(\ell)}$ is space (and time) varying, however it is constant over the depth of the flow. In addition, due to the limited knowledge of the physical processes involved, the beta-factor $\beta_{cw}{}^{(\ell)}$ is limited to the range $1 < \beta_{cw}{}^{(\ell)} < 1.5$.

Remark:
- The $k-\varepsilon$ turbulence closure model has been extended by **Walstra et al. (2000)** to include the three-dimensional effects of waves on the mixing (via the frictional bottom dissipation and wave breaking dissipation).

2.2.3.4 Reference concentration

For non-cohesive sediment (e.g. sand), we follow the method of **Van Rijn (1993)** for the combined effect of waves and currents. The reference height is given by:

$$a = \min\left[\max\left\{k_c, k_w, 0.01h\right\}, 0.20h\right], \tag{2.2.33}$$

where:

a Van Rijn's reference height.

k_c user-specified current-related effective roughness height (see options below).

k_w	user-specified wave-related effective roughness height (see options below).
h	water depth.

Remarks:

- Van Rijn's reference height a is limited to a maximum of 20% of the water depth. This precaution is only likely to come into effect in very shallow areas.
- The currently implemented minimum value of 1 % of the local water depth for the reference height requires further research. Especially in deeper water this would imply unrealistic high reference heights which will result in reduced transport rates. It might be better to prescribe an absolute minimum in the order of 0.01 m.

With the keyword IOPKCW the user has three options to calculate k_c (and k_w):

1) k_c derived from current-related effective roughness height as determined in the FLOW module (spatially varying) and k_w specified by user (constant in space).
2) k_c and k_w specified by the user (constant in space).
3) k_c and k_w determined by the roughness predictor as derived in this report (see also Chapter 3).

The total physical current-related roughness k_c is calculated as:

$$k_c = \left(k_{cr}{}^2 + k_{cmr}{}^2 + k_{cd}{}^2 \right)^{0.5} \tag{2.2.34}$$

which is based on a summation of the current-related roughness due to ripples (k_{cr}), mega-ripples (k_{cmr}) and dunes (k_{cd}, rivers only).

The current-related roughness due to ripples is estimated as:

$$\begin{array}{ll} k_{cr} = 150 d_{50} & and\; 0 \le \psi \le 50 \\ k_{cr} = \left(182.5 - 0.65\psi\right) d_{50} & and\; 50 < \psi < 250 \\ k_{cr} = 20 d_{50} & and\; \psi \ge 250 \end{array} , \tag{2.2.35}$$

The current-related roughness due to mega-ripples reads:

$$\begin{array}{lll} k_{cmr} = 0.0002\psi h & and\; 0 \le \psi \le 50 & and\; h > 1 \; and\; u_c > 0.3 \\ k_{cmr} = \left(0.0125 - 0.00005\psi\right) h & and\; 50 < \psi < 250 & and\; h > 1 \; and\; u_c > 0.3 \\ k_{cmr} = 0 & and\; \psi \ge 250 & and\; h > 1 \; and\; u_c > 0.3 \end{array} \tag{2.2.36}$$

The current-related roughness due to dunes in rivers reads:

$$\begin{aligned}
&k_{cmr} = 0.0004\psi h && and\, 0 \le \psi \le 100 && and\, h > 1 && and\, u_c > 0.3 \\
&k_{cmr} = \left(0.05 - 0.0001\psi\right) h && and\, 100 < \psi < 500 && and\, h > 1 && and\, u_c > 0.3 \\
&k_{cmr} = 0 && and\, \psi \ge 500 && and\, h > 1 && and\, u_c > 0.3
\end{aligned} \tag{2.2.37}$$

in which ψ is the mobility parameter:

$$\psi = \frac{{u_{wc}}^2}{\left(s-1\right) g d_{50}}, \tag{2.2.38}$$

where

$$u_{wc} = \sqrt{{U_w}^2 + {u_c}^2 + 2U_w u_c \left|\cos\varphi\right|}, \tag{2.2.39}$$

in which U_w is the peak orbital velocity near bed based on linear wave theory, u_c is the depth-averaged current velocity, φ is the angle between wave and current motion, H_s the significant wave height, k is the wave number (=2π/L, where L is the wave length derived from $(L/T_p \pm u_c)^2 = gL \tanh(2\pi h/L)/(2\pi)$).

In line with this, it is proposed that the physical wave-related roughness of small-scale ripples is given by:

$$\begin{aligned}
&k_w = 150 d_{50} && and\;\; 0 \le \psi \le 50 \\
&k_w = \left(182.5 - 0.65\psi\right) d_{50} && and\;\; 50 < \psi < 250 \;\;, \\
&k_w = 20 d_{50} && and\;\; \psi \ge 250
\end{aligned} \tag{2.2.40}$$

This predictor is assumed to be valid for relatively fine sand with d_{50} in the range of 0.1 to 0.5 mm. An estimate of the bed roughness for coarse particles (d_{50}>0.5 mm) can be obtained by using Eq. (2.2.34) for d_{50}=0.5 mm. Thus, d_{50}=0.5 mm for $d_{50} \ge 0.5$ mm resulting in a maximum bed roughness height of 0.075 m (upper limit). The lower limit will be $k_w = 15 d_{50}$= 0.0015 m for sand with $d_{50} \le 0.1$ mm.
Larger scale wave-induced ripples (often known as ‘long wave ripples’ may be present, but the physical roughness of these types of ripples is assumed to be zero, as flow separation is not likely to occur.

Calculation of the reference concentration
The reference concentration is calculated in accordance with **Van Rijn (2000)**, but an additional factor η is introduced (and monitored) to reflect the presence of multiple sediment fractions. The resulting expression is:

$$c_a^{(\ell)} = SUS\; \eta^{(\ell)}\; 0.015 \rho_s^{(\ell)} \frac{d_{50}^{(\ell)} \left(T_a^{(\ell)}\right)^{1.5}}{a\left(D_*^{(\ell)}\right)^{0.3}} \tag{2.2.41}$$

where:

$c_a^{(\ell)}$ mass concentration at reference height *a*.

SUS multiplication factor specified in the morphological input file.

In order to evaluate this expression the following quantities must be calculated:

$\eta^{(\ell)}$ relative availability of sediment fraction:

$$\eta^{(\ell)} = \frac{\text{mass of fraction } (\ell) \text{ in mixing layer}}{\text{total mass of sediment in mixing layer}}. \tag{2.2.42}$$

$D_*^{(\ell)}$ non-dimensional particle diameter:

$$D_*^{(\ell)} = d_{50}^{(\ell)} \left[\frac{(s^{(\ell)} - 1) g}{\upsilon^2} \right]^{1/3}. \tag{2.2.43}$$

$T_a^{(\ell)}$ non-dimensional bed-shear stress:

$$T_a^{(\ell)} = \frac{(\mu_c^{(\ell)} \tau_{b,cw} + \mu_w^{(\ell)} \tau_{b,w}) - \tau_{cr}^{(\ell)}}{\tau_{cr}^{(\ell)}}. \tag{2.2.44}$$

$\mu_c^{(\ell)}$ efficiency factor current:

$$\mu_c^{(\ell)} = \frac{f_c'^{(\ell)}}{f_c}. \tag{2.2.45}$$

$f_c'^{(\ell)}$ gain related friction factor:

$$f_c'^{(\ell)} = 0.24 \left[\log_{10} \left(\frac{12h}{3 d_{90}^{(\ell)}} \right) \right]^{-2}. \tag{2.2.46}$$

$f_c^{(\ell)}$ total current-related friction factor:

$$f_c^{(\ell)} = 0.24 \left[\log_{10} \left(\frac{12h}{k_c} \right) \right]^{-2}. \tag{2.2.47}$$

$\tau_{b,cw}$ bed shear stress due to current in the presence of waves.
Note that the bed shear velocity u_* is calculated in such a way that Van Rijn's wave-current interaction factor α_{cw} is not required.

$$\tau_{b,cw} = \rho_w u_*^2, \tag{2.2.48}$$

$\mu_w^{(\ell)}$ efficiency factor waves:

$$\mu_w^{(\ell)} = \max \left(0.063, \frac{1}{8} \left(1.5 - \frac{H_s}{h} \right)^2 \right), \tag{2.2.49}$$

$\tau_{b,w}$ bed shear stress due to waves:

$$\tau_{b,w} = \frac{1}{4} \rho_w f_w \left(\hat{U}_\delta \right)^2, \tag{2.2.50}$$

f_w total wave-related friction factor:

$$f_w = \exp \left[-6 + 5.2 \left(\frac{\hat{A}_\delta}{k_w} \right)^{-0.19} \right]. \tag{2.2.51}$$

$\tau_{cr}^{(\ell)}$ critical bed shear stress:

$$\tau_{cr}^{(\ell)} = (\rho_s^{(\ell)} - \rho_w) g \; d_{50}^{(\ell)} \; \theta_{cr}^{(\ell)} . \tag{2.2.52}$$

$\theta_{cr}^{(\ell)}$ threshold parameter $\theta_{cr}^{(\ell)}$ is calculated according to the classical Shields curve as modelled by **Van Rijn (1993)** as a function of the non-dimensional grain size D*. This avoids the need for iteration. Note that, for clarity, in this expression the symbol D_* has been used where $D_*^{(\ell)}$ would be more correct:

$$\begin{aligned}
\theta_{cr}^{(\ell)} &= 0.24 D_*^{-1} \quad , && 1 < D_* \le 4 \\
\theta_{cr}^{(\ell)} &= 0.14 D_*^{-0.64} \quad , && 4 < D_* \le 10 \\
\theta_{cr}^{(\ell)} &= 0.04 D_*^{-0.1} \quad , && 10 < D_* \le 20 \; . \\
\theta_{cr}^{(\ell)} &= 0.013 D_*^{0.29} \quad , && 20 < D_* \le 150 \\
\theta_{cr}^{(\ell)} &= 0.055, && 150 < D_*
\end{aligned} \tag{2.2.53}$$

a Van Rijn's reference height.

$\hat{A}_\delta$ peak orbital excursion at the bed:

$$\hat{A}_\delta = \frac{T_p \hat{U}_\delta}{2\pi} \tag{2.2.54}$$

$d_{50}^{(\ell)}$ representative sediment diameter.

$d_{90}^{(\ell)}$ 90% sediment passing size:

$d_{90}^{(\ell)} = 1.5 d_{50}^{(\ell)}$.

h water depth.

k_a apparent bed roughness felt by the flow when waves are present. Calculated by DELFT3D-FLOW using the wave-current interaction formulation selected.

$k_a \le 10 k_c$.

k_c user-specified current-related roughness.

k_w user-specified wave-related roughness.

u_z velocity magnitude taken from a near-bed computational layer. In a current-only situation the velocity in the bottom computational layer is used. Otherwise, if waves are active, the velocity is taken from the layer closest to the height of the top of the wave mixing layer δ.

$\hat{U}_\delta$ peak orbital velocity at the bed:

$\sqrt{2} \times$RMS orbital velocity at bed, taken from the wave module.

z_u height above bed of the near-bed velocity (u_z) used in the calculation of bottom shear stress due to current.

Δ_r estimated ripple height, see Eq. (B.8.32)

δ_m thickness of wave boundary mixing layer following **Van Rijn (1993)**:

$3\delta_w$ (and $\delta_m \ge k_a$).

δ_w wave boundary layer thickness:

$$\delta_w = 0.072 \hat{A}_\delta \left(\frac{\hat{A}_\delta}{k_w} \right)^{-0.25} \quad (2.2.55)$$

We emphasise the following points regarding this implementation:

- The bottom shear stress due to currents is based on a near-bed velocity taken from the hydrodynamic calculations, rather than the depth-averaged velocity used by Van Rijn.
- All sediment calculations are based on hydrodynamic calculations from the previous half time-step. We find that this is necessary to prevent unstable oscillations developing.

The apparent roughness felt by the flow (k_a) is dependent on the hydrodynamic wave-current interaction model applied. At this time, Van Rijn's wave-current interaction model is not available in DELFT3D-FLOW and DELFT3D-ONLINE. This means that it is not possible for a user to exactly reproduce results obtained using Van Rijn's full formulations for waves and currents.

2.2.4 Bed load transport

Bed-load transport is calculated for all "sand" sediment fractions by broadly following the approach described by **Van Rijn (1993, 2000)**. This accounts for the near-bed sediment transport occurring below the reference height *a* described above.

The approach first computes the magnitude and direction of the bed-load "sand" transport using by Van Rijn. The computed sediment transport vectors are then relocated from water-level points to velocity points using an "upwind" computational scheme to ensure numerical stability. Finally the transport components are adjusted for bed-slope effects. Here the transport formulations are highlighted, more information on numerical aspects and bed slope effects can be found in the DELFT3D user manual.

For simulations including waves the magnitude and direction of the bed-load transport on a horizontal bed are calculated using an approximation method developed by **Van Rijn et al. (2003)**. The method computes the magnitude of the bed-load transport as:

$$|S_b| = 0.006 \eta \rho_s w_s d_{50}^{(\ell)} M^{0.5} M_e^{0.7} \quad (2.2.56)$$

where:

S_b = bed load transport (kg/m/s)
η = relative availability of the sediment fraction in the mixing layer (-)
M = sediment mobility number due to waves and currents (-)
M_e = excess sediment mobility number (-)

$$M = \frac{{v_{eff}}^2}{(s-1)\,g d_{50}} \tag{2.2.57}$$

$$M_e = \frac{\left(v_{eff} - v_{cr}\right)^2}{(s-1)\,g\,d_{50}} \tag{2.2.58}$$

$$v_{eff} = \sqrt{v_R^2 + U_{on}^2} \tag{2.2.59}$$

in which:

v_{cr} = critical depth averaged velocity for initiation of motion (based on a parameterisation of the Shields curve) (m/s).
v_R = magnitude of an equivalent depth-averaged velocity computed from the velocity in the bottom computational layer, assuming a logarithmic velocity profile (m/s).
U_{on} = near-bed peak orbital velocity (m/s) in onshore direction (in the direction on wave propagation) based on the significant wave height.

U_{on} (and U_{off} used below) are the high frequency near-bed orbital velocities due to short waves and are computed using a modification of the method of **Isobe and Horikawa (1982)**. This method is a parameterisation of fifth-order Stokes wave theory and third-order cnoidal wave theory which can be used over a wide range of wave conditions and takes into account the non-linear effects that occur as waves propagate in shallow water (**Grasmeijer and Van Rijn, 1999**).

The direction of the bed-load transport vector is determined by assuming that it is composed of two parts: part due to current ($S_{b,c}$) which acts in the direction of the near-bed current, and part due to waves ($S_{b,w}$) which acts in the direction of wave propagation. These components are determined, as follows:

$$S_{b,c} = \frac{S_b}{\sqrt{1 + r^2 + 2|r|\cos\varphi}} \tag{2.2.60}$$

$$\left|S_{b,w}\right| = r\left|S_{b,c}\right| \tag{2.2.61}$$

where:

$$r = \frac{\left(\left|U_{on}\right| - v_{cr}\right)^3}{\left(\left|v_R\right| - v_{cr}\right)^3} \tag{2.2.62}$$

$S_{b,w} = 0$ if r<0.01, $S_{b,c} = 0$ if r>100, and φ = angle between current and wave direction. As Eq. (2.2.56) is only based on data with $\varphi = 90°$, the φ-value is fixed to $\varphi = 90°$. This is an important limitation of this wave-averaged approach. Especially under larger wave conditions this can results in deviations in the order 50 % compared to the original intra-wave approach (see e.g. the sensitivity analysis in Section 4.2). It is therefore recommended to include the intra-wave approach in DELFT3D as option.

The bed load transport components in x- and y-direction are:

$$
\begin{aligned}
S_{b,x} &= \frac{u_b}{\left(u_b{}^2 + v_b{}^2\right)^{0.5}} S_{b,c} + S_{b,w} \cos\phi \\
S_{b,y} &= \frac{v_b}{\left(u_b{}^2 + v_b{}^2\right)^{0.5}} S_{b,c} + S_{b,w} \sin\phi
\end{aligned}
\tag{2.2.63}
$$

where u_b and v_b are near-bed current velocities in x- and y-directions, and ϕ is the local angle between the direction of wave propagation and the x-axis of the computational grid.

2.2.5 Wave-related suspended transport

The wave-related suspended transport is an estimation of the suspended sediment transport due to wave velocity asymmetry effects. This is intended to model the effect of asymmetric wave orbital velocities on the transport of suspended material within about 0.5m of the bed (the bulk of the suspended transport affected by high frequency wave oscillations).

This wave-related suspended sediment transport is modelled using an approximation method proposed by **Van Rijn (2002)**:

$$S_{s,w} = f_{\mathrm{SUSW}}\, \gamma U_A\, L_T \tag{2.2.64}$$

where:

$S_{s,w}$	=	wave-related suspended transport (kg/m/s)
f_{SUSW}	=	user specified tuning parameter
γ	=	phase lag coefficient (= 0.2)
U_A	=	velocity asymmetry value (m/s) = $\dfrac{U_{on}^4 - U_{off}^4}{U_{on}^3 + U_{off}^3}$
L_T	=	suspended sediment load (kg/m^2) = $0.007\, \rho_s\, d_{50}\, M_e$

The wave-related suspended transport components in x- and y-directions are:

$$
\begin{aligned}
S_{s,w,x} &= S_{s,w} \cos\phi \\
S_{s,w,y} &= S_{s,w} \sin\phi
\end{aligned}
\tag{2.2.65}
$$

2.2.6 Approximation formulas for current-related suspended transport

The approximation method recently developed by **Van Rijn (2002)** has also been implemented in DELFT3D-ONLINE as a separate transport formulation option (see Table 2.1.2). This method is an extension of **Van Rijn (1993)** who introduced an approximation method for the current-related suspended sand transport in steady flow conditions (in direction of velocity vector), as follows:

$$q_{s,c} \simeq F_c v_R h c_a \tag{2.2.66}$$

where:

$q_{s,c}$ = current-related suspended transport (in kg/s/m, if concentration in kg/m^3),
v_R = depth-averaged current velocity (magnitude of vector),
h = water depth,
c_a = reference concentration (kg/m^3),
F_c = correction factor.

The correction factor F_c is described by:

$$F_c = \frac{\left(\frac{a}{h}\right)^{ZC} - \left(\frac{a}{h}\right)^{1.2}}{\left(1.2 - ZC\right)\left(1 - \frac{a}{h}\right)^{ZC}} \tag{2.2.67}$$

in which:

$$ZC = \frac{w_s}{\beta_c \kappa u_{*,c}} + 2.5\left(\frac{w_s}{u_{*,c}}\right)^{0.8}\left(\frac{c_a}{c_0}\right)^{0.4} \tag{2.2.68}$$

where:

$u_{*,c}$ = current-related bed-shear velocity,
c_o = maximum bed concentration=0.65 (volume),
w_s = fall velocity (based on d_{50} of bed material),
β_c = $1+2(w_s/u_{*,c})^2$ with $\beta_{c,max}$=1.5.

For conditions with currents and waves **Van Rijn (2002)** generalised this method as follows:

$$q_{s,c} = \left(F_c + F_w\right) v_R h c_a \tag{2.2.69}$$

The correction factor F_w is described by:

$$F_w = \frac{\left(\frac{a}{h}\right)^{ZW} - \left(\frac{a}{h}\right)^{1.2}}{\left(1.2 - ZW\right)\left(1 - \frac{a}{h}\right)^{ZW}} \tag{2.2.70}$$

The *ZW* parameter of the approximation method has been determined by computer fitting based on a set of numerically computed suspended transport rates, yielding:

$$ZW = 4\left(\frac{h}{h_{ref}}\right)^{0.6}\left(\frac{w_s T_p}{H_s}\right)^{0.8} \tag{2.2.71}$$

where:

h = water depth (should not be taken smaller than 0.25 m and not larger than 50 m),
h_{ref} = reference water depth (= 5 m),
T_p = peak period of waves,
H_s = significant wave height,
w_s = fall velocity ($w_{s,minimum}$= 0.03 m/s).

$$\begin{aligned} ZC = ZW = 1.19 \qquad & if\, 1.19 < ZC = ZW < 1.20 \\ ZC = ZW = 1.21 \qquad & if\, 1.20 < ZC = ZW < 1.21 \end{aligned} \tag{2.2.72}$$

2.2.7 Numerical aspects

The bed-load transport vector components are computed at the water-level points of the staggered grid (see also **Figure 2.2.2**). The vector components at the velocity-points are determined by taking the appropriate vector components from the adjacent water-level point ½ a grid cell 'upwind'. The upwind direction is based on the computed direction of the bed load transport vectors in the water-level points. If the vector components in adjacent water-level points oppose, then a central scheme is used. The bed load transport components at the velocity-points are modified to include bed-slope effects in longitudinal and in transverse directions (see **Lesser et al. 2003**), as follows:

$$\begin{aligned} S^*_{b,x} &= \alpha_s S_{b,x} - \alpha_n S_{b,y} \\ S^*_{b,y} &= \alpha_s S_{b,y} + \alpha_n S_{b,x} \end{aligned} \tag{2.2.73}$$

where

$$\alpha_s = 1 + \alpha_{bs}\left[\frac{\tan(\phi)}{\cos(\beta_s)\left(\tan(\phi) - \tan(\beta_s)\right)} - 1\right] \tag{2.2.74}$$

and

$$\alpha_n = \alpha_{bn}\left(\frac{\tau_{b,cr}}{\tau_{b,cw}}\right)^{0.5} \tan(\beta_n) \tag{2.2.75}$$

in which α_{bs} and α_{bn} are user-specified tuning parameters, β_s is the bed slope angle in direction of bed load transport vector (positive down), β_n is the bed slope angle normal to bed load transport vector (positive down), ϕ is the internal angle of friction of bed material (assumed to be 30°), $\tau_{b,cr}$ is the critical bed shear stress and $\tau_{b,cw}$ is the bed shear stress due to current and waves.

This upwind shift ensures numerical stability and allows the implementation of a simple morphological updating scheme.

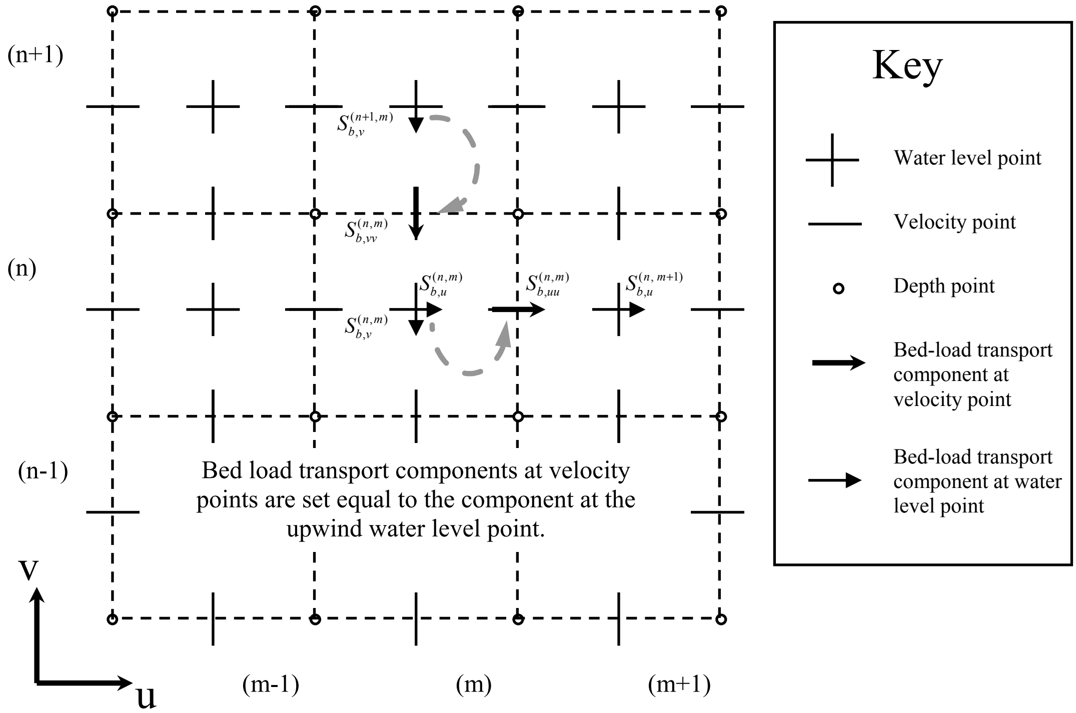

Figure 2.2.2 *Transport vectors in staggered grid in DELFT3D-ONLINE (source Lesser et al.).*

3 Improvement and validation of engineering sand transport formulations

3.1 Derivation of bed roughness predictor

3.1.1 Approach

Nikuradse (1932) introduced the concept of an equivalent or effective sand roughness height (k_s) to simulate the roughness of arbitrary roughness elements of the bottom boundary.

Generally, four types of roughness values can be distinguished:

Grain roughness ($k_{s,grain}$)	→ sand transport modelling
Current-related bed form roughness ($k_{s,c}$)	→ flow modelling → sand transport modelling
Wave-related bed form roughness ($k_{s,w}$)	→ wave modelling → sand transport modelling
Apparent roughness (k_a)	→ flow modelling → sand transport modelling

In case of a movable bed with bed forms the effective bed roughness (k_s) mainly consists of grain roughness (k'_s) generated by skin friction forces and of form roughness (k''_s) generated by pressure forces acting on the bed forms. Similarly, a grain-related bed-shear stress (τ'_b) and a form-related bed-shear stress (τ''_b) can be defined.
The grain roughness is the roughness of the plane bed surface, which is of importance for the motion of the bed load particles and the entrainment of suspended load particles at the upstream side (stoss side) of the bed forms or at a flat bed (if bed forms are absent).

The current-related roughness is the effective roughness of the bed forms as experienced by the current (unidirectional flow). This parameter affects the depth-mean velocity and the vertical distribution of the velocity profile and hence the near-bed velocities, which are of special importance for the sand transport processes. Similarly, the wave-related roughness is the effective roughness of the bed forms as experienced by the orbital motion of the waves (oscillatory flow) in conditions when the bed forms have a length scale smaller than the orbital excursion.

The apparent roughness is the effective roughness experienced by the current when waves are superimposed on the current (wave-current interaction effects) resulting in modification of the velocity profile. Generally, the velocities are reduced in the near-bed region.

The effective bed roughness for a given bed material size is not constant but depends on the flow conditions. Analysis results of k_s-values computed from Mississippi River data (USA) show that the k_s-value strongly decreases from about 0.5 m at low velocities (0.5 m/s) to about 0.001 m at high velocities (2 m/s), probably because the bed forms become more rounded or are washed out at high velocities.
The fundamental problem of bed roughness prediction is that the bed characteristics (bed forms) and hence the bed roughness depend on the main flow and wave variables (depth, velocity, wave height and period) and sediment transport rate (sediment size). These hydraulic variables are, however, in turn strongly dependent on the bed configuration and its roughness.

As the current-related and the wave-related roughness values are strongly related to the bed forms, these latter features are reviewed in Sections 3.1.2 and 3.1.3 with a summary in Section 3.1.4. The bed roughness due to bed forms is reviewed in Section 3.1.5. A new relatively simple bed roughness predictor is proposed in Section 3.1.6.

3.1.2 Bed form characteristics in oscillatory flows

Bedforms are a primary cause of hydraulic roughness of flows over sediment beds and may severely modify the flow field in the near-bed region. In waves or currents, wave ripples or current ripples and dunes play significant roles in the suspension of bed sediments. The bedform height determines the active layer thickness at the bed surface, which is important for transport and morphological computations over sediment mixtures. Moreover, the presence of ripples may lead to large phase differences between sediment suspension in vortex shedding from the ripples and orbital wave motion, which may invert the sediment transport direction. Certain bedform types (ripples and flat bed) occur only in a limited range of flow conditions and sediment sizes. Inversely, the presence of certain (relict) bedform types or their deposits may indicate the flow conditions during their creation.
The dominant bed forms in oscillatory flow with or without a weak current in field conditions often are ripples with a length scale related (smaller or equal) to the near-bed orbital diameter. The ripples are sometimes irregular or have three-dimensional patterns, but are more commonly approximately two-dimensional. Ripples exhibiting the formation of fluid vortices (orbital excursion larger than ripple length) are called vortex-ripples (**Bagnold, 1946**). Field studies have shown that besides vortex-ripples there is a variety of other bed form types and patterns. The variability in bed form morphology is the result of the complex combination of currents and unsteady shoaled waves of many frequencies and directions. Furthermore, the sedimentary bed is composed of a combination of grain sizes.

Most bed roughness models require a priori estimates of the ripple geometry for the given flow and sand bed conditions. A number of empirical bed form prediction formulae have been developed for ripple geometry (e.g. **Vongvisessomjai, 1984; Nielsen, 1992; Wiberg and Harris, 1994; Mogridge et al., 1994**). These formulae are heavily based on empirical data from laboratory and field experiments and predict ripple geometry for the short period, low amplitude flows that are typical of wave-dominated conditions. The predicted ripple characteristics diverge extremely for field-scale conditions (**Mogridge et al. ,1994).**

Ripple geometry predictive formulae generally apply to two-dimensional (2D) ripples, i.e. long-crested, parallel ripples with height and length constant over a large bed area. However, three-dimensional (3D) ripples have been frequently observed in most field conditions.

The most simple expressions describing ripple dimensions have been given by **Kos'yan (1988),** who found that the ripple height and length in depths up to about 15 m can be roughly described by Δ_r= 200d_{50} and λ_r= 1000d_{50}.

Mogridge et al. (1994) have re-examined data on bed form geometry provided by various researchers, with the objective of improving the predictive methods and determining where uncertainties remain. According to their results, the bed forms (ripples) reach a maximum height and length, which are dependent on the particle size (d_{50}), wave period (T_p) and peak near-bed orbital velocity (U_w). The maximum length is in the range of 100d_{50} to 5000d_{50}; the maximum height is in the range of 10d_{50} to 500d_{50}. **Mogridge et al.** concluded that the scatter of existing bed form data is such that the prediction accuracies are poor.

Hume et al. (1999) have studied bed form changes during a tropical storm by using an instrumented tripod on a bed of 0.4 mm sand in 25 m depth off Cape Rodney headland on the northeast coast of New Zealand. Three-dimensional short-crested ripples with a height of about 0.03 m (Δ_r= 7.5d_{50}) and a length of about 0.45 m (λ_r= 110d_{50}) were present during pre-storm conditions, but changed to a long-crested ripples with a height of 0.1 m (Δ_r= 25d_{50}) and a length of about 1 m (λ_r= 250d_{50}) during passage of the storm (maximum significant wave height of about 3 m; peak period of about 10 s). The ripples were aligned normal to the wave approach. The maximum peak orbital velocities were in the range of 0.6 to 0.8 m/s. The maximum wave orbital diameters were in the range of 1 to 1.5 m during passage of the storm. Mean current speeds near the bed were in the range of 0.2 to 0.3 m/s. Analysis of velocity profiles shows k_a-values in the range of 1.5 to 3 m (ratio $k_a/k_{s,c}$ is in the range of 15 to 30 assuming $k_{s,c}\cong\Delta_r$; the ratio U_w/u_c is about 2).

Hanes et al. (2001) have analysed an extensive data set of ripples observed in the nearshore zone of the Duck site (North Carolina, USA) in water depths ranging from 1 to 7 m, grain sizes ranging from 0.12 to 1.6 mm and wave heights ranging from 0.2 to 1.2 m. Ripples with two different ranges of wave lengths were observed: shorter ripples (SWR) with heights of 0.003 to 0.02 m and lengths of 0.05 to 0.25 m and longer ripples (LWR) with heights of 0.003 to 0.06 m and lengths of 0.35 to 2 m. Each of these types sometimes occurred alone and at other times both types were superimposed. The LWR have relatively low relief with a steepness (= height-length ratio) of 0.01 when compared to the SWR with a steepness of 0.15. The behaviour of the SWR is rather well correlated to the significant near-bed mobility number $\psi=(U_w)^2/((s-1)g\ d_{50})$. The LWR were almost always present and were not clearly correlated to the forcing conditions. The SWR disappeared at high ψ-values. No SWR were observed for $\psi>185$. SWR were present 85% of the time when $\psi<65$, but SWR were only present 13% of the time for $65<\psi<185$. Mobility numbers greater than 150 result in the reduction of SWR height. Ripple reformation can occur within a minute or so after flattening, when the ψ-value decrease to a value below 150 but larger than about 50. For $\psi<50$ ripple movement is slow. The dimensions of the SWR are predictable by models to within a factor of 2.

The origin of the LWR is not quite clear. The models are not able to reproduce the relatively low steepness values. Numerical simulation of the oscillatory flow over the LWR indicates weak separation and turbulence production with significant enhancement of these processes when SWR are superimposed upon the LWR. Hence, the effective form roughness of the LWR is almost zero.

SWR and LWR were also observed by **Grasmeijer (2002)** in the nearshore zone of the Egmond site (The Netherlands). SWR were dominantly present for ψ<50 and were almost absent for ψ>150. LWR were always present (20% of time for ψ<50), but dominated (90% of time) for ψ>150.

SWR (with lengths of about 0.1 to 0.3 m and estimated heights of 0.01 to 0.03 m) were also observed by **Amos et al. (1999)** in field conditions (Sable Banks, Nova Scotia, Canada) with depths of about 20 m and fine sand beds (0.23 mm) under low-energy conditions (oscillatory flows plus weak tidal currents) and by **Slaattelid and Myrhaug (1994)** in depths of 70 m (North Sea) with fine sand beds (0.2 mm).

The results of recent wave tunnel experiments (see Section 3.3.3) with oscillatory flows and combined oscillatory and steady flows also show the presence of LWR for ψ-values larger than 65 (up to 370). SWR with vortex shedding phenomena were only observed for ψ-values smaller than 50.

grain size (mm)	**water depth (m)**			
	4 – 10	**10 – 20**	**20 – 35**	**35 – 60**
0.1–0.3	Hanes et al. 2001 *(wave ripples; 0.5-5 cm; 2-120 cm; sheet flow)*	Boyd et al. 1988 *(wave ripples; ?-14 cm)*		Slaattelid-Myrhaug, 1994 *(wave ripples; 1-3 cm; 10-20 cm)* Li and Amos 1999b *(no motion to sheet flow; ?-10 cm)*
0.3–0.5		Traykovski et al. 1999 *(wave ripples; ?-70 cm)* Van Lancker et al. 2000 *(current dunes; 2-100 cm)*	Williams and Rose 2001 *(wave ripples; 0.6-60 cm)*	Li and Amos 1998, 1999a *(wave-current ripples; 1.4-12 cm)*
> 0.5				

wave height (m)	**current velocity (m/s)**			
	< 0.1	**0.1 – 0.5**	**0.5 – 1.0**	**> 1.0**
< 1	Hanes et al. 2001	Traykovski et al. 1999 Li and Amos 1999b	Van Lancker et al. 2000	Boyd et al. 1988 Van Lancker et al. 2000
1–3	Hanes et al. 2001	Li and Amos 1999b Traykovski et al. 1999	Williams and Rose 2001	Boyd et al. 1988 Li and Amos 1998, 1999a
> 4		Li and Amos 1999b		

Table 3.1.1 *Bed form data outside the surfzone reported in literature classified according to conditions. Bedform type and indicative dimensions (height-length in cm) are given in italic print*

Traykovski and Goff (2003) have analysed time series of small-scale bed forms in field conditions (south coast of the island of Martha's Vineyard, USA) showing the presence of ripples with heights of 0.02 to 0.03 m and lengths of 0.2 to 0.3 m in depths of about 15 m with fine sand beds (0.1 to 0.2 mm) and heights of 0.05 to 0.2 m and lengths of 0.3 to 1.5 m in coarse sand beds (0.5 to 0.7 mm) under low-energy conditions. The fine sand ripples were always washed out in high-energy conditions.

Doucette (2002) found similar bed forms in shallow water (Australia): relatively large SWR (heights of 0.05 to 0.15 m and lengths of 0.3 to 1.5 m) in coarse sand beds (0.7 mm). Low-amplitude SWR (heights<0.02 m) were observed in fine sand beds (0.2 mm).

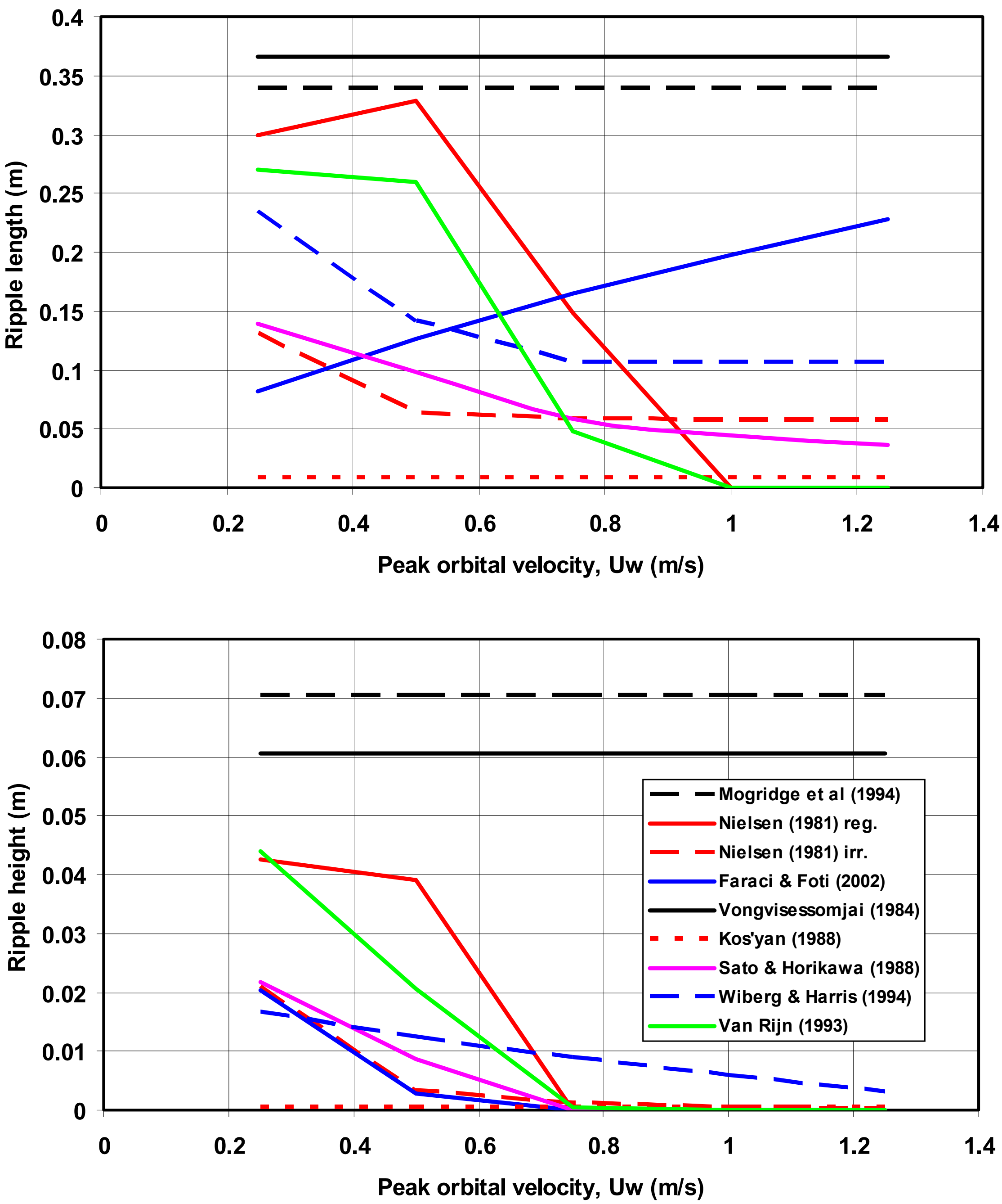

Figures 3.1.1 *Computed ripple height and length; d_{50}=0.2 mm, T=6 s*

Kleinhans (2003) has performed a literature survey of bed form characteristics measured in coastal seas. The most relevant and detailed datasets concern the following sites:

Duck (USA), Nova Scotia (Canada), New Jersey (USA), Southern Australia, New Zealand, Middelkerke banks (Belgium) and the Dutch sector of the North Sea.
Table 3.1.1 based on the review of **Kleinhans (2003)** shows the field datasets of small-scale bedforms that are available for certain ranges of water depth, grain size, wave height and current velocity outside the surfzone. Hardly any data sets are available for deep water with depths larger than 10 m.

Foti (2003) applied the most popular ripple prediction models to compute the ripple height and ripple length for sediment with d_{50}= 0.2 mm and a range of wave conditions (wave period T= 6 s, peak orbital velocities U_w=0.25, 0.50, 0.75, 1.0 and 1.25 m/s). The results are shown in Figure 3.1.1. As can be observed, there is a wide range in computed ripple heights and lengths. The ripple heights vary between 0.07 and 0 m; the ripple lengths vary between 0.37 and 0.01 m. Most methods yield a ripple height decreasing with increasing peak orbital velocity, as the ripples will be washed out for large peak orbital velocities (> 1 m/s). Some methods yield a constant ripple height. One method yields an increasing ripple length with increasing peak orbital velocity

3.1.3 Bed form characteristics in combined oscillatory and weak, steady flows

The generation of bed forms (ripples) under oscillatory flows (wave motion) or under steady flows is much better documented and understood than that under combined oscillatory and steady flows. In fact, purely unidirectional, steady flows and purely oscillatory flows represent the extreme conditions of natural flows, particularly if the steady flow is at an arbitrary angle with the direction of the oscillatory motion. There have been few studies of bed forms generated by combined oscillatory and steady flows. Most of the studies concern bed forms generated under oscillatory flows in combination with following or opposing steady flows as present in flumes.

Van Rijn and Havinga (1995) have published bed form data for oblique (60^o and 120^o) and perpendicular (90^o) oscillatory flow superimposed on a steady flow over a bed of fine sand (0.1 mm) in a basin. The ripple configurations can be described, as (see Figure 3.1.2):

- 2D patterns with straight crests perpendicular to the wave direction (waves only);
- 2.5D patterns with wavy crests in combined oscillatory and relatively weak flows;
- 3D patterns (honeycomb-pattern) in combined oscillatory and relatively strong flows.

Wave-related ripples generated in the wave direction were always reasonably symmetric, whereas the current-related ripples generated in the current direction were asymmetric. The length of both types of ripples increased with increasing strength of the current and peak orbital velocity. The ripple heights of both types were in the range of 0.006 and 0.013 m; the ripple lengths were in the range of 0.05 and 0.11 m. The angle between the wave and current directions had no significant influence on the ripple dimensions.

Field observations of ripple generation under the combined influence of waves and weak currents are discussed by various authors (see review of **Kleinhans, 2003**). In most of these studies the ripples are strongly wave-dominated (storm waves) and the effect of the currents on ripple dimensions is rather limited (not measurable).

Li and Amos (1998) studied various ripple-type bed forms using an instrumented tripod in water depths of about 40 m near Sable Island bank (0.34 mm sand) situated about 180 km southeast of Nova Scotia, Canada. Analysis of seabed photos shows the presence of various types of ripples: current-dominant ripples (CR), wave-dominant ripples (SWR), large wave ripples (LWR) and combined wave-current ripples (CWR). CR are predominantly asymmetrical in shape with sharp brink points. SWR are predominantly symmetrical in shape with sharp crests and bifurcations. LWR are wave-generated ripples with a length larger than 0.3 m. CWR are composed of superimposed wave and current ripples with roughly equal magnitudes. Except LWR, nearly all ripples of the data set have a height in the range of 0.01 to 0.02 m ($30d_{50}$ to $60d_{50}$) and a length of in the range of 0.1 to 0.15 m ($300d_{50}$ to $450d_{50}$). As only two velocity meters were used, the bed roughness values could not be determined accurately. According to Li and Amos, the various ripple types can be separated, as follows:

- Wave-dominant ripples (SWR) for $(u_{*,w}/u_{*,c})^{/}>1.25$
- Current-dominant ripples (CR) for $(u_{*,w}/u_{*,c})^{/}<0.75$
- Combined wave-current ripples (CWR) for $0.75<(u_{*,w}/u_{*,c})^{/}<1.25$

with: $(u_{*,w})^{/}$= wave-related grain shear velocity and $(u_{*,c})^{/}$= current-related grain-shear velocity.

Khelifa and Quellet (2000) have tried to include the effect of weak steady currents in ripple prediction methods. Their results show that empirical expressions proposed for the prediction of ripple geometry under pure wave motion are not applicable for the prediction of ripple dimensions observed under combined waves and currents. According to their results, the effect of a current on the ripple dimensions can be included by two parameters (Δ_r, λ_r=f(ψ,A)):

an effective fluid orbital diameter:

$$A=\frac{U_w T_r}{2\pi} \tag{3.1.1}$$

and a corresponding mobility parameter:

$$\psi=\frac{U_{wc}{}^{2}}{\left(s-1\right)gd_{50}} \tag{3.1.2}$$

with:

$$U_{wc}{}^{2}=U_w{}^{2}+u_c{}^{2}+2U_w u_c\left|\cos\varphi\right| \tag{3.1.3}$$

and: U_w= peak orbital velocity near bed= $\pi H/(T_r \sinh(2kh))$, u_c= depth-averaged current velocity, φ= angle between wave and current motion, H= wave height, k=2π/L, L= wave length derived from $(L/T\pm u_c)^2=gL\tanh(2\pi h/L)/(2\pi)$, T_r= $T/((1-(u_cT/L)\cos\varphi)$= relative wave period, T= wave period, h= water depth.

The substitution of u_c=0 should give a ripple length equal to that for pure wave motion and U_w=0 a ripple length equal to that for a pure current.

A special class of bed forms in combined oscillatory flow and quasi-steady tidal flow is that of the mega-ripples (Δ_{mr}=0.01h to 0.03 h, λ_{mr}=0.4h to 1h, h= water depth), which have been observed quite frequently in field conditions (**Van Rijn, 1993**). Analysis of bottom soundings in various areas of the Dutch Sector of the North Sea with depths of 20 to 35 m shows the presence of transverse sand waves superimposed by migrating mega-ripples. The peak tidal velocities are in the range of 0.5 to 0.8 m/s; the bed material is sand with d_{50} in the range of 0.25 to 0.5 mm.

Large-scale dunes may be present in steady or quasi-steady unidirectional flow conditions (rivers or tidal rivers). Generally, the height of dunes is of the order of 5% to 15% of the water depth. The length scale of the dunes is of the order of 5 to 10 times the water depth. Thus, Δ_d=0.05h to 0.15h, λ_d=5h to 10h (h= water depth).

Herein, it is assumed that the:

- mega-ripple height is Δ_{mr}=0.02h for ψ=50, Δ_{mr}=0 for ψ=0 and ψ=250; the physical bed roughness of these mega-ripples is of the order of half the mega-ripple height; thus $k_{s,c,mr} \cong 0.5\Delta_{mr}$= 0.01h for ψ=50;
- dune height is Δ_d=0.08h for ψ=100, Δ_{mr}=0 for ψ=0 and ψ=500; the physical bed roughness of the dunes is of the order of half the dune height; thus $k_{s,c,d} \cong 0.5\Delta_d$= 0.04h for ψ=100.

The effective roughness of the (symmetrical) sand waves is assumed to be zero, because flow separation does not occur. The large-scale sand waves can be seen as topography for the flow system.

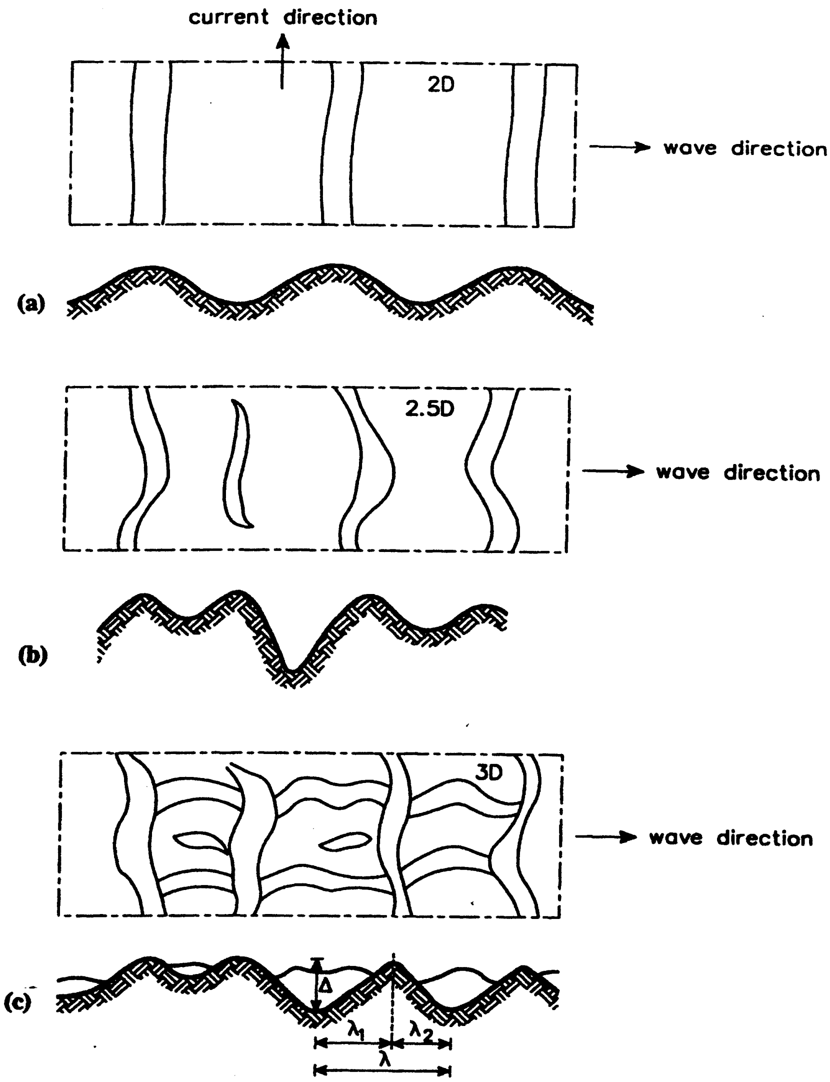

Figure 3.1.2 *Ripple patterns in combined oscillatory flows and steady flows*

3.1.4 Summary

Analysis of field data shows the presence of short wave ripples (SWR) and long wave ripples (LWR) in conditions with combined waves and weak currents.

SWR are dominant for $\psi=(U_w)^2/((s-1)g\ d_{50})$ in the range of 50 to 150 and disappear for $\psi>150$. SWR reformation can occur within a minute or so after flattening, when the ψ-value decrease to a value below 150 but larger than about 50. For $\psi<50$ ripple movement is slow. SWR have the following dimensions:

- ***fine sand bed (0.1-0.3 mm)***
  - height of 0.01 to 0.03 m or Δ_r/d_{50}=50 to 300,
  - length of 0.1 to 0.3 m or λ_r/d_{50}=500 to 3000,
  - steepness (Δ_r/λ_r) of 0.05 to 0.15;
- ***coarse sand bed (0.3 to 1 mm),***
  - height of 0.03 to 0.1 m or Δ_r/d_{50}= 10 to 300,
  - length of 0.3 to 1.2 m or λ_r/d_{50}= 100 to 3000.

The dimensions of the SWR are predictable by models to within a factor of 2. As flow separation and vortex production are basic phenomena of SWR, these ripples have a relatively large form roughness of the order of the ripple height ($k_s \cong$ ripple height).

LWR are low-relief bed features (steepness of about 0.01) and are always present on the bed surface, but are dominantly present for ψ>150. LWR have a height of 0.01 to 0.02 m and a length of 1 to 2 m in a fine sand bed (0.1 to 0.3 mm). The origin of the LWR is not quite clear. The prediction models are not able to reproduce the relatively low steepness values. Numerical simulation of the oscillatory flow over the LWR indicates weak separation and turbulence production with significant enhancement of these processes when SWR are superimposed upon the LWR. Hence, the effective form roughness of the LWR is almost zero ($k_s \cong 0$). Mega-ripples and large-scale dunes may be present at specific locations, but this is not yet predictable

Based on these results, it is concluded that a generally-accepted method for the accurate prediction of ripple characteristics is not yet available. In line with this it is concluded that the prediction of bed roughness from predicted ripple dimensions will not lead to very accurate results. Instead of that it is proposed to relate the bed roughness (k_s) directly to hydrodynamic and sediment-dynamic parameters ($k_s/d_{50}=f(\psi)$).

3.1.5 Analysis of measured bed-roughness values

Four types of bed-roughness values can be distinguished (see **Van Rijn, 1993**):

- grain roughness ($k_{s,grain}$);
- physical wave-related bed form roughness ($k_{s,w}$);
- physical current-related bed form roughness ($k_{s,c}$);
- apparent bed-roughness (k_a).

The physical wave-related bed form roughness value ($k_{s,w}$) of ripples can be derived from analysis of measured instantaneous velocity profiles within the wave boundary layer or from the attenuation of measured wave heights over a certain distance. In the latter case a numerical model is required for simulation of measured wave heights due to bottom friction. The $k_{s,w}$ parameter is strongly related to flow separation and vortex shedding due to oscillatory flow (wave motion) over ripples. Data analysis shows values in the range of 1 to 3 times the ripple height ($k_{s,w}/\Delta_r$=1 to 3).

The physical current-related bed roughness value ($k_{s,c}$) of ripples is the roughness experienced by the current in condition with and without waves. However, this roughness can only be derived from measured velocity profiles in the absence of waves over a rippled bed surface (see Figure 3.1.3). This is due to the fact that the current-related bed roughness requires detailed measurements very close to the bed in conditions with waves. With the present technology this is not possible. In stead, the approach is to run conditions with flow and waves to generate the ripples, next the wave motion is stopped and the current-related bed roughness can be measured. Consequently, field data can only be used when the (tidal) velocity profiles have been measured directly after cessation of the wave motion immediately after a storm. The tidal currents need to be relatively small (range of 0.2 to 0.3 m/s), so that they can not modify the bed forms generated under combined wave-current conditions.

The apparent bed-roughness (k_a) can be derived from measured velocity profiles in the presence of waves over a rippled bed surface using the velocity data outside the wave boundary layer (see Figure 3.1.3).
Herein, the attention is focussed on the $k_{s,c}$, $k_{s,w}$ and k_a-values of rippled beds.

Physical current-related bed roughness ($k_{s,c}$)
Havinga (1992) and **Van Rijn and Havinga (1995)** have presented results based on analysis of velocity profiles measured above a fine-sand bed (0.1 mm) with ripples in a wave-current basin. The k_s-values are in the range of 0.1 to 1.5 times the ripple height (or k_s/Δ_r=0.1 to 1.5 with a mean value of 0.75). A similar data analysis of measured velocity profiles over a bed of ripples (sand of 0.1 and 0. 2 mm) in a wave-current flume (**Van Rijn et al., 1993**) shows k_s-values in the range of 1 to 10 times the ripple height.

Fredsøe et al. (1999) have studied the effective roughness of artificial ripples (concrete ripples) based on measured velocity profiles in a wave-current flume. The experiments were performed in a flume (width of 0.6 m, depth of 0.8 m and length of 28 m). The bed of the flume was covered with sharp-crested wave-type ripples (length of 0.22 m and height of 0.35 m) made of concrete. Three types of experiments were carried out: current-alone, waves-alone and combined waves-current. The k_s-values were determined by regression-analysis of velocity profiles (theoretical bed at $0.25\Delta_r$ below the ripple crest) from the current-alone experiments (three different discharges, water depth of 0.415 m; depth-averaged velocities of 0.22, 0.135 and 0.096 m/s) resulting in k_s-values in the range of 0.074 to 0.08 m or 2.1 to 2.3 times the ripple height (k_s/Δ_r=2.1 to 2.2).

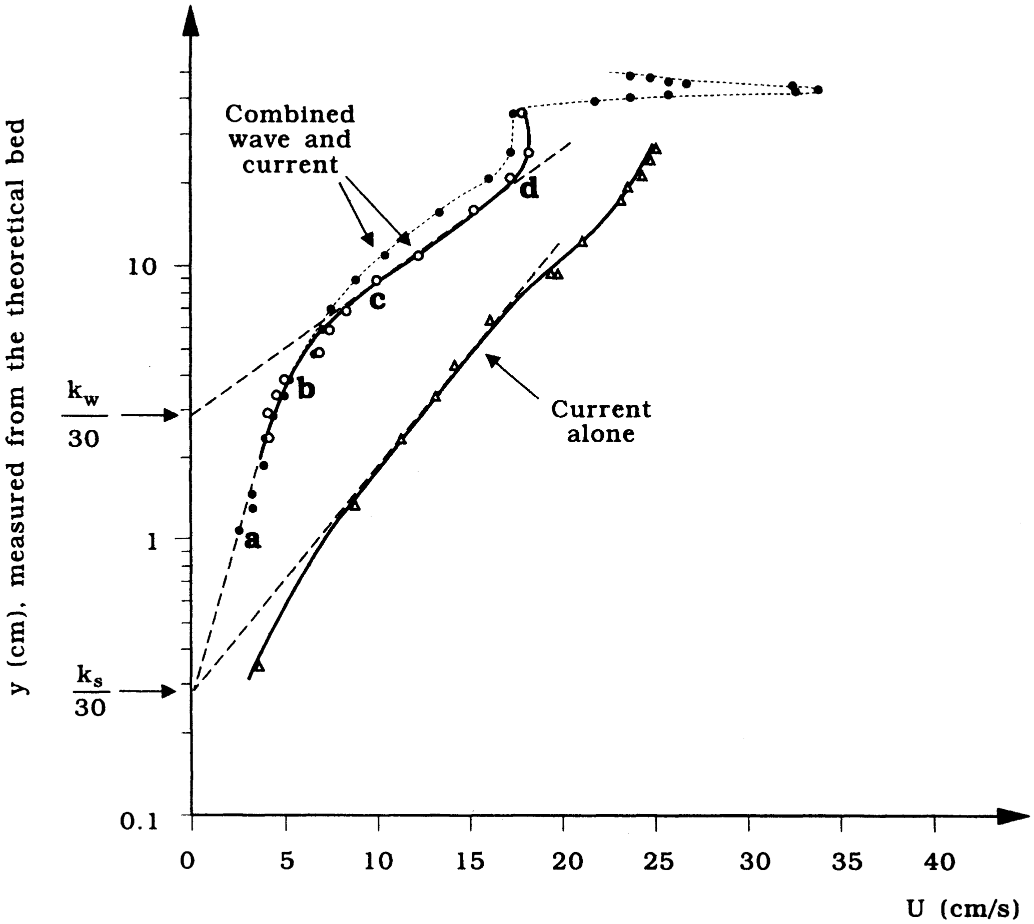

Figure 3.1.3 *Velocity profiles in current-alone and combined current-waves conditions (k_s= physical roughness; k_w= apparent roughness); Fredsøe et al. (1999)*

The k_s-values derived from data in a wave-current basin are substantially smaller (factor 3 to 5) those measured in a wave-current flume. It seems that the width-depth ratio of the flow system (about 1.5 to 2 for the flume and about 10 for the basin) has a significant effect on the measured k_s-values. Herein, the values based on flume data have not been used because of the relatively large effect of side wall roughness on the velocity profile.

Summarizing, it is included that the physical current-related bed roughness k_s of the small-scale ripples is approximately equal to the ripple height (Δ_r) or height of the bed irregularities. Thus, $k_{s,c,r} \cong \Delta_r$.

The small-scale ripples may be superimposed on mega-ripples and/or large-scale dunes at specific locations. The physical bed roughness of these mega-ripples is of the order of half the mega-ripple height ($k_{s,c,mr} \cong 0.5\Delta_{mr}$). The physical bed roughness of large-scale dunes similarly is of the order of half the dune height ($k_{s,c,d} \cong 0.5\Delta_d$). The effective roughness of the (symmetrical) sand waves is approximately zero, because flow separation does not occur. The large-scale sand waves can be seen as topography for the flow system.

Bayram et al. (2003) re-examined the physical bed roughness of a plane bed under both steady flows and oscillatory flows (sand size in the range of 0.13 to 0.7 mm).

The k_s-values are in the range of $2d_{50}$ to $5d_{50}$ with a mean value of about $2.5d_{50}$ for $\theta<1$ (with $\theta=u_*^2/((s-1)gd_{50})$) and in the range of $5d_{50}$ to $100d_{50}$ with a mean value of $15d_{50}$ for $\theta>1$.

Physical wave-related bed roughness ($k_{s,w}$)
The physical wave-related bed roughness can only be determined from experiments in waves flumes and wave tunnels by measuring instantaneous velocity profiles within the wave cycle (intra-wave measurements of velocity) or by measuring the attenuation of wave height over a long stretch (distance). Generally, these experiments concern the oscillatory flow over a rigid bed (artificial ripples).

Detailed field experiments of oscillatory flow over a rippled bed (natural movable ripples) with high-resolution velocity profiles (spatial and temporal) in the wave boundary layer are not yet available. **Sayao (1982)** found $k_{s,w,r}\cong 3\Delta_r$ based on the wave tunnel data set of **Carstens et al. (1969)** for conditions with orbital excursions much larger than the ripple length (vortex ripple range).

Hitching and Lewis (1999) performed experiments in a wave flume with artificial polystyrene ripples (height of 0.0103 m and length of 0.065 m) having a parabolic shape. The ripple surface was roughened by dusting with grains of 0.21 mm sand (after painting). A two-component LDV was used to measure instantaneous velocity profiles along 12 profiles between ripple crest and trough. Analysis of the measured velocity profiles within the boundary layer (logarithmic portion of the profile) shows $k_{s,w}$ values of about 3 times the ripple height. Thus, $k_{s,w,r} \cong 3\Delta_r$.

Bayram et al. (2003) re-examined the physical bed roughness of a plane bed under both steady flow and oscillatory flow (sand size in the range of 0.13 to 0.7 mm).
The k_s-values are in the range of $2d_{50}$ to $5d_{50}$ with a mean value of about $2.5d_{50}$ in the lower regime with $\theta<1$ ($\theta=u_*^2/((s-1)gd_{50})$) and in the range of $5d_{50}$ to $100d_{50}$ with a mean value of about $20d_{50}$ in the upper regime with $\theta>1$.

Field data are scarce, but the wave attenuation data over an offshore reef near Australia **(Nelson, 1996)** can be used to estimate the hydraulic roughness of the bed surface. The experimental data were collected from John Brewer Reef, located inside the line of the Barrier Reef approximately 70 km north east of Townsville, Australia. The reef is elliptical in shape (6 km by 3 km) with a major axis approximately normal to the prevailing south-easterly winds. High water depths (spring tide) over the reef platform seldom exceed 3 m. Wave heights were measured simultaneously at two stations (H_1 and H_4) at a distance of 141 m. Assuming that all wave energy dissipation between the two stations is due to bed friction only, the friction coefficients can be computed from the wave attenuation function using the measured wave heights. The wave heights differences were in the range of 0.05 to 0.1 m; the wave heights measured at the most upwave station (H_1) were in the range of 0.34 and 0.63 m. The hydraulic roughness was computed from: $f_w=\exp(5.21(k_{s,w}/A_w)^{0.194}- 6)$ resulting in values of $k_{s,w}$= 0.06 to 0.07 m for the reef top surface. Nelson compared these values with those of movable bed experiments and found that a movable bed of 0.6 mm sand produces approximately the same roughness due to the presence of small-scale bed forms (ripples).

Apparent bed roughness (k_a)

The apparent roughness (k_a) is much larger than the physical roughness (k_s) depending on the relative strength of the peak orbital velocity (U_w) and the depth-averaged current velocity (u_c) and the angle between the wave direction and the current direction. Based on analysis of laboratory data (sand ripples in movable-bed experiments) in a wave-current basin (**Van Rijn, 1993**) has proposed the following empirical expression:

$$\frac{k_a}{k_{s,c}} = \exp\left(\frac{\gamma U_w}{u_c}\right) \; and \left(\frac{k_a}{k_{s,c}}\right)_{MAX} = 10 \tag{3.1.4}$$

with: $\gamma=0.8+\varphi-0.3\varphi^2$ and φ= angle between wave direction and current direction (in radians between 0 and π; $0.5\pi= 90^o$, $\pi= 180^o$). Characteristic γ-values are γ=0.8 for 0, γ=1 for $\pi= 180^o$ and γ=1.63 for $0.5\pi= 90^o$. The γ-value is maximum γ=1.63 for $\varphi= 0.5\pi= 90^o$.

Fredsøe et al. (1999) have summarized the k_a–values for artificial ripples in laboratory flumes and basins (9 data sets). Most values of the k_a/k_s-ratio are in the range 1 and 15 depending on the relative strength of the wave and current motion, the wave height and the wave direction. Eq. (3.1.4) was applied by Fredsøe et al. to their experimental values with good results. These authors also presented an expression for the friction coefficient (f_{cw}) in combined waves and currents based on numerical results of a detailed hydrodynamic model, as follows:

$$f_{cw} = f_c\left(1+0.68\left(\frac{U_w}{u_c}\right)^{0.88}\right) \tag{3.1.5}$$

with: f_c= friction coefficient in current alone; f_{cw} approaches f_c for U_w approaching 0.

Garcez Faria et al. (1998) have analysed a large data set from the Duck94 experiment (USA). Velocity profiles of the longshore current were measured in the surf zone of the Duck beach site (sand of 0.15 to 0.2 mm). Water depths are in the range of 1.5 to 4 m; depth-mean current velocities are in the range of 0.2 to 1 m/s, significant wave heights are in the range of 0.8 to 1.8 m. Bed irregularities (k_r) were measured with a 1MHz sonic altimeter mounted on the CRAB (11 m high, motorized, three wheel vehicle) at 70 cm from the bed and presented as rms-values in the range of 0.0005 and 0.11 m. The k_a-values were determined from the z-intercept ($z_a=k_a/30$) of the linear regression on a semilog-plot of z versus velocity u(z), resulting in k_a-values in the range of 0.001 to 2 m. Based on a data set of 19 values, the ratio k_a/k_r varies in the range of 0.3 and 50, with a mean value of about 11. The ratio of U_w and u_c varies in the range of 0.9 to 5.4, with a mean value of 1.9. Thus, $k_a/k_r\cong11$ for $U_w/u_c\cong1.9$ and $\varphi\cong90^o$. The data do not show a clear correlation between k_a/k_r and U_w/u_c. Eq. (3.1.4) yields a value of 10 for these conditions.
The friction coefficient f_{cw} was determined from the known values of $u_{*,cw}$ and u_c ($u_{*,cw}$ based on regression analysis of velocity profiles). The results can be represented by:

$$f_{cw} = 0.9\left(\frac{k_a}{h}\right)^{0.36} \tag{3.1.6}$$

Houwman and Van Rijn (1999) have shown that the apparent roughness is almost constant (see dotted curve in Figure 3.1.4) over a wide range of peak orbital velocities (0.3 to 1.5 m/s). This behaviour is caused by the strong decrease of the physical bed roughness for increasing orbital velocity due to the disappearance of the bed ripples (ripples are washed at relatively high orbital velocities in the sheet flow regime), while the amplification effect (ratio k_a/k_p) strongly increases for increasing orbital velocities. A constant apparent bed roughness of 0.1 m was found to give the best agreement between all measured and predicted current velocities (0.3 to 0.5 m/s at 1.2 m above the bed) at two sites (water depths of 5 to 10 m, sand of 0.2 mm; orbital velocities up to 0.6 m/s) near the island of Terschelling in the Dutch sector of the North Sea.

Finally, the results of **You (1995)** are discussed. He re-examined most of the available flume data and found that the increase of the current bottom shear stress in the presence of waves is linearly proportional to the near-bed wave orbital velocity amplitude (U_w) and is practically independent of the relative bed roughness (k_s/A_w) and the angle between the wave direction and the current direction. He proposes to use (see also **You and Nielsen, 1996**):

$$k_a = k_{s,c}\left(1 + \frac{U_w}{u_c}\right) \tag{3.1.7}$$

$$u_{*,cw} = u_{*,c} + 0.026U_w \tag{3.1.8}$$

with: $u_{*,c}$= current-related bed-shear velocity, U_w=ωA_w=$2\pi A_w/T_p$= peak orbital velocity, A_w= peak orbital excursion near the bed, T_p= peak wave period.

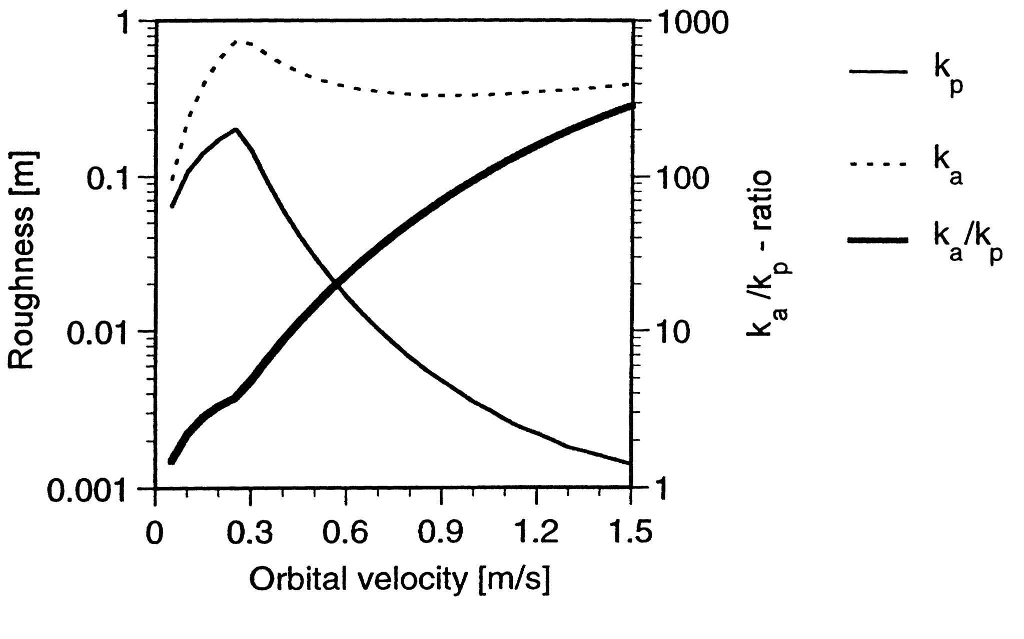

Figure 3.1.4 *Apparent roughness (k_a) and physical bed roughness (k_p=k_s) as function of peak orbital velocity; constant current velocity*

3.1.6 Derivation of bed roughness predictor

Physical current-related roughness of movable bed $k_{s,c}$

It is assumed that the physical bed roughness of movable ripples (SWR) in natural conditions is approximately equal to the ripple height: $k_{s,c}$=Δ_r. Furthermore, it is assumed that ripples (SWR) are fully developed with a height equal to Δ_r=150d_{50} for $\psi \leq 50$ in the lower wave-current regime and that the ripples (SWR) disappear with Δ_r=0 for $\psi \geq 250$ (see

Section 3.1.2) in the upper wave-current regime (sheet flow conditions). In the former case the bed roughness is fully determined by form roughness, while in the latter case the physical roughness is fully determined by the moving grains in the sheet flow layer. LWR may be present in the upper regime, but the form roughness of LWR is assumed to be zero (no vortex generation). In line with this, it is proposed that the physical current-related roughness of small-scale ripples is given by:

$$\begin{aligned}
k_{s,c,r} &= 150 d_{50} && for\,\psi \le 250 \text{ (lower wave-current regime, SWR ripples)} \\
k_{s,c,r} &= 20 d_{50} && for\,\psi \ge 250 \text{ (upper wave-current regime, sheet flow)} \\
k_{s,c,r} &= \left(182.5 - 0.65\psi\right) d_{50} && for\; 50 < \psi < 250 \text{ (linear approach in transitional regime)}
\end{aligned} \tag{3.1.9}$$

with: ψ= mobility parameter=$U_{wc}^2/((s-1)gd_{50}))$, $(U_{wc})^2= (U_w)^2+ u_c^2+2(U_w)\,(u_c)\,|\cos\varphi|$

U_w= peak orbital velocity near bed= $\pi H_s/(T_r \sinh(2kh))$, u_c= depth-averaged current velocity, φ= angle between wave and current motion, H_s= significant wave height, $k=2\pi/L$, L= wave length derived from $(L/T_p \pm u_c)^2=gL\tanh(2\pi h/L)/(2\pi)$,

$T_r= T_p/((1-(u_cT_p/L)\cos\varphi)$= relative wave period, T_p= peak wave period, h= water depth.

Eq. (3.1.9) includes the grain roughness and is assumed to be valid for relatively fine sand with d_{50} in the range of 0.1 to 0.5 mm. An estimate of the bed roughness for coarse particles (d_{50}>0.5 mm) can be obtained by using Eq. (3.1.9) for d_{50}=0.5 mm. Thus, d_{50}=0.5 mm for $d_{50}\ge$0.5 mm resulting in a maximum bed roughness height of 0.075 m (upper limit). The lower limit will be $k_{s,c}=20d_{50}$= 0.002 m for sand with $d_{50}\le$0.1 mm.

Finally, it is remarked that (besides SWR) often mega-ripples and/or dunes are present on the seabed (if h=water depth>1 m and u_c=depth-averaged velocity>0.3 m/s). The physical bed form roughness ($k_{s,c,mr}$) of the mega-ripples and dunes is roughly of the order of half the mega-ripple height and can be expressed as (grain roughness is neglected; only form roughness):

$$\begin{aligned}
k_{s,cmr} &= 0.0002\psi h && and\; 0 \le \psi \le 50 && and\; h > 1 \; and\; u_c > 0.3 \\
k_{s,cmr} &= \left(0.0125 - 0.00005\psi\right) h && and\; 50 < \psi < 250 && and\; h > 1 \; and\; u_c > 0.3 \\
k_{s,cmr} &= 0 && and\; \psi \ge 250 && and\; h > 1 \; and\; u_c > 0.3
\end{aligned} \tag{3.1.10}$$

for mega-ripples and

$$\begin{aligned}
k_{s,c,d} &= 0.0004\psi h && and\; 0 \le \psi \le 100 && and\; h > 1 && and\; u_c > 0.3 \\
k_{s,c,d} &= \left(0.05 - 0.0001\psi\right) h && and\; 100 < \psi < 500 && and\; h > 1 && and\; u_c > 0.3 \\
k_{s,c,d} &= 0 && and\; \psi \ge 500 && and\; h > 1 && and\; u_c > 0.3
\end{aligned} \tag{3.1.11}$$

for dunes.

Eq. (3.1.10) yields: $k_{s,c,mr}$=0 for ψ=0, $k_{s,c,mr}$=0.01h for ψ=50 and $k_{s,c,mr}$=0 for ψ=250. Hence, the maximum value is $k_{s,c,mr}$=0.01h.

Eq. (3.1.11) yields: $k_{s,c,d}$=0 for ψ=0, $k_{s,c,d}$=0.04h for ψ=100 and $k_{s,c,d}$=0 for ψ=500. Hence, the maximum value is $k_{s,c,d}$=0.04 h.

When mega-ripples and/or dunes are present, these values should be added to the physical bed roughness of the small-scale ripples by quadratic summation, see Eq. (3.1.12).

The total physical current-related roughness ($k_{s,c}$) is:

$$k_{s,c} = \left(k_{s,c,r}{}^2 + k_{s,c,mr}{}^2 + k_{s,c,d}{}^2\right)^{0.5} \tag{3.1.12}$$

The current-related friction coefficient (based on the Darcy-Weisbach approach: $f=8g/C^2$) can be computed as:

$$f_c = \frac{8g}{\left(18\log\left(\frac{12h}{k_{s,c}}\right)\right)^2} = \frac{0.24}{\left(\log\left(\frac{12h}{k_{s,c}}\right)\right)^2} \tag{3.1.13}$$

Figure 3.1.5 shows the current-related ripple roughness ($k_{s,c,r}$) and the wave-related ripple roughness ($k_{s,w,r}$) as a function of the mobility parameter (ψ). The values range from 0.015 and 0.075 m for ψ<50 and from 0.002 m to 0.01 m for ψ>250; linear interpolation for intermediate values.

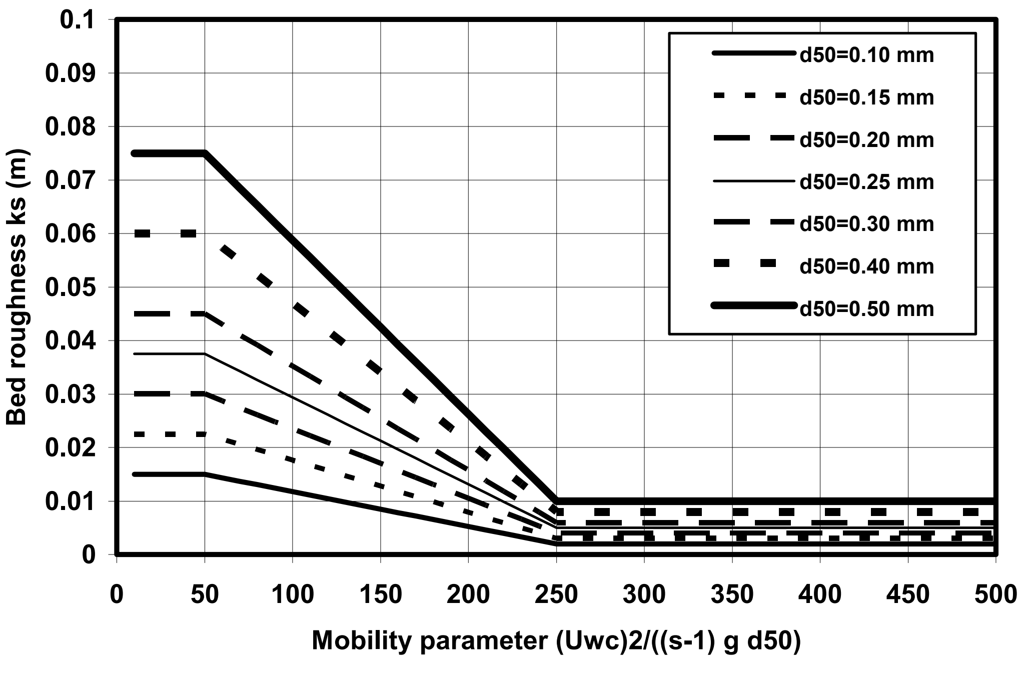

Figure 3.1.5 *Current-related ($k_{s,c,r}$) and wave-related ripple ($k_{s,w,r}$) roughness as function of mobility parameter for sand in the range of 0.1 to 0.5 mm*

Physical wave-related roughness of movable bed $k_{s,w}$

As regards the physical wave-related bed roughness, only bed forms (ripples) with a length scale of the order of the wave orbital diameter near the bed are relevant. Bed forms (mega-ripples, ridges, sand waves) with a length scale much larger than the orbital diameter do not contribute to the wave-related roughness. It is assumed that the physical wave-related roughness of movable small-scale ripples (SWR) in natural conditions is approximately equal to the ripple height: $k_{s,w}=\Delta_r$. Furthermore, it is assumed that ripples (SWR) are fully developed with a height equal to $\Delta_r=150d_{50}$ for $\psi\leq 50$ in the lower wave-current regime and that the ripples (SWR) disappear with $\Delta_r=0$ for $\psi\geq 250$ (see Section 3.1.2) in the upper wave-current regime (sheet flow conditions). In the former case the bed roughness is fully determined by form roughness, while in the latter case the physical roughness is fully determined by the moving grains in the sheet flow layer. LWR may be present in the upper regime, but the form roughness of LWR is assumed to be zero (no vortex generation).

In line with this, it is proposed that the physical wave-related roughness of small-scale ripples is given by:

$$\begin{aligned} k_{s,w,r} &= 150 d_{50} \quad && for\,\psi \leq 250 \text{ (lower wave-current regime, SWR ripples)} \\ k_{s,w,r} &= 20 d_{50} \quad && for\,\psi \geq 250 \text{ (upper wave-current regime, sheet flow)} \\ k_{s,w,r} &= \left(182.5 - 0.65\psi\right) d_{50} && for\, 50 < \psi < 250 \text{ (linear approach in transitional regime)} \end{aligned} \tag{3.1.14}$$

with: ψ= mobility parameter=$U_{wc}^2/((s-1)g\ d_{50})$), $(U_{wc})^2= (U_w)^2+ u_c^2+2(U_w)\ (u_c)\ |\cos\varphi|$ U_w= peak orbital velocity near bed= $\pi H_s/(T_r\sinh(2kh))$, u_c= depth-averaged current velocity, φ= angle between wave and current motion, H_s= significant wave height, $k=2\pi/L$, L= wave length derived from $(L/T_p\pm u_c)^2=gL\tanh(2\pi h/L)/(2\pi)$,
$T_r= T_p/((1-(u_cT_p/L)\cos\varphi)$= relative wave period, T_p= peak wave period, h= water depth.

Eq. (3.1.14) includes grain roughness and is assumed to be valid for relatively fine sand with d_{50} in the range of 0.1 to 0.5 mm (see Figure 3.1.5). An estimate of the bed roughness for coarse particles (d_{50}>0.5 mm) can be obtained by using Eq. (3.1.14) for d_{50}=0.5 mm. Thus, d_{50}=0.5 mm for $d_{50}\geq$0.5 mm resulting in a maximum bed roughness height of 0.075 m (upper limit). The lower limit will be $k_{s,w}=20d_{50}$= 0.002 m for sand with $d_{50}\leq$0.1 mm.

The wave-related friction coefficient can be computed as:

$$f_w = \exp\left(5.2\left(\frac{A_w}{k_{s,w}}\right)^{-0.19} - 6\right) \tag{3.1.15}$$

Apparent bed roughness for flow over a movable bed
It is proposed to use the existing expression (see Eq. (3.1.4)):

$$\frac{k_a}{k_{s,c}} = \exp\left(\frac{\gamma U_w}{u_c}\right) and \left(\frac{k_a}{k_{s,c}}\right)_{MAX} = 10 \tag{3.1.16}$$

with: $\gamma=0.8+\varphi-0.3\varphi^2$ and φ= angle between wave direction and current direction (in radians between 0 and π; $0.5\pi= 90^o$, $\pi= 180^o$). Characteristic γ-values are γ=0.8 for 0, γ=1 for $\pi= 180^o$ and γ=1.63 for $0.5\pi= 90^o$. The γ-value is maximum γ=1.63 for $\varphi= 0.5\pi= 90^o$.

Eq. (3.1.16) should only be applied to the small-scale ripples (SWR). The mega-ripples and/or dunes should be excluded.

The current-related apparent friction coefficient (based on the Darcy-Weisbach approach: *f=8g/C*) can be computed as:

$$f_{c,a} = \frac{8g}{\left(18\log\left(\frac{12h}{k_a}\right)\right)^2} = \frac{0.24}{\left(\log\left(\frac{12h}{k_a}\right)\right)^2} \tag{3.1.17}$$

3.2 Verification of bed-load transport

3.2.1 Approach and formulations

Various field data sets from the literature and new data sets (laboratory and field) collected within the SANDPIT project have been used to verify/improve the bed-load transport formulations of the TRANSPOR2000 model. The median particle size for all data sets is in the range of 0.2 to 0.5 mm. The following data sets have been used:

Existing data of bed load transport in tidal flow (no waves):
- Puget Sound, Washington, USA (1964),
- Salmon Bank, Washington, USA (1968),
- ridge south of IJ-channel, North Sea, Netherlands (1994),

Existing data of bed load transport in coastal conditions:
- Skerries Bank, Start Bay, UK (1979),
- Sable Island Bank, Scotian Shelf, Canada (1999),
- Spratt Sand, Teignmouth, UK (2001).

New data of bed load transport (collected within SANDPIT Project):
- wave tunnel experiments of Delft Hydraulics,
- Noordwijk site, North Sea, Netherlands.

Bed load transport model
The net bed-load transport rate in conditions with uniform bed material is obtained by time-averaging (over the wave period T) of the instantaneous transport rate using the bed-load transport model (quasi-steady approach), as follows:

$$q_b = \left(\frac{1}{T}\right)\int q_{b,t}\,dt \tag{3.2.1}$$

with $q_{b,t}$ = F(instantaneous hydrodynamic and sediment transport parameters).

The formula applied, reads as:

$$q_b = 0.5\rho_s d_{50} D_*^{-0.3} \left(\frac{\tau'_{b,cw}}{\rho}\right)^{0.5} \left(\frac{\tau'_{b,cw} - \tau_{b,cr}}{\tau_{b,cr}}\right) \tag{3.2.2}$$

in which:

$\tau'_{b,cw}$ = nstantaneous grain-related bed-shear stress due to both current and wave motion = 0.5 ρ $f'_{cw}\,(U_{\delta,cw})^2$,

$U_{\delta,cw}$ = instantaneous velocity due to current and wave motion at edge of wave boundary layer,

f'_{cw} = grain friction coefficient due to current and wave motion= $\alpha\beta f'_c + (1-\alpha) f'_w$,

f'_c = current-related grain friction coefficient =$0.24(\log(12h/k_{s,grain}))^{-2}$,

f'_w = wave-related grain friction coefficient=$\mathrm{Exp}[-6+5.2(A_{\delta,w}/k_{s,grain})^{-0.19}]$,

α = coefficient related to relative strength of wave and current motion: $\alpha = \dfrac{\hat{U}_{\delta,cw}}{u_c}$,

$\hat{U}_{\delta,cw}$ = the peak orbital velocity, u_c is the depth averaged current,

β = coefficient related to vertical structure of velocity profile,

$A_{\delta,w}$ = peak orbital excursion,

$\tau_{b,cr}$ = critical bed-shear stress according to Shields,

ρ_s = sediment density,

ρ = fluid density,

d_{50} = particle size,

D_* = dimensionless particle size.

Eq. (3.2.2) is based on the assumption that the sediment particles respond instantaneously (quasi-steady) to the oscillatory fluid motion near the bed. The net transport rate will always be in the direction of the largest peak orbital velocity. This assumption is reasonably valid for the sheet flow regime with sediment particles larger than about 0.2 mm (**Dohmen-Janssen, 1999**). According to **Dohmen-Janssen (1999)**, phase-lag effects will occur for sediments smaller than 0.2 mm. These phase lags can be very well represented by the parameter $p=\delta_s\omega/w_s$ with δ_s= thickness of sheet flow layer (order of 0.01 m), $\omega=2\pi/T$=angular frequency, w_s= sediment fall velocity, T= wave period. Phase-lag effects (p>0.25) are important for fine sediment, large peak orbital velocities and small wave periods. **Dohmen-Janssen (1999)** proposed to correct the bed-load transport rates based on quasi-steady expressions, using a correction factor dependent on the p-parameter. Thus:

$$q_{b,net} = r q_{b,net,steady} \tag{3.2.3}$$

with r=F(p)=correction factor between 0 and 1 (r= 1, 0.8, 0.6 and 0.4 for p=0, 0.5, 1 and 10), $q_{b,net,\,steady}$=net bed-load transport according to quasi-steady expression (for example Eq. (3.2.2)). Using this approach, the net bed-load transport rate will be reduced but the net transport rate can not be reversed into the direction of the smallest peak velocity. Herein, phase lag effects have been neglected.

The two most influential parameters of Eq. (3.2.2) are:

$$f'_{cw} = \alpha\beta f'_c + (1-\alpha) f'_w \tag{3.2.4}$$

$$k_{s,grain} = \alpha_{grain} d_{50} \tag{3.2.5}$$

The grain roughness generally varies in the range of 1d_{90} to 3d_{90} (α_{grain} in the range of 1-3) for conditions with d_{50}<0.5 mm (**Van Rijn, 1993**). Up to now $k_{s,grain}$=3d_{90} has been used in most studies. In this study both values have been used to evaluate what is the best approach.

Koelewijn (1994) has shown that Eq. (3.2.4) yields relatively large bed-shear stress values compared with the results of the parameterization method of Soulsby/Ockenden (see Figure 3.2.1). This latter method is based on parameterized results of detailed mathematical models and is therefore assumed to give the most accurate values. According to Koelewijn, more accurate results can be obtained by using:

$$f_{cw}^{'} = \alpha^{0.5} \beta f_{c}^{'} + \left(1 - \alpha^{0.5}\right) f_{w}^{'} \tag{3.2.6}$$

Both Eq. (3.2.4) referred to as 'f_{cw}-original' and Eq. (3.2.6) referred to as 'f_{cw}-modified' have been used in this study to compute the bed-load transport. In all computations the wave-induced streaming in the near-bed region was neglected. This effects of this latter parameter is studied in Section 3.4

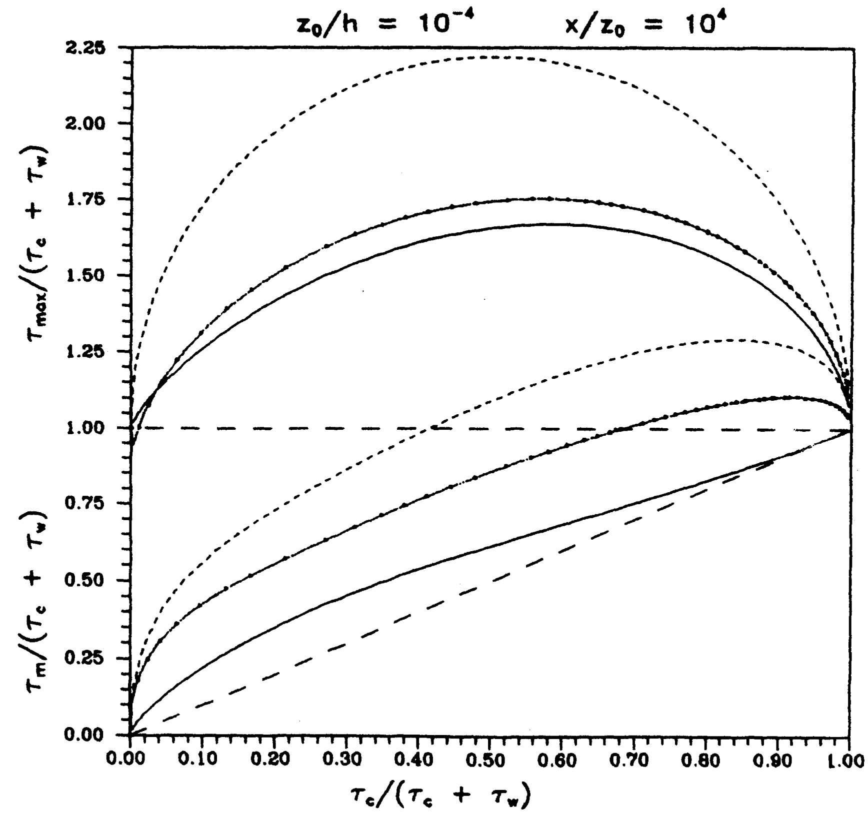

Figure 3.2.1 *Bed-shear stresses for currents and waves*
--------based on Eq. (3.2.4)
_____ based on friction factor of Soulsby/Ockenden
-.-.-.-. based on Eq. (3.2.6)

3.2.2 Bed load transport in tidal flow: Puget Sound, Washington, USA, 1964

During November 1964 a series of measurements was made of sediment transport in a tidal channel within the Puget Sound, Washington (**Sternberg, 1967**). These data consisted of direct observations of the sea bed (using underwater television and stereo cameras). Data were collected with an instrumented tripod. The tidal channel depth was about 23 m. The maximum tidal range was about 4 m. Bottom ripples were present (mean height of 0.015 to 0.024 m, mean length of 0.16 m) in a semiregular pattern with crests oriented in a cross-channel direction. The bed was composed primarily of sand-sized particles which had a mean diameter of 0.43 mm. Coarse shell fragments were present in the ripple troughs. Ripple migration rates were determined yielding a mean value of about 1 cm per 5 min over a period of 40 minutes (12 cm per hour). The observed current velocity during this period was about 0.4 m/s at about 1 m above the bed. The depth-mean current velocity was about 0.48 m/s. Using a ripple height of 0.02 m and q_b= 0.6 ρ_s (1-p) Δ_r C_r (with p= porosity= 0.4, Δ_r = ripple height= 0.02 m, C_r = ripple migration velocity= 0.12 m/hr), the bed load transport is found to be about q_b=0.00065 kg/s/m (±50%).

Measured depth-averaged velocity (m/s)	**Measured bed-load transport (kg/m/s)**	**Computed Bed-load transport (kg/s/m)**	
		$k_{s,grain}$= 1d_{90}	$k_{s,grain}$= 3d_{90}
0.48	0.00065	0.00021	0.0012

Table 3.2.1 *Measured and computed bed-load transport rates, Puget Sound, USA; d_{50}=0.43 mm*

The bed-load transport model of TRANSPOR2000 was used to estimate the bed-load transport, using h= 23 m, v_{mean}= 0.48 m/s, d_{50}= 0.43 mm, d_{90}= 0.86 mm, $k_{s,c}$= 0.03 m, temperature= 15 ^{o}C and salinity= 30 promille. The computed bed-load transport rates for $k_{s,grain}$= 1d_{90} and 3d_{90} are presented in Table 3.2.1. As can be observed, the grain roughness has a rather large effect on the computed transport rate. The computed bed-load transport is too small (factor 3) for $k_{s,grain}$=1d_{90} and too large (factor 2) for $k_{s,grain}$=3d_{90}. The computed suspended transport was much smaller than the computed bed-load transport confirming that bed load transport was dominant at this field site.

3.2.3 Bed load transport in tidal flow: Salmon bank, Washington, USA, 1968

On July 11, 1968 a series of measurements was made of sediment transport on a tidal bank at the southern end of San Juan Island, Washington (**Kachel and Sternberg, 1971**). These data consisted of direct observations of the sea bed (using stereo cameras). Data were collected with an instrumented tripod. The local depth was about 31 m. Bottom ripples were present with mean height of 0.01 to 0.05 m and mean length of 0.1 to 0.5 m. The bed was composed primarily of sand-sized particles which had a mean diameter of d_{50}=0.37 mm.

Coarse shell fragments were present in the ripple troughs. Ripple migration rates were determined from the measured ripple displacements over time. The bed-load transport was derived from the ripple heights and the ripple migration velocities. Two cases have been taken from the data set:

- measured velocity of about 0.5 m/s at 1 m above bed; depth-mean velocity of 0.65 m/s; $q_{b,measured}$= 0.005 kg/s/m (±50%);
- measured velocity of about 0.6 m/s at 1 m above bed; depth-mean velocity of 0.78 m/s; $q_{b,measured}$= 0.01 kg/s/m (±50%).

The bed-load transport model of TRANSPOR2000 was used to estimate the bed-load transport, using h= 31 m, d_{50}= 0.37 mm, d_{90}= 0.74 mm, $k_{s,c}$= 0.03 m, temperature= 15 ^oC and salinity= 30 promille. The computed values are presented in Table 3.2.2 for two values of the grain roughness of the bed. The best agreement is obtained for a grain roughness equal to $k_{s,grain}$=1 d_{90}. The computed suspended transport was much smaller than the computed bed-load transport confirming that bed-load transport was dominant at this field site.

Measured depth-averaged velocity (m/s)	**Measured bed-load transport (kg/m/s)**	**Computed Bed-load transport (kg/s/m)**	
		$k_{s,grain}$= 1d_{90}	$k_{s,grain}$= 3d_{90}
0.65	0.005 (±0.0025)	0.0045	0.007
0.78	0.01 (±0.005)	0.011	0.015

Table 3.2.2 *Measured and computed bed-load transport rates, Salmon bank, USA; d_{50}=0.37 mm*

3.2.4 Bed-load transport in tidal flow: ridge south of IJ-channel, North Sea (1994)

Van de Meene (1994) performed bed-load transport measurements using a mechanical bed-load transport instrument during spring tidal conditions at a ridge location south of the IJ-channel (approach channel to harbour of IJmuiden and Amsterdam), on 14 and 15 August 1990. The water depth varied between 13 and 15 m with a spring tidal range of 2 m. The maximum bottom currents (at 0.45 m above the bed) were around 0.45 m/s. The depth-averaged velocity was about 0.8 m/s. The weather was fair; the significant wave height varied between 0.3 and 0.8 m. The small-scale bed forms consisted of mini-ripples (length of 0. 2 m and height of 0.03 m) superimposed on mega-ripples with an average length of 10 m and an average height of 0.2 to 0.3 m. The bed material was sand with d_{50}= 0.28 mm and d_{90}= 0.33 mm. The measured bed-load transport rates (clustered in three groups) are given in Table 3.2.3.

Measured depth-averaged velocity (m/s)	**Measured bed-load transport (kg/m/s)**	**Computed Bed-load transport (kg/s/m)**	
		$k_{s,grain}$= 1d_{90}	$k_{s,grain}$= 3d_{90}
0.35	0.0003 (±0.0003)	0	0
0.48	0.0008 (±0.0004)	0.0005	0.0012
0.60	0.0028 (±0.0015)	0.003	0.0048

Table 3.2.3 *Measured and computed bed-load transport rates, North Sea; d_{50}=0.28 mm*

The bed-load transport model of TRANSPOR2000 was used to estimate the bed-load transport, using h= 14 m, d_{50}= 0.28 mm, d_{90}= 0.33 mm, $k_{s,c}$= 0.03 m, temperature= 15 ^oC and salinity= 30 promille. Two values of the grain roughness were used: $k_{s,grain}$=1d_{90} and $k_{s,grain}$=3d_{90}. The best agreement of measured and computed values is obtained for $k_{s,grain}$=1d_{90} (see Table 3.2.3).

3.2.5 Bed-load transport in coastal conditions (steady and oscillatory flow): Skerries bank, Start Bay, UK, 1979

During several tidal cycles in September (5 to 13 September, 1979), a series of measurements was made of sediment transport on top of the Skerries bank in Start Bay, UK (**Langhorne, 1981**). These data consisted of direct observations of sand wave migration (height of 3.5 m and length of 180 m) at the sea bed. The local depth was about 10 m. In order to measure the erosion and deposition volumes at the sand wave crest, a line of reference stakes was hammered into the seabed at 0.5 m intervals (total length covered was about 12 m). Measurements of bed levels were taken over a period of a few hours within the tidal cycle using divers. Flow measurements were taken at the sand wave crest using a vertical array of four bottom-mounted velocity sensors. Based on analysis of the velocity data, the equivalent bed roughness of Nikuradse was found to be about k_s= 0.18 m. A wave rider buoy was used to measure the local wave heights, yielding a significant wave height of about 0.4 to 0.8 m and a period of 5 to 7 s. The bed was composed primarily of sand-sized particles which had a mean diameter of 0.32 mm. The sand transport rates were derived from the observed erosion and deposition volumes.

Two cases have been taken from the data set:
- measured velocity of about 0.5 m/s at 1 m above bed; depth-mean velocity of 0.6 m/s; $q_{measured}$=0.025 kg/s/m (±50%);
- measured velocity of about 0.6 m/s at 1 m above bed; depth-mean velocity of 0.7 m/s; $q_{measured}$=0.06 kg/s/m (±50%).

The precise mode of transport is not quite clear, as both the bed load and suspended load transport will contribute to the sand wave migration.

The TRANSPOR2000 model was used to estimate both the bed-load and suspended load transport, using h= 10 m, H_s= 0.6 m, T_p=6 s and wave-current angle= 90 ^{o}, d_{50}= 0.32 mm,

d_{90}= 0.64 mm, d_s=d_{50}= 0.32 mm, $k_{s,c}$=$k_{s,w}$= 0.03 m, temperature= 15 °C and salinity= 30 promille. The results are presented in Table 3.2.4. The suspended load transport is of the same order as the bed load transport and most likely occurring in the near-bed region and may therefore not be neglected. The best agreement is obtained for a grain roughness of $k_{s,grain}$=3d_{90}. The measured transport rates are somewhat (factor 1.5 to 2.0) larger than the computed total load transport values. The effect of the modified f_{cw}-friction factor is marginally small (slightly smaller bed-load transport values are obtained).

Measured depth-averaged velocity (m/s)	**Measured transport (kg/m/s)**	**Computed transport (kg/m/s)**		**Computed transport (kg/m/s)**	
		$k_{s,grain}$= 1d_{90} f_{cw}-original	$k_{s,grain}$= 3d_{90} f_{cw}-original	$k_{s,grain}$= 1d_{90} f_{cw}-modified	$k_{s,grain}$= 3d_{90} f_{cw}-modified
0.6	0.025 (±0.0125)	q_b=0.006 q_s=0.0074 q_t=0.0134	0.011 0.009 0.02	0.0055 0.0075 0.013	0.01 0.009 0.019
0.7	0.06 (±0.03)	q_b=0.011 q_s=0.015 q_t=0.026	0.018 0.02 0.038	0.01 0.015 0.025	0.016 0.02 0.036

Table 3.2.4 *Measured and computed transport rates, Skerries bank, Start Bay, UK; d_{50}=0.32 mm*

3.2.6 Bed-load transport in coastal conditions: Sable Island bank, the Scotian Shelf, Canada (1999)

Amos et al. (1999) measured bed state, ripple migration and bed form transport of fine sand with d_{50} of 0.23 mm in 22 m of water on Sable Island bank, Scotian Shelf, Canada. Near-bed wave and steady flows (at about 1 m above the bed) were also recorded during a period of 12 days (see Table 3.2.5). The instrument package was mounted in a free-standing frame. Sand transport occurred under conditions where oscillatory and steady flows were orthogonal. The near-bed current was dominated by semi-diurnal tidal flows reaching up to 0.35 m/s. Two periods (days 182 and 186) of moderate waves with H_s between 1 and 1.5 m (wave period of about 9 s) were present in the measurement records. The latter part of the experiment was relatively wave-free (days 188 to 192). Bed form transport was derived from ripple migration rates and estimated ripple heights. The measured values are shown in Figure 3.2.2. The bed-load transport rates are relatively small just beyond initiation of motion. The bed load transport rate increases strongly (factor 4) with increasing velocities in the range of 0.25 to 0.35 m/s. The bed-load transport increases strongly (factor 2) with increasing wave height from 0.5 to 1 m.

Test code	H_S (m)	T_P (s)	$u_{z=1\ m}$ (m/s)	q_b (kg/s/m)
Day 188-192	0.5	9	0.25	0.00025
Day 188-192	0.5	9	0.3	0.0005
Day 188-192	0.5	9	0.35	0.001
Day 182,186	1 to 1.5	9	0.22	0.00075
Day 182,186	1 to 1.5	9	0.3	0.001

Table 3.2.5 *Bed-form transport in 22 m of water on Sable Island bank, Scotian Shelf, Canada; d_{50}= 0.23 mm*

Measured depth-averaged velocity (m/s) and sign. wave height (m)	Measured transport (kg/m/s)	Computed bed load tr. (kg/m/s)		Computed bed load tr. (kg/m/s)	
		$k_{s,grain}$= 1d_{90} f_{cw}-original	$k_{s,grain}$= 3d_{90} f_{cw}-original	$k_{s,grain}$= 1d_{90} f_{cw}-modified	$k_{s,grain}$= 3d_{90} f_{cw}-modified
u=0.35; H_s=0.5	0.00025	0	0.00016	0	0.00008
u=0.3; H_s=0.5	0.0005	0.00012	0.0008	0.0001	0.00055
u=0.35; H_s=0.5	0.001	0.0009	0.0024	0.0008	0.002
u=0.22; H_s=1	0.00075	0.00025	0.0007	0.00025	0.0006
u=0.3; H_s=1	0.001	0.0008	0.0018	0.0008	0.0016

Table 3.2.6 *Measured and computed bed-load transport rates, Sable Island bank, Scotian Shelf, Canada; d_{50}=0.23 mm*

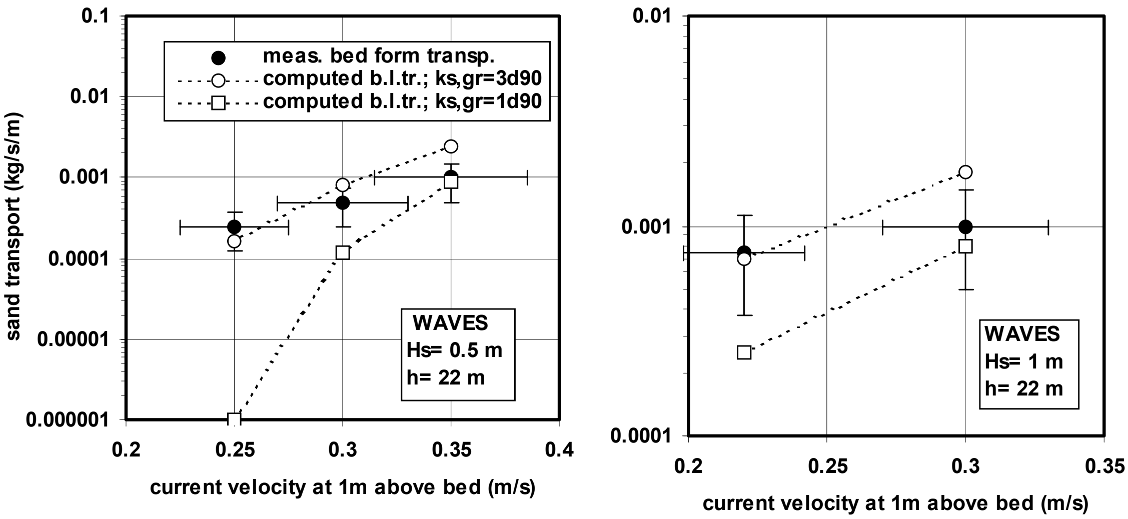

Figure 3.2.2 *Measured and computed bed-load transport rates, Sable Island bank, Scotian Shelf, Canada; d_{50}=0.23 mm and f_{cw}-original*

The bed-load transport model of TRANSPOR2000 has been used to compute bed-load transport rates (Table 3.2.6) for conditions near Sable Island bank, Scotian Shelf, Canada (**Amos et al., 1999**) using measured input data (water depth, current velocity, wave height, wave period, sand size). The depth-averaged current velocity was assumed to be 1.4 $\mathbf{u_{z=1m}}$.

The wave height was assumed to be H_s= 1 m for moderate wave conditions; whereas H_s= 0.5 m was used for wave-free conditions. The bed roughness was assumed to be equal to the ripple height ($k_{s,c}$=$k_{s,w}$=0.03 m) given by Amos et al. (1999). Two values of the grain roughness have been used: $k_{s,grain}$=1d_{90} and $k_{s,grain}$=3d_{90}. Other input data are: d_{50}= 0.23 mm, d_{90}= 0.5 mm, angle current-waves= 90^o, temperature= 10 ^{o}C, salinity= 30 promille. The computed bed-load transport (based on f_{cw}-original) is shown in Figure 3.2.2. Comparison of measured and computed values shows reasonable agreement for $k_{s,grain}$=3d_{90}. The application of a modified f_{cw}-friction factor yields somewhat smaller values.

3.2.7 Bed-load transport in coastal conditions: Spratt Sand, Teignmouth, South-west coast of England (2001)

Hoekstra et al. (2001) measured bed form dimensions, bed form migration and bed form transport of sand with d_{50} of 0.3 mm (d_{90} of about 1 mm) in shallow depth on Spratt Sand near the village of Teignmouth (Coast3D project, Autumn 1999). The tidal range was about 4 to 5 m. The water depths were between 1 and 4 m. Near-bed wave and current conditions (at about 1 m above the bed) were also recorded during the tidal cycle (time-averaged values are given in Table 3.2.7). The instrument package was mounted in a free-standing tripod.

Depth **h** **(m)**	**Sign. wave height** **H_s** **(m)**	**Peak period** **T_p** **(s)**	**Depth-mean velocity** **u** **(m/s)**	**Angle waves and current** **(degrees)**	**Ripple height** **(m)**	**Ripple length** **(m)**	**Meas. b.f.tr.** **q_b** **(kg/s/m)**
1.55 ±0.2	0.3 ±0.05	6 ±0.5	0.55 ±0.05	70 ±10	0.07 ±0.03	0.9 ±0.5	0.022 ±0.011
1.85 ±0.1	0.27 ±0.07	7 ±2	0.55 ±0.1	75 ±25	0.06 ±0.02	0.9 ±0.2	0.018 ±0.009
2.1 ±0.1	0.43 ±0.07	6 ±0.5	0.52 ±0.12	60 ±10	0.055 ±0.025	0.7 ±0.2	0.026 ±0.016
2.4 ±0.1	0.43 ±0.1	5.5 ±1	0.4 ±0.15	100 ±50	0.06 ±0.02	0.9 ±0.3	0.008 ±0.006
2.65 ±0.1	0.4 ±0.15	7 ±2	0.65 ±0.1	45 ±15	0.05 ±0.025	0.95 ±0.2	0.023 ±0.013
3.1 ±0.2	0.55 ±0.15	5.5 ±0.5	0.5 ±0.15	55 ±10	0.055 ±0.025	0.85 ±0.25	0.021 ±0.015

Table 3.2.7 *Bed-form transport in shallow depth on Spratt Sand near Teignmouth, England; d_{50}= 0.3 mm*

The current velocities were measured by an electro-magnetic current meter; the wave heights were derived from pressure sensor measurements. The measured bed-form transport rates were determined from bed form tracking analysis. These latter results were in good agreement with transport rates estimated from ripple migration and ripple height data, using: q_{bf}=0.6 (1-p) ρ_s Δ_r m_r, where q_{bf}= bed form transport, Δ_r= ripple height, m_r= ripple migration velocity, p= porosity factor=0.4. About 75 individual data points were available, which were clustered in 6 depth classes. The original transport rates were given in m^2/s (including pores), which were converted to kg/s/m using a bulk density of 1600 kg/m^3. Data points with roughly the same time-averaged current velocity within each depth class were averaged resulting in 6 cases, see Table 3.2.7. The variation ranges of the parameters are: about 10% for depth, 20% for wave height, 25% for velocity, 25% for bed form dimensions and 50% to 75% for bed form transport. The bed-load transport model of TRANSPOR2000 was used to compute the bed load transport based on the input data of Table 3.2.7. The water temperature was taken as 10 degrees Celsius and salinity as 30 promille. The bed roughness was taken as $k_{s,c}= k_{s,w}= 0.03$ m.

Measured depth-av. velocity (m/s) and sign. wave height (m)	**Measured transport (kg/m/s)**	**Computed bed load tr. (kg/m/s)**		**Computed bed load tr. (kg/m/s)**	
		$k_{s,grain}= 1d_{90}$ f_{cw}-original	$k_{s,grain}= 3d_{90}$ f_{cw}-original	$k_{s,grain}= 1d_{90}$ f_{cw}-modified	$k_{s,grain}= 3d_{90}$ f_{cw}-modified
u=0.55; H_s=0.3	0.022	0.018	0.033	0.016	0.027
u=0.55; H_s=0.27	0.018	0.013	0.024	0.012	0.021
u=0.52; H_s=0.43	0.026	0.024	0.041	0.021	0.034
u=0.40; H_s=0.43	0.008	0.0053	0.011	0.0046	0.0087
u=0.65; H_s=0.4	0.023	0.032	0.055	0.029	0.046
u=0.50; H_s=0.55	0.021	0.022	0.039	0.02	0.032

Table 3.2.8 *Measured and computed bed-load transport rates (d_{50}=0.3 mm), Spratt Sand near Teignmouth, England*

The results are given in Table 3.2.8. Comparison of measured and computed bed load transport rates (bed form transport is assumed to be equal to bed load transport) shows good agreement (within factor 2) for $k_{s,grain}=1d_{90}$. The computed bed load transport rates are significantly larger (factor 1.5 to 2) for $k_{s,grain}=3d_{90}$. The application of a modified f_{cw}-friction factor yields somewhat smaller values (20%).

3.2.8 Bed-load and suspended load transport data from new experiments (within Sandpit-project) in wave tunnel

Experimental set-up Wave tunnel

Experiments have been performed by the University of Twente (**J. van der Werf**) in cooperation with Delft Hydraulics in the large-scale wave tunnel of Delft Hydraulics within the framework of the SANDPIT-Project with the aim to obtain information of the bed form characteristics and sand transport rates under various wave and current conditions as present in the North Sea at a depth in the range of 10 to 20 m. Two types of sand representative for field conditions in the North Sea have been used: relatively fine sand with d_{50} of 0.22 mm (V-series) and relatively coarse sand with d_{50} of 0.35 mm (T- and U-series). All experiments were done in the ripple bed regime as present in deeper water (10 to 20 m). Both regular and irregular wave signals have been used in the coarse sand experiments. Only irregular wave signals have been used in the fine sand experiments. The wave signals in these latter tests were based on data series measured at the Noordwijk field site (SANDPIT measurements; Spring 2003) and on the Egmond field site (COAST3D measurements; Autumn 1998) to simulate field conditions as close as possible. A steady flow between 0.18 and 0.45 m/s (colinear; angle between wave and current direction is zero) was imposed in some tests.
The detailed objectives of the experimental programme were focussed on:

- the ripple bed form characteristics;
- the time-averaged suspended sand concentrations in the ripple regime;
- the net sand transport rates in the ripple regime.

Herein, only the results of tests with irregular wave motion above the fine sand bed of 0.22 mm have been used for verification of the TRANSPOR2000 model. The test results with irregular wave motion above the coarse sand bed of 0.35 mm are also analyzed, but the results have not yet been used for verification. The results are not fully reliable because the bed forms are relatively large and irregular (too large compared with wave tunnel dimensions). The test results with regular wave motion above the coarse sand bed of 0.35 mm have been described by **Van der Werf (2003)**.

Each test was repeated two to three times. The first test was always started from a flat bed, whereas the second and third repetition-tests were started with a rippled bed as obtained at the end of the previous test. Velocity time series (using electro-magnetic sensors) and net transport rates were measured during all tests. ABS-concentrations (Acoustical Back Scatter method) were measured in most tests (see **Van der Werf, 2003**). Time-averaged sand concentrations (based on simultaneous pump samples over about 5 to 10 minutes) were only measured in the second and third repetition-tests. The transport rates were determined from: (1) the sand masses collected in the traps on both sides of the tunnel, (2) the sand mass collected in the settling tank in the return pipe (tests with steady flow only) and (3) bed level soundings (using an optical system) measured before and after each test. Based on these measured quantities and assuming a bed porosity of 0.4, the net sand transport rate along the test section can be calculated. Since the net transport is not uniform along the test section (influence of boundaries, instruments and bed forms), an average is taken over a certain tunnel section length where the gradient of the transport is smallest. A detailed description of the measuring instruments and analysis methods is given by **Van der Werf (2003)**.

Sediment characteristics

The sediment characteristics are presented in Table 3.2.9. The settling velocities were determined from bulk samples; samples at the same level above the bed but from different tests were put together into a bulk sample.

Test No.	Bed material sizes (mm)	Settling velocity of bed material (m/s) at Te= 20 ^oC	Settling velocity of suspended material (m/s) at Te= 20 ^oC
U-series	d_{10}= 0.22 mm d_{50}= 0.35 mm d_{90}= 0.46 mm	w_{10}=0.035 m/s w_{50}=0.056 m/s w_{90}=0.070 m/s	z = 0.01 m 0.03 m 0.065 m 0.10 m a. b. w_{10}=0.030 0.024 0.016 0.014 m/s w_{50}=0.051 0.046 0.033 0.029 m/s w_{90}=0.068 0.064 0.050 0.047 m/s
V-series	d_{10}= 0.15 mm d_{50}= 0.22 mm d_{90}= 0.28 mm	w_{10}=0.018 m/s w_{50}=0.027 m/s w_{90}=0.039 m/s	z= 0.01 m to 0.02 m above bed. w_{10}=0.012 m/s w_{50}=0.023 m/s w_{90}=0.035 m/s

Table 3.2.9 *Sediment characteristics of wave tunnel experiments*

Experimental results

The experimental values (averages and variation ranges over two or three test results) are given in Table 3.2.10. The suspended sand concentrations (pump-data and ABS-data of V-series; pump-data of U-series) are given in Table 3.2.11. Reasonably good agreement can be observed between both data sets. The pump-data of Test V25-wc20 were used to calibrate the ABS-data. The ABS-data of the U-series are reported by **Van der Werf (2003)**.

The bed forms in the V-series (fine sand of 0.22 mm) generally were flat wavy ripples, generated by the oscillatory flow, but also induced by the presence of a scour hole at the upwave end of the tunnel and the presence of instruments in the tunnel. Small-scale sub-ripples with height of 5 mm and length of 100 mm were generated during passage of smaller waves of the spectrum, but these latter sub-ripples were washed out immediately by the larger waves of the spectrum. Vortex motion and flow separation at ripple crests were not observed during the tests of the V-series. Sediment suspension was only observed in a layer with a maximum thickness of about 10 cm; the maximum concentration was about 0.35 kg/m^3 at 0.01 m above the local bed surface. The net transport rates were positive (in the wave and flow direction) in these tests.

The bed forms in the U-series (coarse sand of 0.35 mm) generally were fairly sharp-crested, 2D/3D bed forms and ripples. Relatively strong vortex motion and flow separation at the ripple crests were clearly observed during the tests of the U-series. Sediment suspension was observed in a layer with a maximum thickness of about 0.4 m; the maximum concentration was about 10 kg/m^3 at 0.01 m above the local bed surface. The net transport rates were negative (against the wave and flow direction) in these tests.

Velocity data

Time-averaged velocity data (approx. 0, 0.2 and 0.45 m/s) are based on measurements using standard Electro-Magnetic Sensors (EMS). During test 1 only one EMS was used, roughly positioned at 0.5 m above the bed. During test 2 and test 3, velocity data were obtained using two sensors simultaneously at two different locations. The second EMS was attached to the pump sampling rack (TSS) at 0.3 m above the lowest intake tube. This latter intake tube was placed as close as possible above the bed (0.01 to 0.03 m depending on test conditions). Hence, the second EMS-instrument was at 0.31 to 0.33 m above the bed. The velocity data are given in Table 3.2.12. The irregular velocity time-series measured at about 0.25 m above the local bed surface are represented by the $U_{1/3,on}$ and $U_{1/3,off}$ values, which are defined as the average values of the highest one-third part of the peak orbital velocities in onshore (in forward) and in offshore (in backward) directions after subtraction of the time-averaged velocities. The RMS-velocity of the orbital motion is also given.

Velocity profile information can be obtained from the Thesis of **M. Dohmen-Janssen (1999).** The experimental conditions are as follows: fixed bed; flat bed surfaces of 0.13, 0.21 and 0.32 mm sand were used(see Fig 5.22. page 142 of Thesis).

z= 0.001 m above bed surface	$u/u_{0.1}$=0.35
z=0.0055 m	$u/u_{0.1}$=0.52
z=0.0110 m	$u/u_{0.1}$=0.60
z=0.0330 m	$u/u_{0.1}$=0.75
z=0.0550 m	$u/u_{0.1}$=0.88
z=0.1 m	$u/u_{0.1}$=1.0

with: $u_{0.1}$= time-averaged velocity measured at 0.1 m above bed surface.
Time-averaged velocities at elevations higher than 0.1 m are approximately constant (equal to $u_{0.1}$). Measurements below z=0.01 m were done above the fixed bed and above the 0.32 mm sand bed (no suspension).

V-Tests	Peak orbital velocity RMS velocity			Mean current $u_{0.25}$	Wave period $T_{1/3}$	Sand d_{50}	size d_{90}	Net sand transport	Ripples
	$U_{1/3,on}$ (m/s)	$U_{1/3,off}$ (m/s)	U_{rms} (m/s)	(m/s)	(s)	(mm)	(mm	(kg/s/m)	(m)
V25-w (B2223 Noordwijk)	0.52 (± 0.02)	0.52	0.25	0 (± 0.02)	9.3 (± 0.3)	0.22	0.28	0	Δ=0.015 to 0.03 m λ= 0.8 to 1.2 m flat, wavy bed forms
V25-wc20 (B2223, Noordwijk)	0.52 (± 0.02)	0.52	0.25	0.2 (± 0.02)	9.3 (± 0.3)	0.22	0.28	0.006 (± 0.0005)	Δ=0.01 to 0.015 m λ= 1 to 1.5 m flat, wavy bed forms
V34-w (B2210, Noordwijk)	0.70 (± 0.05)	0.70	0.34	0 (± 0.02)	9.3 (± 0.3)	0.22	0.28	0	Δ=0.02 to 0.04 m λ= 0.8 to 1.2 m flat, wavy bed forms
V34-wc20 (B2210, Noordwijk)	0.70 (± 0.05)	0.70	0.34	0.20 (± 0.02)	9.3 (± 0.3)	0.22	0.28	0.009 (± 0.002)	Δ=0.005 to 0.015 m λ=1.5 to 2 m long flat, wavy bed forms
V34-wc45 (B2210, Noordwijk)	0.70 0.34 (± 0.05)	0.70	0.34	0.45 (± 0.03)	9.3 (± 0.3)	0.22	0.28	0.04 (± 0.01)	Δ=0 to 0.02 m λ= 1.5 to 2 m long flat, wavy bed forms
V38-w (B9436, Egmond)	0.88 (± 0.05)	0.72	0.38	0 (± 0.05)	8.5 (± 0.5)	0.22	0.28	0.008 (± 0.001)	Δ=0.02 to 0.03 m λ= 1 to 1.5 m flat, wavy bed forms
V15-w (B2228, Noordwijk)	0.35	0.35	0.15	0	6	0.22	0.28	not measured	Δ=0.03 to 0.05 m λ= 0.1 to 0.2 m 3D ripples; bed load transport only
U-Tests	**Peak orbital velocity RMS velocity**			**Mean current $u_{0.25}$**	**Wave period $T_{1/3}$**	**Sand d_{50}**	**size d_{90}**	**Net sand transport**	**Ripples**
	$U_{1/3,on}$ (m/s)	$U_{1/3,off}$ (m/s)	U_{rms} (m/s)	(m/s)	(s)	(mm)	(mm	(kg/s/m)	(m)
U36-w (Jonswap)	0.85 (± 0.03)	0.62	0.36	0 (± 0.03)	6.5 (± 0.2)	0.35	0.46	-0.004 (± 0.002)	Δ=0.04 to 0.06 m λ= 0.4 to 0.6 m irregular 2D/3D fairly sharp-crested ripples
U36-wc20 (Jonswap)	0.85 (± 0.03)	0.62	0.36	0.18 (± 0.03)	6.5 (± 0.2)	0.35	0.46	-0.01 (± 0.003)	Δ=0.05 to 0.15 m λ= 0.6 to 1.2 m regular 2D fairly sharp-crested ripples
U44-w (Jonswap)	1.02 (± 0.05)	0.80	0.44	0 (± 0.03)	6.5 (± 0.2)	0.35	0.46	-0.01 (± 0.003)	Δ=0.0.5 to 0.15 m λ= 0.6 to 1.2 m irregular 2D/3D rounded bedforms and 2D/3D fairly sharp-crested ripples

Table 3.2.10 *Summary of net transport rates measured in wave tunnel; 0.22 and 0.35 mm sand; $u_{0.25}$= measured time-averaged velocity at 0.25 m above bed*

Height above bed (m)	**Test V25-w (kg/m^3)**	**Test V25-wc20 (kg/m^3)**	**Test V34-w (kg/m^3)**	**Test V34-wc20 (kg/m^3)**	**Test V34-wc45 (kg/m^3)**	**Test V38-w (kg/m^3)**
0.005	0.35	0.46	0.145	0.275		0.32
0.0075						0.19
0.01	0.35 0.23	0.35	0.105	0.170		0.13
0.015			0.21		0.74	0.12 0.09
0.02	0.15 0.12	0.12 0.21	0.065	0.09	0.55	
0.025			0.12			0.05
0.03	0.05 0.07	0.06 0.13	0.05	0.05 0.06	0.35	0.04
0.035			0.07		0.1	0.06
0.04		0.03 0.09	0.04	0.04 0.045	0.23	
0.045	0.03 0.045					
0.045					0.06	
0.05	0.035	0.064	0.05 0.035	0.04	0.17	0.04
0.055						
0.06	0.033	0.05	0.035	0.035	0.14	0.025
0.07	0.028	0.043	0.03	0.03	0.05 0.12	0.03
0.09	0.024	0.029	0.025	0.03	0.045 0.09	0.025 0.03
0.105						
0.12	0.022	0.024	0.025	0.025	0.07	0.01 0.022
0.14	0.022	0.022	0.025	0.025	0.01 0.06	

Table 3.2.11 *Sand concentration data (left=pump samples; right=ABS-data) of V-series*

Height above bed (m)	**Test U36-w (kg/m^3) (0.22 to 0.25 m left of crest 0.55 m right of crest)**	**Test U36-wc20 (kg/m^3) (0.05 m left of crest; 0.45 m right of crest)**	**Test U44-w (kg/m^3) (0.22 m left of crest; 1 m left of large ripple above trough)**
0.005	7.6		
0.01	12.2		
0.015	2.9		
0.02	1.4-5.8	3.84	1.44
0.025	1.9		
0.03	1.2-3.2	2.84	1.16
0.04	0.6-1.0	1.93	0.6
0.045	1.2		
0.055	0.54	1.39	0.54
0.06	1.05		
0.075	0.41	1.16	
0.08	0.8		
0.085	0.54		
0.095	0.3	0.84	0.3
0.11	0.67		
0.115	0.36		
0.125	0.23	0.63	0.23
0.13-0.14		0.84-0.96	
0.15-0.165	0.14-0.39	0.36-0.75	0.14
0.20-0.215	0.08-0.27	0.22-0.32	0.08
0.235-0.245			0.39-0.41
0.26-0.275	0.09-0.27	0.13-0.15	0.09-0.19
0.325-0.385		0.02-0.03	0.15-0.18
0.43-0.49			0.13-0.14

Table 3.2.12 *Sand concentration data (pump samples) of U-series*

Verification results

The bed-load transport model of TRANSPOR 2000 was used to estimate the bed-load transport, using (see Table 3.2.10): h= 15 m, wave-current angle= 0 ^{o}, d_{50}= 0.22 mm, d_{90}= 0.28 mm, d_s=d_{50}= 0.22 mm, $k_{s,c}$= 0.01 m, temperature= 15 ^{o}C and salinity= 0 promille. The measured peak orbital velocities (average value of $U_{1/3,on}$ and $U_{1/3,off}$; see Table 3.2.10) have been translated to a representative significant wave height in a water depth of 15 m using linear wave theory. The measured current velocities at z=0.25 m above the sand bed have been translated to a depth-averaged current velocity in a water depth of 15 m. The input data are presented in Table 3.2.13.
To verify the bed-load transport model, two approaches have been used:

- measured peak orbital velocities specified as input values;
- representative wave heights specified as input values; peak orbital velocities (velocity asymmetry) are based on Isobe-Horikawa method.

The current-related bed roughness was set to $k_{s,c}$=0.01 m to obtain the best representation of the velocity profile in the near-bed layer (see previous Section).
Two values of the grain roughness have been used: $k_{s,grain}$=1d_{90} and $k_{s,grain}$=3d_{90}. The $k_{s,w}$-value is assumed to be equal to $k_{s,grain}$ (no bed form roughness). Both the original f_{cw}-friction factor and the modified f_{cw}-friction factor have been used.
The computed and measured bed-load transport rates based on input of measured peak orbital velocities are presented in Table 3.2.14 and Figure 3.2.3. The computed values are slightly too large (but within a factor of 2) for $k_{s,grain}$=1d_{90}. The computed values are much too large (factor of 2 to 3) for $k_{s,grain}$=3d_{90}. The effect of a modified f_{cw}-friction factor is marginal.

The computed wave-asymmetry related suspended load transport ($q_{s,w}$) is about zero in the tests V25-wc20, V34-wc20 and V34-wc45, because the velocity asymmetry of the orbital velocities is about zero (see Table 3.2.10). The computed $q_{s,w}$-value in the test V38-w is about 0.001 kg/s/m and is negligible small compared with the bed-load transport ($q_{b,w}$).
The bed-load transport rates (values in brackets; Table 3.2.14) have also been computed by using the representative wave height as input. The results are as follows:

- cases V25-wc20 and V34-wc20; computed bed load transport rates are slightly larger (10%) than those based on the measured peak orbital velocities as input values, because the predicted peak orbital velocities are slightly different (asymmetric waves) whereas the measured values are equal (symmetric waves);
- case V34-wc45; computed bed load transport rates are almost the same (transport rate is dominated by the current);
- case V38-w; computed bed load transport rates are smaller than those based on the measured peak orbital velocities as input values, because the predicted peak orbital velocities are too small compared with the measured values.

Test No.	Water depth h (m)	Depth-averaged current velocity u (m/s)	Significant wave height H_s (m)	Peak wave period T_p (s)	Angle between wave and current direction φ (°)	Ripple height and length Δ, λ (m)	Measured peak orbital velocity $U_{1/3,on}$ $U_{1/3,off}$ (m/s)	Measured bed load transport q_b (kg/s/m)
V25-wc20	15	0.3	1.7	9.3	0	0.012; 1.25	0.52; 0.52	0.006
V34-wc20	15	0.27	2.2	9.3	0	0.01; 2.0	0.70; 0.70	0.009
V34-wc45	15	0.67	2.2	9.3	0	0.01; 1.75	0.70; 0.70	0.04
V38-w	15	0	2.8	8.5	0	0.02; 1.75	0.90; 0.73	0.008

Table 3.2.13 *Input parameters related to wave tunnel data; d_{10}=0.15 mm, d_{50}=0.22 mm; d_{90}=0.28 mm; temperature=15 °C, salinity=0 promille (fresh water); flat wavy ripples*

Test No.	Measured bed-load transport (kg/m/s)	Computed Bed-load transport (kg/s/m)			
		$k_{s,grain}$= 1d_{90} f_{cw}-original	$k_{s,grain}$= 3d_{90} f_{cw}-original	$k_{s,grain}$= 1d_{90} f_{cw}-modified	$k_{s,grain}$= 3d_{90} f_{cw}-modified
V25-wc20	0.006	0.01 (0.011)	0.016 (0.017)	0.01 (0.0125)	0.015 (0.015)
V34-wc20	0.009	0.014 (0.015)	0.022 (0.024)	0.014 (0.016)	0.021 (0.024)
V34-wc45	0.04	0.05 (0.049)	0.074 (0.072)	0.052 (0.052)	0.072 (0.07)
V38-w	0.008	0.011 (0.0051)	0.016 (0.0075)	0.011 (0.005)	0.016 (0.0075)

Table 3.2.14 *Measured and computed bed-load transport rates for new wave tunnel data based on measured peak orbital velocities as input (computed values based on representative wave heights are given in brackets)*

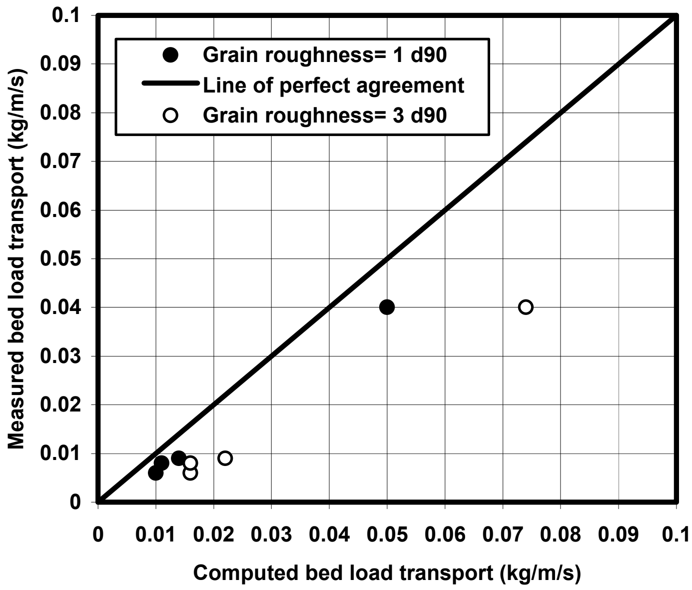

Figure 3.2.3 *Measured and computed bed-load transport rates for new wave tunnel data; d_{50}=0.22 mm; f_{cw}-original (measured peak orbital velocities used as input data)*

3.2.9 Bed-load transport from new experiments (within Sandpit-Project) at field site Noordwijk of North Sea

Kleinhans (2002) performed bed-load transport measurements using a mechanical bed-load transport instrument during spring tidal conditions at a location off the coast of Noordwijk, on 5 March 2003. The water depth varied between 11 and 13 m with a spring tidal range of about 2 m. The maximum bottom currents (at 0.55 m above the bed) were around 0.5 m/s. The weather was fair; the significant wave height was negligible small. The bed material was sand with d_{50}= 0.21 mm and d_{90}= 0.3 mm. Herein only the bed-load transport rates measured around peak tidal flow with near-bed velocities in the range of 0.4 to 0.5 m/s are considered. The depth-averaged velocity is assumed to be 10% larger than the measured near-bed velocities. The measured bed-load transport rates (clustered in two groups) are given in Table 3.2.15.

The bed-load transport model of TRANSPOR2000 was used to estimate the bed-load transport, using h= 12 m, d_{50}= 0.21 mm, d_{90}= 0.3 mm, $k_{s,c}$= 0.03 m, temperature= 15 ^{o}C and salinity= 30 promille. Two values of the grain roughness were used: $k_{s,grain}$=1d_{90} and $k_{s,grain}$=3d_{90}. The best agreement of measured and computed values is obtained for $k_{s,grain}$=1d_{90} (see Table 3.2.12).

Measured depth-averaged velocity (m/s)	Measured bed-load transport (kg/m/s)	Computed Bed-load transport (kg/s/m)	
		$k_{s,grain}$= $1d_{90}$	$k_{s,grain}$= $3d_{90}$
0.45	0.0004 (±0.0003)	0.00032	0.0009
0.55	0.0008 (±0.0006)	0.002	0.0033

Table 3.2.15 *Measured and computed bed-load transport rates, North Sea;* d_{50}*=0.21 mm*

3.2.10 Conclusions of bed load verification results

The following conclusions were drawn:

- The measured bed-load transport in quasi-steady tidal flow can be reasonably well described (about 65 % within factor of 2 of measured values; 6 cases; see Figure 3.2.4) by the TRANSPOR2000 model for sand in the range of 0.2 to 0.5 mm using a grain roughness value of $1d_{90}$.

- The net bed-load transport rate in conditions with combined steady and oscillatory flow over a sand bed can be reasonably well described (about 80 % within factor of 2 of measured values; 19 cases; see Figure 3.2.4) by time-averaging (over the wave period) of the instantaneous transport rates using a quasi-steady bed-load transport formula approach with grain roughness of $1d_{90}$ for sand in the range of 0.2 to 0.5 mm in the ripple regime without adjustment of model coefficients.

- The bed-load transport is mainly affected by the grain roughness. The best results are obtained for a grain roughness equal to $1d_{90}$. The computed bed load transport rates are significantly larger (factor 1.5 to 2) for a grain roughness of $3d_{90}$.

The bed-load transport in combined steady and oscillatory flow is only marginally dependent on a somewhat more accurate description of the wave-current friction factor (f_{cw}). The modified f_{cw}-method yields slightly smaller transport rates (20% to 30%).

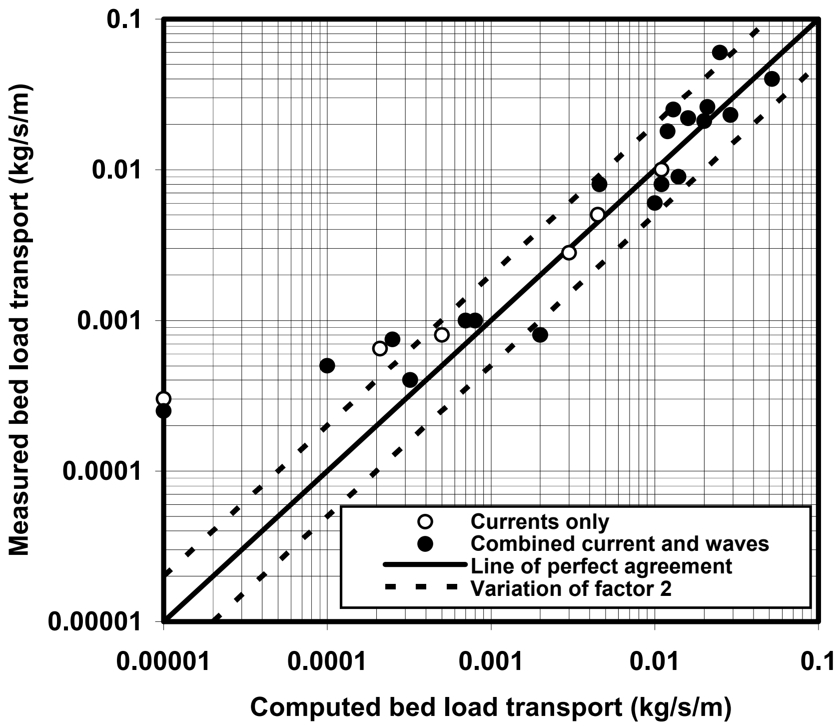

Figure 3.2.4 *Comparison of computed and measured bed load transport (25 cases).*

3.3 Verification of oscillatory suspended load transport

3.3.1 Approach and formulations

Various data sets from the literature have been used to verify/improve the oscillatory suspended load transport of the TRANSPOR2000 model. The median particle size for all data sets is in the range of 0.2 to 0.5 mm.

The following data sets have been used:

Experimental results from large-scale Delta flume,
Field data from COAST3D project at Egmond site, The Netherlands.

The engineering method implemented in the TRANSPOR2000 model has been introduced by **Houwman and Ruessink (1996)**. Experimental data are required to determine the empirical coefficient involved. The wave-related suspended transport component is modelled as:

$$q_{s,w} = \gamma \frac{U_{on}^4 - U_{off}^4}{U_{on}^3 + U_{off}^3} \int c dz \qquad (3.3.1)$$

with: $U_{on}=U_{\delta,f}$= near-bed peak orbital velocity in onshore direction (in wave direction) and $U_{off}=U_{\delta,b}$= near-bed peak orbital velocity in offshore direction (against wave direction), c= time-averaged concentration and γ= phase lag function.

Eq. (3.3.1) is based on an instantaneous response of the suspended sand concentrations (C) and transport ($q_{s,w}$) to the near-bed orbital velocity (C proportional to U^3 and q_s to U^4). This approach may be valid for the near-bed layer (say 1 to 5 times the wave boundary layer thickness), but at higher levels a delayed response of the sand concentrations (phase lag effects) will be more realistic, particularly for fine sediments. For very fine sediment the wave-related suspended transport may even be opposite to the wave propagation direction.
Phase lag effects are supposed to be accounted for by the γ-function. As phase lag effects are related to the wave conditions, sand size and bed geometry, the γ-function is supposed to be a complicated function of the former parameters (yielding negative values for very fine sand). A detailed discussion of phase lag effects and functions is given by **Dohmen-Janssen (1999)**.

Simulation of the wave-related suspended transport according to Eq. (3.3.1) requires computation of the time-averaged sand concentration profile and integration of the time-averaged sand concentration profile in vertical direction. Herein, the integration is taken over a near-bed layer with a thickness equal to about 0.5 m, assuming that the suspended sand above this layer is not much effected by the high-frequency wave motion with periods in the range of T= 5 to 10 s. This assumption is satisfied if the fall time of a suspended sand particle over a distance of 0.5 m is much larger than the wave period (T_{fall}= 0.5/w_s yielding about 25 s for d= 0.2 mm with w_s= 0.02 m/s). Furthermore, the data of the Delta flume (**Chung and Grasmeijer, 1999**) show that most of the wave-related suspended transport occurs in the near-bed layer with a thickness of about 0.5 m (10 to 20 times the ripple height).

Chung and Grasmeijer (1999) have determined the γ-function by fitting of Eq. (3.3.1) to the measured wave-related transport rates. The peak onshore and offshore orbital velocities as well as the time-averaged sand concentrations were taken from the measured data. Amazingly, the γ-function was found to be a constant value of about 0.2 for all test results (relative standard error of about 30 %). Any influence of the wave conditions and/or the sand size on the γ-function could not be detected, implying relatively small phase lag effects for the five data sets used. It is noted that the γ-value of 0.2 is based on data with rather pronounced ripples observed in a large scale 2D wave tank. The γ-value may be considerably smaller (say between 0.1 and 0.2) for field conditions with less pronounced 3D-ripples (**Grasmeijer, 2002**).

3.3.2 Data from large-scale Delta flume

Experiments in the large-scale Delta flume (length= 200 m, depth= 7 m, width= 5 m) of Delft Hydraulics have been carried out to study the wave-related suspended transport under controlled conditions (**Chung and Grasmeijer, 1999**). The experimental conditions (ripple regime) are given in Table 3.3.1.

A horizontal sand bed layer was placed in the wave tank from position x = 100 meters to x = 140 meters. The water depth was about 4.5 m in all experiments. Two types of sand have been used: fine sand with median diameter of 0.16 mm and coarse sand with median diameter of 0.33 mm. The experimental set-up is two dimensional, but local processes are three dimensional due to the generation of ripples on the bed. Irregular waves with a single-topped spectrum were generated in the flume. The peak wave period was 5 s.

The basic data for wave height and peak orbital velocity are:

Test 1A	H_s=1.0 m	$U_{s,on}$=0.40 m/s	$U_{s,off}$=0.36 m/s
Test 1B	H_s=1.25 m	$U_{s,on}$=0.50 m/s	$U_{s,off}$=0.45 m/s
Test 1C	H_s=1.0 m	$U_{s,on}$=0.46 m/s	$U_{s,off}$=0.42 m/s
Test 1D	H_s=1.25 m	$U_{s,on}$=0.55 m/s	$U_{s,off}$=0.50 m/s
Test 1E	H_s=1.50 m	$U_{s,on}$=0.58 m/s	$U_{s,off}$=0.53 m/s

Source	**Test**	**h** m	**H_S** m	**T_P** s	**d_{50}** mm	**d_{90}** mm	**d_S** mm	**Δ_b** m	**λ_b** m	**$k_{s,w}$** m	**$q_{s,w,CR}$** kg/s/m	**Te** °C
Chung and	1A (Set I)	4.55	1	5	0.33	0.7	0.26	0.05	0.25	0.03	0.003	15
Grasmeijer	1B (set II)	4.55	1.25	5	0.33	0.7	0.26	0.05	0.25	0.03	0.0056	15
1999	1C (set III)	4.50	1	5	0.16	0.3	0.16	0.03	0.7	0.02	0.0016	15
	1D (Set IV)	4.50	1.25	5	0.16	0.3	0.16	0.05	0.75	0.02	0.0035	15
	1E (Set V)	4.50	1.5	5	0.16	0.3	0.16	0.05	0.75	0.02	0.0042	15

h = water depth, H_s = significant wave height, T_P = peak wave period
d_S = representative suspended sand size (estimated)
$k_{s,w}$ = wave-related bed form roughness (not measured, but estimated)
$q_{s,w,CR}$ = wave-related (high freq.) cross-shore suspended sand transport (- offshore, + onshore)
Δ_b = bed form height (pl= plane bed), λ_b = bed form length, Te= temperature (Celsius)

Table 3.3.1 *Summary of wave-related suspended sand transport data for large-scale wave tank (Delta flume of Delft Hydraulics)*

An acoustic instrument (ASTM) was used to measure the instantaneous fluid velocities and sand concentrations at five points above the bed simultaneously. The measurement levels above bed were (most tests): z= 0.075; 0.125; 0.225; 0.475 and 1.075m above bed. The precise position of the instrument sensors with respect to the ripple crests could not be measured. Two pump sampling systems (2x5 intake nozzles) located along the flume wall (intake nozzles at about 0.3 m from the wall) and close to the ASTM-instrument were used to measure the time-averaged sand concentrations. A sand ripple profiler of Proudman Oceanographic Laboratory (UK) was used to measure bed-form dimensions. Bed forms were also inspected by visual observation after drainage of the flume. The ASTM-instrument and pump nozzles were mounted in a tripod, which was placed on the horizontal sand bed at location x = 125 m. During each test the instruments were operated for about 15 minutes to sample over a representative wave record. Each test was repeated many times to include the effect of the (migrating) ripples on the instantaneous sand concentrations and fluid velocities. The sampling records had a maximum duration of about 2 hours. In all, 35 tests have been done, which have been grouped to 5 data sets (Table 3.3.1).

The measured instantaneous velocity and sediment concentration at each level above the bed have been separated into time-averaged, high frequency and low frequency components. Using these parameters, the various suspended transport components have been computed: current-related, high-frequency and low-frequency wave-related and net transport (**Chung and Grasmeijer, 1999; Grasmeijer et al., 1999**). The current-related suspended transport in these experiments is caused by the presence of a very weak net offshore-directed current in the near-bed layer, which is generated due to interaction of the wave-boundary layer hydrodynamics with the rippled bed. Analysis of the results showed that, in general, the high-frequency wave-related transport rates are slightly dominant and tend to be onshore-directed. The current-related transport rates are slightly smaller than the high-frequency wave-related transport rates and are offshore-directed. The low-frequency wave-related transport rates are of minor importance and have a tendency for the offshore direction similar to the current-related transport components. The suspended sediment transport mainly occurs in the near-bed layer with thickness of about 0.3 to 0.5 m, which is roughly equivalent to 10 to 20 times the ripple height.

In order to obtain the depth-integrated transport rates, the transport terms have been integrated between the lowest and highest measurement points. The results (mean values and errors) for all available tests are shown in Figure 3.3.1. The measured values represent the depth-integrated values between the lowest measurement point z= 0.075 m and the highest point z= 1.075 m. The wave-related suspended transport in the unmeasured zone between z= 0.01 m and z= 0.075 m has been estimated by extrapolation (**Chung and Grasmeijer, 1999**). The wave-related suspended transport in the unmeasured zone is about 0.5 times the measured values shown in Figure 3.3.1. It is realized that this type of extrapolation is rather tricky, but the main aim is to get a rough estimate of the suspended transport in the unmeasured zone. Based on these results, it is evident that the high-frequency suspended sand transport rate below 0.075m down to 0.01 m is an essential part of the total depth-integrated transport rate and can not be neglected. For field measurements this has the consequence that measured values down to 0.01 m above the bed are required to determine accurate values of the total depth-integrated suspended transport rate, which is a challenging task for field workers.

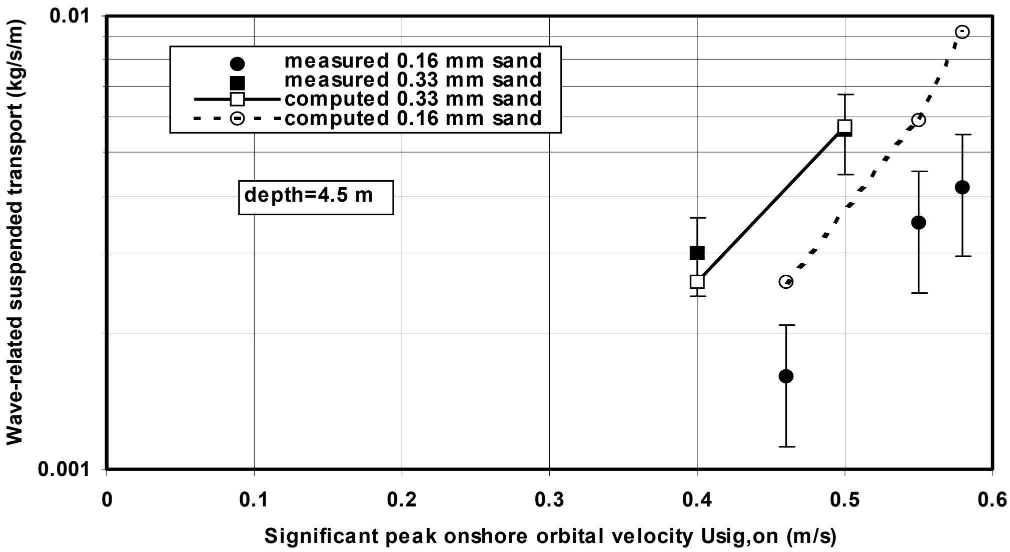

Figure 3.3.1 *Depth-integrated wave-related suspended transport (measured and computed) as a function of significant peak onshore orbital velocity and sand size*

In Figure 3.3.1 the high-frequency wave-related suspended transport rates are shown as a function of significant peak onshore orbital velocity and sand size. In all conditions with irregular waves the wave-related suspended transport is onshore-directed (in wave direction). From Figure 3.3.1 it can be observed that the wave-related suspended transport increases with increasing peak orbital velocity and decreases with decreasing particle size. This latter effect can be understood from the ripple dimensions; the ripples generated on the 0.33 mm sand bed are much more pronounced than those on the 0.16 mm sand bed (see Table 3.3.1) resulting in larger vortex motions and stronger associated suspension processes. The standard error of the wave-related transport is relatively large (about 50%) for one Test 1E (data set V; sand bed of 0.16 mm and a peak onshore velocity of 0.58 m/s), expressing relatively large variability because only 3 data records of 15 minutes were available. It stresses the importance of relatively long data sets in case of a rippled bed.

Eq. (3.3.1) as implemented in the TRANSPOR2000 model has been used to compute the wave-related suspended transport for the five Delta flume cases 1A to 1E. The near-bed orbital velocities during the onshore and offshore phase of the wave cycle are represented by sine-functions based on the measured near-bed peak orbital velocities. Input values are shown in Table 3.3.1. The computed wave-related suspended transport rates based on measured peak orbital velocities are shown in Figure 3.3.1. The computed values are roughly 1.5 to 2 times the measured values for the 0.16 mm sand. The computed values for the 0.33 mm sand are somewhat too small (about 25%). It should be realized that the measured transport rates have a relatively large inaccuracy range (about factor 2 to 3), because the transport rate in the unmeasured zone between z= 0.01 and 0.075m is not included. The computed wave-related suspended transport rates are much too large (Table 3.3.2), if the near-bed peak orbital velocity is computed by the method of **Isobe and Horikawa (1982)**. This latter method considerably overpredicts the peak orbital velocities (up to 30%) for these experiments in the Delta flume and hence the transport rates. This can be compensated by using a smaller γ-value of 0.1.

Overall, it can be concluded that the proposed approach yields wave-related suspended transport rates of the right order of magnitude, if the near-bed velocity asymmetry is predicted with sufficient accuracy. Proper predictive modelling of the oscillating suspended transport component ($q_{s,w}$) requires an accurate description of the near-bed orbital fluid velocity, especially in conditions with shoaling and breaking waves (non-linear wave motion).

Case	H_s (m)	$U_{s,on}$ (m/s)	$U_{s,off}$ (m/s)	d_{50} (mm)	d_{90} (mm)	d_s (mm)	$k_{s,w}$ (m)	$q_{s,w,\ meas}$ (kg/s/m)	$q_{s,w,comp}$ based on measured orb. vel. (kg/s/m)	$q_{s,w,comp}$ based on computed orb. vel. Isobe (kg/s/m)
1A	1	0.4	0.36	0.33	0.7	0.3	0.03	0.003	0.0026	0.0044
1B	1.25	0.5	0.45	0.33	0.7	0.3	0.03	0.0056	0.0057	0.011
1C	1	0.46	0.42	0.16	0.3	0.16	0.02	0.0016	0.0026	0.0045
1D	1.25	0.55	0.5	0.16	0.3	0.16	0.02	0.0035	0.0059	0.0122
1E	1.5	0.58	0.53	0.16	0.3	0.16	0.02	0.0042	0.0092	0.026

Table 3.3.2 *Measured and computed wave-related suspended transport rates for Delta flume experiments (h= 4.5 m, T_p= 5 s, d_s and $k_{s,w}$ are estimated)*

3.3.3 Data from Egmond field site

Coastal conditions: Egmond site 1989-1992, The Netherlands
Some information of the wave-related transport component can be obtained from the field data collected at the Dutch coast. **Kroon (1994)** and **Wolf (1997)** measured instantaneous velocities and sand concentrations at one or two points above the bed in the inner surf/swash zone (water depths between 0.5 and 1.5 m) at the beach site of Egmond. **Houwman and Ruessink (1996)** performed similar measurements in the shoreface zone and in the surf zone (water depths between 4 and 9 m) at the site of Terschelling. At both sites the sediments are in the range between 0.15 and 0.3 mm. Analysis of the available data reveals that the local (in a specific point above bed) $q_{s,w}$-component generally is onshore-directed near the bed and significant compared to the (offshore-directed) $q_{s,c}$-component.

Typical values are:
In the inner surf/swash zone: $|q_{s,w}|$ =0.2 to 0.3 $|q_{s,c}|$
In the shoreface and surf zone: $|q_{s,w}|$ =0.5 to 1 $|q_{s,c}|$
The vertical resolution of the data is not sufficient to obtain depth-integrated values of the wave-related suspended transport.

Coastal conditions: Egmond site 1998, The Netherlands
Figure 3.3.2 shows measured values of the depth-integrated wave-related (high frequency) suspended transport component ($q_{s,w}$) at the inner bar crest of the Egmond site 1998 (COAST3D project; see **Grasmeijer, 2002**). The basic data are given by **Grasmeijer (2002)**. Onshore-directed as well as offshore-directed values have been observed. The variation range of the $q_{s,w}$-transport component for the largest peak onshore orbital velocity of 1.25 m/s is relatively large, because it is based on only two data points. Computed values are also shown in Figure 3.3.2.

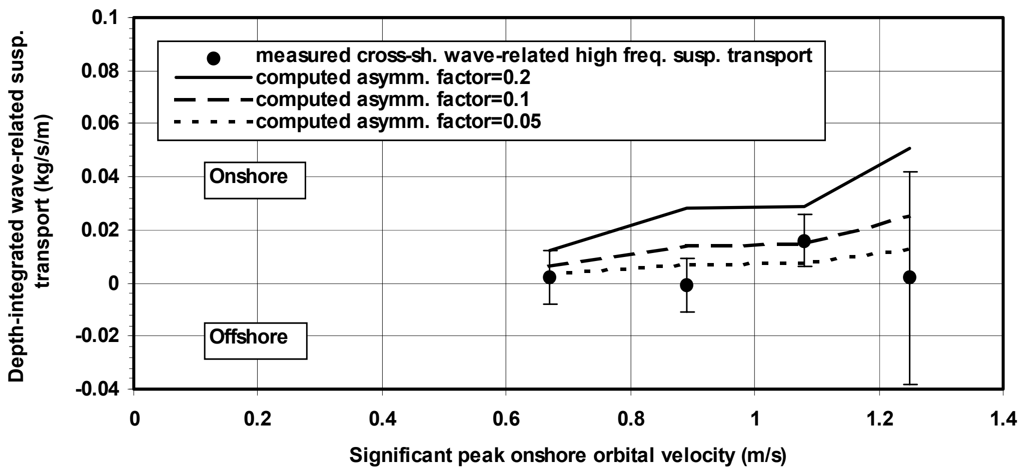

Figure 3.3.2 *Measured and computed wave-related high frequency suspended transport; Egmond 1998 site, The Netherlands*

Eq. (3.3.1) implemented in the TRANSPOR2000 model has been used to compute the wave-related suspended transport for the data of the Egmond site 1998 (6 cases). The measured and computed results are shown in Figure 3.3.2. The computed wave-related suspended transport rates are based on three different γ-values, being γ=0.2, 0.1 and 0.05. The best results are obtained for γ of about 0.1. Thus, the γ-value representing the Egmond data is considerably smaller (factor 2) than that derived from the data of the Delta flume, which may be related to the type of bed forms generated in nature and in the 2D wave flume. The bed forms at the Egmond site generally were somewhat longer and flatter than those in the Delta flume resulting in less pronounced vortex motions and hence smaller wave-related suspended transport rates. Given the presence of relatively flat ripples in field conditions with fine sand in the range of 0.2 to 0.3 mm, it is recommended to use a value of γ=0.1.

3.4 Effect of near-bed wave-induced streaming on bed load and suspended load transport

3.4.1 Introduction

The cross-shore sand transport rate in the near-bed region of shallow waters (near the coast) is strongly affected by small residual (net) currents induced by the wave motion. This was clearly observed by **Bijker et al. (1974)** who measured streaming velocities over the full depth at the toe of a sloping beach (See Figure 3.4.6). Above a smooth bed they found that the measured streaming was in reasonable agreement with the streaming predicted by using the conduction-solution of **Longuet-Higgins (1953)**. However, when the same incident waves propagated above a flat sand-roughened bed, the near-bed streaming, while still being in the onshore direction, was greatly reduced in magnitude. When the bed was rippled, the near-bed streaming was further reduced to approximately zero, while the streaming just above the bottom boundary layer was directed offshore.

Various mechanisms are responsible for the generation of these net currents near the bed:

- wave-induced streaming velocities in and directly above the wave boundary layer due to the turbulence structure near the bed;
- return (offshore-directed) currents due to onshore-directed Lagrangian and Eulerian mass fluxes in the upper part of the water depth.

The magnitude and even direction of these net currents are rather uncertain and therefore the accuracy of models of coastal sand transport depends strongly upon reliable predictions of the detailed hydrodynamic processes leading to these net currents.

3.4.2 Lagrangian and Eulerian streaming velocities in near-bed region

Stokes (1847) first pointed out that the fluid particles do not describe exactly closed orbital trajectories in case of small-amplitude sinusoidal surface waves in perfect irrotational (non-viscous) conditions. The fluid particles have a second-order mean Lagrangian velocity (called Stokes-drift) in the direction of wave propagation resulting from the fact that the horizontal orbital velocity increases slightly with distance above the bed. Consequently, a particle at the top of an orbit beneath the wave crest has a greater forward velocity than it has at the bottom of the orbit beneath the wave trough. As the waves enter shallow water, the orbits become more elliptical and the drift velocities increase to appreciable values (order 0.1 m/s). The depth-integrated mass flux associated with waves propagating in a horizontally unbounded domain is given by M = $gH^2/(8c)$ with H = wave height and c = wave propagation velocity. Assuming a zero mass flux (bounded domain; near coast or in wave tank) over the water depth, the onshore mass flux in the upper part of the depth is balanced by an Eulerian return mass flux in the near-bed region of the water column.

Besides the Lagrangian mass flux, there also is an Eulerian mass flux in the region near the water surface due to the presence of the wave form. This Eulerian mass flux can be determined by integration over time and space of the instantaneous horizontal velocities between the wave trough level and the wave crest level. In this region there is an asymmetry of the horizontal velocity; more fluid moves forward in the crest region than backward in the trough region. Both methods (Lagrangian and Eulerian) yield the same value of the mass flux, but a different distribution over the depth. In a bounded domain (near the coast or in a wave tank) the onshore-directed Lagrangian and Eulerian mass fluxes are compensated by an Eulerian return (offshore-directed) flow near the bed.

Longuet-Higgins (1953) first explained theoretically that for real fluids with viscosity ν ; there is a time-averaged net downward transfer of momentum into the wave boundary layer by viscous diffusion producing a mean Eulerian streaming in addition to the Lagrangian Stokes drift. Furthermore **Longuet-Higgins (1953)** also explained theoretically that progressive waves on a free surface give rise to vertical velocities within the wave boundary layer as a consequence of the continuity principle. Both effects lead to a non-zero, cycle-averaged, shear stress and hence, to a mean component of velocity in the direction of wave propagation. At the edge of the laminar wave boundary layer above a smooth flat bottom, the Eulerian streaming velocity was found to be $u_{LH}=0.75((U_{\delta,w})^2/c$ with $U_{\delta,w}$= peak orbital velocity at edge of boundary layer and c = wave propagation velocity. **Longuet-Higgins (1958)** showed that, if the assumption of a constant (in time and space) eddy viscosity is made, then the streaming at the edge of the turbulent boundary layer above a smooth bottom is still given by $u_{LH}=0.75((U_{\delta,w})^2/c$. These results remains valid even if height variation of the eddy viscosity is introduced (**Johns, 1970**).

Assuming a zero mass flux over the depth, Longuet-Higgins found a vertical distribution as given in Figure 3.4.1 (based on 'conduction solution'). The wave-induced streaming in the boundary layer is onshore-directed and of the order of $(U_{\delta,w})^2/c$ with $U_{\delta,w}$= peak orbital velocity at edge of boundary layer and c = wave propagation velocity.

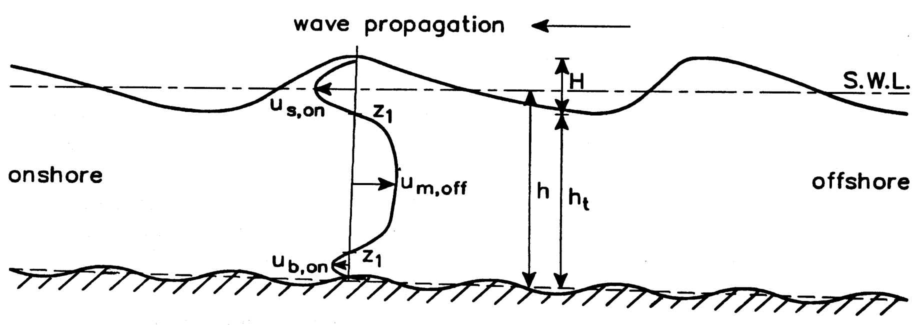

Figure 3.4.1 *Streaming velocities according to Longuet-Higgins (1953)*

Various researchers have successfully developed mathematical models to describe the Eulerian wave-induced streaming near the bed. **Davies and Villaret (1997, 1998, 1999)** have summarized model and experimental results. Experimental and theoretical studies involving plane rough beds in the turbulent flow regime have shown that the near-bed streaming depends rather critically upon the bed roughness, as well as on the degree of wave asymmetry. The effect of bed roughness is to reduce the phase lead of the bottom velocity in comparison with the lead of $\pi/4$ given by the classical Stokes' solution. This causes the Eulerian streaming to be reduced (i.e., $u_\delta c/U^2<0.75$), as shown by **Towbridge and Madsen (1984)**. Their two-layer eddy viscosity model included both height variation of the eddy viscosity and also a reference elevation (i.e. bed roughness length scale $z_o=k_{s,w}/30$; $k_{s,w}$=wave-related roughness).

In addition to the streaming associated with the vertical velocity field, any asymmetry in the turbulence intensity in successive wave half cycles will give rise to a near-bed residual streaming component. For a plane bed, this component is in the offshore direction as demonstrated, in isolation from other processes, by **Ribberink and Al-Salem (1995)** for asymmetrical waves in an oscillating water tunnel. These two competing mechanisms were considered by **Towbridge and Madsen (1984)**, whose model included an asymmetrically time-varying eddy viscosity. In this and other modelling studies, it has been found that, above plane rough beds ($A_{\delta,w}/k_{s,w}>10$), the effect of asymmetry in the turbulence in successive half cycles is to reduce the Eulerian streaming with a reversal in the direction of streaming occurring for very long waves.

Davies and Villaret (1999) also present a semi-analytical approach for the generation of net currents over very rough and rippled bottoms ($A_{\delta,w}/k_{s,w}<5$). Above such bottoms, momentum transfer is dominated by the spatially well organized process of vortex shedding, rather than by random turbulent processes. A simplified, time-varying convective eddy viscosity K has been defined to characterize this vortex-shedding process in a standard, one-dimensional, gradient diffusion approach. Their convective eddy viscosity includes symmetrical and asymmetrical time-varying components, with phase angles such that the peak value of K occurs at about the time of flow reversal following the passage of each (steep) wave crest. The Eulerian streaming velocity in the bottom wave boundary layer comprises contributions that arise from:

- wave Reynolds stress associated with the lowest order velocity field;
- asymmetry terms arising from time-varying components of K.

Following **Sleath (1991)** and **Nielsen (1992)** respectively, the thickness of the wave boundary layer is described by (**Davies and Villaret, 1999**):

$$
\begin{aligned}
\delta_w &= 0.355 A_{\delta w}\left(\frac{A_{\delta w}}{k_{s,w}}\right)^{-0.25} \qquad && for\ \frac{A_{\delta w}}{k_{s,w}} > 2.5 \\
\delta_w &= 0.45 k_s\left(\frac{A_{\delta w}}{k_{s,w}}\right)^{-0.25} \qquad && for\ \frac{A_{\delta w}}{k_{s,w}} \le 2.5
\end{aligned}
\tag{3.4.1}
$$

with: $A_{\delta,w}$= peak orbital excursion near the bed, k_s= effective bed roughness.

The streaming velocity distribution (u-velocity profile) within the wave boundary layer with thickness δ_w has the following features (see Figures 3.4.2 and 3.4.3):

- a near-bed jet of fluid in the direction of wave propagation;
- a level of zero-velocity within the wave bounder layer;

- a reversal in the direction of the velocity extending to the edge of the wave boundary layer; the offshore-directed streaming velocity at the edge of the wave boundary layer depends on the relative wave height (H/h), the degree of velocity asymmetry ($U_{\delta,on}/U_{\delta,off}$) and the relative roughness ($A_{\delta,w}/k_{s,w}$).

It should be realized that this boundary layer model is a model based on a rigid lid approach at the water surface in an unbounded domain (zero mass flux over the depth is not imposed). Hence, the onshore Lagrangian and Eulerian mass fluxes due to presence of real waves and the corresponding near-bed return flow in a bounded domain are not included. Also the 'asymmetry terms' referred to above are beneath a rigid lid. However, the wave Reynolds stress term (also referred to above) which is a streaming-type term that arises as a result of the vertical wave velocity field, is fully included.

Figures 3.4.2 shows the streaming velocity distribution within the wave boundary layer for an asymmetry factor $B=U_2/U_1=0.75kA_{\delta,w}/((\sinh(kh))^2=0.1$, $\alpha=(\omega/K_o)^{0.5}$ and standard model settings. U_2=second-order velocity amplitude, U_1=first order velocity amplitude. The model has been tuned for conditions with a very rough bed (for $A_{\delta,w}/k_{s,w}<5$). The solution of **Longuet-Higgins (1953)** is shown for comparison. The edge of the wave boundary layer is at $\alpha z=5$ (on vertical axis). The horizontal scale of Figure 3.4.2 represents the parameter: $(u_\delta c)/(U_{\delta,w})^2$, with u_δ=streaming velocity at edge of wave boundary layer, c= wave propagation speed and $U_{\delta,w}$= peak orbital velocity at edge of wave boundary layer (first order value).

Figures 3.4.3 and 3.4.4 show similar profiles for other values of $c/U_{\delta,w}$ and B. The parameter $c/U_{\delta,w}$ is a measure of relative wave length ($L/A_{\delta,w}$); longer waves for larger $c/U_{\delta,w}$-values. The B-parameter expresses the asymmetry of the peak orbital velocities (B=0 for symmetric waves and B=0.2 for very asymmetric waves). Very asymmetric waves (relatively large H/h values) result in a relatively strong jet flow velocity near the bed, but a relatively small onshore-directed residual flow velocity at the edge of the wave boundary layer. Symmetric waves (relatively small H/h value) yield the opposite behaviour with a relatively weak jet flow near the bed, but a relatively strong negative (offshore-directed) residual flow at the edge of the wave boundary layer.

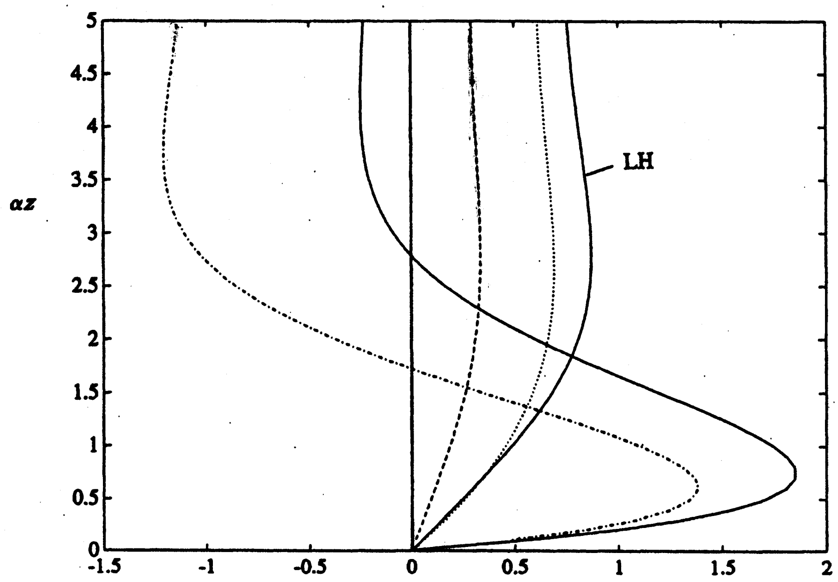

Figure 3.4.2 *Streaming velocity profile in wave boundary layer according to* ***Davies-Villaret 1999*** *(full line represents residual flow; dotted lines represent various contributions; $c/U_{\delta,w}=10$; $B=0.1$; $A_{\delta,w}/k_{s,w}<5$) and according to* ***Longuet-Higgins 1953*** *(LH); horizontal axis represents $u_\delta c/(U_{\delta,w})^2$*

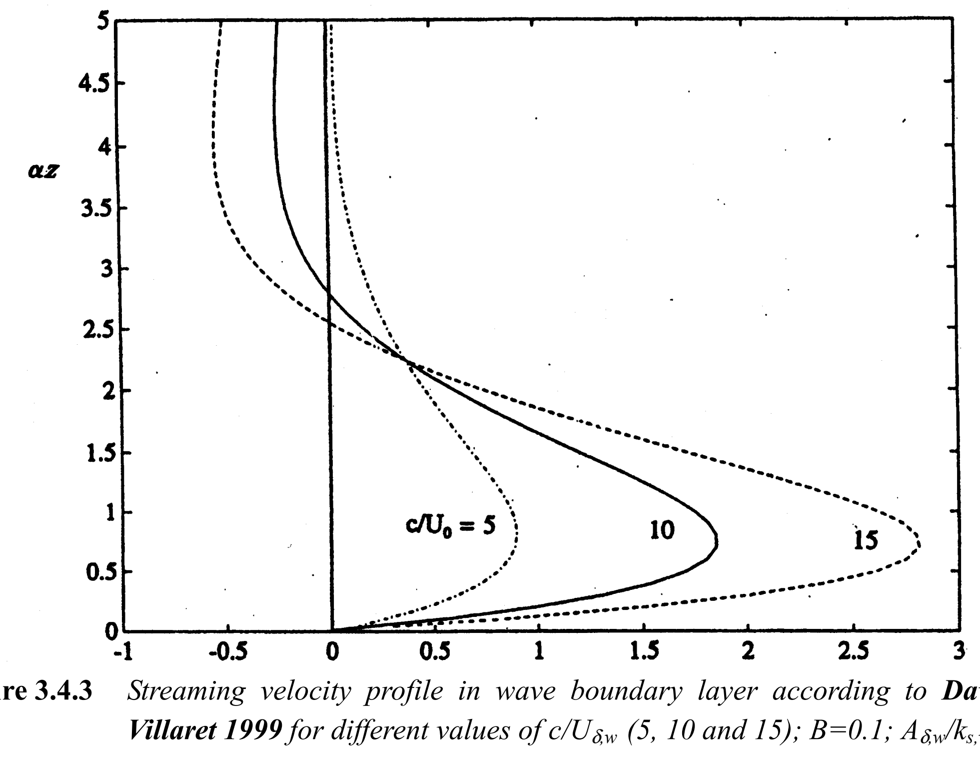

Figure 3.4.3 *Streaming velocity profile in wave boundary layer according to* ***Davies-Villaret 1999*** *for different values of $c/U_{\delta,w}$ (5, 10 and 15); $B=0.1$; $A_{\delta,w}/k_{s,w}<5$*

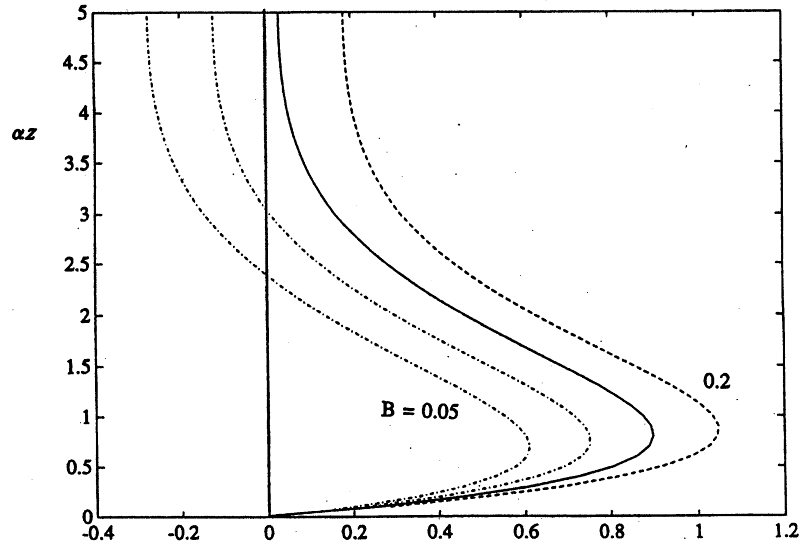

Figure 3.4.4 *Streaming velocity profile in wave boundary layer according to* ***Davies-Villaret 1999*** *for different values of B=0.05, 0.1, 0.15 and 0.2; $c/U_{\delta w}$ =10; $A_{\delta w}/k_{s,w}$<5*

It is still open for debate whether these results of **Davies and Villaret (1999)** are sufficiently accurate for the streaming distribution over rippled beds, as the modelling of flow separation phenomena around rippled beds basically require a two-dimensional horizontal and vertical approach using higher order turbulence closure models **(Hansen et al., 1994; Utnes et al., 1996; Fredsøe et al.„ 1999).** The streaming velocity at the edge of the wave boundary layer produced by the model of **Davies and Villaret** certainly is of the right order of magnitude compared with the available laboratory data sets, but the vertical streaming distribution within the boundary layer is not yet severely tested (see Figures 9 to 11 from **Davies and Villaret, 1999**).

Some additional information can be obtained from the model results of **Malarkey (2001)**. Figure 3.4.5 shows Malarkey's spatially averaged results for waves of three different asymmetries over a symmetrical, steep ripple (steepness=0.16 with A/wavelength = 2.4). Three different wave asymmetries are shown. The boundary layer thickness should be taken to be $y/\lambda = 0.5$ at most. Due to the constraint of zero mean velocity at the top ($y/\lambda = 1$), the residual at the 'edge' of the w.b.l. should probably be taken as the peak offshore value at about $y/\lambda = 0.3$.

The results are from a discrete vortex Cloud-in-Cell model, and are to be compared only with the asymmetry term in the model of **Davies and Villaret** (1999; i.e. rigid lid is assumed, no vertical velocities, no streaming). The vertical axis goes up to a height of one ripple length above the trough; the wave boundary (vortex) layer extends up to about 0.5, which corresponds to about 2 ripple heights above the crest. The basic structure of the model of **Davies and Villaret (1999)** is apparent: a forward jet (though this is mainly below the crest level) and a return flow within the wave boundary layer above this. The spatially averaged profile is constrained to go to zero at the top of the plot, and so the peak offshore residual could probably be taken as the velocity at the edge of the boundary layer. However the structure within the wave boundary layer is clear and confirms the 1D-model results.

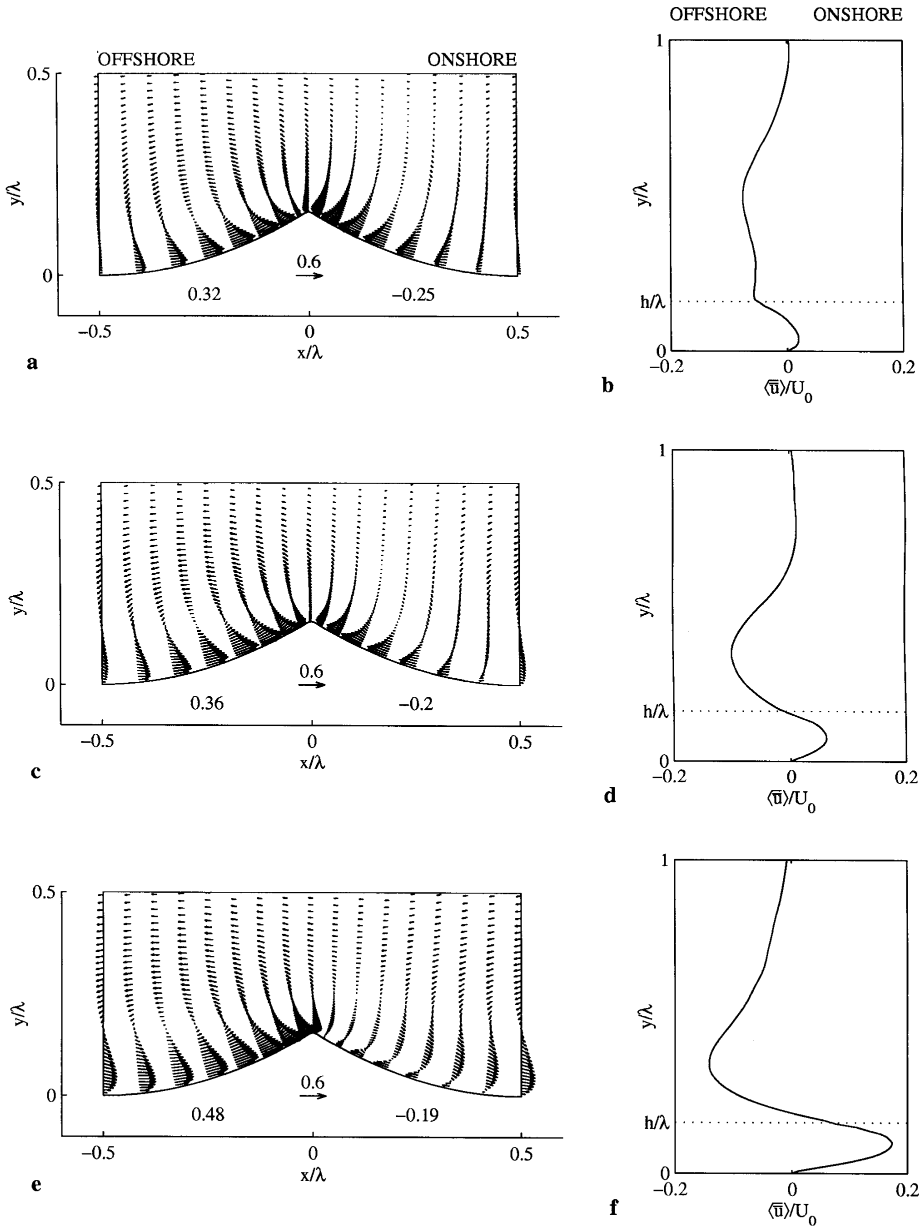

Figure 3.4.5 *Streaming velocity profile in wave boundary layer according to 2D model of Malarkey (2001); λ_L/λ=0.5, h/λ=0.16, A_o/λ=2.4, T=8.46 s, λ=0.22 m;*

h=ripple height, λ=ripple length, λ_L=half ripple length, $\bar{\bar{u}}$ =horizontally averaged mean velocity, $U_0 = U_{\delta,w}$ =peak orbital velocity,

$A_0 = A_{\delta,w}$ =peak orbital excursion;

a,c,e: local streaming profiles (ensemble-averaged)
b,d,f: horizontally-averaged streaming profiles
a and b: wave asymmetry $(U_1+U_2)/U_1$=1.1
c and d: wave asymmetry $(U_1+U_2)/U_1$=1.2
e and f: wave asymmetry $(U_1+U_2)/U_1$=1.44

Davies and Villaret (1998, 1999) have reviewed the available experimental datasets of streaming velocities in the near-bed region. The data sets have been classified by using the relative bed roughness parameter ($A_{\delta,w}/k_{s,w}$) as discriminating parameter. Very rough rippled beds can be defined as conditions with $A_{\delta,w}/k_{s,w}<10$, rough plane beds as conditions with $A_{\delta,w}/k_{s,w}=10$ to 1000 and smooth plane beds as $A_{\delta,w}/k_{s,w}>1000$.

Analysis of the datasets shows that the wave-induced streaming at the edge of the wave boundary layer is negative (against wave propagation direction) or positive as a function of relative roughness $A_{\delta,w}/k_{s,w}$ (**Davies and Villaret, 1999**). The streaming velocities at the edge of wave boundary layer become more negative for decreasing relative roughness values ($A_{\delta,w}/k_{s,w}$).

Some values are: $u_\delta=\beta(U_{\delta,w})^2/c$ with $\beta=-0.2$ for $A_{\delta,w}/k_{s,w}=5$, $\beta=-1$ for $A_{\delta,w}/k_{s,w}=1$, $\beta=-1.5$ for $A_{\delta,w}/k_{s,w}=0.5$. Using $\beta=0.75$ (Longuet-Higgins) for $A_{\delta,w}/k_s>100$, these results can roughly be approximated by:

$$
\begin{aligned}
u_\delta &= \left(-1+0.875\log\left(\frac{A_{\delta,w}}{k_s}\right)\right)\left(\frac{U_{\delta,w}^2}{c}\right) && for\, 1<\frac{A_{\delta w}}{k_s}<100 \\
u_\delta &= 0.75\left(\frac{U_{\delta,w}^2}{c}\right) && for\, \frac{A_{\delta w}}{k_s}\geq 100 \\
u_\delta &= -\left(\frac{U_{\delta,w}^2}{c}\right) && for\, \frac{A_{\delta w}}{k_s}\leq 1
\end{aligned}
\tag{3.4.2}
$$

This expression yields:

$u_\delta=\ 0.75(U_{\delta,w})^2/c$	for $A_{\delta,w}/k_{s,w}\geq 100$
$u_\delta=\ 0$	for $A_{\delta,w}/k_{s,w}=13.9$
$u_\delta=-0.125(U_{\delta,w})^2/c$	for $A_{\delta,w}/k_{s,w}=10$
$u_\delta=\ -(U_{\delta,w})^2/c$	for $A_{\delta,w}/k_{s,w}=1$

The data of **Davies and Villaret (1999)** and Eq. (3.4.2) are shown in Figure 3.4.6. Two additional data points related to the flume tests of **Klopman (1994),** four data points related to the Delta flume tests of **Chung and Grasmeijer (1999)** and four data points related to related to small-scale flume experiments of **Grasmeijer-Van Rijn (1999)** are also shown. These latter three experiments are described below.

The data points related to the relatively strong negative streaming values for relatively large roughness values *($A_{\delta,w}/k_{s,w}<1$)* are based on experimental results with rather steep, artificial triangular 2D-ripples (Mathisen and Madsen, 1996a,b). The data points related to these artificial ripples have not been taken into account to derive expression (3.4.2), as this latter type of ripples do not represent natural (more rounded) sand ripples. The maximum negative velocity is assumed to be of the order of $\frac{-U_{\delta,w}{}^2}{c}$.

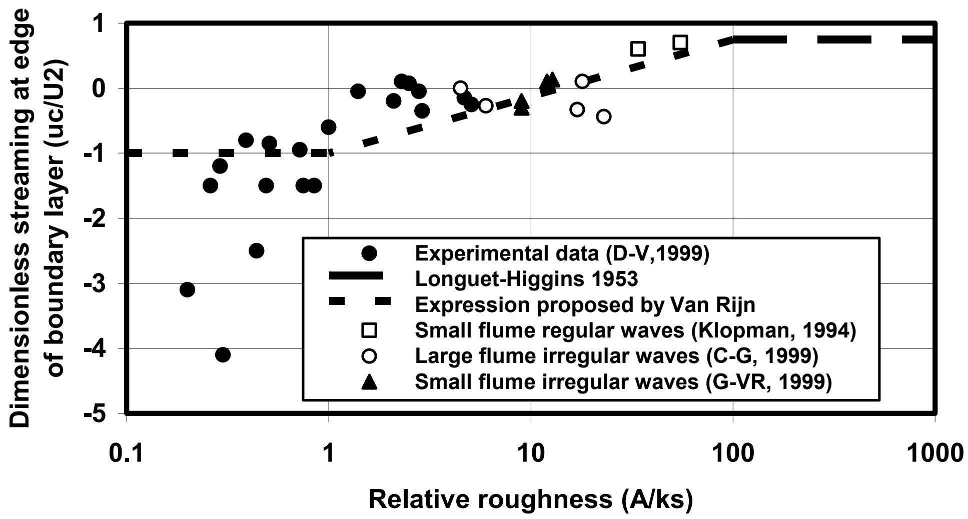

Figure 3.4.6 *Streaming velocity ($u_{\delta c}/(U_{\delta w})^2$) at edge of wave boundary layer as function of relative roughness ($A_{\delta,w}/k_{s,w}$)*

Finally, it is noted that the determination of the residual streaming at the edge of the wave boundary from datasets of wave tanks and flumes is rather tricky, as the data will always include the near-bed return flow due to the onshore mass fluxes in the upper part of the water depth, whereas the near-bed streaming velocities of interest are boundary layer effects to be separated from the return flow related to mass fluxes higher up in the water depth. The streaming velocity values at the edge of the wave boundary layer given by **Davies and Villaret (1999)** are based on the implicit assumption that boundary layer processes are dominant in the near-bed region. This assumption was made on the basis of an experimental verification of this particular point by **Mathisen and Madsen (1996)**.

Hereafter, measured streaming velocity profiles of **Bijker et al. (1974)**, **Klopman (1994), Mathisen and Madsen (1996a,b)** and **Chung and Grasmeijer (1999)** are shown in Figures 3.4.7 to 3.4.14.

Bijker et al. (1974) have performed flume experiments on the mass transport on a sloping bottom. Three different rigid beach slopes were applied (1 to 10; 1 to 25 and 1 to 40; water depth upwave of beach =0.45 m). The bottom roughness consisted of concrete, glued sand grains (1.6 to 2 mm) and artificial ripples (height=0.018 m; length=0.08 m). The mass transport velocities (Lagrangian + Eulerian) were determined by filming the displacement of small rigid particles (diameter of 5 mm) with about the same density as water. In all experiments the amplitude of the free second harmonic component did not exceed 10% of the value of the first harmonic component (Second order Stokes waves). The results are given in Figure 3.4.7.

- smooth and rough bottom: onshore-directed streaming in the near-bed region and near-surface region; offshore-directed streaming in middle of depth; streaming in near-bed region is smaller above a rough bottom; the onshore-directed near-bed streaming decreases slightly with increasing beach slope above a smooth bottom;
- very rough rippled bottom; the initially forward streaming in the near-bed region of the horizontal section is reduced to about zero in the sloping section.

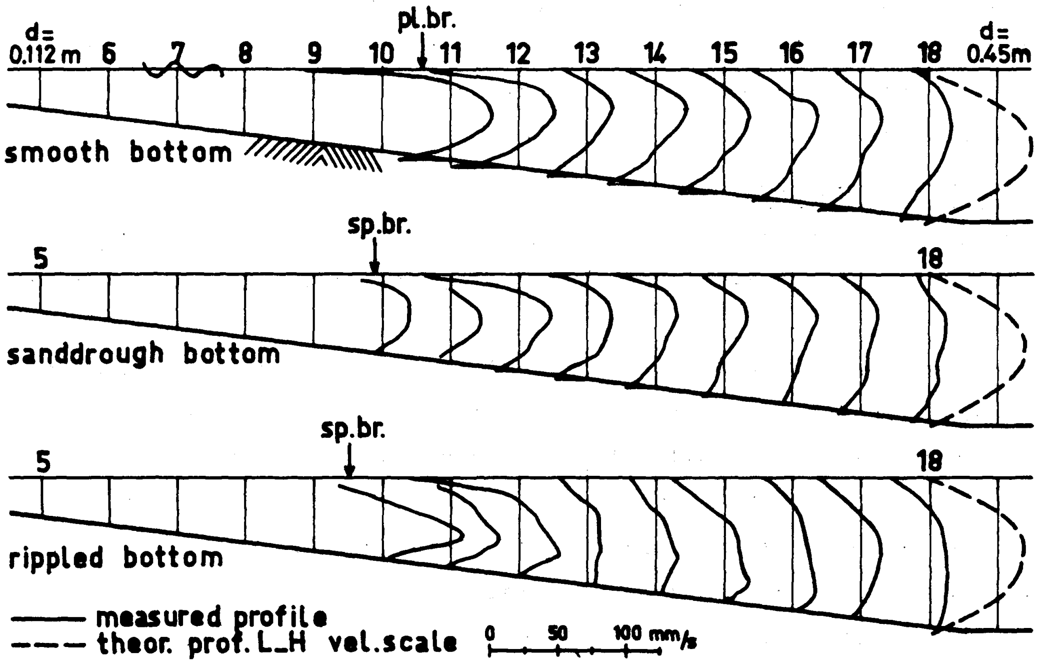

Figure 3.4.7 *Measured streaming velocities above a sloping beach of 1 to 25; bottom of smooth concrete, sand grains and artificial ripples (Bijker et al, 1974)*

Klopman (1994) performed a detailed experimental flume study of wave-induced streaming in non-breaking waves over both plane and sloping bottoms by using Laser-Doppler velocimetry. Monochromatic and random waves were generated. Active wave absorption boards were used to eliminate wave reflection and resonance. The flume bottom consisted of gravel particles (0.002 m) with an effective Nikuradse roughness of 0.0012 m. The relative bed roughness is in the range of $A_{\delta,w}/k_{s,w}$=30 to 100. The thickness of the wave boundary layer is about 5 to 15 mm. Figure 3.4.8 shows the mean horizontal velocities over a horizontal and a sloping bottom, as measured by Klopman.

In case of monochromatic waves over a horizontal bottom the wave-induced streaming shows maximum values of about 0.01 m/s in the wave propagation direction (approx. 6% of peak orbital velocity of $U_{\delta,w}$=0.18 m/s; $A_{\delta,w}$=0.041 m; c=1.9 m/s; L=2.7 m). The dimensionless streaming is $u_\delta=+0.6(U_\delta)^2/c$ for $A_{\delta,w}/k_{s,w}$=35. The thickness of the layer with wave-induced streaming is about 20 mm which is about 4 times the wave boundary layer thickness. Above the streaming layer a return flow layer balancing the mean mass-flux between the wave trough and crest can be observed.

In case of random waves over a horizontal bottom maximum streaming velocities of about 0.015 to 0.02 m/s can be observed; the thickness of the streaming layer shows a significant increase to about 0.1 m. The dimensionless streaming is $u_\delta=+0.7(U_{\delta,w})^2/c$ for $A_{\delta,w}/k_{s,w}$=55 ($U_{\delta,w}$=0.24 m/s; $A_{\delta,w}$=0.065 m; c=1.95 m/s; L=3.3).

In case of monochromatic and random waves (non-breaking) over a plane sloping bottom the maximum streaming velocities are smaller (0.009 to 0.004 m/s). The layer thickness is about 0.01 m which is considerably smaller than that in case of a horizontal bottom. As the relative wave heights were quite high (0.39 to 0.51) in these latter two tests, the near-bed streaming may have been affected by the return flow associated with onshore mass flux near the water surface.

The experimental results of **Klopman (1994)** show the presence of onshore-directed wave-induced streaming velocities near the bed similar to those above smooth plane beds as explained by the theoretical results of **Longuet-Higgins (1953)** and also verified by various datasets for smooth bed. The magnitude of the wave-induced streaming above a rough bed is overestimated (factor 2) by the theoretical results of Longuet-Higgins (see Figure 3.4.8).

Grasmeijer and Van Rijn (1999) performed various experiments in a small flume above a test section comprising of fine sand of about 0.1 mm. The water depth varied between 0.6 and 0.3 m due to the presence of a triangular sand bar. The wave period is 2.3 s. The ripple height is about Δ_r=0.007 to 0.01 m; the ripple length is about λ_r=0.045 m. The effective bed roughness is assumed to be about k_s=1 to 2Δ_r.

Offshore-directed near-bed velocities (at about 0.02 m above the mean bed) were measured in Profiles 3 and 6 (section with non-breaking waves).
Profile 1: h=0.6 m, H_s=0.19 m, $A_{\delta,w}$=0.12 m, $U_{\delta,w}$=0.32 m/s, c=2.2 m/s, u_δ=-0.015 m/s,
Profile 3: h=0.6 m, H_s=0.19 m, $A_{\delta,w}$=0.12 m, $U_{\delta,w}$=0.32 m/s, c=2.2 m/s, u_δ=-0.01 m/s.

Onshore near-bed velocities (at about 0.02 m above the mean bed) were measured in Profiles 17 and 20 (section with non-breaking waves).
Profile 17: h=0.45 m, H_s=0.15 m, $A_{\delta,w}$=0.11 m, $U_{\delta,w}$=0.31 m/s, c= 1.95 m/s, u_δ=+0.006 m/s,
Profile 20: h=0.40 m, H_s=0.15 m, $A_{\delta,w}$=0.11 m, $U_{\delta,w}$=0.33 m/s, c=1.9 m/s, u_δ=+0.008 m/s.

The relative roughness values are in the range of $A_{\delta,w}/k_{s,w}$= 6 to 16; the dimensionless streaming velocities are in the range of $u_\delta c/(U_{\delta,w})^2$= -0.3 to 0.12 and fit the other data well (Figure 3.4.6).

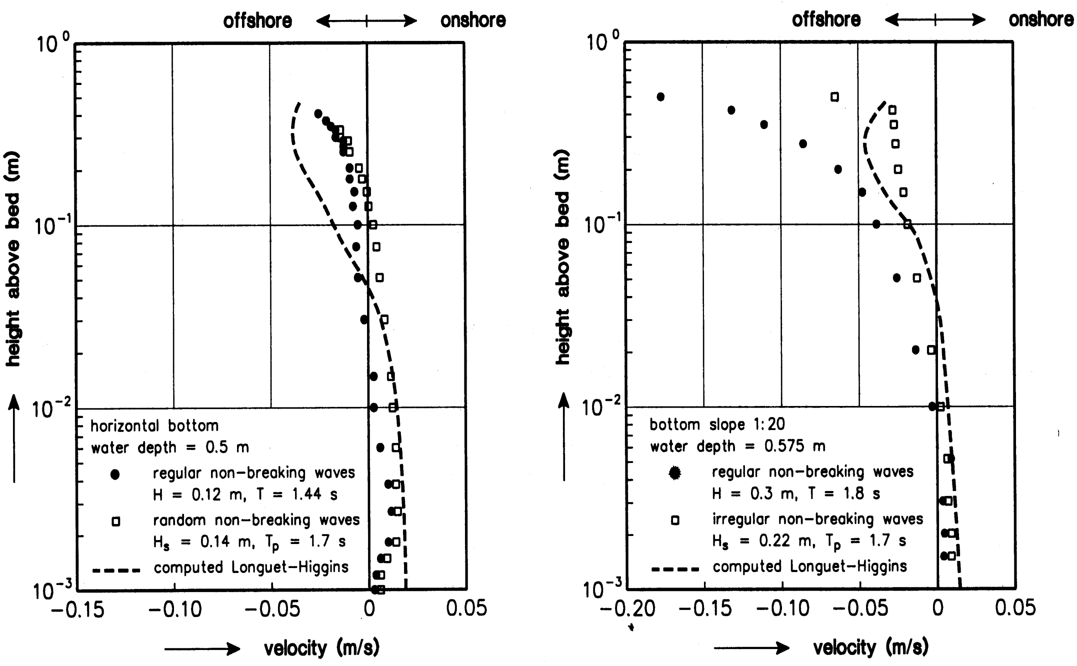

Figure 3.4.8 *Measured wave-induced streaming velocities in near-bed region based on tests in small-scale wave flume (Klopman, 1994);*
Left: regular and irregular waves over plane bottom
Right: regular and irregular waves over sloping bottom

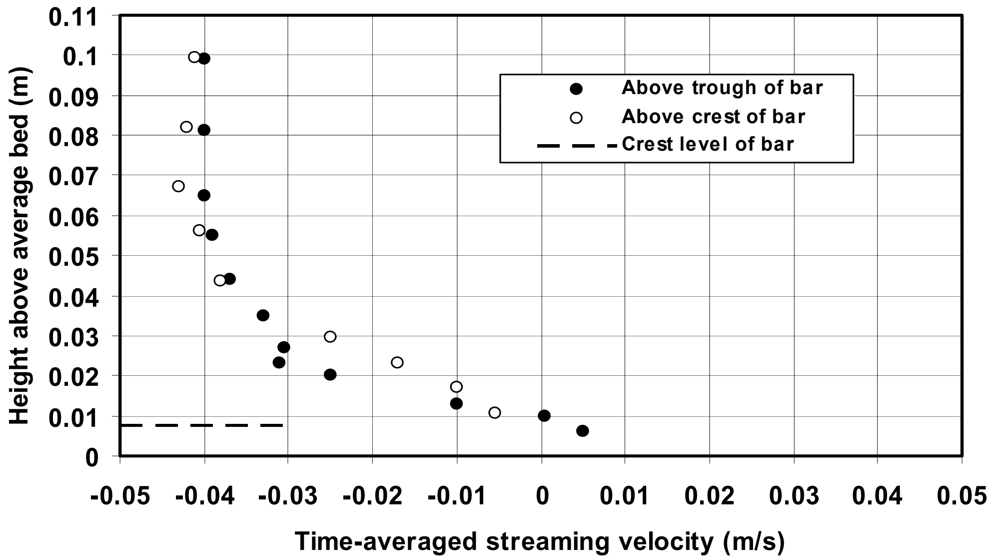

Figure 3.4.9 *Measured wave-induced streaming velocities in near-bed region based on tests in small-scale wave flume with fixed triangular bars; H=0.106 m, h=0.6 m (Mathisen-Madsen, 1996a,b)*

Mathisen and Madsen (1996a,b) performed various experiments in a 28 m long flume above a test section comprising transverse 2D triangular bars with a height of 0.015 m and a spacing of 0.1 m. The water depth was 0.6 m. The results of experiment MMc are shown in Figure 3.4.9. The wave period is 2.89 s. The wave height is 0.106 m. The peak orbital velocity is 0.193 m/s. Other parameters are: $A_{\delta,w}$= 0.089 m, B=0.177, kh=0.57, $c/U_{\delta,w}$=12.

Eulerian streaming profiles were measured above both crests and troughs of the bars. The effective equivalent roughness of the triangular bars was determined from experiments involving currents alone resulting in $k_{s,c}=k_{s,w}=0.213$ m for the bar spacing of 0.1 m, yielding $A_{\delta,w}/k_{s,w}=5.2$. The thickness of the wave boundary layer is estimated to be 0.062 m.

Chung and Grasmeijer (1999) analysed measured velocities of experiments performed in the large-scale Delta flume (length=200 m, depth= 7 m, width=5 m) of Delft Hydraulics. The experiments are described in detail in Section 3.3.2. The experimental conditions (ripple regime) are given in Table 3.4.1. The relative bed roughness ($A_{\delta,w}/k_{s,w}$) is in the range of 5 to 20. The bed roughness of Test 1A and 1B is assumed to be 0.05 to 0.1 m ($1\Delta_r$ to $2\Delta_r$). The bed roughness of Tests 1C to 1E is assumed to be 0.015 to 0.025 m ($0.5\Delta_r$). Tests 1A and 1B seem to be vortex ripples of height 0.05 m, and so a wave boundary layer thickness of 0.1 m or so is expected. The other data for fine sand (1C, 1D, 1E) produces relatively long low ripples outside the vortex regime. The wave boundary layer thickness is estimated to be about 0.05 m. The measured streaming velocities are shown in Figures 3.4.10 to 3.4.14. The velocities in the region with z>0.4 m most likely represent the return velocities due to the onshore mass flux in the upper part of the water depth. The streaming velocities show small positive values at a level of about 0.2 m above the bed (Tests 1A, 1B, 1D and 1E). Below this level of 0.2 m the streaming velocities show a strong tendency to become negative at levels closer to the bed. These velocity profile values represent local profile data measured at arbitrary positions with respect to the movable ripple crests. As the average values represent the data from 7 to 9 repeated measurements at different positions along the ripple (ripples were moving), these values are assumed to represent horizontally-averaged values.

Source	Test	h m	H_S m	T_P s	$U_{w,on}$ m/s	$U_{w,off}$ m/s	u_δ m/s	d_{50} mm	d_{90} mm	Δ_b m	λ_b m	$q_{s,c}$ kg/s/m	Te °C
Chung and	1A (Set I)	4.55	1	5	0.4	0.36	0.005 to -0.005	0.33	0.7	0.05	0.25	-0.00004	15
Grasmeijer	1B (set II)	4.55	1.25	5	0.5	0.45	0 to -0.02	0.33	0.7	0.05	0.25	-0.0011	15
1999	1C (set III)	4.50	1	5	0.46	0.42	-0.01 to -0.02	0.16	0.3	0.03	0.7	-0.0016	15
	1D (Set IV)	4.50	1.25	5	0.55	0.5	-0.01 to -0.02	0.16	0.3	0.05	0.75	-0.003	15
	1E (Set V)	4.50	1.5	5	0.58	0.53	0.01 to 0	0.16	0.3	0.05	0.75	-0.0022	15

h = water depth, H_s = significant wave height, T_P = peak wave period
$q_{s,c}$ = current-related (high freq.) suspended sand transport (- offshore, + onshore)
Δ_b = bed form height (pl= plane bed), λ_b = bed form length, Te= temperature (Celsius)

Table 3.4.1 *Summary of streaming-related suspended sand transport data for large-scale wave tank (Delta flume of Delft Hydraulics)*

The results of Test 1E are not reliable in this sense because only three repetition-tests have been done, whereas the other test are based on 7 to 9 repetition-tests. The streaming velocities at the edge of the wave boundary layer (roughly at 0.10 m above the mean bed) are estimated to be in the range of 0.005 to -0.02 m/s in Tests 1A, 1B, 1C, 1D and 1E. These results can be roughly approximated by:

- Test 1A and 1B: $u_\delta \cong 0$ to $-0.3(U_{\delta,w})^2/c$ for $A_{\delta,w}/k_{s,w}$= 4.5 and 6 ($U_{\delta,w}$=0.4 to 0.5 m/s, c=6 m/s and $k_{s,w}$=1 to 2 Δ_r);
- Test 1C, 1D and 1E: $u_\delta \cong -0.5(U_{\delta,w})^2/c$ to $+0.1(U_{\delta,w})^2/c$ for $A_{\delta,w}/k_{s,w}$= 23, 17 and 18 ($U_{\delta,w}$=0.45 to 0.55 m/s, c=6 m/s and $k_{s,w}$=0.5Δ_r).

These results are plotted in Figure 3.4.6.

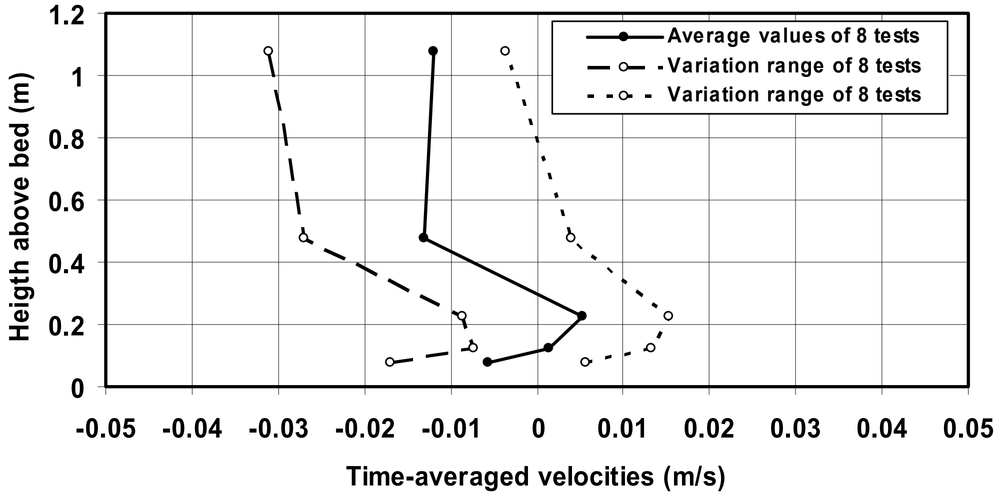

Figure 3.4.10 *Measured streaming velocities (D-flume); H_s=1 m; d_{50}=0.33 mm; Case 1A*

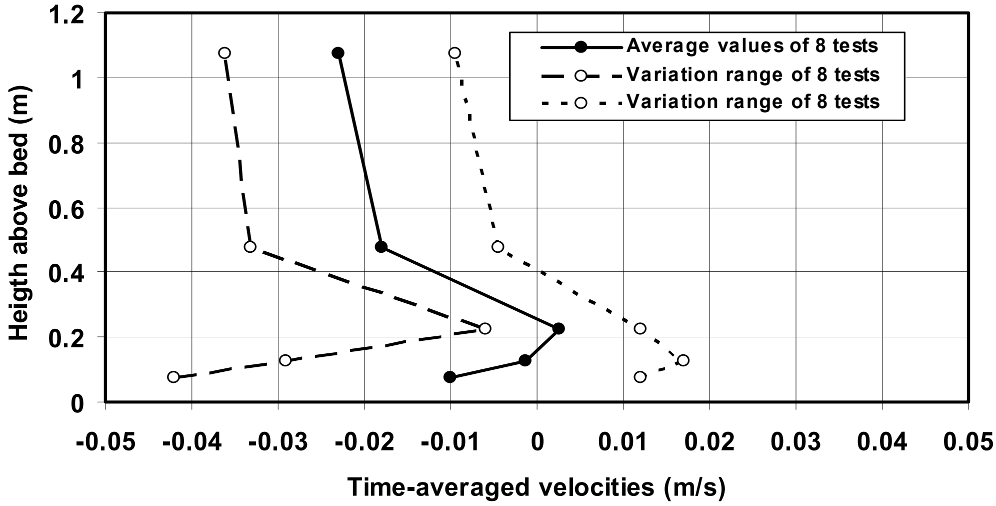

Figure 3.4.11 *Measured streaming velocities (D-flume); H_s=1.25 m;d_{50}=0.33 mm; Case 1B*

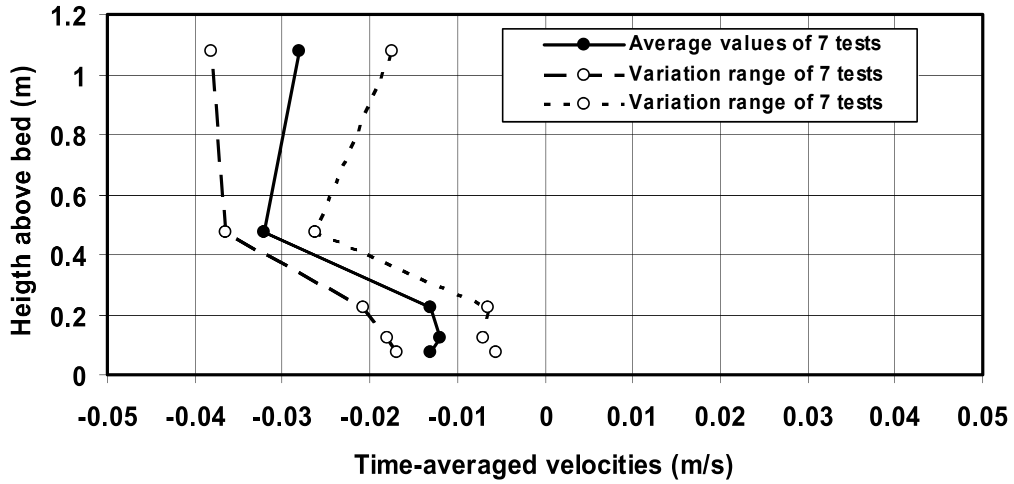

Figure 3.4.12 *Measured streaming velocities (D-flume); H_s=1.0 m; d_{50}=0.16 mm; Case 1C*

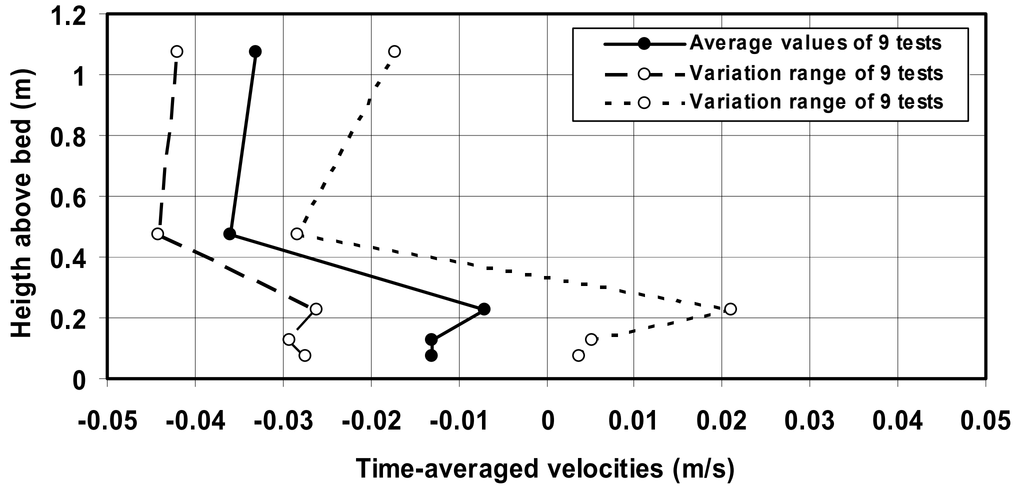

Figure 3.4.13 *Measured streaming velocities (D-flume); H_s=1.25 m; d_{50}=0.16 mm; Case 1D*

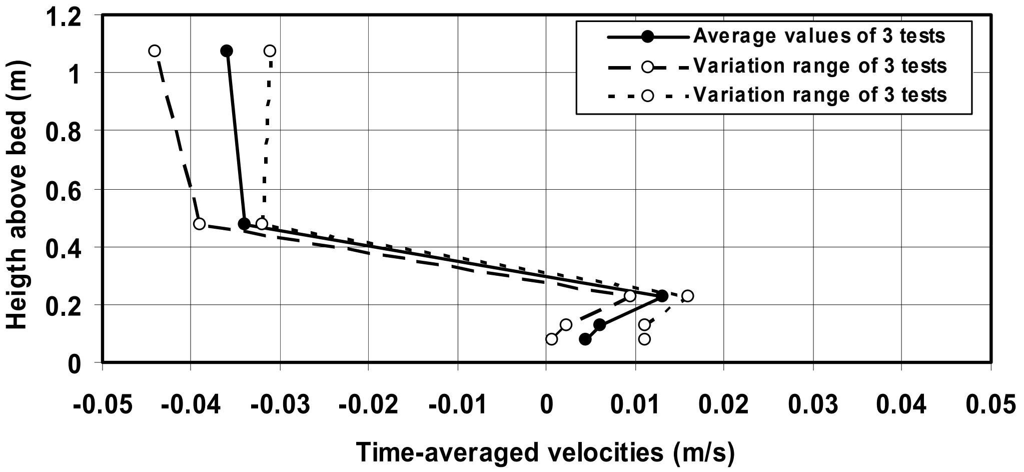

Figure 3.4.14 *Measured streaming velocities (D-flume); H_s=1.50 m; d_{50}=0.16 mm; Case 1E*

3.4.3 Modelling of Eulerian streaming in DELFT3D

As described in **Walstra et al. (2000)** Eulerian streaming is accounted for in DELFT3D by imposing a phase-averaged shear stress on the water column in wave boundary layer. This phase-averaged shear stress is based on the wave bottom dissipation (D_f) and is assumed to decrease linearly to zero across the wave boundary layer (**Fredsøe and Deigaard, 1992**):

$$\frac{\partial}{\partial x_j}\left(\overline{\tilde{u}\tilde{w}}\right) = -\frac{1}{\delta}\frac{D_f}{c} \tag{3.4.3}$$

where c is the phase velocity and D_f, the dissipation due to bottom friction, is written as:

$$D_f = \frac{1}{2\sqrt{\pi}}\rho f_w U_{\delta,w}{}^3 \tag{3.4.4}$$

where $U_{\delta,w}$ is the orbital velocity near the bed based on linear theory with the root mean square wave height and f_w is the friction factor according to **Soulsby et al. (1993)**. The additional shear stress due to streaming decreases linearly to zero across the wave boundary layer (see also Figure 3.4.15):

$$\tau_{str}\left(z`\right) = \frac{D_f}{c}\left(1-\frac{d+\overline{\zeta}-z`}{\delta}\right) \; for \; d+\overline{\zeta}-\delta \le z` \le d+\overline{\zeta} \tag{3.4.5}$$

In fact, streaming is modelled in the same way as the forces breaking waves exert on the top of the water column (again see Figure 3.4.15).

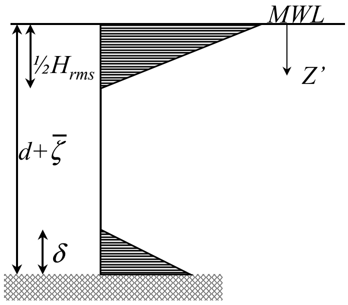

Figure 3.4.15 *Vertical distribution of shear stresses due to wave breaking and Eulerian streaming.*

Furthermore, DELFT3D is solved in a GLM reference frame which implies that the Lagrangian drift should be taken into account to obtain Eulerian velocities, see Section 2.1. This is achieved by subtracting the Lagrangian (Stokes) drift from the GLM velocities. In a 3D model this approach offers the opportunity to take account of the vertical structure of the Stokes drift. The effects of these implementations are highlighted in Figure 3.4.16 where the model is applied on one the **Klopman (1994)** experiments.

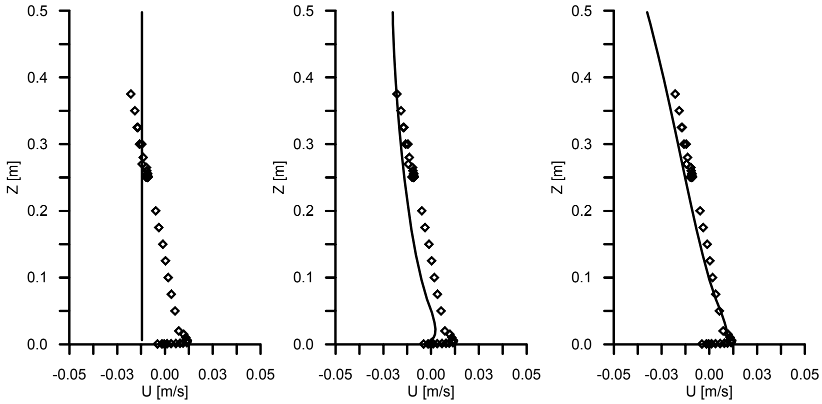

Figure 3.4.16 *Comparison of model (solid) with measurements (symbols); left: uniform mass flux no Eulerian streaming, middle: uniform mass flux with Eulerian streaming included, right: non-uniform mass flux with Eulerian streaming included.*

In Figure 3.4.16 the model is compared with measurements for the case with waves only. The left graph shows the model results if a uniform mass flux is applied and Eulerian streaming effects are excluded. Because the equations are solved for GLM velocities, which are corrected to Eulerian velocities at the bottom to determine the bottom shear stress, the wave motion induces no (wave-averaged) bottom shear stress. A significant improvement can already be seen in the middle graph when the Eulerian streaming effect is included. In the graph on the right hand side the 2^{nd} order analytical expression for the Stokes drift is used to convert the GLM velocities back to Eulerian velocities. The computed velocity profile now compares well with the measurements. In the lower part of the water column the correspondence is excellent. In the upper part some deviations can be observed.

Although this approach has not yet been verified extensively it seems to give velocities of the right order of magnitude. A major drawback of this approach is that it can only be applied for relative roughness values ($A_{\delta,w}/k_{s,w}$) larger than about 20-50 because velocities opposing the wave propagation direction can not be accounted for.

3.4.4 Sand transport associated with wave-induced streaming in the near-bed region

The wave-induced streaming velocities in the near-bed region will have substantial effect on the sand transport processes in the near-bed region. **Chung and Grasmeijer (1999)** determined the suspended load transport associated with the measured streaming velocities in the near-bed region. Their results are presented in Table 3.4.1. The suspended transport values associated with the streaming velocities are somewhat smaller than those associated with the asymmetrical orbital velocities presented in Table 3.3.2, but they can not be neglected.
Herein, it is proposed to correct the wave-related suspended transport component according to Eq. (3.3.1) by including the streaming velocity at the edge of the wave boundary layer, as follows:

$$q_{s,w} = \gamma \left(\frac{U_{on}^4 - U_{off}^4}{U_{on}^3 + U_{off}^3} + u_\delta \right) \int c dz \qquad (3.4.6)$$

with: $U_{on}=U_{\delta,f}$= near-bed peak orbital velocity in onshore direction (in wave direction) and $U_{off}=U_{\delta,b}$= near-bed peak orbital velocity in offshore direction (against wave direction), u_δ= wave-induced streaming at edge of wave boundary layer based on Eq. (3.4.2), c= time-averaged concentration and γ= phase lag function.

The wave-related suspended transport will be larger for positive values of u_δ and smaller for negative values of u_δ. Similarly, the bed load transport in the wave boundary layer just above the bed can be corrected by adding the streaming velocity to the instantaneous velocity vector. The (current-related) suspended load transport related to the near-bed return flow (u_r) due to onshore mass flux in the upper part of the water depth should be taken into account separately ($q_{s,c}=\int(u_r c)dz$).

3.4.5 Sensitivity computation results related to streaming velocity and bed roughness

The effect of the streaming velocity and bed roughness on cross-shore bed load transport and cross-shore wave-related suspended transport based on the TRANSPOR model is shown in Figures 3.4.17 and 3.4.18 for an example case. The water depth is assumed to be 15 m. The wave heights are in the range of 1 to 6 m. The shore-parallel tidal current is assumed to be 0.7 m/s. The angle between the current and wave direction is 90^o. The bed material is assumed to be sand with d_{50}=0.2 mm and d_{90}=0.3 mm; d_s=0.2 mm. Other parameters are: temperature= 15^o C and salinity=30 promille.

The grain roughness was set to $k_s=1d_{90}$ and the modified wave-current friction factor ($f_{cw\text{-}modified}$) was used. Tables 3.4.2, 3.4.3 and 3.4.4 present the computed values of the bed load transport and the wave-related suspended load transport for different approaches of the streaming velocity and bed roughness.

The effect of variable bed roughness (k_s-values in range of 0.0156 and 0.004 m) on the streaming velocity is presented in Figure 3.4.17Bottom, showing values up to 0.18 m/s. The streaming has a small negative value (against the wave propagation direction) for a wave height of 1 m. The streaming values are smaller for larger bed roughness values (k_s=0.03 m). The streaming is not affected by bed roughness for wave heights of 5 and 6 m.

The effect of variable bed roughness and variable streaming on the bed load transport and wave-related suspended transport is shown in Figure 3.4.17Top and 3.4.17Middle. Both transport rates are negative for a wave height of 1 m, if the streaming velocity is included and positive if the streaming is excluded. The bed load transport is significantly larger (factor 2 to 3), if the streaming is included. The bed form roughness has not much effect on the bed-load transport, since this latter parameter is mainly affected by grain roughness (Figure 3.4.17Top). The bed form roughness only has a weak effect on the near-bed velocity profile of the tidal current and, hence, on the bed shear stress and bed load transport.

The effect of variable streaming on the wave-related suspended transport is relatively small (10% to 20%). The suspended transport is larger if the streaming is included.

H_s (m)	T_p (s)	$k_{s,w}$; $k_{s,c}$ (m)	u_δ (m/s)	q_b (kg/s/m)	$q_{s,w}$ (kg/s/m)
1	5	0.03; 0.03	-0.0005	-0.00014	-0.0000002
2	6	0.03; 0.03	0.0024	0.0003	0.00034
3	7	0.03; 0.03	0.021	0.0053	0.0067
4	8	0.03; 0.03	0.065	0.0291	0.046
5	9	0.03; 0.03	0.121	0.0874	0.172
6	10	0.03; 0.03	0.181	0.187	0.447

Table 3.4.2 *Computed bed load and wave-related suspended transport; depth=15 m; Streaming velocity according to Equation (3.4.2); Bed roughness=constant= 0.03 m*

H_s (m)	T_p (s)	$k_{s,w}$; $k_{s,c}$ (m)	u_δ (m/s)	q_b (kg/s/m)	$q_{s,w}$ (kg/s/m)
1	5	0.03; 0.03	0	0.00000041	0.0000003
2	6	0.03; 0.03	0	0.00013	0.00029
3	7	0.03; 0.03	0	0.002	0.0054
4	8	0.03; 0.03	0	0.011	0.037
5	9	0.03; 0.03	0	0.036	0.142
6	10	0.03; 0.03	0	0.081	0.376

Table 3.4.3 *Computed bed load and wave-related suspended transport; depth=15 m; Streaming velocity=0; Bed roughness=constant= 0.03 m*

H_s (m)	T_p (s)	$k_{s,w}$; $k_{s,c}$ (m)	u_δ (m/s)	q_b (kg/s/m)	$q_{s,w}$ (kg/s/m)
1	5	0.0156; 0.069	-0.00014	-0.0000032	-0.00000016
2	6	0.0106; 0.039	0.0077	0.00074	0.000114
3	7	0.004; 0.004	0.033	0.0064	0.0022
4	8	0.004; 0.004	0.071	0.029	0.0154
5	9	0.004; 0.004	0.121	0.083	0.074
6	10	0.004; 0.004	0.181	0.179	0.222

Table 3.4.4 *Computed bed load and wave-related suspended transport; depth=15 m; Streaming velocity according to Equation (3.4.2); Bed roughness according to Equations ((3.1.9), (3.1.10), (3.1.12) and (3.1.14))*

The effect of variable bed roughness is relatively large (factor 2). The suspended transport is largest for a constant bed roughness of 0.03 m, because the sand concentrations are much larger for a constant bed roughness of 0.03 m compared with a variable bed roughness (values between 0.016 and 0.004 m).

Figure 3.4.18 shows a comparison of the bed load transport and the wave-related suspended transport. The suspended transport is dominant for a constant bed roughness ($k_{s,c}$=$k_{s,w}$=0.03 m). The bed load transport is slightly dominant for a variable bed roughness.

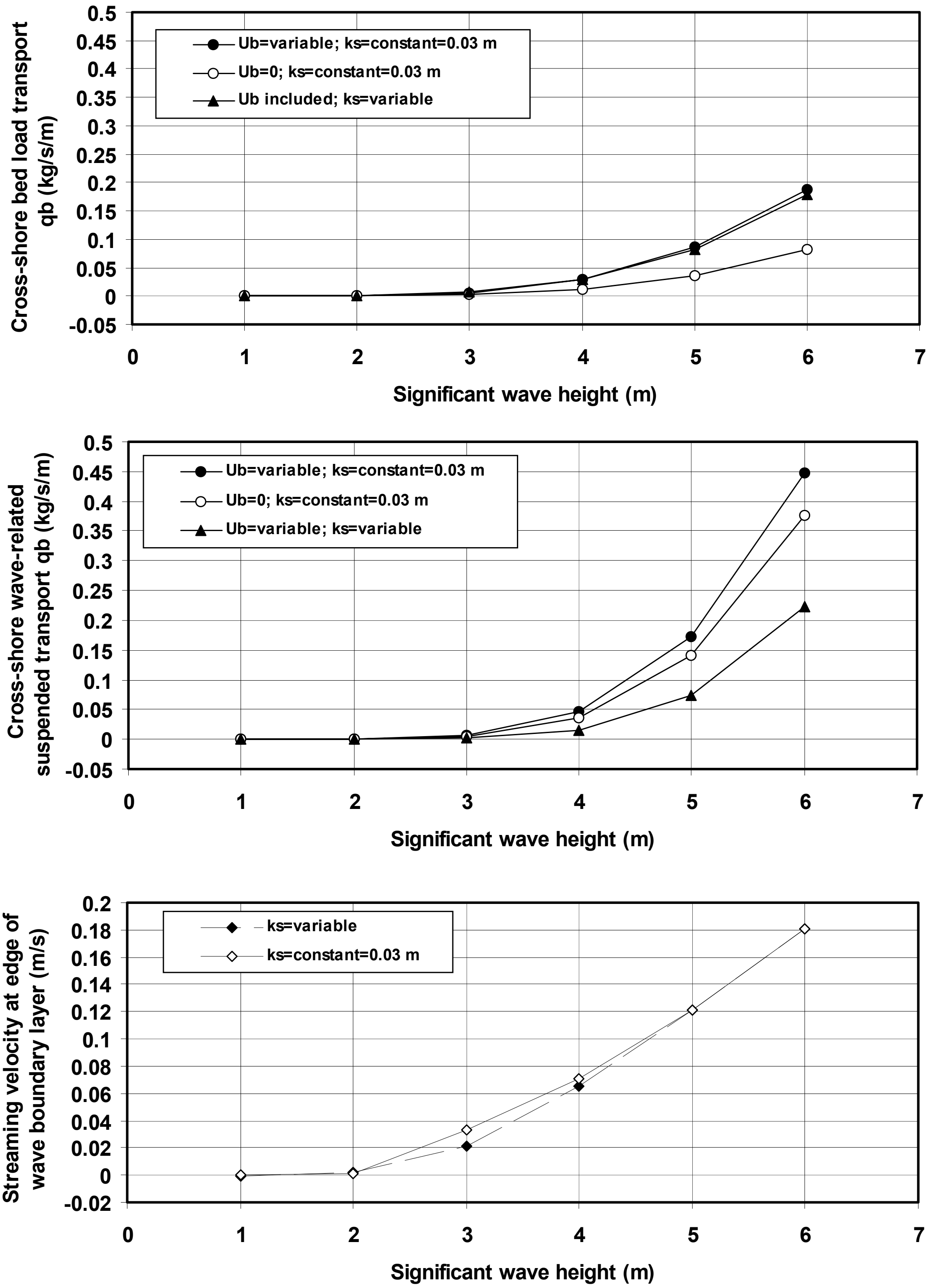

Figure 3.4.17 *Effect of near-bed streaming and bed roughness on bed load transport and wave-related suspended load transport*
Top: Cross-shore bed load transport
Middle: Cross-shore wave-related suspended load transport
Bottom: Streaming velocity

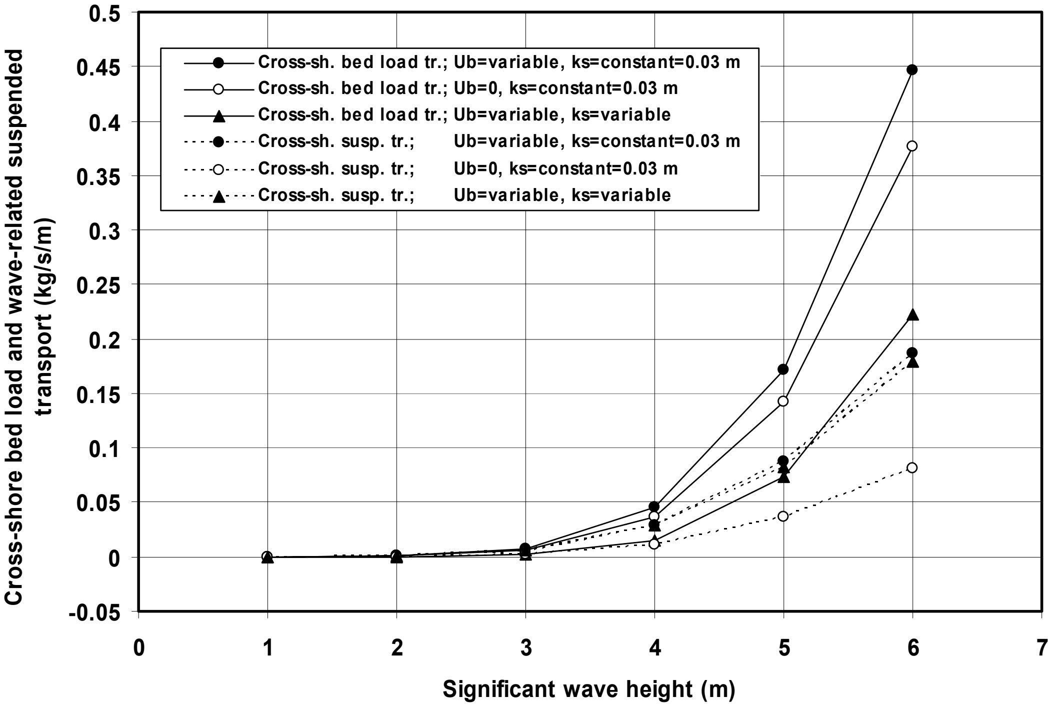

Figure 3.4.18 Effect of near-bed streaming and bed roughness on bed load transport and wave-related suspended load transport

4 Application and Verification of TRANSPOR2000 in deep water conditions

4.1 Introduction

In this chapter Van Rijn's TR1993 and TR2000 engineering sand transport formulations are applied to deep water conditions to investigate the influence of wave angles, to determine the residual transports at 20 m water and to validate the upgraded DELFT3D-ONLINE model.

In Section 4.2, sand transport is calculated at a depth of 10 m using the SUTRENCH93 and SUTRENCH2000 formulations. In Section 4.3 the net yearly-averaged sand transport is calculated at a depth of 20 m using both the TRANSPOR93 and TRANSPOR2000 formulations, which have been incorporated in UNIBEST-TC Version 2.04 and 2.10, respectively. In Section 4.4, the upgraded DELFT3D-ONLINE model is verified. This verification aims to illustrate the performance of the TR2000 formulation in DELFT3D and the application of the various other transport formulas which have been included in the upgraded DELFT3D-ONLINE version.

4.2 Effect of various parameters on sand transport in deep water

4.2.1 Introduction

In **Walstra et al. (2002b)** it was shown that the total sediment transport calculated with SUTRENCH93 is very sensitive to the angle between waves and currents. They stated that: *"The incident wave angles severely influence transports. The magnitude of the bedload transport can vary a factor 10, and can even switch sign. Moreover, the reactions of the suspended transports are not in accordance with the latest knowledge developments. It can be concluded that the bedload and suspended transport relations in Sutrench require further examination with respect to the wave angle.*" In the referred study it was outside the scope to perform a more detailed investigation. However a recommendation was given to further investigate the behaviour of SUTRENCH regarding the sensitivity for the incident wave angle. It is noted that the water depth for the calculations in **Walstra et al. (2002b)** is 10 m. This section follows up on this recommendation. As a first step the implemented formulations in the SUTRENCH model are reviewed in detail. Next, the simulations as carried out in **Walstra et al. (2002b)** are rerun as a check. Based on these two steps some conclusions are drawn.

4.2.2 Results

Contribution of waves

A number of simulations were executed in debugging mode, enabling a close monitoring of the parameter values during the calculations. Using a wave period of T_p = 6.8 s and a significant wave height of H_s = 2.35 m, this results in a near-bed peak orbital velocity of 0.82 m/s (at edge of the wave boundary layer) at a water depth of 10 m according to:

$$\hat{U}_\delta = \frac{\pi H_s}{T_p' \sinh\left(2\pi h / L'\right)} \tag{4.2.1}$$

At a water depth of 20 m, the near-bed peak orbital velocity is 0.36 m/s using the same wave condition.

Contribution of tide

The wave contribution should be compared with the tidal contribution. At a water depth of 10 m, the depth-averaged tidal peak velocity is v_R = 0.6 m/s for the case described in **Walstra et al. (2002b)**. At a depth of 20 m, the tidal peak velocity is v_R = 0.7 m/s.

According to the formulations of **Van Rijn (1993),** (Appendix A), the bed load transport is evaluated at a level δ, which is the maximum of $3\delta_w$ (with δ_w= the wave boundary layer thickness) and $k_{s,c}$ (=the current-related roughness). Thus: $\delta = \max(3\delta_w, k_{s,c})$, where

$$\delta_w = 0.072 \hat{A}_\delta \left(\hat{A}_\delta / k_{s,w} \right)^{-0.25} \tag{4.2.2}$$

For the applicable conditions, δ is typically about 0.05 m. Subsequently, the current velocity at this level is evaluated according to

$$v_{R,\delta} = \frac{\overline{v}_R \ln\left(30\delta / k_a\right)}{-1 + \ln\left(30h / k_a\right)} \tag{4.2.3}$$

where v_R is the depth-averaged tidal velocity and k_a is the apparent bed roughness, which is typically about 0.5 m for the conditions applied. This high value is caused by the interaction between waves and current. As a result, the tidal velocity at level δ is well into the current boundary layer and is much reduced compared to the value outside the boundary layer. Typically, $v_{R,\delta}$ = 0.12 m/s at a water depth of 10 m and 0.22 m/s at 20 m.

In the SUTRENCH-model the wave and tidal contributions are added, taking into account the angle between the two directions. Based on the presented analysis, which has shown that the peak orbital velocities can be of the same order of magnitude as the tidal currents, it seems logical that at a depth of 10 m the computed sediment transport rates are very sensitive to the wave angle. Even at a depth of 20 m, a strong dependency remains.

Results on total sediment transport for the case described in **Walstra et al. (2002b)** are shown in **Figure 4.2.1**.

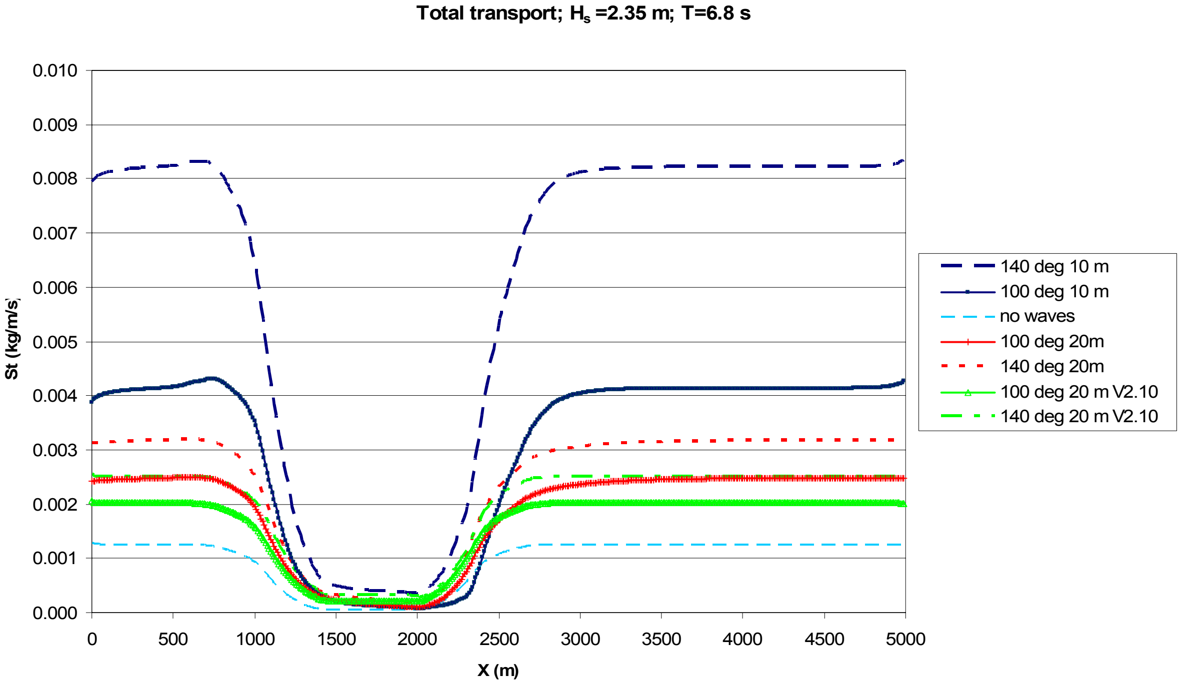

Figure 4.2.1 *Total transport calculated along a trench with SUTRENCH93 and SUTRENCH2000.*
Significant wave height=2.35 m; wave period=6.8 s.
Angle between waves and current=100 and 140 deg.;
water depth=10 m (SUTRENCH93) and 20 m (SUTRENCH93 and 2000).
Total transport based on SUTRENCH93 for current only case (no waves)

4.2.3 Conclusions

The sensitivity of sediment transport calculated by SUTRENCH93 and SUTRENCH2000 to the angle between waves and currents can be well explained with the formulations used in this model. If this sensitivity is not observed in measurements under similar conditions, it is recommended to improve the formulations used in Sutrench. However, this is beyond the scope of this study.

4.3 Net sand transport rates

4.3.1 Introduction

In **Van Rijn (1995)** the yearly-averaged sand transport rates at the -20 and -8 m NAP depth contours of the Jarkus-profiles 14, 40, 76 and 103 are presented.

Using the same forcing, the yearly-averaged sand transport rates at the -20 m NAP depth contours of the Jarkus-profile 76 (Noordwijk) are recalculated in the present study using the UNIBEST-TC model which contains formulations for wave- and current-driven sand transport (TR1993 and TR2000 are included in UNIBEST-TC Versions 2.04 and 2.10, respectively).

Similarities and differences between the present and 1995 calculations are subsequently discussed.

4.3.2 Method

4.3.2.1 Forcing

The forcing applied for the present calculations is identical to that applied in the **Van Rijn (1995)** study. Wave height and wind velocity data for each wind direction for Profile 76 is derived from Table 3.3.3A from **Van Rijn (1995)**. This table is reproduced in Appendix A of the present report.

The percentage of occurrence of wave data (all year) for profile 76 is derived from Table 3.3.7 from **Van Rijn (1995)**. This table is reproduced in Appendix B of the present report. It is remarked that the direction classes between 60 and 180 degrees have not been used. This is in accordance with **Van Rijn (1995)**.

The current velocities and water levels based on the TRIWAQ-model are derived from Table 3.4.3A in **Van Rijn (1995)**. They are shown per wind direction and wave height class at depth of 20 m for Profile 76. This table is reproduced in Appendix C of the present report.

4.3.2.2 Coefficients

The following parameter settings have been used in the reference calculation:

- wave breaking parameter $\gamma = 0.7$ (−)
- friction factor for bottom friction $f_w = 0.01$ (−)
- friction factor for mean current $r_k = 0.05$ (−)
- water depth $d = 20$ m (flat bed over length of 100 m, 5 computational cells)
- $d_{50} = 250$ µm
- $d_{90} = 500$ µm
- $d_{SS} = 250$ µm
- current-related roughness $k_c = 0.1$ m
- wave-related roughness $k_w = 0.05$ m
- temperature $T = 15$ ºC
- salinity $S = 30$ ppt

4.3.2.3 Model

The UNIBEST-TC model has been used to calculate the year-averaged sand transport. For the reference calculation version 2.04 has been used, which includes formulations similar to the formulations in the TRANSPOR1993 model. Sensitivity calculations are carried out with UNIBEST-TC version 2.10, which includes formulations similar to the formulations in the TRANSPOR2000 model.

4.3.3 Results

4.3.3.1 Base case

Table 4.3.1 shows the results of the base case in comparison with the results from the study by **Van Rijn (1995)**. It is observed that both the gross and net bed load transport is much smaller for the present calculation compared to that by **Van Rijn (1995)**.

Both waves and currents contribute to bed load transport. For the present calculations, apparently the wave contribution dominates over the current contribution. The near-bed orbital velocity is 0.22 m/s for water depth d = 20 m, wave height H_s = 2.0 m and wave period T_p = 6 s. The maximum current-induced velocity at 1 cm from the bed (which is by default used as input for the bed load transport calculations in UNIBEST-TC) is only 0.15 m/s.

Wave dominance explains the symmetry of the bed load transport, as at a water depth of 20 m waves with H_s = 2.0 m and T_p = 6 are nearly symmetric. For the calculations in **Van Rijn (1995)** the tidal velocity used to calculate bed load transport is taken at a level higher above the bed, i.e. 10 cm. In that case the effect of tidal currents becomes larger and the asymmetry in the bed load transport is increased.

To enable a better comparison, the UNIBEST-TC calculations were made taking the tidal current at 10 cm from the bed as representative tidal forcing for the bed load transport. This level is approximately equal to the thickness of the wave boundary layer. Therefore this calculation is judged to be more realistic than the calculation with a tidal current reference height of 1 cm. Results are shown in Table 4.3.2. It is noted that the change in reference level has only consequences for the bed load transport; the suspended load transport remains unchanged. It is concluded that with the TRANSPOR1993 formulations in UNIBEST-TC version 2.04 a yearly-averaged transport rate is calculated, which is very close to the values reported by **Van Rijn (1995)** for Run CN09 without density effects. The TR2000 results show larger transport rates, particularly in the cross-shore direction (see below).

Summarizing, the computed total transport rates (no density gradient; current at 0.1 m a.b.) are:

Cross-shore

Present-TR1993:	-0.7 m^3/m/year
Present-TR2000:	-10.5 m^3/m/year
Previous-Van Rijn (1995):	-0.1 m^3/m/year

Longshore

Present-TR1993: 33.1 m^3/m/year
Present-TR2000: 45 m^3/m/year
Previous-Van Rijn (1995): 30.5 m^3/m/year

The ranges reported in Van Rijn et al. (1995) are ± 5 m^3/m/year and ± 10 m^3/m/year for the cross-shore and longshore directions respectively.

Transport mode	TR1993 (V2.04)			No Density	Including Density		
	total 1 cm	onshore/north 1 cm	offs/south 1 cm	total CN09 (VR 95)	total CN01 (VR95)	onshore/north CN01 (Van Rijn 95)	offshore/south CN01 (Van Rijn 95)
bed cross	0.2	2.7	-2.5	0.4	9.5	11.0	-1.5
bed long	0.1	5.2	-5.2	19.4	17.3	43.7	-26.4
sus cross	-0.9	0.0	-0.9	-0.6	1.4	1.7	-0.3
sus long	16.4	29.9	-13.5	11.2	11.0	17.6	-6.5
tot cross	-0.7	2.7	-3.4	-0.1	10.9	12.4	-1.5
tot long	16.4	35.1	-18.7	30.5	28.4	61.3	-33.0

Table 4.3.1 *Comparison between presently computed yearly-averaged transport rate (in m^3/m/year) at a depth of 20 m in cross-shore Profile 76 (Noordwijk) (columns 2−4) and previous results reported in Van Rijn (1995) (columns 5−7). Of these results, the total transport is shown for case CN09 (without density gradients). The positive and negative transport is shown for case CN01 (including density gradients), as these values are not reported in Van Rijn (1995) for case CN09.* ***In the present calculation the tidal forcing on bed load transport is taken at a level of 1 cm, much smaller than the value in Van Rijn (1995) (10 cm).***

Transport mode	TR1993 (V2.04)			No Density	Including Density		
	total 10 cm	onshore/north 10 cm	offs/south 10 cm	total CN09 (VR 95)	total CN01 (VR95)	onshore/north CN01 (Van Rijn 95)	offshore/south CN01 (Van Rijn 95)
bed cross	0.1	7.1	-6.9	0.4	9.5	11.0	-1.5
bed long	16.8	50.0	-33.2	19.4	17.3	43.7	-26.4
sus cross	-0.9	0.0	-0.9	-0.6	1.4	1.7	-0.3
sus long	16.4	29.9	-13.5	11.2	11.0	17.6	-6.5
tot cross	-0.7	7.1	-7.8	-0.1	10.9	12.4	-1.5
tot long	33.1	79.8	-46.7	30.5	28.4	61.3	-33.0

Table 4.3.2 *Comparison between presently computed yearly-averaged transport rate (in m^3/m/year) at a depth of 20 m in cross-shore Profile 76 (Noordwijk) (columns 2−4) and previous results reported in Van Rijn (1995) (columns 5−7). Of these results, the total transport is shown for case CN09 (without density gradients). The positive and negative transport is shown for case CN01 (including density gradients), as these values are not reported in Van Rijn (1995) for case CN09.* ***In the present calculation the tidal forcing on bed load transport is taken at a level of 10 cm, equal to the value in Van Rijn (1995).***

4.3.3.2 Sensitivity runs

First the calculations were remade with UNIBEST-TC version 2.10, which is based on the TRANSPOR2000 formulations (see Table 4.3.3). Compared with version 2.04, which is based on the TRANSPOR1993 formulations, the total yearly-averaged longshore transport increases with 36%. The gross longshore transports in both directions along the coast increases by a factor of 2 to 3. **Figure 4.3.1** and **Figure 4.3.2** show the momentary bed load, suspended load and total transport rates for the UNIBEST-TC Version 2.10 calculations with a reference height for tide-induced bed load transport of 10 cm, respectively weighed and unweighed for frequency of occurrence of wind and wave climate. All 73 wind and wave classes are shown in **Figure 4.3.1** and **Figure 4.3.2**, each representing a single tide of 12.5 h. The wind and wave classes applied are shown in Appendix A, the tidal forcing in Appendix C. Note that classes between 60^o and 180^o have not been used.

A comparison of **Figure 4.3.1** and **Figure 4.3.2** shows that although extreme wave conditions result in the highest sediment transport, these conditions do not dominate the yearly-averaged sediment transport, as their frequency of occurrence is low. The middle wave height classes (see Appendix B) have the highest contribution to yearly-averaged transport.

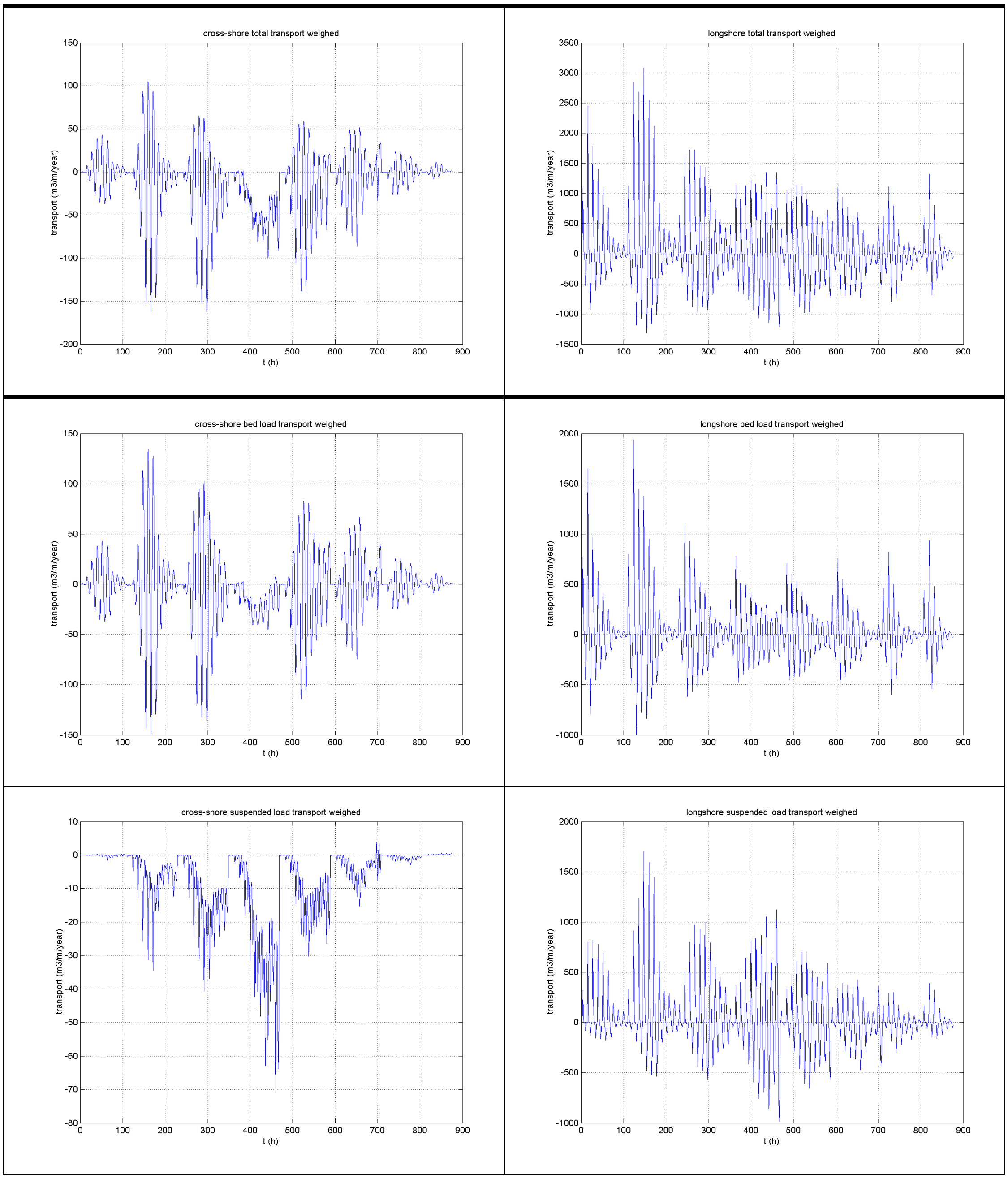

Figure 4.3.1 *Cross-shore (left) and longshore (right) bed load (top), suspended load (middle) and total (bottom) transport, weighted for frequency of occurrence. UNIBEST-TC 2.10, velocity reference height for bed load transport set at 10 cm. Horizontal axis = time (hours) and vertical axis = transport (m^3/m/year). Notice different scales on vertical axis.*

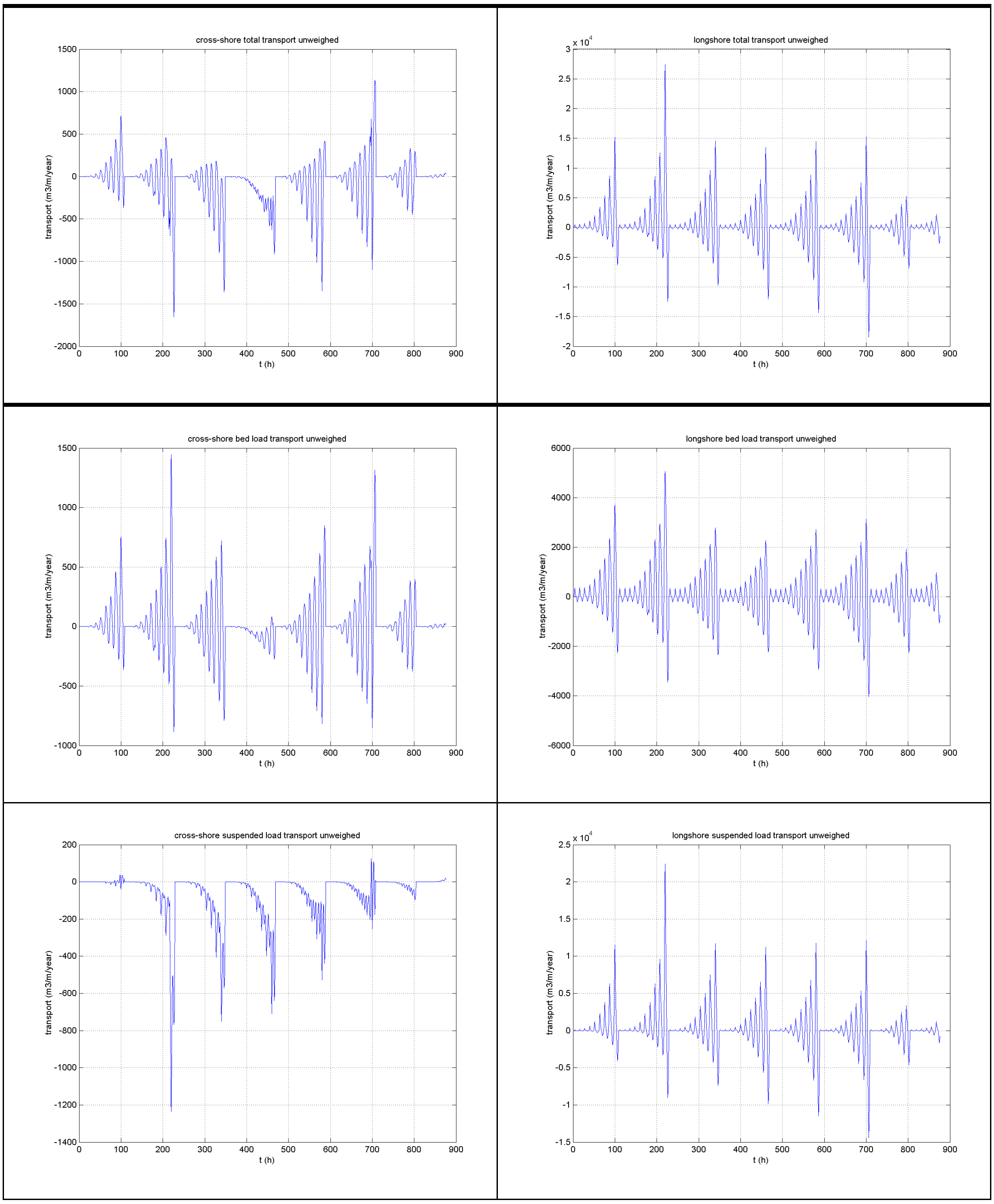

Figure 4.3.2 *Cross-shore (left) and longshore (right) bed load (top), suspended load (middle) and total (bottom) transport, not weighed for frequency of occurrence. UNIBEST-TC 2.10, velocity reference height for bed load transport set at 10 cm. Horizontal axis = time (hours) and vertical axis = transport (m^3/m/year). Notice different scales on vertical axis.*

Subsequently, a number of runs were made to investigate the sensitivity of the yearly-averaged transport rate on a number of input parameters. As reference calculation, the run with UNIBEST-TC version 2.10 was taken with a reference height for tide-induced bed load transport of 1 cm. Results are shown in Table 4.3.4 and visualised in **Figure 4.3.3** and **Figure 4.3.4**. The following parameters were varied:

- d_{50} high: d_{50} = 275 μm; d_{90} = 550 μm
- d_{50} low: d_{50} = 225 μm; d_{90} = 450 μm
- No wind: wind speed set to zero
- No vert. tide: vertical tide set to zero
- +10% ebb: ebb current increased with 10%, flood current remains unchanged
- $k_a = k_c$: the apparent bed roughness k_a is set equal to the current related roughness of 0.1 m (this option required modifications in the code and is not an option available in the standard version).
- $k_c = k_w = 0.01$: the wave and current related bed roughness are both set at 0.01 m.

	total TR2000 (10 cm)	positive TR2000 (10 cm)	negative TR2000 (10 cm)	total TR1993 (10 cm)	positive TR1993 (10 cm)	negative TR1993 (10 cm)
bed cross	-3.6	9.0	-12.6	0.1	7.1	-6.9
bed long	18.5	93.7	-75.3	16.8	49.9	-33.2
sus cross	-6.9	0.0	-6.9	-0.9	0.0	-0.9
sus long	26.5	94.8	-68.3	16.4	29.9	-13.5
tot cross	-10.5	9.0	-19.5	-0.7	7.1	-7.8
tot long	45.0	188.5	-143.6	33.1	79.8	-46.7

Table 4.3.3 *Comparison between UNIBEST-TC 2.04 (based on TRANSPOR1993 formulations) and UNIBEST-TC 2.10 (based on TRANSPOR2000 formulations).*
Yearly-averaged transport rate (in m^3/m/year) at a depth of 20 m in cross-shore Profile 76 (Noordwijk).

	RT2000 10 cm	TR2000 1 cm	d_{50} high	d_{50} low	no wind	no vert. tide	+10% ebb	$k_a = k_c$= 0.1 m	$k_c = k_w$= 0.01 m
bed load x	-3.6	1.4	1.5	1.3	4.9	1.7	1.3	1.4	1.4
bed load y	18.5	-0.2	-0.3	-0.2	0.5	2.8	-2.8	-0.2	1.0
sus load x	-6.9	-6.9	-5.5	-9.1	-0.2	-7.2	-7.1	-8.1	-0.4
sus load y	26.5	26.5	19.8	38.9	27.6	40.7	4.2	31.6	8.4
total x	-10.5	-5.5	-4.0	-7.7	4.7	-5.5	-5.8	-6.7	0.9
total y	45.0	26.3	19.5	38.6	28.2	43.5	1.3	31.3	9.3

Table 4.3.4 *Sensitivity calculations of total yearly-averaged transport rate (in m^3/m/year) at a depth of 20 m in cross-shore Profile 76 (Noordwijk); TR2000 results*

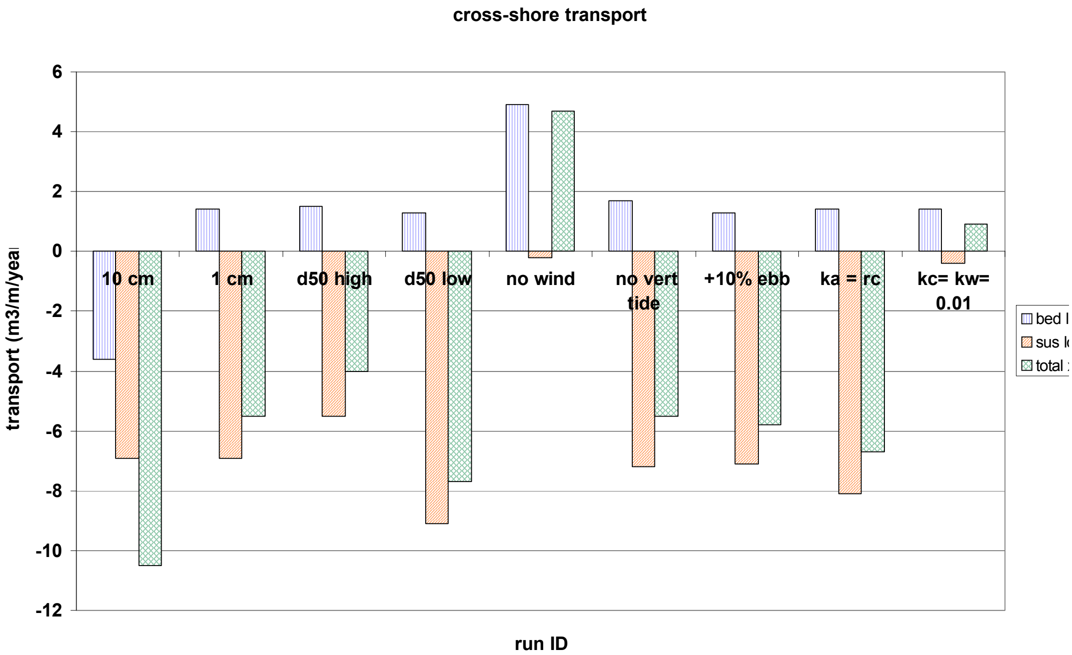

Figure 4.3.3 *Cross-shore yearly-averaged transport rate (in m^3/m/year) at a depth of 20 m in cross-shore Profile 76 (Noordwijk). See also Table 4.3.4; TR2000 results*

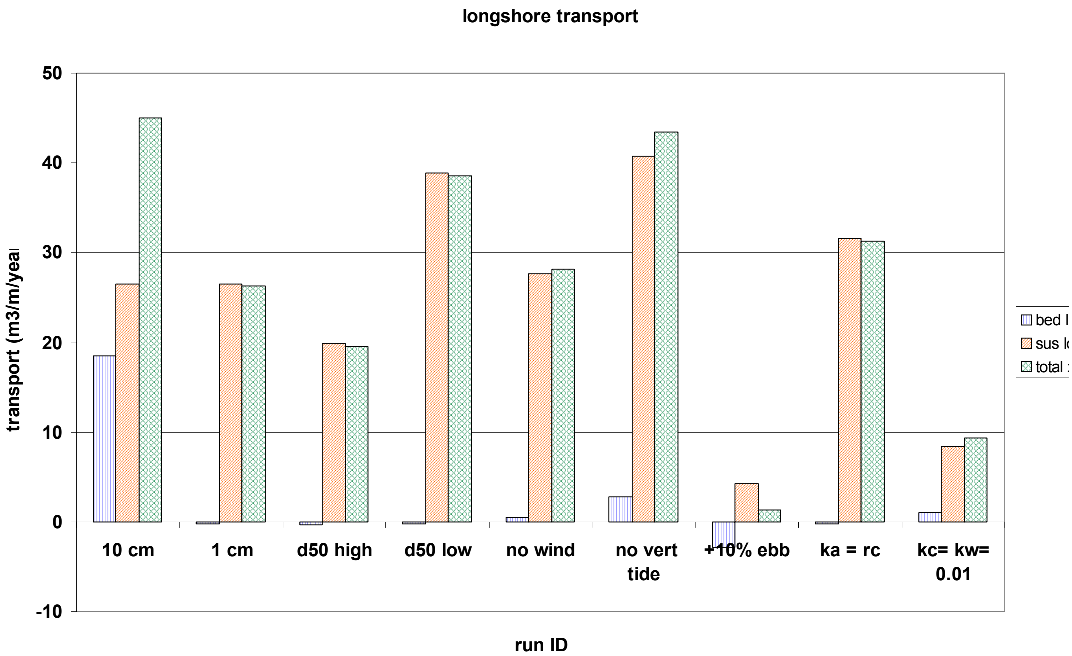

Figure 4.3.4 *Longshore yearly-averaged transport rate (in m^3/m/year) at a depth of 20 m in cross-shore profile 76 (Noordwijk). See also Table 4.3.4; TR2000 results*

From the sensitivity runs, the following is observed:

Grain size
The total transport is reduced with 26% for a 10% smaller grain size. The total transport is increased with 47% for a 10% larger grain size. Suspended load transport is very sensitive to changes in grain size, but bed load transport is much less sensitive to these changes.

Wind
Longshore transport (both bed load and suspended load) is not very sensitive to wind forcing. Cross-shore transport is quite sensitive to wind forcing, probably because the positive and negative contributions are nearly balanced. A small change in these contribution then results in a relatively large change in net cross-shore transport. It is remarked that a part of the wind effect is included in the tidal forcing, which remained unchanged in this simulation. Therefore indirect wind effects are still included in this simulation.

Vertical tide
If the vertical tide is neglected, substantially more transport (65%) is observed in the direction of flood current. Including vertical tide, the water depth is relatively high during flood. Excluding vertical tide, the water depth is less and wave-stirring of sediment from the bottom is enhanced. This may explain the calculated increase in transport.

Ebb current
Model results are very sensitive to a 10% increase in ebb current velocity. As a result, the net longshore transport nearly changes from northward to southward. Changes in gross positive and negative transport are less: the positive transport is reduced with about 10%, the negative transport is increased with about 25% (not shown in Table 4.3.4). The cross-shore transport is also much less affected.

Apparent bed roughness k_a
The sensitivity of the model results to the apparent bed roughness k_a is very mild.

Wave and current related roughness k_w and k_c
Model results are very sensitive to the wave-related roughness k_w and the current-related roughness k_c. For the present calculations default values of k_c = 0.1 m and k_w = 0.05 m have been applied, which are representative for mild to average wave conditions along the Dutch coast according to Van Rijn (1995, Table 3.7.1). However, for rough conditions sheet flow prevails and values for both k_c and k_w of 0.01 m are more suitable (**Van Rijn, 1995**). Application of these values to all condition (note that UNIBEST-TC only allows to apply constant k_w and k_c values) results in a strongly reduced transport (65% less). Hence, the simulations with k_c = 0.1 m and k_w = 0.05 m may considerably overestimate the sand transport in rough conditions.

4.3.3.3 Sensitivity runs (continued)

After the first set of sensitivity calculations, an additional set of runs was made to investigate the sensitivity of the cross-shore transport to a net onshore velocity caused by gravity circulation. To this end, an onshore velocity of 3, 5 and 10 cm/s was superimposed on the original velocity signal. Results are shown for both UNIBEST-TC 2.04 and 2.10 in

Tables 4.3.5 and 4.3.6, respectively. The reference height for tidal forcing on the bed load transport was set at 10 cm.

These calculations show that the direction and magnitude of the cross-shore transport is very sensitive to the net cross-shore velocity. The sensitivity of UNIBEST-TC version 2.10 is higher than that of UNIBEST-TC version 2.04. The calculations with version 2.04 with u_{cross} = 3 cm/s and 5 cm/s show the closest match with the calculation CN01 in **Van Rijn (1995)** (see Table 4.3.1), in which the gravitation circulation was taken into account.

Transport mode	**u_{cross} = 0 cm/s**			**u_{cross} = 3 cm/s**			**u_{cross} = 5 cm/s**			**u_{cross} = 10 cm/s**		
	tot	pos	*neg*	**tot**	pos	*neg*	**tot**	pos	*neg*	**tot**	pos	*neg*
bed x	**0.1**	7.1	*-6.9*	**6.0**	10.7	*-4.6*	**10.0**	13.7	*-3.7*	**20.2**	22.4	*-2.2*
bed y	**16.8**	49.9	*-33.2*	**17.0**	50.5	*-33.4*	**17.2**	50.8	*-33.7*	**17.6**	52.1	*-34.4*
sus x	**-0.9**	0.0	*-0.9*	**1.5**	1.5	*-0.0*	**3.1**	3.1	*0.0*	**7.4**	7.4	*0.0*
sus y	**16.4**	29.9	*-13.5*	**16.6**	30.4	*-13.8*	**16.8**	30.7	*-14.0*	**17.3**	32.1	*-14.8*
tot x	**-0.7**	7.1	*-7.8*	**7.5**	12.1	*-4.7*	**13.0**	16.8	*-3.7*	**27.6**	29.8	*-2.2*
tot y	**33.1**	79.8	*-46.7*	**33.7**	80.7	*-47.2*	**34.1**	81.5	*-47.6*	**34.8**	84.2	*-49.2*

Table 4.3.5 *Sensitivity calculations of total yearly-averaged transport rate (in m^3/m/year) at a depth of 20 m in cross-shore Profile 76 (Noordwijk). UNIBEST-TC 2.04 based on TR1993. Sensitivity to net onshore velocity. Reference height for tidal forcing on bed load transport at 10 cm.*

Transport mode	**u_{cross} = 0 cm/s**			**u_{cross} = 3 cm/s**			**u_{cross} = 5 cm/s**			**u_{cross} = 10 cm/s**		
	tot	pos	*neg*	**tot**	pos	*neg*	**tot**	pos	*neg*	**tot**	pos	*neg*
bed x	**-3.6**	9.0	*-12.6*	**8.7**	16.0	*-7.3*	**16.8**	22.0	*-5.2*	**37.2**	39.4	*-2.0*
bed y	**18.5**	93.7	*-75.3*	**18.9**	94.3	*-75.4*	**19.2**	94.6	*-75.5*	**19.9**	95.9	*-76.0*
sus x	**-6.9**	0.0	*-6.9*	**3.4**	3.8	*-0.4*	**10.4**	10.4	*0.0*	**28.5**	28.5	*0.0*
sus y	**26.5**	94.8	*-68.3*	**26.9**	95.9	*-69.1*	**27.2**	97.1	*-69.8*	**28.0**	100.3	*-72.2*
tot x	**-10.5**	9.0	*-19.5*	**12.1**	19.8	*-7.7*	**27.2**	32.4	*-5.2*	**65.7**	67.9	*-2.0*
tot y	**45.0**	188.5	*-143.6*	**45.7**	190.2	*-144.4*	**46.4**	191.7	*-145.3*	**47.9**	196.2	*-148.2*

Table 4.3.6 *Sensitivity calculations of total yearly-averaged transport rate (in m^3/m/year) at a depth of 20 m in cross-shore profile 76 (Noordwijk). UNIBEST-TC 2.10 based on TR2000. Sensitivity to net onshore velocity. Reference height for tidal forcing on bed load transport at 10 cm.*

Finally, a calculation was made with UNIBEST-TC version 2.10 based on TR2000 in which the new bed roughness height predictor was included. For this simulation a reference height for tidal forcing on bed load transport of 1 cm was applied (default value). A comparison with the results obtained with the original version of UNIBEST-TC 2.10 based on TR2000 is shown in Table 4.3.7. It is concluded that the new bed roughness height predictor hardly influences the bed load transport, but that the suspended load is reduced with about 50%.

Transport mode	***with new bed roughness height predictor (based on TR2000)***			***standard UNIBEST-TC 2.10 (based on TR2000)***		
	tot	pos	*neg*	**tot**	pos	*neg*
bed load x	**1.4**	5.3	*-3.9*	**1.4**	5.4	*-4.0*
bed load y	**-0.5**	19.5	*-20.0*	**-0.2**	20.1	*-20.3*
sus load x	**-1.4**	0.3	*-1.7*	**-6.9**	0.0	*-6.9*
sus load y	**15.2**	44.5	*-29.1*	**26.5**	94.8	*-68.3*
total load x	**-0.1**	5.6	*-5.6*	**-5.5**	5.5	*-10.9*
total load y	**14.8**	63.7	*-48.9*	**26.3**	114.9	*-88.6*

Table 4.3.7 *Effect of new bed roughness height predictor on yearly-averaged transport rate (in $m^3/m^2/year$) at a depth of 20 m in cross-shore Profile 76 (Noordwijk). UNIBEST-TC 2.10 based on TR2000. Reference height for tidal forcing on bed load transport at 1 cm.*

4.3.4 Conclusions

It is shown that calculation of the yearly-averaged longshore transport rate at the -20 m NAP depth contour of the Jarkus-Profile 76 with UNIBEST-TC version 2.04, which is based on the TRANSPOR1993 formulations, results in rate of 33.1 $m^3/m/year$, which is very close the rate of 30.5 $m^3/m/year$ reported in **Van Rijn (1995)**. If UNIBEST-TC version 2.10 is used, which includes new formulations from TRANSPOR2000, the total transport is increased with nearly 40% to 45 $m^3/m/year$.

The values reported are found if the tidal forcing for bed load transport is applied at a level approximately equal to the wave boundary layer thickness (0.1 m). This approach is equal to that followed in the **Van Rijn (1995)** study. However, in UNIBEST-TC the tidal forcing for bed load transport is by default applied at a level of 1 cm, which results in an underestimation of the bed load transport. The suspended load transport is equal for both cases.

Sensitivity runs show that the transport rate is very sensitive to grain size, vertical tide, wave and current related roughness k_w and k_c, the relative strength of the ebb current, and much less so to the apparent bed roughness k_a.

The bed roughness height predictor, Eqs. (2.2.34) and (2.2.40), built into UNIBEST-TC 2.10 hardly influences the bed load transport, but reduces the suspended load with about 50%.

4.4 DELFT3D validation runs

4.4.1 Introduction

The upgraded DELFT3D-ONLINE model described in Chapter 2 was verified using data from the Havinga experiment (**Havinga, 1992**). This experiment is also used in the EU-Sandpit project as a benchmark test to intercompare various models. A brief description of this experiment is given in the next sub-section. This is followed by a discussion of a number of validation simulations with various transport formulations and bottom roughness settings.

4.4.2 Description of Havinga experiment

This laboratory experiment was carried out in a wave-current basin. A channel with a sediment bed consisting of fine sand (d_{50} = 100 µm, d_{90} = 130 µm) was present at the end of the basin. The movable bed surface was at the same level as the cement floor of the surrounding basin. Irregular waves were generated by a directional wave generator. The wave spectrum (JONSWAP form) was single-topped with a peak frequency of 0.4 Hz. The water depth was about 0.4 m in all tests. Three different wave conditions were used with significant wave heights of 0.07, 0.1 and 0.14 m for each wave direction. In all, three wave directions were considered 60°, 90° and 120° (angle between wave orthogonal and current direction). A pump system was used to generate a current in the channel. Guiding boards were used to confine the current in the movable-bed channel (width = 4 m). The guiding boards were placed normal to the wave crests in all experiments to allow free passage of the waves. Three different current velocities (0.1, 0.2 and 0.3 m/s) were generated by varying the pump discharge. The velocity distribution across the channel was found to be almost uniform (current alone). The vertical distribution of the velocity in the middle of the channel was perfectly logarithmic in all tests (current alone).

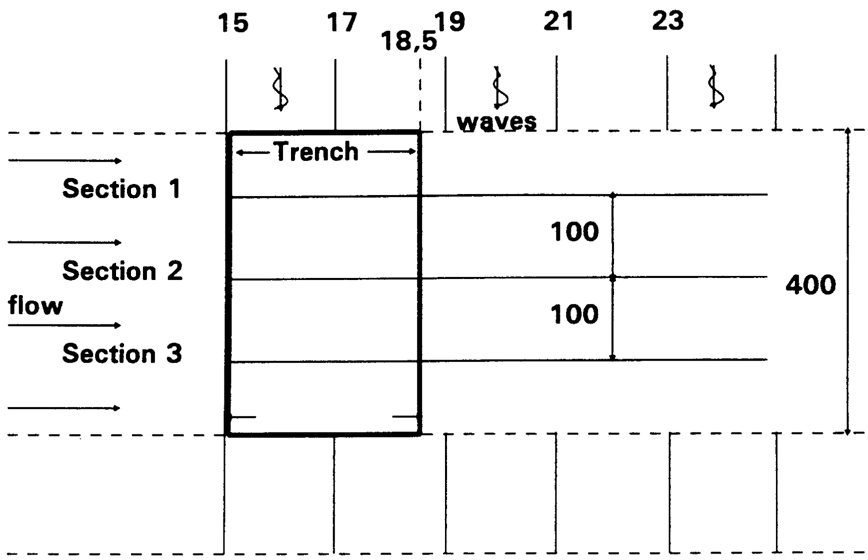

Figure 4.4.1 *Plan view of experimental set-up of Benchmark Test 1* ***(Walstra et al., 1998)***

In the selected benchmark test (wave height of about 0.1 m, current velocity of about 0.2 m/s and wave approach angle of 90^o, normal to channel) a trench was present in the movable-bed channel. The trench (longest axis) was situated normal to the current and parallel to the wave propagation direction (see **Figure 4.4.1**). The sedimentation in the trench was recorded by performing regular soundings (over about 25 hours) in three sections. The dimensions of the initial trench profile are: depth of about 0.2 m, bottom width of about 0.5 m, side slopes of about 1 to 8. The basic data upstream of the trench are listed in the table below:

Table 4.4.1 *Basic data of Havinga experiment.*

Parameter	Value
water depth	0.42 m
Significant wave height	0.105 m
peak wave period	2.2 s
depth-mean velocity	0.245 m/s
angle between current and waves	90^o
characteristic particle sizes of bed	d_{10} = 70 μm d_{50} = 100 μm d_{90} = 130 μm d_s = 90 μm
fall velocity of suspended sediment	0.006 m/s
Suspended sand transport	0.018 to 0.024 kg/s/m
ripple height	0.007 m
ripple length	0.084 m

4.4.3 Modelling Approach

The computational grid (**Figure 4.4.2**) covers a horizontal domain of about 12 m with an increased resolution (dx=0.10 m) in the vicinity of the trench decreasing to the model boundaries (dx=0.40 m). All simulations were carried out in 3D-mode with 10 horizontal layers and an exponential vertical distribution (high resolution near the bed). For the wave model the flow grid was extended in longitudinal direction by about 3 m to avoid boundary effects. The flow and wave modules are executed in a loop during of 120 s, with a morphological scaling factor of 90 it would require 8.5 loops to simulate 25.5 hrs of morphology. To spin up the model an additional 11 minutes are used, so the total number of loops was 14. The flow model uses a time step 0.24 s, White-Colebrook was used with a roughness of height 0.01 m. The flow model uses an upstream discharge boundary and a water level boundary downstream. The remaining input parameters were set to the suggested measured values.

The following transport formulations/settings were applied:
1) Bijker in 3D-model with k_c=k_w=0.01 m and FACDSS=0.8 (i.e. d_s/d_{50}),
2) Soulsby-Van Rijn formula in 3D-model with k_c=k_w=0.01 m and FACDSS=0.8,
3) TRANSPOR1993 in 3D-model with k_c=k_w=0.01 m and FACDSS=0.8,
4) TRANSPOR2000 in 3D-model with k_c=k_w=0.01 m and FACDSS=0.8,
5) TRANSPOR2000 in 2DH-model with k_c=k_w=0.01 m and FACDSS=0.8,
6) TRANSPOR2000 in 3D-model with variable roughness (predictor, see Chapter 3) and FACDSS=0.8,
7) TRANSPOR2000-Approximation formulas in 2DH-model with k_c=k_w=0.01 m and FACDSS=0.8,
8) TRANSPOR2000 in 3D-model with variable roughness and mixing based on $k-\varepsilon$ model and FACDSS=0.8,
9) TRANSPOR2000 in 2DH-model with suspended sediment diameter based on Eq. (2.2.23),
10) TRANSPOR2000 in 2DH-model with suspended sediment diameter equal to d_{50} (FACDSS=1).

To enable a comparison between the various model simulations the upstream transports were scaled to the measured values (approximately 0.021 kg/m/s).

Furthermore, the Bijker and Soulsby-Van Rijn transport formulations require some additional input parameters which are listed in the tables below

Table 4.4.2 *Input parameters for Bijker transport formula.*

Parameter	**Value**
BS (Coefficient b for shallow water)	5 (default)
BD (Coefficient b for deep water)	2 (default)
CS (shallow water criterion)	0.4 (default)
CD (deep water criterion)	0.05 (default)
D90	130 μm
Kc (roughness height for current)	0.01 m
WS (Fall velocity)	0.002 m/s
POR (porosity)	0.4 (-)

Table 4.4.3 *Input parameters for Soulsby-Van Rijn transport formula.*

Parameter	**Value**
ACAL (calibration coefficient)	1 (default)
FACD90 (ratio of d50 and d90)	1.3
Z0 (roughness height)	0.01 m

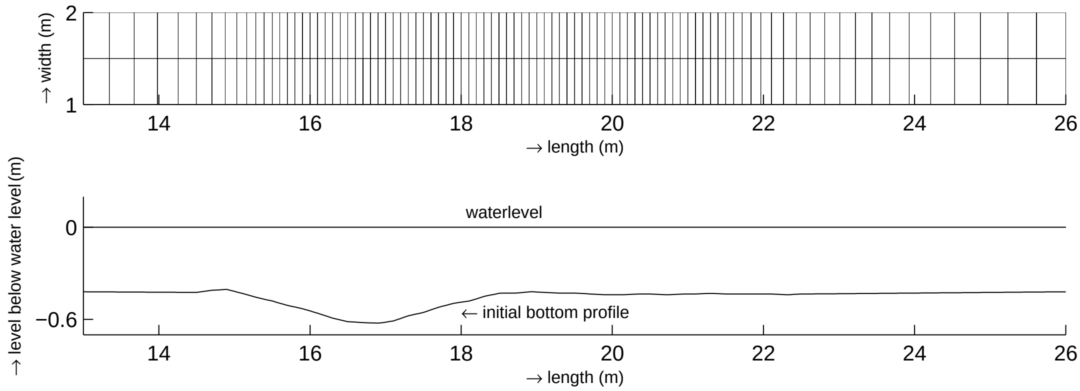

Figure 4.4.2 *Computational flow grid and bathymetry for Havinga experiment.*

4.4.4 Discussion on results

The applied transport scaling factors are summarised in **Table 4.4.4** illustrate the relative large deviations for the three transport formulations that are used. Bijker over-estimates the transports by more than a factor 7, whereas TRANSPOR1993 underestimates the transports by about 700 %. Even though, the various simulations with TRANSPOR2000 also have large deviations these simulations in general give a better estimate of the order of magnitude of the transports. The difference between the approximation method and the original implementation is negligible. With the roughness predictor the best estimate of the upstream transports is achieved. The roughness predictor estimated k_c and k_w at about 0.013 m which compares well with the value of 0.01 m applied in the other simulations. Soulsby-Van Rijn gives zero transports which is not surprising as it is applied outside its validity range (critical velocity threshold is not exceeded). This is consistent with results obtained in the Sandpit experiment by other partners who applied Soulsby-Van Rijn on this case. The last two simulations investigated the effect of the suspended sediment diameter. It can be seen that the predictor for d_s based on d_{10} and the mobility number see Eq. (2.2.23) results in a d_s which is very close to d_{50}.This is to be expected as the measured sediment composition was rather uniform.

Table 4.4.4 *Transport scaling Factors for DELFT3D simulations of Havinga experiment.*

Run Number	Type of Simulation	Scaling Factor
1	3D-model; Bijker	0.14
2	3D-model; Soulsby-Van Rijn	-
3	3D-model-TRANSPOR1993	7.36
4	3D-model TRANSPOR2000	3.4
5	2DH-model TRANSPOR2000	3.4
6	3D-model TRANSPOR2000 with variable roughness	2.58
7	2DH-model TRANSPOR2000-Approximation	3.3
8	3D-model TRANSPOR2000 with variable roughness and mixing based on $k-\varepsilon$ model	6.1

9	2DH-model TRANSPOR2000-FACDSS=F(D10,M)	4.39
10	2DH-model TRANSPOR2000-FACDSS=1.0	4.39

Below the results of the various simulations are discussed. In this discussion the focus is on the distribution of the initial transports across the trench and the morphological development, as the table above illustrates the differences in magnitude. The results are presented along the following lines:

- the differences between 2DH and 3D, which implies a comparison between Galappatti's Quasi-3D approach and a 3D advection-diffusion equations for the suspended sediment,
- comparison between the TRANSPOR2000-approximation formulations and the TRANSPOR2000 version,
- comparison between TRANSPOR2000, TRANSPOR1993, Bijker and Soulsby-Van Rijn transport formulations,
- evaluation of the performance of the bed roughness predictor,
- evaluation of some of the available sediment mixing options: parametric mixing according to **Van Rijn (2002)** or based on $k-\varepsilon$ model,
- investigation of the sensitivity of the results to variations in the diameter of the suspended sediment.

2DH versus 3D

Comparison of the 2DH with the 3D simulations (Runs 4 and 5, see **Figure 4.4.3**) shows that the modelling approach regarding lag effects has a significant influence on the transports across the trench. In 2DH the Quasi-3D approach of Galappatti is used whereas in 3D the 3D advection-diffusion equation is used. It seems that, based on a comparison with the measured trench development, the 2DH model over-predicts the amount of sediment settling in the trench. Although the upstream magnitude of sediment transport is approximately the same (also same scaling factors) the resulting trench development differs significantly.

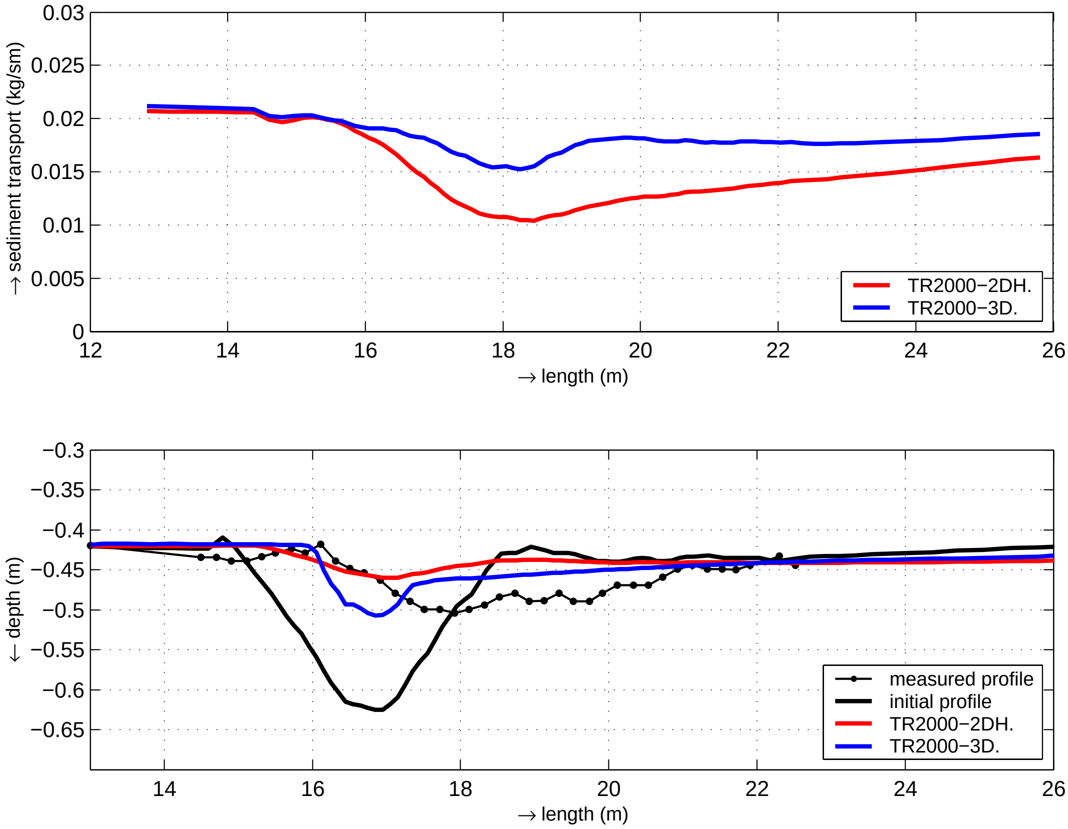

Figure 4.4.3 *2DH versus 3D. Initial suspended transports (top plot) and profile predictions (bottom plot) for various DELFT-model simulations.*

TR2000 versus TR2000 approximated

The difference between the TRANSPOR2000-approximation formulas and the TRANSPOR2000 version (Runs 5 and 7, both in 2DH mode) is small and also shows similar morphological behaviour (**Figure 4.4.4**) because both runs use Galappatti's Quasi 3D approach. The difference of the predicted sediment transport is also negligible (identical scaling factors) which implies that the approximation functions are able to give a fairly good estimate of the transports predicted by the original transport relations for the considered case. However, in cases where the angle between waves and currents differs from 90 degrees considerable deviations between both models should be expected.

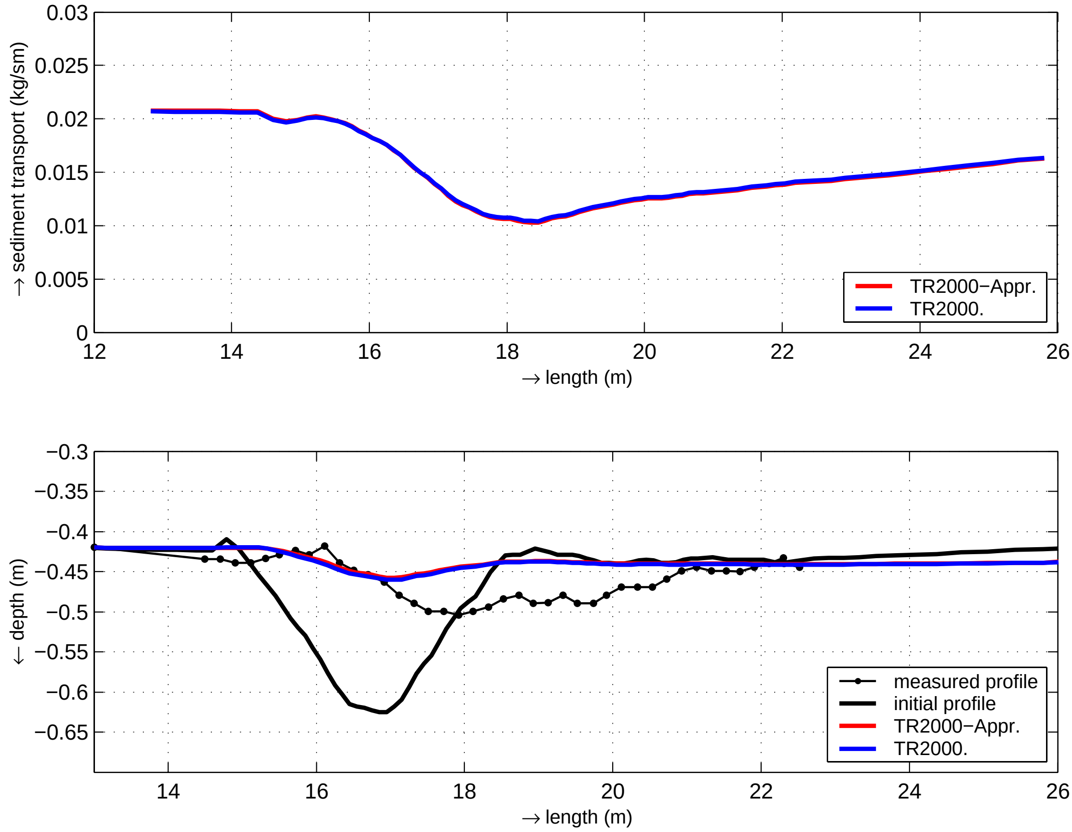

Figure 4.4.4 *TR2000 approximation formula versus TR2000. Initial suspended transports (top plot) and profile predictions (bottom plot) for 2DH simulations.*

TRANSPOR2000, TRANSPOR1993, Soulsby-Van Rijn and Bijker

A comparison between different transport formulations in the 3D-model is shown in **Figure 4.4.5** for the various transport formulas (Runs 1 to 4). Although the transports have been scaled to common values in the simulations, the prediction of the suspended sediment across the trench is significantly different (the Soulsby-Van Rijn formula could not be scaled as it predicts negligible transports as the threshold velocity is not exceeded) .This is also the case for the resulting morphological predictions.

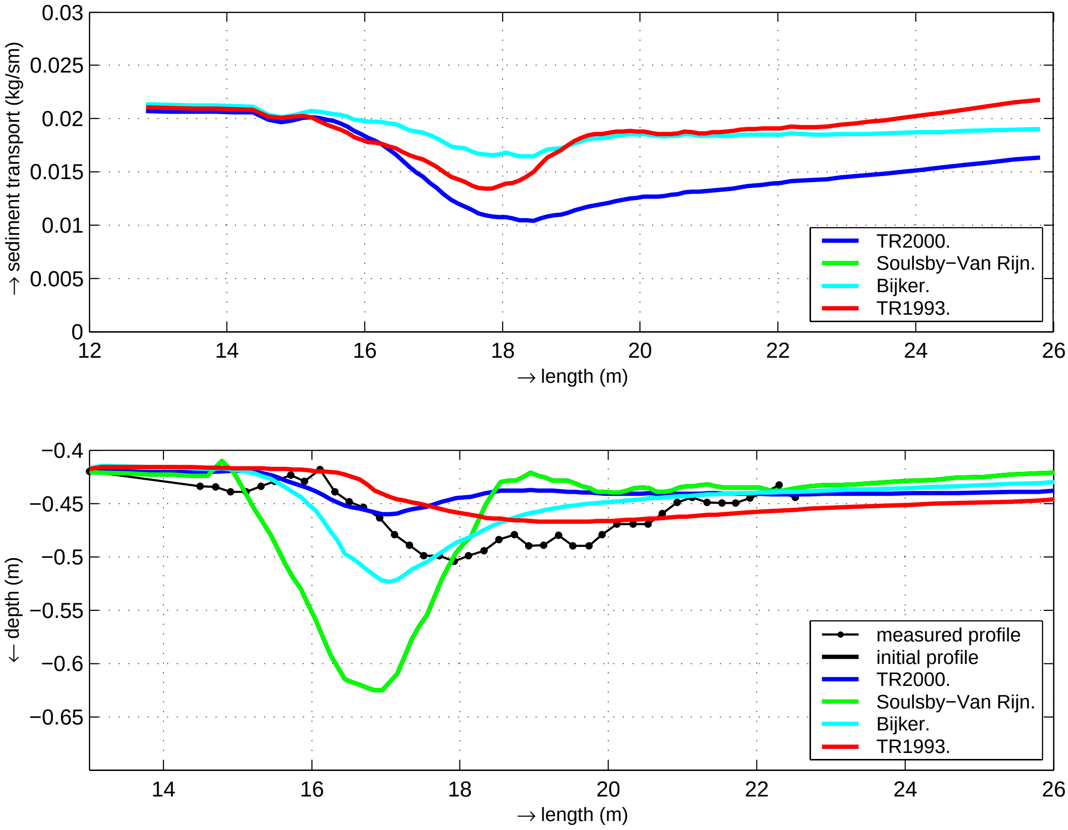

Figure 4.4.5 *Comparison of various transport formulations. Initial suspended transports (top plot) and profile predictions (bottom plot) for various 3D simulations.*

Bed roughness predictor

Bed roughness predictor and constant value give a comparable initial sediment transport distribution across the trench (Runs 4 and 6, see **Figure 4.4.6**). Interestingly the predicted trench developments for both runs do show some differences. Especially the trench slopes have flattened slightly more with the roughness prediction run. However, the amount of backfilling is approximately similar.

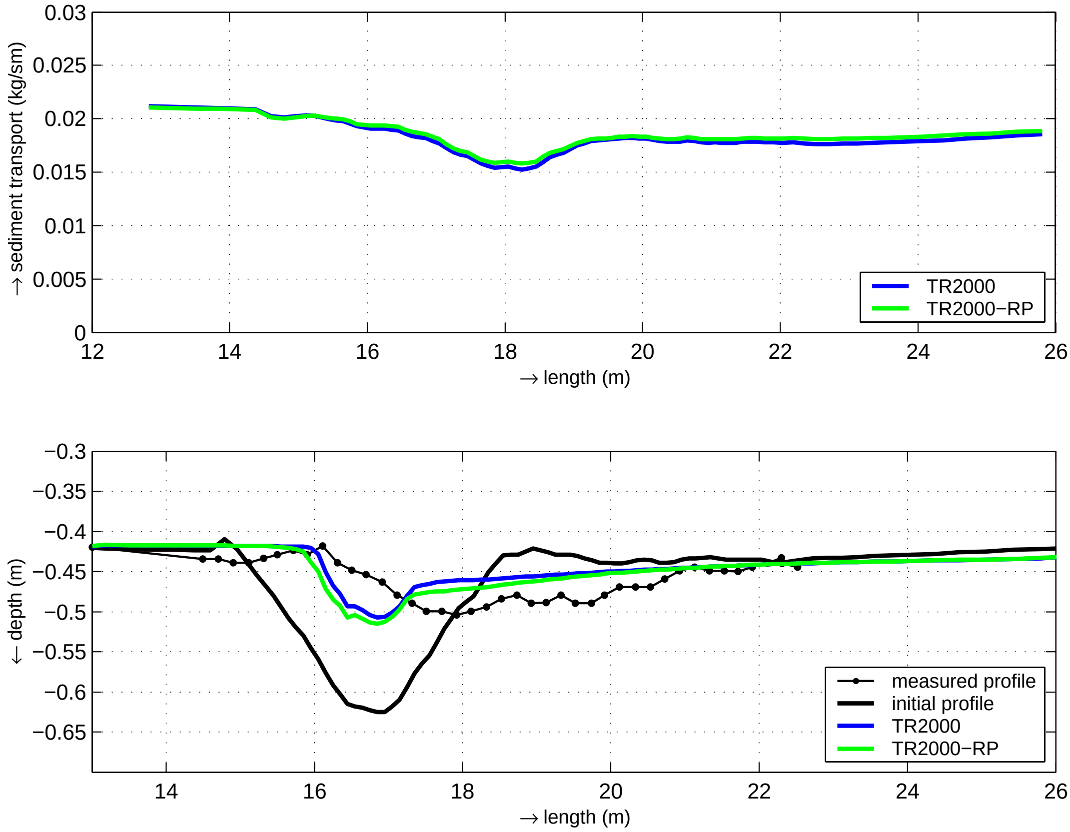

Figure 4.4.6 *Influence of roughness predictor. Initial suspended transports (top plot) and profile predictions (bottom plot) for various 3D simulations.*

Parametric mixing vs. mixing based on $k-\varepsilon$ model

The magnitude of the transports is under-estimated by the simulation with the mixing of the $k-\varepsilon$ model compared to a simulation using Van Rijn's parametric mixing relations (used in the algebraic eddy viscosity closure model), given the scaling of transports by respectively 6.1 and 3.3. However, the measured morphological development is reproduced remarkably well with a mixing based on the $k-\varepsilon$ model (Runs 6 and 8, see **Figure 4.4.7**). It is thought that the parametric mixing relations are not suitable for laboratory scale simulations. Especially the thickness of the near bed mixing layer is over-estimated, see Eq. (2.2.27). This results in an over-estimation of the vertical mixing of sediment. This is illustrated in **Figure 4.4.8** where the concentration profiles are compared. It is recommended that carry out more research into Van Rijn's parametric mixing relations.

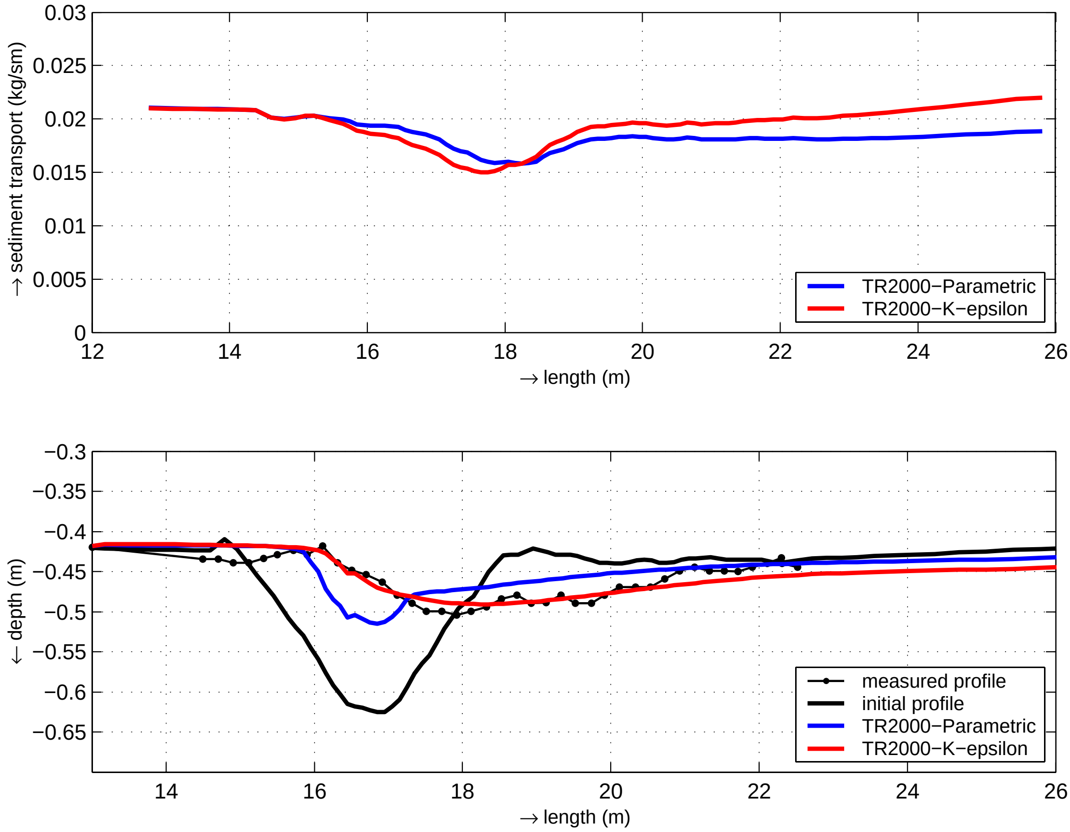

Figure 4.4.7 *Influence of sediment mixing coefficients. Initial suspended transports (top plot) and profile predictions (bottom plot) for various 3D simulations.*

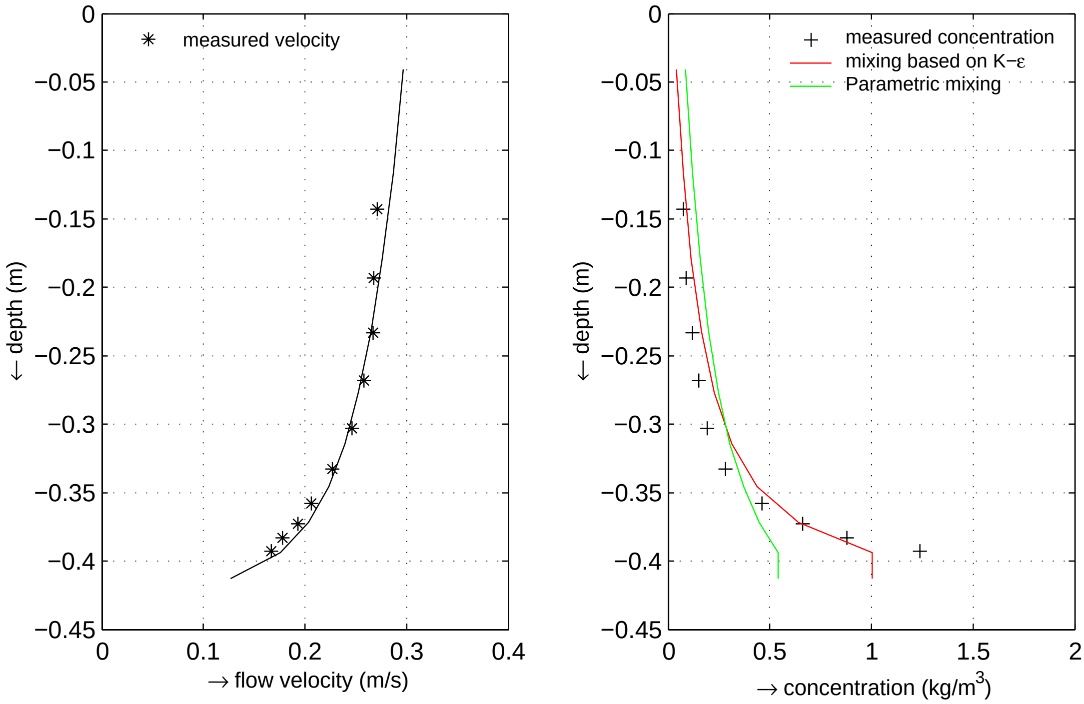

Figure 4.4.8 *Comparison of upstream velocity (left) and concentration profiles (right).*

Varying the diameter of suspended sediment diameter

Figure 4.4.9 reveals that the value of the suspended sediment diameter, d_s, has a large influence on the amount of sediment that is trapped in the trench. Furthermore, the d_s predictor gives an estimate of d_s which is very close to the d_{50} value. This is to be expected as the sediment used in the Havinga experiment is very uniform and hence d_s should be close to d_{50}. The measured value of d_s is 90 µm which is also shown. It is surprising to see that the difference between a d_s of 90 and 80 µm is rather large.

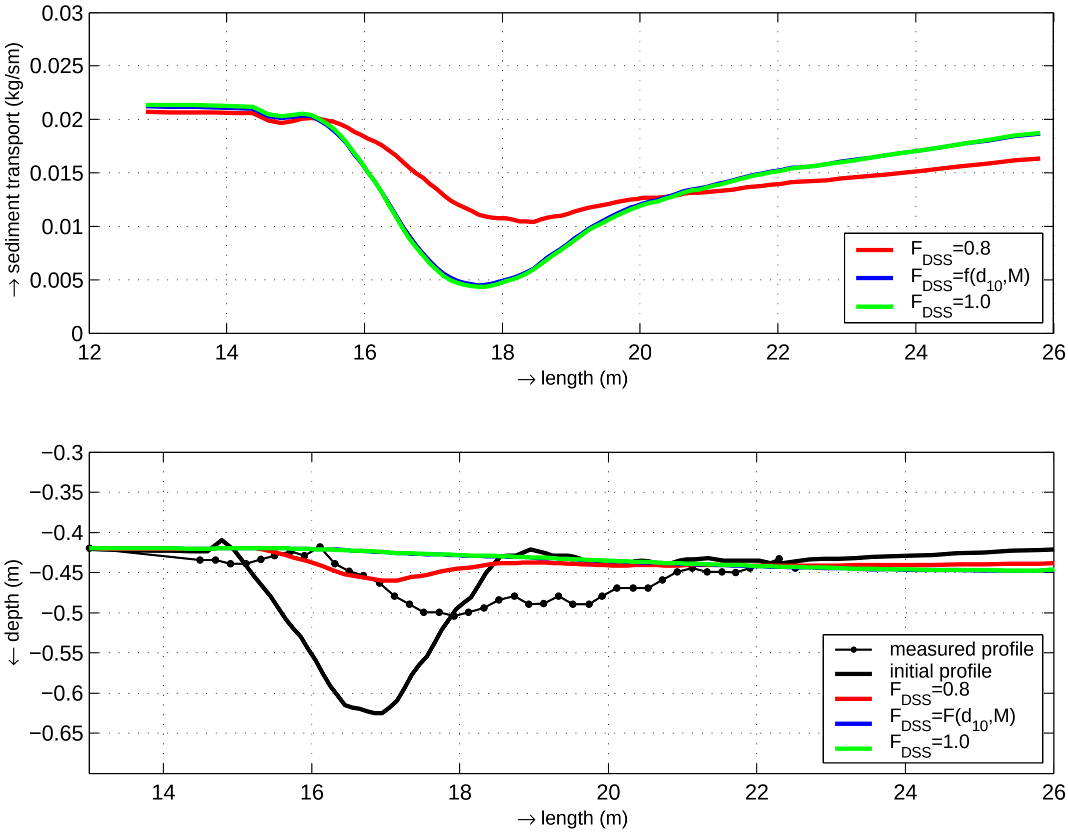

Figure 4.4.9 *Influence of varying the diameter of the suspended sediment. Initial suspended transports (top plot) and profile predictions (bottom plot) for various 2DH simulations.*

5 Summary and conclusions

5.1 Sand transport formulations in DELFT3D model

A detailed description of the updated transport relations of TRANSPOR2000 has been given in this report. The presented validation runs showed that the model is now capable of using various transport formulations in both 2DH (using Galappatti) and 3D (advection-diffusion equation). Because only one case was considered it is not yet possible to draw definite conclusion on the models performance. However, it did seem that 3D applications yielded better results than the 2DH simulations.

5.2 Ripples and bed roughness

Analysis of field data shows the presence of short wave ripples (SWR) and long wave ripples (LWR) in conditions with combined waves and weak currents. The bed form dimensions can be related to particle size d_{50} and a dimensionless mobility parameter $\psi=(U_w)^2/((s-1)g\ d_{50})$.

SWR are dominant for $\psi=(U_w)^2/((s-1)g\ d_{50})$ in the range of 50 to 150 and disappear for $\psi>150$. SWR reformation can occur within a minute or so after flattening, when the ψ-value decrease to a value below 150 but larger than about 50. For $\psi<50$ ripple movement is slow. The dimensions of the SWR are predictable by models to within a factor of 2. As flow separation and vortex production are basic phenomena of SWR, these ripples have a relatively large form roughness of the order of the ripple height ($k_s \cong$ ripple height).

LWR are low-relief bed features (steepness of about 0.01) and are always present on the bed surface, but are dominantly present for $\psi>150$. LWR have a height of 0.01 to 0.02 m and a length of 1 to 2 m in a fine sand bed (0.1 to 0.3 mm). The origin of the LWR is not quite clear. The prediction models are not able to reproduce the relatively low steepness values.

Mega-ripples and large-scale dunes may be present at specific locations, but this is not yet predictable.

It is concluded that a generally-accepted method for the accurate prediction of ripple characteristics is not yet available. In line with this it is concluded that the prediction of bed roughness from predicted ripple dimensions will not lead to very accurate results. Instead of that it is proposed to relate the bed roughness (k_s) directly to hydrodynamic and sediment-dynamic parameters ($k_s/d_{50}=f(\psi)$).

Four types of bed-roughness values can be distinguished: grain roughness ($k_{s,grain}$), physical wave-related bed form roughness ($k_{s,w}$), physical current-related bed form roughness ($k_{s,c}$) and apparent bed-roughness (k_a).

In case of a movable bed with bed forms the effective bed roughness (k_s) mainly consists of grain roughness generated by skin friction forces and of form roughness generated by pressure forces acting on the bed forms.

The grain roughness is the roughness of the plane bed surface, which is of importance for the motion of the bed load particles and the entrainment of suspended load particles at the upstream side (stoss side) of the bed forms or at a flat bed (if bed forms are absent).

The current-related roughness is the effective roughness of the bed forms as experienced by the current (unidirectional flow). This parameter affects the depth-mean velocity and the vertical distribution of the velocity profile and hence the near-bed velocities, which are of special importance for the sand transport processes. Similarly, the wave-related roughness is the effective roughness of the bed forms as experienced by the orbital motion of the waves (oscillatory flow) in conditions when the bed forms have a length scale smaller than the orbital excursion.

The apparent roughness is the effective roughness experienced by the current when waves are superimposed on the current (wave-current interaction effects) resulting in modification of the velocity profile. Generally, the velocities are reduced in the near-bed region.

Simple engineering expressions have been proposed to represent each type of bed roughness; the bed roughness (k_s) is related directly to bulk hydrodynamic and sediment-dynamic parameters ($k_s/d_{50}=f(\psi)$).

5.3 Verification of bed load transport model

Various field data sets from the literature and new data sets (laboratory and field) collected within the SANDPIT project have been used to verify/improve the bed-load transport formulations of the TRANSPOR2000 model. The median particle size for all data sets is in the range of 0.2 to 0.5 mm. The following data sets have been used:

Existing data of bed load transport in tidal flow (no waves):
- Puget Sound, Washington, USA (1964),
- Salmon Bank, Washington, USA (1968),
- ridge south of IJ-channel, North Sea, Netherlands (1994).

Existing data of bed load transport in coastal conditions:
- Skerries Bank, Start Bay, UK (1979),
- Sable Island Bank, Scotian Shelf, Canada (1999),
- Spratt Sand, Teignmouth, UK (2001).

New data of bed load transport (collected within SANDPIT Project):
- wave tunnel experiments of Delft Hydraulics,
- Noordwijk site, North Sea, Netherlands.

Bed load transport model
The net bed-load transport rate in conditions with uniform bed material can be obtained by time-averaging (over the wave period T) of the instantaneous transport rate using a quasi-steady bed-load transport model.

Verification results
The following conclusions are given:

- The measured bed-load transport in quasi-steady tidal flow can be reasonably well described (within factor 2 to 3) by the TRANSPOR2000 model for sand in the range of 0.2 to 0.5 mm using a grain roughness value of $1d_{90}$.
- The net bed-load transport rate in conditions with combined steady and oscillatory flow over a sand bed can be reasonably well described (within factor 2 to 3) by time-averaging (over the wave period) of the instantaneous transport rates using a quasi-steady bed-load transport formula approach with grain roughness of $1d_{90}$ for sand in the range of 0.2 to 0.5 mm in the ripple regime without adjustment of model coefficients.
- The bed-load transport is mainly affected by the grain roughness. The best results are obtained for a grain roughness equal to $1d_{90}$. The computed bed load transport rates are significantly larger (factor 1.5 to 2) for a grain roughness of $3d_{90}$.

The bed-load transport in combined steady and oscillatory flow is only marginally dependent on a somewhat more accurate description of the wave-current friction factor (f_{cw}). The modified f_{cw}-method yields slightly smaller transport rates (20% to 30%).

5.4 Verification of oscillatory suspended load transport model

Experimental results from the large-scale Delta flume and from the COAST3D project at the Egmond site (The Netherlands) have been used to verify/improve the oscillatory suspended load transport of the TRANSPOR2000 model. The median particle size for all data sets is in the range of 0.2 to 0.5 mm.

The engineering method implemented in the TRANSPOR2000 model is based on an instantaneous response of the suspended sand concentrations (C) and transport ($q_{s,w}$) to the near-bed orbital velocity (C proportional to U^3 and q_s to U^4). This approach is assumed to be valid for the near-bed layer (say 1 to 5 times the wave boundary layer thickness). Phase lag effects can be included, but are neglected at present stage of research. Application of this approach requires computation of the time-averaged sand concentration profile and integration of the time-averaged sand concentration profile in vertical direction.

This method is implemented in the TRANSPOR2000 model. This latter model has been used to compute the wave-related suspended transport for the five Delta flume cases 1A to 1E. Based on these results, it can be concluded that the proposed approach yields wave-related suspended transport rates of the right order of magnitude, if the near-bed velocity asymmetry is predicted with sufficient accuracy.

5.5 Effect of near-bed wave-induced streaming on bed load transport and suspended load transport

The cross-shore sand transport rate in the near-bed region of shallow waters (near the coast) is strongly affected by small residual (net) currents induced by the wave motion. This was clearly shown by results of various laboratory data sets. Above a smooth bed it was found that the measured streaming was in reasonable agreement with the streaming predicted by using the conduction-solution of **Longuet-Higgins (1953)**. However, when the same incident waves propagated above a flat sand-roughened bed, the near-bed streaming, while still being in the onshore direction, was greatly reduced in magnitude. When the bed was rippled, the near-bed streaming was further reduced to approximately zero, while the streaming just above the bottom boundary layer was directed offshore.

Various mechanisms are responsible for the generation of these net currents near the bed:

- wave-induced streaming velocities in and directly above the wave boundary layer due to the turbulence structure near the bed;
- return (offshore-directed) currents due to onshore-directed Lagrangian and Eulerian mass fluxes in the upper part of the water depth.

The magnitude and even direction of these net currents are rather uncertain and therefore the accuracy of models of coastal sand transport depends strongly upon reliable predictions of the detailed hydrodynamic processes leading to these net currents.

Various researchers have successfully developed mathematical models to describe the Eulerian wave-induced streaming near the bed. In the modelling studies, it has been found that, above plane rough beds ($A_{\delta,w}/k_s>10$), the effect of asymmetry in the turbulence in successive half cycles (due to asymmetry of the wave motion) is to reduce the Eulerian streaming, with a reversal to offshore-directed streaming for very long waves. **Davies and Villaret (1999)** have presented a semi-analytical approach for the generation of net currents over very rough rippled bottoms ($A_{\delta,w}/k_s<5$). Above such bottoms, momentum transfer is dominated by the spatially well organized process of vortex shedding, rather than by random turbulent processes. Based on their results, the streaming velocity distribution (u-velocity profile) within the wave boundary layer has the following features:

- a near-bed jet of fluid in the direction of wave propagation;
- a level of zero-velocity within the wave boundary layer;
- a reversal in the direction of the velocity extending to the edge of the wave boundary layer; the offshore-directed streaming velocity at the edge of the wave boundary layer depends on the relative wave height (H/h), the degree of velocity asymmetry and the relative roughness ($A_{\delta,w}/k_{s,w}$).

Davies and Villaret (1998, 1999) have reviewed the available experimental datasets of streaming velocities in the near-bed region. The data sets have been classified by using the relative bed roughness parameter ($A_{\delta,w}/k_s$) as the most important discriminating parameter. Very rough rippled beds can be defined as conditions with $A_{\delta,w}/k_s<10$, rough plane beds as conditions with $A_{\delta,w}/k_s=10$ to 1000 and smooth plane beds as $A_{\delta,w}/k_s>1000$.

Analysis of the datasets shows that the wave-induced streaming at the edge of the wave boundary layer is negative (against wave propagation direction) or positive as a function of relative roughness $A_{\delta,w}/k_s$. The streaming velocities at the edge of wave boundary layer become more negative for decreasing relative roughness values ($A_{\delta,w}/k_s$).

The wave-induced streaming velocities in the near-bed region will have substantial effect on the sand transport processes in the near-bed region, as shown by a series of Delta flume measurements. The suspended transport values associated with the streaming velocities are somewhat smaller than those associated with the asymmetrical orbital velocities, but they can not be neglected.

It is proposed to include the streaming effects by correcting the wave-related suspended transport component and the bed load transport component. These transport components will be larger for positive values of u_δ and smaller for negative values of u_δ.

The (current-related) suspended load transport related to the near-bed return flow (u_r) due to onshore mass flux in the upper part of the water depth should be taken into account separately.

5.6 Application of engineering sand transport formulations in deep water

Sensitivity of sediment transport to angle between wave and current direction
The sensitivity of sediment transport calculated by SUTRENCH93 and SUTRENCH2000 to the angle between waves and currents can be well explained with the formulations used in this model. The wave and tidal contributions are added, taking into account the angle between the two directions. Based on this, the peak orbital velocities can be of the same order of magnitude as the tidal currents and, hence, it is logical that at a depth of 10 m the computed sediment transport rates are very sensitive to the wave angle. Even at a depth of 20 m, a strong dependency remains.

Yearly-averaged sediment transport at 20 m depth in Jarkus-Profile 76
It is shown that calculation of the yearly-averaged transport rate at the -20 m NAP depth contour of the Jarkus-Profile 76 with UNIBEST-TC version 2.04, which is based on the TRANSPOR1993 formulations, results in rate of 33.1 m^3/m/year, which is very close the rate of 30.5 m^3/m/year reported in **Van Rijn (1995)**. If UNIBEST-TC version 2.10 is used, which includes new formulations from TRANSPOR2000, the total transport is increased with nearly 40% to 45 m^3/m/year. The results on cross-shore transport show the best agreement with results from **Van Rijn (1995)** if a net onshore current is superimposed on the original velocity profile of 3 to 5 cm/s to simulate the onshore-directed near-bed currents due to fluid density gradients. This is done to incorporate the effect of gravity circulation, which is not included in UNIBEST-TC.

These values are found if the tidal forcing for bed load transport is applied at a level approximately equal to the wave boundary layer thickness (0.1 m). This approach is equal to that followed in the **Van Rijn (1995)** study. However, in UNIBEST-TC the tidal forcing for bed load transport is by default applied at a level of 1 cm, which results in an underestimation of the bed load transport. The suspended load transport is equal for both cases.

Sensitivity runs show that the transport rate is very sensitive to grain size, vertical tide, wave and current related roughness k_w and k_c, the relative strength of the ebb current, and much less so to apparent bed roughness k_a.

A new bed roughness height predictor built into UNIBEST-TC 2.10 hardly influences the bed load transport, but reduces the suspended load with about 50%.

DELFT3D validation runs
The validation runs were primarily used to illustrate the new extended capabilities the DELFT3D-ONLINE model now has. Although, the model requires further testing the validation runs showed that:

- All transport formulations which were previously available in DELFT3D-MOR are now also operational in DELFT3D-ONLINE.
- Simulations in 2DH and 3D showed identical results (for the present case).
- The TRANSPOR2000 approximation formulations give a very good estimate of the original expressions.
- The bed roughness predictor and suspended sediment diameter predictor derived in this report have both been implemented successfully in DELFT3D-ONLINE and give reasonable estimates (for the considered case).
- When the transports can be scaled, the DELFT3D simulation which used the ε of the $k-\varepsilon$ turbulence model for the sediment mixing coefficient, gives a very good estimate of the backfilling of the considered trench.

5.7 Recommendations

The present project has resulted in some major improvements which have been implemented and validated successfully. In our view this project constitutes a major leap forward regarding the quality of the transport relations (including roughness predictors, etc.) and the morphological models in which they have been implemented. However, there are some inevitable items that could not be covered in the present study. In view of the good progress we made it is strongly advised to consider the following topics for further research:

- The new roughness predictor should be seen as part of the TR2000 formulations. It is therefore recommended to recalibrate TR2000 with the roughness predictor with an emphasis on the reference concentration (c_a) and near bed mixing layer thickness (δ_s) and to implement these new parameters in the DELFT-ONLINE model.
- It was shown in this study that the effects the wave angle has on the bed load transports can be in the order of 50 %. However, at present only the approximated formulations are available in DELFT3D-ONLINE. It is therefore recommended to include the original **Van Rijn (2000)** intra-wave approach for bed load transport as well.
- The currently implemented minimum value of 1 % of the local water depth for the reference height requires further research. Especially in deeper water this would imply unrealistic high reference heights which will result in reduced transports. It might be better to prescribe an absolute minimum in the order of 0.01 m. At present little is known about the effects of these limitations on the transports in deeper water. It is therefore recommended to carry out a limited number of sensitivity simulations to investigate this aspect and come to realistic limitations for the reference height.

- The roughness predictor and the formulation for the apparent roughness are at present only included in the transport module (apparent roughness itself is obtained from the flow model, but limits are based on TR2000). To come to a more consistent model it is vital that these formulations are also included in the FLOW-module. Using this approach they are automatically available in the ONLINE module.
- Various total load transport formulations are available in DELFT3D. Using these formulations, it is assumed that the total load consists of bed load only. As this approach is not always realistic, it is recommended to split the total load into a suspended load and a bed load component using an available expression (**Van Rijn, 1993**). Furthermore, the critical velocity of the Soulsby-Van Rijn model should be improved.
- The DELFT3D-ONLINE model includes the option of schematizing the bed material into a number of fractions. However, the interaction of the fractions (hiding-exposure effect) is not yet included. It is recommended to improve the fractional approach using the formulations of **Van Rijn (2000)**. This would require a small-scale laboratory experiment concerning a trench infill with graded sediment.
- Options should be available in the algebraic eddy-viscosity turbulence-closure model to include hindered settling and turbulence damping effects using simple algebraic expressions.
- On code level the above described improvements are relative small modifications and it is recommended to update the SUTRENCH and UNIBEST-TC in concert with DELFT3D. Particularly, the level above the bed at which the current velocity is applied in the UNIBEST-model is not correct and should be improved (in line with TR2000). This will allow easier testing procedures as these models are easier to run and can be used to perform morphological longer time scales against little extra cost.
- In line with the testbank facility of the UNIBEST-model, it is recommended to compose a similar testbank database for the DELFT3D- model and to use the relevant data sets for model verification/validation. Basic data sets which should be included are:
  - Laboratory flume: three trenches (different slopes) in currents only; detailed velocity and concentration profiles are available,
  - Vinje-laboratory basin: trench in combined current and waves,
  - Laboratory flume: rived bend experiment,
  - Field: trial dredge trench in Westerschelde estuary (tidal current only),
  - Field: Scheveningen Trench in North Sea (tidal current with waves),
  - Field: PUTMOR pit data North Sea (see **Walstra et al., 2002a**),
  - Field: Artificial bar in North Sea near Hoek van Holland (Wiersma bar).

6 References

Amos, C.L. et al., 1999. *Ripple migration and sand transport under quasi-orthogonal combined flows on the Scotian Shelf. Journal of Coastal Research, Vol. 15, No. 1, pp 1-14*

Andrews, D.G. and Mcintyre, M.E., 1978: *An exact theory of non-linear waves on a Lagrangian-mean flow. J. Fluid Mech., Vol. 89 (4), pp. 609-646.*

Bagnold, R.A., 1946. *Motion of waves in shallow water: interaction of waves and sand bottoms. Proc. R. Soc. London, Ser. A, 187, p. 1-15*

Bayram, A., Benoit, C. and Larson, M., 2003. *Equivalent roughness under sheet flow conditions. Coastal Sediment, Florida, USA*

Bijker, E.W., Kalkwijk, J.P.Th. and Pieters, T., 1974. *Mass transport in gravity waves on a sloping bottom, proc. 14th ICCE, p. 447-465*

Carstens, M.R., Neilson, F.M. and Altinbilek, H.D., 1969. *Bed forms generated in the laboratory under an oscillatory flow. CERC, Techn. Memo 28, USA*

Chung, D.H. and Grasmeijer, B.T. , 1999. *Analysis of sand transport under regular and irregular waves in large-scale wave flume. Report R99-05, Dep. of Physical Geography, Univ. of Utrecht, The Netherlands*

Davies, A.G. and Villaret, C., 1997. *Oscillatory flow over rippled beds. In J.N. Hunt (ed.), Gravity waves in water of finite depth: Chapter 6, p. 215-254. Advances in fluid mechanics, Computational Mechanics Publications*

Davies, A.G. and Villaret, C., 1998. *Wave-induced currents above rippled beds, p. 187-199. In: Physics of Estuaries and Coastal Seas, edited by J. Dronkers and M. Scheffers, Balkema, Brookfield*

Davies, A.G. and Villaret, C., 1999. *Eulerian drift induced by progressive waves above rippled and very rough bed, p. 1465-1488. Journal of Geophysical Research, Vol. 104, No. C1*

Delft Hydraulics, 1999. *Voortschrijdend Onderzoek Programma (VOP); Generiek kustonderzoek voor de jaren 2000-2004. Report Z2478, Delft, The Netherlands*

Dingemans, M.W., Radder, A.C. and De Vriend, H.J., 1987. *Computation of the Driving Forces of Wave-Induced Currents. Coastal Engineering. 11: 539-563.*

Dohmen-Janssen, M., 1999. *Grain size influence on sediment transport in oscillatory sheet flow. Doc. Thesis. Dep. of Civil Engineering, Univ. of Twente, The Netherlands*

Doucette, J.S., 2002. *Bedform migration and sediment dynamics in the nearshore of a low-energy sandy beach in southwestern Australia, p. 576-591. Journal of Coastal Research, Vol. 18, No. 3*

Forester, C.K., 1979: *Higher Order Monotonic Convective Difference Schemes. Journal of Computational Physics, Vol. 23, 1-22.*

Foti, E., 2003. *Literature review of bed form predcition models. University of Catania, Catania, Sicily, Italy*

Fredsøe, J., 1984. *Turbulent boundary layer in wave-current interaction. Journal of Hydraulic Engineering, ASCE, Vol. 110, 1103-1120.*

Fredsøe, J., Andersen, K.H. and Sumer, B.M., 1999. *Wave plus current over a ripple-covered bed, p. 177-221. Coastal Engineering 38.*

Fredsøe, J. and R. Deigaard,1992. *Mechanics of Coastal Sediment Transport. Advanced series on ocean engineering - Vol. 3, World Scientific Publishing.*

Garcez Faria, A.F. et al., 1998. *Vertical profiles of longshore currents and related bed shear stress and bottom roughness, p. 3217-3232. Journal of Geophysical Research, Vol. 103, No. C2*

Grasmeijer, B.G., 2002. *Process-based cross-shore modelling of barred beaches. Doctoral Thesis, Department of Physical Geography, University of Utrecht, Utrecht, The Netherlands*

Grasmeijer, B.T., Chung, D.H. and Van Rijn, L.C., 1999. *Depth-integrated sand transport in the surf zone. Coastal Sediments, Long Island, USA, p.325-340*

Grasmeijer, B.T. and Van Rijn, L.C., 1999. *Transport of fine sands by currents and waves, Part III: Breaking waves over barred profile with ripples. Journal of Waterway, Port, Coastal and Ocean Engineering, Vol. 125, No. 2*

Groeneweg, J. and Klopman, G., 1998. *Changes of the mean velocity profiles in the combined wave-current motion in a GLM formulation, J. Fluid Mech., Vol 370, pp. 271-296.*

Groeneweg, J., 1999. *Wave-current interactions in a generalised Lagrangian Mean formulation, PhD thesis, Delft University of Technology, Delft.*

Hanes, D.M., Alymov, V. and Chang, Y.S., 2001. *Wave-formed sand ripples at Duck, North Carolina, p. 22592-22592. Journal of Geophysical research, Vol. 106, No. C10*

Hansen, E.A., Fredsøe, J. and Deigaard, R., 1994. *Distribution of suspended sediment over wave-generated ripples, p. 37-55. Journal of Waterway, Port, Coastal and Ocean Engineering, Vol. 120*

Havinga, F.J., 1992. *Sediment concentrations and transport in case of irregular non-breaking waves with a current.Report H840 Parts E, F, G. Delft Hydraulics, Delft, The Netherlands*

Hitching, E and Lewis, A.W., 1999. *Bed roughness over vortex ripples, p. 18-32. Coastal Sediments, Long Island, USA*

Hoekstra, P., Bell, P., Van Santen, P and Roode, N., 2001. *Intertidal bedforms and bedload transport measurements on Spratt Sand, Teignmouth (UK). Coastal Dynamics, Lund, Sweden*

Holthuijsen, L.H., N. Booij and T.H.C. Herbers, 1989. *A prediction model for stationary, short-crested waves in shallow water with ambient currents. Coastal Engineering, 13, pp. 23-54.*

Holthuijsen, L.H., N. Booij and R.C. Ris, 1993. *A spectral wave model for the coastal zone. Proc. of the 2nd Int. Symposium on Ocean Wave Measurement and Analysis, New Orleans, 630-641.*

Houwman, K.T. and Ruessink, B.G., 1996. *Sediment transport in the vicinity of the shoreface nourishment of Terschelling. Dep. of Physical Geography. Univ. of Utrecht, The Netherlands*

Houwman, K.T. and Van Rijn, L.C., 1999. *Flow resistance in the coastal zone, p. 261-273. Coastal Engineering, 38*

Huang, C.J and Dong, C.M., 2002. *Propagation of water waves over rigid rippled beds, p. 190-201 Journal of Waterway, Port, Coastal and Ocean Engineering.*

Huang, W. and Spaulding, M., 1996. *Modelling horizontal diffusion with sigma coordinate system, Journal of Hydraulic Eng., Vol. 122, No. 6, 349-352.*

Hume, T.M., Green, M.O. and Oldman, J.W., 1999. *What happens at the seabed off a headland during a tropical cyclone, p. 1836-1851. Coastal Sediments, Long Island, USA*

Isobe, M. and Horikawa, K., 1982. *Study on water particle velocities of shoaling and breaking waves. Coastal Engineering in Japan, Vol. 25.*

Johns, B., 1970. *On the mass transport induced by oscillatory flow in a turbulent boundary layer. Journal Fluid Mechanics, 43 (1), p. 177-185*

Kachel, N. B. and Sternberg, R.W., 1971. *Transport of bedload as ripples during an ebb current. Marine Geology 10, p. 229-244*

Khelifa, A. and Quellet, Y, 2000. *Prediction of sand ripple geometry under waves and currents, p. 14-22. Journal of Waterway, Port, Coastal and Ocean Engineering, Vol. 126, No. 1*

Kleinhans, M.G., 2002. *Personal Communication on Bed load transport measurements in North Sea under tidal conditions at location Noordwijk, Sandpit Project, Dep. of Physical Geography, University of Utrecht, Utrecht, The Netherlands*

Kleinhans, M.G., 2003. *Sediment dynamics on the shoreface and upper continental shelf, a review. Dep. of Physical Geography, University of Utrecht, Utrecht, The Netherlands*

Klopman, G., 1994. *Vertical structure of the flow due to waves and currents, Parts 1 and 2. Report H840.30, Delft Hydraulics, Delft, The Netherlands*

Koelewijn, H., 1994. *Sediment transport under sheetflow conditions. MsC. Thesis, Dep. of Civil Engineering, Delft University of Technology, Delft, The Netherlands*

Kolmogorov, A. N., 1942. *Equations of turbulent motion of an incompressible fluid. IZV Akad. Nauk. USSR, Ser. Phys., Vol. 6, pp. 56-58. (translated into English by D.B. Spalding, as Imperial College, Mechanical Engineering Department Report ON/6, 1968, London, U.K.).*

Kos'yan, R., 1988. *On the dimensions of passive ripple marks in the nearshore zone, p. 149-153. Marine Geology, Vol. 80*

Kroon, A., 1994. *Sediment transport and morphodynamics of the beach and nearshore zone near Egmond, The Netherlands. Doc. Thesis, Dep. of Physical Geography, Univ. of Utrecht, The Netherlands*

Langhorne, D.N., 1981. *An evaluation of Bagnold's dimensionless coefficient of proportionality using measurements of sandwave movement. Marine Geology 43, p. 49-64*

Leendertse, J.J., 1987. *A three-dimensional alternating direction implicit model with iterative fourth order dissipative non-linear advection terms. WD-333-NETH, The Netherlands Rijkswaterstaat.*

Lesser, G. et al., 2003. *Development and validation of a three-dimensional morphological model. In press.*

Li, M.Z. and Amos, C.L., 1998. *Predicting ripple geometry and bed roughness under combined waves and currents in a continental shelf environment, p. 941-970. Continental Shelf Research, Vol. 18*

Longuet-Higgins, M.S., 1953. *Mass transport in water waves, p. 535-581. Philos.Ttrans. R.. Soc., London, Ser. A 245 (03)*

Longuet-Higgins, M.S., 1958. *The mechanics of the boundary layer near the bottom in a progressive wave, p. 184-193.Proc. 6th ICCE, Florida, USA*

Malarkey, J., 2001. *Modelling Oscillatory Flow over Vortex Ripples using the Discrete Vortex Method. PhD Thesis, University of Wales Bangor.*

Mathisen, P.P. and Madsen, O.S., 1996a. *Waves and currents over a fixed rippled bed, Part 1: Bottom roughness experienced by waves in the presence and absence of currents, p. 16533-16542. Journal of Geophysical Research, Vol. 101,C7*

Mathisen, P.P. and Madsen, O.S., 1996b. *Waves and currents over a fixed rippled bed, Part 1: Bottom and apparent roughness experienced by currents in the presence of waves, p. 16543-16550. Journal of Geophysical Research, Vol. 101,C7*

Mellor, G.L. and A.F. Blumberg, 1985. *Modelling vertical and horizontal diffusivities and the sigma coordinate system. Monthly Weather Review, Vol. 113, 1379-1383.*

Mogridge, G.R., Davies, M.H. and Willis, D.H., 1994. *Geometry prediction for wave-generated bedforms, p. 255-286. Coastal Engineering 22*

Nelson, R.C., 1996. *Field measurement of bed roughness for waves on an offshore reef, p. 3143-3154. 25th ICCE, Orlando, USA*

Nielsen, P., 1992. *Coastal Bottom Boundary Layers and Sediment Transport, 324 pp, World Science*

Nikuradse, J., 1932. *Gesetzmässigkeiten der Turbulente Strömung in Glatten Rohren. Ver. Deut. Ing. Forschungsheft 356*

Prandtl, L., 1945. *Uber ein neues formelsystem fur die ausgebildete turbulenz (On a new formation for fully developed turbulence). Nachr. Akad. Wiss. (Report of Academy of Sciences) Gottingen, Germany.*

Ribberink, J.S. and Al-Salem, A.A., 1995. *Sheet flow and suspension of sand in oscillatory boundary layers, Coastal Engineering 25, p. 205-225*

Rodi, W., 1984. *Turbulence models and their application in Hydraulics, State-of-the-art paper article sur l'etat de connaissance. Paper presented by the IAHR-Section on Fundamentals of Division II: Experimental and Mathematical Fluid Dynamics, The Netherlands.*

Sayao, O.D.S.F.J., 1982. *Beach profiles and littoral sand transport. Queen's University, Kingston, Ontario, USA*

Simonin, O., R.E. Uittenbogaard, F. Baron, and P.L. Viollet, 1989. *Possibilities and limitations to simulate turbulence fluxes of mass and momentum, measured in a steady stratified mixing layer. In Proc. XXIII IAHR Congress, Ottawa, August 21-25, published by National Research Council Canada, pp. A55-A62.*

Slaattelid, O.H. and Myrhaug, D., 1994. *Data from near-bottom measurements of flow velocity and sediment concentration in the North Sea. Report No. 401515.00.01.94, Marintek, Sintef Group, Norway*

Sleath, J.F.A., 1991. *Velocities and shear stresses in wave-current flows, Journal Geophysical Research, 96 (C8), p.15237-15244.*

Soulsby, R.L., L. Hamm, G. Klopman, D. Myrhaug, R.R. Simons, and G.P. Thomas, 1993. *Wave-current interaction within and outside the bottom boundary layer. Coastal Engineering, 21 (1993) 41-69, Elsevier Science Publishers B.V., Amsterdam.*

Stelling, G.S., 1983. *On the construction of computational methods for shallow water flow problems. Ph.D. Thesis, Delft Univ. of Techn., Delft.*

Stelling, G.S. and Kester, van J.A.T.M., 1994. *On the approximation of horizontal gradients in sigma coordinates for bathymetry with steep bottom slopes. Int. J. Num. Meth. Fluids, Vol. 18, 915-955.*

Stelling, G.S. and Leendertse, J.J., 1991. *Approximation of Convective Processes by Cyclic ACI methods. Proceeding 2nd ASCE Conference on Estuarine and Coastal Modelling, Tampa.*

Sternberg, R.W., 1967. *Measurements of sediment movement and ripple migration in a shallow marine environment. Marine Geology 5, p. 195-205*

Stive, M.J.F. and Wind, H.G., 1986. *Cross-shore mean flow in the surf zone. Coastal Eng., 10, pp. 235-340.*

Stokes, G.G., 1847. *On the theory of oscillatory waves, p. 441-455. Trans. Cambridge Phil. Soc., Vol. 8*

Svendsen, I.A., 1985. *On the formulation of the cross-shore wave-current problem. Proc. Workshop "European Coastal Zones". Athens, pp. 1.1-1.9.*

Towbridge, J.H. and Madsen, O.S., 1984. *Turbulent wave boundary layers, 1, Model formulation and first-order solution, p. 7989-7997. Journal Geophysical Research, 89 (C5)*

Towbridge, J.H. and Madsen, O.S., 1984. *Turbulent wave boundary layers, 2, Second-order theory and mass transport, p. 7999-8007. Journal Geophysical Research, 89 (C5)*

Traykovski, P. and Goff, J.A., 2003. *Observations and modelling of large and small-scale bedforms at the Martha's Vineyard coastal observatory. Coastal Sediments, Florida, USA*

Uittenbogaard, R.E., 1998. *Model for eddy diffusivity and viscosity related to sub-grid velocity and bed topography. Note, WL | Delft Hydraulics.*

Utnes, T., and Eidsvik, K.J. 1996. *Turbulent flows over mountains modelled by the Reynolds equations, p. 393-416. Boundary Layer Meteorology Vol. 79*

Van de Meene, J.W.H, 1994. *The shoreface-connected ridges along the central Dutch coast. Doctoral Thesis, Department of Physical Geography, University of Utrecht, Utrecht, The Netherlands*

Van der Werf, J, 2003. *Sand transport processes in the ripple regime, Data report Series T, U. Department of Civil Engineering, Water Engineering and Management, University of Twente, The Netherlands*

Van Rijn, L.C., 1993. *Principles of sediment transport in rivers, estuaries and coastal seas. Aqua Publications, The Netherlands*

Van Rijn, L.C., 1995. *Yearly-averaged sand transport at the -20 and -8 m NAP depth contours of the Jarkus-profiles 14, 40, 76 and 103. Delft Hydraulics, report H1887, project kustgenese.*

Van Rijn, L.C. and Havinga, F.J., 1995. *Transport of fine sands by currents and waves, Part II, p. 123-133. Journal of Waterway, Port, Coastal and Ocean Engineering, Vol. 121, No. 2*

Van Rijn, L.C. et al., 1993. *Transport of fine sands by currents and waves, p. 123-143. Journal of Waterway, Port, Coastal and Ocean Engineering, Vol. 119, No. 2*

Van Rijn, L.C., 2000. *General view on sand transport by currents and waves, Report Z2899.20-Z2099.30-Z2824.30, Delft Hydraulics, Delft, The Netherlands*

Van Rijn, L.C., 2002. *Approximation formulae for sand transport by currents and waves and implementation in DELFT-MOR. Report Z3054.20, Delft Hydraulics, Delft, The Netherlands.*

Van Rijn, L.C., 2003. *Sand Transport by currents and waves; general approximation formulae. Coastal Sediments 1999, ASCE, Long Island New York.*

Van Vossen, B., 2000. *Horizontal Large Eddy Simulations; evaluation of computations with DELFT3D-FLOW. Report MEAH-197, Delft University of Technology.*

Verboom, G.K. and Slob, A., 1984. *Weakly reflective boundary conditions for two-dimensional water flow problems. 5th Int. Conf. on Finite Elements in Water Resources, June 1984, Vermont. Also Adv. Water Resources, Vol. 7, December 1984, Delft Hydraulics publication No. 322.*

Vongvisessomjai, S., 1984. *Oscillatory ripple geometry, p. 247-266. Journal of Hydraulic Engineering, Vol. 110, No. 3*

Walstra D.J.R., L.C. van Rijn, S. Hoogewoning and Aarninkhof, S.G.J., 1998. *Modelling of sedimentation of dredged trenches and channels under the influence of tidal currents and waves. Coastal Sediments 1999, ASCE, Long Island New York.*

Walstra D.J.R., L.C. van Rijn and M.A.G. van Helvert, 2002a. *Morphology of Pits, Channels and Trenches. Part II:Model verification of DELFT3D with PUTMOR dataset. WL | Delft Hydraulics report no. Z3223.*

Walstra D.J.R., L.C. van Rijn and G. de Boer, 2002b. *Morphology of Pits, Channels and Trenches. Part III: Investigation of the longshore and cross-shore impact of various pit designs. WL | Delft Hydraulics report no. Z3223.30.*

Walstra, D.J.R., J.A. Roelvink and J. Groeneweg, 2000: *Calculation of wave-driven currents in a 3D mean flow model. In: Coastal Engineering 2000, Billy Edge (ed.), Vol. 2, ASCE, New York, pp. 1050-1063.*

Wiberg, P.L.and Harris, C.K., 1994. *Ripple geometry in wave-dominated environments, p. 775-789. Journal of Geophysical Research, Vol. 99*

Wolf, F.C.,J., 1997. *Hydrodynamics, sediment transport and daily morphological development of a bar-beach system. Doc. Thesis, Dep. of Physical Geography, Univ. of Utrecht, The Netherlands*

You, Z.L.,1995. *Increase of current bottom shear stress due to waves, p. 291-295. Coastal Engineering, 26*

You, Z.L. and Nielsen, P., 1996. *Movable bed roughness in the flow of irregular waves and currents over movable beds, p. 3495-3505. 25th ICCE, Orlando, USA*

A Wave height and wind velocity data

STATION	:	Raai	76	
WINDRICHTINGS SECTOR	:	180 - 209	GRADEN	
Hm0 (m)	Tm02 (s)	alfa golf	W (m/s)	alfa wind
0.01	3.77	273	0	195
0.35	3.77	273	4.4	195
0.73	4.01	247	6.7	195
1.21	4.36	233	9.4	195
1.72	4.75	228	12.3	195
2.2	5.18	228	13.9	195
2.73	5.54	232	15.8	195
3.18	5.76	230	17	195
3.67	6.34	232	18	195
0	0	0	0	195
4.59	6.9	232	19.3	195

STATION	:	Raai	76	
WINDRICHTINGS SECTOR	:	210 - 239	GRADEN	
Hm0 (m)	Tm02 (s)	alfa golf	W (m/s)	alfa wind
0.01	3.69	281	0	225
0.35	3.69	281	4.4	225
0.75	4.06	260	6.4	225
1.24	4.45	245	9.1	225
1.72	4.87	240	11.5	225
2.21	5.28	239	13.3	225
2.72	5.69	240	14.7	225
3.21	5.97	239	16.3	225
3.74	6.48	238	18	225
4.28	6.85	243	18.2	225
5.72	7.65	256	23.4	225

STATION	:	Raai	76	
WINDRICHTINGS SECTOR	:	240 - 269	GRADEN	
Hm0 (m)	Tm02 (s)	alfa golf	W (m/s)	alfa wind
0.01	3.8	300	0	255
0.36	3.8	300	3.5	255
0.75	4.2	286	5.4	255
1.23	4.58	270	7.9	255
1.73	5	263	10.1	255
2.23	5.4	260	11.8	255
2.71	5.78	259	13.5	255
3.22	6.21	263	14.9	255
3.7	6.51	266	15.8	255
4.18	6.89	262	18.3	255
4.97	7.13	266	19.8	255

STATION	:	Raai	76	
WINDRICHTINGS SECTOR	:	270 - 299	GRADEN	
Hm0 (m)	Tm02 (s)	alfa golf	W (m/s)	alfa wind
0.01	3.85	318	0	285
0.35	3.85	318	3	285
0.76	4.28	310	4.8	285
1.24	4.7	303	6.8	285
1.72	5.07	296	9	285
2.21	5.46	293	11.1	285
2.73	5.91	294	12.7	285
3.24	6.26	293	14.2	285
3.72	6.63	292	15.5	285
4.23	6.96	291	16.4	285
4.96	7.41	290	18	285

STATION	:	Raai	76	
WINDRICHTINGS SECTOR	:	300 - 329	GRADEN	
Hm0 (m)	Tm02 (s)	alfa golf	W (m/s)	alfa wind
0.01	3.82	332	0	315
0.35	3.82	332	2.9	315
0.76	4.35	330	4.3	315
1.24	4.72	329	6.6	315
1.72	5.11	327	8.7	315
2.22	5.53	325	10.6	315
2.72	5.98	327	12	315
3.23	6.41	324	13.1	315
3.75	6.79	325	14	315
4.24	7.16	328	14.6	315
4.96	7.66	324	16.4	315

STATION	:	Raai	76	
WINDRICHTINGS SECTOR	:	330 - 359	GRADEN	
Hm0 (m)	Tm02 (s)	alfa golf	W (m/s)	alfa wind
0.01	3.75	346	0	345
0.33	3.75	346	3.4	345
0.76	4.33	345	4.7	345
1.22	4.66	344	6.5	345
1.72	5.06	344	8.6	345
2.21	5.48	344	10.3	345
2.69	5.91	345	11.5	345
3.18	6.39	344	12.8	345
3.62	6.69	342	13.6	345
4.1	7.02	347	14.3	345
5.04	8.04	336	16.2	345

STATION	:	Raai	76	
WINDRICHTINGS SECTOR	:	0 - 29	GRADEN	
Hm0 (m)	Tm02 (s)	alfa golf	W (m/s)	alfa wind
0.01	3.75	355	0	15
0.33	3.75	355	3.7	15
0.74	4.13	357	5.3	15
1.21	4.58	357	6.8	15
1.69	4.92	358	8.5	15
2.23	5.46	353	10.5	15
2.73	5.88	354	11.9	15
3.25	6.35	353	12.6	15
3.78	6.37	2	16.9	15
4.38	7	7	13.3	15
0	0	0	0	15

STATION	:	Raai	76	
WINDRICHTINGS SECTOR	:	30 - 59	GRADEN	
Hm0 (m)	Tm02 (s)	alfa golf	W (m/s)	alfa wind
0.01	3.84	358	0	45
0.34	3.84	358	3.7	45
0.75	4.16	8	5.6	45
1.18	4.52	11	7.2	45
1.71	4.94	15	9.8	45
2.17	5.06	21	11.2	45
2.68	5.59	26	13.8	45
3.1	6.4	342	13.3	45
3.74	6.3	24	8.9	45
0	0	0	0	45
0	0	0	0	45

STATION	:	Raai	76	
WINDRICHTINGS SECTOR	:	60 - 89	GRADEN	
Hm0 (m)	Tm02 (s)	alfa golf	W (m/s)	alfa wind
0.01	3.77	13	0	75
0.34	3.77	13	4.7	75
0.72	4.05	24	6.7	75
1.17	4.31	32	9.4	75
1.66	4.7	39	12.1	75
2.17	5.85	44	11.5	75
2.54	6	48	13.2	75
0	0	0	0	75
0	0	0	0	75
0	0	0	0	75
0	0	0	0	75

STATION	:	Raai	76	
WINDRICHTINGS SECTOR	:	90 - 119	GRADEN	
Hm0 (m)	Tm02 (s)	alfa golf	W (m/s)	alfa wind
0.01	3.7	18	0	105
0.34	3.7	18	4.6	105
0.66	3.94	37	6.5	105
1.11	4.81	28	7.3	105
1.51	6.2	359	1.6	105
0	0	0	0	105
2.56	5.9	22	4.8	105
3.02	6.4	78	6.6	105
0	0	0	0	105
0	0	0	0	105
0	0	0	0	105

STATION	:	Raai	76	
WINDRICHTINGS SECTOR	:	120 - 149	GRADEN	
Hm0 (m)	Tm02 (s)	alfa golf	W (m/s)	alfa wind
0.01	3.56	43	0	135
0.33	3.56	43	4.8	135
0.64	3.92	87	5.9	135
1.14	5.09	356	4.7	135
1.55	3.9	157	14.1	135
0	0	0	0	135
0	0	0	0	135
0	0	0	0	135
0	0	0	0	135
0	0	0	0	135
0	0	0	0	135

STATION	:	Raai	76	
WINDRICHTINGS SECTOR	:	150 - 179	GRADEN	
Hm0 (m)	Tm02 (s)	alfa golf	W (m/s)	alfa wind
0.01	3.81	266	0	165
0.33	3.81	266	4.5	165
0.69	4.11	241	5.8	165
1.18	4.45	219	8.4	165
1.67	4.62	214	11.3	165
2.27	4.99	212	13.4	165
2.95	5.4	208	13.7	165
0	0	0	0	165
0	0	0	0	165
0	0	0	0	165
0	0	0	0	165

Table A: Wave height and wind velocity data for each wind direction for profile 76. After Van Rijn (1995), Table 3.3.3A. See Section 4.3 of report.

B The percentage of occurrence of wave data

Significant				Wave	Direc -tion	(deg. N)							
Wave													
Height	0	30	60	90	120	150	180	210	240	270	300	330	
(m)	30	60	90	120	150	180	210	240	270	300	330	360	Total
<0.5	1.39	1.28	2.25	3.3	3.15	2.42	2.2	2.3	1.33	1.02	0.88	1.16	22.7
0.50:1.00	2.66	2.72	3.37	2.57	1.53	2.62	4.33	5.35	3.24	2.48	2.29	2.45	35.6
1.00:1.50	1.71	1.38	1.14	0.15	0.1	0.5	2.57	4.1	2.85	2.03	1.91	1.74	20.19
1.50:2.00	0.6	0.38	0.18	0	0	0.12	1.27	2.98	1.89	1.44	1.41	0.97	11.26
2.00:2.50	0.12	0.1	0.02	0	0	0.03	0.56	1.38	0.93	0.94	0.82	0.46	5.35
2.50:3.00	0.09	0.03	0	0	0	0	0.22	0.64	0.54	0.55	0.42	0.29	2.79
3.00:3.50	0.03	0	0	0	0	0	0.05	0.16	0.24	0.3	0.18	0.1	1.05
3.50:4.00	0.01	0	0	0	0	0	0.02	0.05	0.11	0.24	0.1	0.03	0.56
4.00:4.50	0	0	0	0	0	0	0	0.03	0.06	0.11	0.06	0.02	0.28
>4.5	0	0	0	0	0	0	0.01	0.01	0.03	0.1	0.05	0.03	0.22
Total	6.61	5.91	6.96	6.03	4.79	5.7	11.23	17	11.21	9.22	8.1	7.24	100

Table B: The percentage of occurrence of wave data (all year) for profile 76. After Van Rijn (1995), Table 3.3.7. See Section 4.3 of report.

C Current velocities and water levels

#	Raai	76											
water	depth:	20	m										
	wind	direction											
	number	sector	direction										
	1	180-210	195										
#no.	class	wave	height										
	1	0	0										
u	(m/s)	-0.05	0.14	0.32	0.28	0.18	0.12	0.01	-0.09	-0.18	-0.26	-0.24	-0.18
v	(m/s)	-0.14	0.13	0.49	0.59	0.48	0.33	0.12	-0.16	-0.41	-0.5	-0.47	-0.38
h	(m)	-0.39	-0.04	0.61	0.87	0.67	0.42	0.1	-0.2	-0.26	-0.28	-0.4	-0.44
#no.	class	wave	height										
	2	.00-0.50	0.25										
u	(m/s)	-0.044	0.146	0.326	0.286	0.184	0.124	0.012	-0.084	-0.174	-0.254	-0.236	-0.176
v	(m/s)	-0.13	0.14	0.498	0.596	0.488	0.336	0.128	-0.15	-0.4	-0.49	-0.46	-0.37
h	(m)	-0.392	-0.042	0.608	0.868	0.67	0.42	0.1	-0.202	-0.264	-0.28	-0.4	-0.442
#no.	class	wave	height										
	3	.50-1.00	35										
u	(m/s)	-0.032	0.158	0.338	0.298	0.192	0.132	0.016	-0.072	-0.162	-0.242	-0.228	-0.168
v	(m/s)	-0.11	0.16	0.514	0.608	0.504	0.348	0.144	-0.13	-0.38	-0.47	-0.44	-0.35
h	(m)	-0.393	-0.046	0.604	0.864	0.67	0.42	0.1	-0.206	-0.272	-0.28	-0.4	-0.446
#no.	class	wave	height										
	4	1.00-1.50	1.25										
u	(m/s)	-0.02	0.17	0.35	0.31	0.2	0.14	0.02	-0.06	-0.15	-0.23	-0.22	-0.16
v	(m/s)	-0.09	0.18	0.53	0.62	0.52	0.36	0.16	-0.11	-0.36	-0.45	-0.42	-0.33
h	(m)	-0.4	-0.05	0.6	0.86	0.67	0.42	0.1	-0.21	-0.28	-0.28	-0.4	-0.45
#no.	class	wave	height										
	5	1.50-2.00	1.75										
u	(m/s)	-0.007	0.183	0.357	0.317	0.207	0.143	0.027	-0.05	-0.137	-0.217	-0.21	-0.15
v	(m/s)	-0.07	0.207	0.55	0.637	0.53	0.373	0.177	-0.087	-0.337	-0.433	-0.4	-0.31
h	(m)	-0.4	-0.047	0.597	0.857	0.667	0.417	0.097	-0.213	-0.283	-0.28	-0.4	-0.453
#no.	class	wave	height										
	6	2.00-2.50	2.25										
u	(m/s)	0.007	0.197	0.363	0.323	0.213	0.147	0.033	-0.04	-0.123	-0.203	-0.2	-0.14
v	(m/s)	-0.05	0.233	0.57	0.653	0.54	0.387	0.193	-0.063	-0.313	-0.417	-0.38	-0.29
h	(m)	-0.4	-0.043	0.593	0.853	0.663	0.413	0.093	-0.217	-0.287	-0.28	-0.4	-0.457
#no.	class	wave	height										
	7	2.50-3.00	2.75										
u	(m/s)	0.02	0.21	0.37	0.33	0.22	0.15	0.04	-0.03	-0.11	-0.19	-0.19	-0.13
v	(m/s)	-0.03	0.26	0.59	0.67	0.55	0.4	0.21	-0.04	-0.29	-0.4	-0.36	-0.27
h	(m)	-0.4	-0.04	0.59	0.85	0.66	0.41	0.09	-0.22	-0.29	-0.28	-0.4	-0.46

#no.	class	wave	height										
	8	3.00-3.50	3.25										
u	(m/s)	0.04	0.23	0.383	0.34	0.23	0.157	0.05	-0.017	-0.093	-0.173	-0.173	-0.11
v	(m/s)	0.003	0.29	0.613	0.687	0.57	0.417	0.23	-0.013	-0.26	-0.37	-0.33	-0.243
h	(m)	-0.393	-0.037	0.583	0.84	0.653	0.403	0.087	-0.227	-0.293	-0.28	-0.4	-0.463
#no.	class	wave	height										
	9	3.50-4.00	3.75										
u	(m/s)	0.06	0.25	0.397	0.35	0.24	0.163	0.06	-0.003	-0.077	-0.157	-0.157	-0.09
v	(m/s)	0.037	0.32	0.637	0.703	0.59	0.433	0.25	0.013	-0.23	-0.34	-0.3	-0.217
h	(m)	-0.387	-0.033	0.577	0.83	0.647	0.397	0.083	-0.233	-0.297	-0.28	-0.4	-0.467
#no.	class	wave	height										
#	10	4.00-4.50	4.25										
u	(m/s)	0.08	0.27	0.41	0.36	0.25	0.17	0.07	0.01	-0.06	-0.14	-0.14	-0.07
v	(m/s)	0.07	0.35	0.66	0.72	0.61	0.45	0.27	0.04	-0.2	-0.31	-0.27	-0.19
h	(m)	-0.38	-0.03	0.57	0.82	0.64	0.39	0.08	-0.24	-0.3	-0.28	-0.4	-0.47
#no.	class	wave	height										
#	11	4.50-9.99	extr										
u	(m/s)	0.08	0.27	0.41	0.36	0.25	0.17	0.07	0.01	-0.06	-0.14	-0.14	-0.07
v	(m/s)	0.07	0.35	0.66	0.72	0.61	0.45	0.27	0.04	-0.2	-0.31	-0.27	-0.19
h	(m)	-0.38	-0.03	0.57	0.82	0.64	0.39	0.08	-0.24	-0.3	-0.28	-0.4	-0.47
#	wind	direction											
#	number	sector	direction										
#	2	210-240	225										
#no.	class	wave	height										
#	1	0	0										
u	(m/s)	-0.05	0.14	0.32	0.28	0.18	0.12	0.01	-0.09	-0.18	-0.26	-0.24	-0.18
v	(m/s)	-0.14	0.13	0.49	0.59	0.48	0.33	0.12	-0.16	-0.41	-0.5	-0.47	-0.38
h	(m)	-0.39	-0.04	0.61	0.87	0.67	0.42	0.1	-0.2	-0.26	-0.28	-0.4	-0.44
#no.	class	wave	height										
#	2	.00-0.50	0.25										
u	(m/s)	-0.044	0.146	0.324	0.284	0.184	0.122	0.012	-0.086	-0.176	-0.256	-0.238	-0.176
v	(m/s)	-0.132	0.138	0.496	0.594	0.486	0.334	0.126	-0.152	-0.402	-0.492	-0.464	-0.374
h	(m)	-0.378	-0.028	0.622	0.882	0.682	0.432	0.112	-0.188	-0.25	-0.268	-0.386	-0.428
#no.	class	wave	height										
#	3	.50-1.00	0.75										
u	(m/s)	-0.032	0.158	0.332	0.292	0.192	0.126	0.016	-0.078	-0.168	-0.248	-0.234	-0.168
v	(m/s)	-0.116	0.154	0.508	0.602	0.498	0.342	0.138	-0.136	-0.386	-0.476	-0.452	-0.362
h	(m)	-0.354	-0.004	0.646	0.906	0.706	0.456	0.136	-0.164	-0.23	-0.244	-0.358	-0.404
#no.	class	wave	height										
#	4	1.00-1.50	1.25										
u	(m/s)	-0.02	0.17	0.34	0.3	0.2	0.13	0.02	-0.07	-0.16	-0.24	-0.23	-0.16
v	(m/s)	-0.1	0.17	0.52	0.61	0.51	0.35	0.15	-0.12	-0.37	-0.46	-0.44	-0.35
h	(m)	-0.33	0.02	0.67	0.93	0.73	0.48	0.16	-0.14	-0.21	-0.22	-0.33	-0.38

#no.	class	wave	height										
#	5	1.50-2.00	1.75										
u	(m/s)	-0.01	0.183	0.35	0.31	0.207	0.137	0.027	-0.06	-0.147	-0.227	-0.22	-0.15
v	(m/s)	-0.083	0.19	0.537	0.623	0.52	0.363	0.167	-0.103	-0.35	-0.447	-0.42	-0.333
h	(m)	-0.3	0.05	0.697	0.953	0.757	0.51	0.19	-0.113	-0.183	-0.187	-0.3	-0.353
#no.	class	wave	height										
II	6	2.00-2.50	2.25										
u	(m/s)	0	0.197	0.36	0.32	0.213	0.143	0.033	-0.05	-0.133	-0.213	-0.21	-0.14
v	(m/s)	-0.067	0.21	0.553	0.637	0.53	0.377	0.183	-0.087	-0.33	-0.433	-0.4	-0.317
h	(m)	-0.27	0.08	0.723	0.977	0.783	0.54	0.22	-0.087	-0.157	-0.153	-0.27	-0.327
#no.	class	wave	height										
#	7	2.50-3.00	2.75										
u	(m/s)	0.01	0.21	0.37	0.33	0.22	0.15	0.04	-0.04	-0.12	-0.2	-0.2	-0.13
v	(m/s)	-0.05	0.23	0.57	0.65	0.54	0.39	0.2	-0.07	-0.31	-0.42	-0.38	-0.3
h	(m)	-0.24	0.11	0.75	1	0.81	0.57	0.25	-0.06	-0.13	-0.12	-0.24	-0.3
#no.	class	wave	height										
#	8	3.00-3.50	3.25										
u	(m/s)	0.03	0.23	0.383	0.34	0.23	0.16	0.05	-0.023	-0.1	-0.18	-0.18	-0.113
v	(m/s)	-0.02	0.263	0.59	0.667	0.553	0.407	0.217	-0.04	-0.28	-0.39	-0.35	-0.27
h	(m)	-0.19	0.163	0.793	1.043	0.853	0.61	0.293	-0.017	-0.087	-0.073	-0.193	-0.253
#no.	class	wave	height										
	9	3.50-4.00	3.75										
u	(m/s)	0.05	0.25	0.397	0.35	0.24	0.17	0.06	-0.007	-0.08	-0.16	-0.16	-0.097
v	(m/s)	0.01	0.297	0.61	0.683	0.567	0.423	0.233	-0.01	-0.25	-0.36	-0.32	-0.24
h	(m)	-0.14	0.217	0.837	1.087	0.897	0.65	0.337	0.027	-0.043	-0.027	-0.147	-0.207
#no.	class	wave	height										
#	10	4.00-4.50	4.25										
u	(m/s)	0.07	0.27	0.41	0.36	0.25	0.18	0.07	0.01	-0.06	-0.14	-0.14	-0.08
v	(m/s)	0.04	0.33	0.63	0.7	0.58	0.44	0.25	0.02	-0.22	-0.33	-0.29	-0.21
h	(m)	-0.09	0.27	0.88	1.13	0.94	0.69	0.38	0.07	0	0.02	-0.1	-0.16
#no.	class	wave	height										
#	11	4.50-9.99	extr										
u	(m/s)	0.07	0.27	0.41	0.36	0.25	0.18	0.07	0.01	-0.06	-0.14	-0.14	-0.08
v	(m/s)	0.04	0.33	0.63	0.7	0.58	0.44	0.25	0.02	-0.22	-0.33	-0.29	-0.21
h	(m)	-0.09	0.27	0.88	1.13	0.94	0.69	0.38	0.07	0	0.02	-0.1	-0.16
	wind	direction											
	number	sector	direction										
	3	240-270	255										
#no.	class	wave	height										
	1	0	0										
u	(m/s)	-0.05	0.14	0.32	0.28	0.18	0.12	0.01	-0.09	-0.18	-0.26	-0.24	-0.18
v	(m/s)	-0.14	0.13	0.49	0.59	0.48	0.33	0.12	-0.16	-0.41	-0.5	-0.47	-0.38
h	(m)	-0.39	-0.04	0.61	0.87	0.67	0.42	0.1	-0.2	-0.26	-0.28	-0.4	-0.44

#no.	class	wave	height										
	2	.00-0.50	0.25										
u	(m/s)	-0.046	0.142	0.322	0.282	0.182	0.122	0.01	-0.088	-0.178	-0.258	-0.238	-0.178
v	(m/s)	-0.136	0.132	0.492	0.592	0.482	0.332	0.122	-0.156	-0.406	-0.498	-0.466	-0.378
h	(m)	-0.374	-0.024	0.626	0.886	0.686	0.436	0.116	-0.184	-0.244	-0.264	-0.382	-0.424
t,													
#no.	class	wave	height										
	3	.50-1.00	0.75										
u	(m/s)	-0.038	0.146	0.326	0.286	0.186	0.126	0.01	-0.084	-0.174	-0.254	-0.234	-0.174
v	(m/s)	-0.128	0.136	0.496	0.596	0.486	0.336	0.126	-0.148	-0.398	-0.494	-0.458	-0.374
h	(m)	-0.342	0.008	0.658	0.918	0.718	0.468	0.148	-0.152	-0.212	-0.232	-0.346	-0.392
#no.	class	wave	height										
	4	1.00-1.50	1.25										
u	(m/s)	-0.03	0.15	0.33	0.29	0.19	0.13	0.01	-0.08	-0.17	-0.25	-0.23	-0.17
v	(m/s)	-0.12	0.14	0.5	0.6	0.49	0.34	0.13	-0.14	-0.39	-0.49	-0.45	-0.37
h	(m)	-0.31	0.04	0.69	0.95	0.75	0.5	0.18	-0.12	-0.18	-0.2	-0.31	-0.36
#no.	class	wave	height										
	5	1.50-2.00	1.75										
u	(m/s)	-0.027	0.16	0.337	0.297	0.197	0.133	0.017	-0.073	-0.163	-0.24	-0.227	-0.167
v	(m/s)	-0.11	0.153	0.507	0.603	0.497	0.343	0.14	-0.133	-0.383	-0.48	-0.443	-0.36
h	(m)	-0.267	0.083	0.737	0.993	0.793	0.543	0.227	-0.077	-0.14	-0.153	-0.263	-0.317
#no.	class	wave	height										
6	200- 230	2.25											
u	(m/s)	-0.023	0.17	0.343	0.303	0.203	0.137	0.023	-0.067	-0.157	-0.23	-0.223	-0.163
v	(m/s)	-0.1	0.167	0.513	0.607	0.503	0.347	0.15	-0.127	-0.377	-0.47	-0.437	-0.35
h	(m)	-0.223	0.127	0.783	1.037	0.837	0.587	0.273	-0.033	-0.1	-0.107	-0.217	-0.273
#no.	class	wave	height										
#	7	2.50-3.00	2.75										
u	(m/s)	-0.02	0.18	0.35	0.31	0.21	0.14	0.03	-0.06	-0.15	-0.22	-0.22	-0.16
v	(m/s)	-0.09	0.18	0.52	0.61	0.51	0.35	0.16	-0.12	-0.37	-0.46	-0.43	-0.34
h	(m)	-0.18	0.17	0.83	1.08	0.88	0.63	0.32	0.01	-0.06	-0.06	-0.17	-0.23
#no.	class	wave	height										
#	8	3.00-3.50	3.25										
u	(m/s)	-0.01	0.19	0.357	0.317	0.217	0.143	0.037	-0.05	-0.137	-0.21	-0.21	-0.15
v	(m/s)	-0.08	0.193	0.53	0.62	0.517	0.36	0.167	-0.103	-0.353	-0.447	-0.417	-0.327
h	(m)	-0.113	0.237	0.893	1.14	0.943	0.697	0.383	0.073	0.003	0.007	-0.107	-0.167
#no.	class	wave	height										
#	9	3.50-4.00	3.75										
u	(m/s)	0	0.2	0.363	0.323	0.223	0.147	0.043	-0.04	-0.123	-0.2	-0.2	-0.14
v	(m/s)	-0.07	0.207	0.54	0.63	0.523	0.37	0.173	-0.087	-0.337	-0.433	-0.403	-0.313
h	(m)	-0.047	0.303	0.957	1.2	1.007	0.763	0.447	0.137	0.067	0.073	-0.043	-0.103
#no.	class	wave	height										
#	10	4.00-4.50	4.25										
u	(m/s)	0.01	0.21	0.37	0.33	0.23	0.15	0.05	-0.03	-0.11	-0.19	-0.19	-0.13

v	(m/s)	-0.06	0.22	0.55	0.64	0.53	0.38	0.18	-0.07	-0.32	-0.42	-0.39	-0.3
h	(m)	0.02	0.37	1.02	1.26	1.07	0.83	0.51	0.2	0.13	0.14	0.02	-0.04
#no.	class	wave	height										
#	11	4.50-9.99	extr										
u	(m/s)	0.01	0.21	0.37	0.33	0.23	0.15	0.05	-0.03	-0.11	-0.19	-0.19	-0.13
v	(m/s)	-0.06	0.22	0.55	0.64	0.53	0.38	0.18	-0.07	-0.32	-0.42	-0.39	-0.3
h	(m)	0.02	0.37	1.02	1.26	1.07	0.83	0.51	0.2	0.13	0.14	0.02	-0.04
#	wind	direction											
#	number	sector	direction										
#	4	270-300	285										
#no.	class	wave	height										
#	1	0	0										
u	(m/s)	-0.05	0.14	0.32	0.28	0.18	0.12	0.01	-0.09	-0.18	-0.26	-0.24	-0.18
v	(m/s)	-0.14	0.13	0.49	0.59	0.48	0.33	0.12	-0.16	-0.41	-0.5	-0.47	-0.38
h	(m)	-0.39	-0.04	0.61	0.87	0.67	0.42	0.1	-0.2	-0.26	-0.28	-0.4	-0.44
#no.	class	wave	height										
#	2	.00-0.50	0.25										
u	(m/s)	-0.048	0.14	0.32	0.282	0.182	0.12	0.01	-0.088	-0.18	-0.26	-0.24	-0.18
v	(m/s)	-0.138	0.13	0.49	0.588	0.48	0.328	0.12	-0.16	-0.41	-0.5	-0.47	-0.38
h	(m)	-0.376	-0.028	0.624	0.884	0.684	0.434	0.114	-0.186	-0.246	-0.266	-0.386	-0.426
#no.	class	wave	height										
#	3	.50-1.00	0.75										
u	(m/s)	-0.044	0.14	0.32	0.286	0.186	0.12	0.01	-0.084	-0.18	-0.26	-0.24	-0.18
v	(m/s)	-0.134	0.13	0.49	0.584	0.48	0.324	0.12	-0.16	-0.41	-0.5	-0.47	-0.38
h	(m)	-0.348	-0.004	0.652	0.912	0.712	0.462	0.142	-0.158	-0.218	-0.238	-0.358	-0.398
#no.	class	wave	height										
#	4	1.00-1.50	1.25										
u	(m/s)	-0.04	0.14	0.32	0.29	0.19	0.12	0.01	-0.08	-0.18	-0.26	-0.24	-0.18
v	(m/s)	-0.13	0.13	0.49	0.58	0.48	0.32	0.12	-0.16	-0.41	-0.5	-0.47	-0.38
h	(m)	-0.32	0.02	0.68	0.94	0.74	0.49	0.17	-0.13	-0.19	-0.21	-0.33	-0.37
#no.	class	wave	height										
#	5	1.50-2.00	1.75										
u	(m/s)	-0.04	0.143	0.323	0.29	0.19	0.12	0.01	-0.08	-0.177	-0.257	-0.24	-0.18
v	(m/s)	-0.133	0.13	0.49	0.58	0.48	0.32	0.12	-0.16	-0.41	-0.5	-0.47	-0.38
h	(m)	-0.273	0.07	0.73	0.99	0.787	0.54	0.22	-0.08	-0.143	-0.163	-0.277	-0.32
#no.	class	wave	height										
#	6	2.00-2.50	2.25										
u	(m/s)	-0.04	0.147	0.327	0.29	0.19	0.12	0.01	-0.08	-0.173	-0.253	-0.24	-0.18
v	(m/s)	-0.137	0.13	0.49	0.58	0.48	0.32	0.12	-0.16	-0.41	-0.5	-0.47	-0.38
h	(m)	-0.227	0.12	0.78	1.04	0.833	0.59	0.27	-0.03	-0.097	-0.117	-0.223	-0.27
#no.	class	wave	height										
#	7	2.50-3.00	2.75										
u	(m/s)	-0.04	0.15	0.33	0.29	0.19	0.12	0.01	-0.08	-0.17	-0.25	-0.24	-0.18

v	(m/s)	-0.14	0.13	0.49	0.58	0.48	0.32	0.12	-0.16	-0.41	-0.5	-0.47	-0.38
h	(m)	-0.18	0.17	0.83	1.09	0.88	0.64	0.32	0.02	-0.05	-0.07	-0.17	-0.22
#no.	class	wave	height										
#	8	3.00-3.50	3.25										
u	(m/s)	-0.037	0.15	0.33	0.29	0.193	0.123	0.013	-0.077	-0.167	-0.247	-0.237	-0.177
v	(m/s)	-0.137	0.13	0.487	0.58	0.48	0.32	0.12	-0.16	-0.407	-0.497	-0.467	-0.377
h	(m)	-0.107	0.243	0.903	1.16	0.953	0.713	0.393	0.093	0.023	0.003	-0.097	-0.147
#no.	class	wave	height										
#	9	3.50-4.00	3.75										
u	(m/s)	-0.033	0.15	0.33	0.29	0.197	0.127	0.017	-0.073	-0.163	-0.243	-0.233	-0.173
v	(m/s)	-0.133	0.13	0.483	0.58	0.48	0.32	0.12	-0.16	-0.403	-0.493	-0.463	-0.373
h	(m)	-0.033	0.317	0.977	1.23	1.027	0.787	0.467	0.167	0.097	0.077	-0.023	-0.073
#no.	class	wave	height										
#	10	4.00-4.50	4.25										
u	(m/s)	-0.03	0.15	0.33	0.29	0.2	0.13	0.02	-0.07	-0.16	-0.24	-0.23	-0.17
v	(m/s)	-0.13	0.13	0.48	0.58	0.48	0.32	0.12	-0.16	-0.4	-0.49	-0.46	-0.37
h	(m)	0.04	0.39	1.05	1.3	1.1	0.86	0.54	0.24	0.17	0.15	0.05	0
#no.	class	wave	height										
#	11	4.50-9.99	extr										
u	(m/s)	-0.03	0.15	0.33	0.29	0.2	0.13	0.02	-0.07	-0.16	-0.24	-0.23	-0.17
v	(m/s)	-0.13	0.13	0.48	0.58	0.48	0.32	0.12	-0.16	-0.4	-0.49	-0.46	-0.37
h	(m)	0.04	0.39	1.05	1.3	1.1	0.86	0.54	0.24	0.17	0.15	0.05	0
#	wind	direction											
#	number	sector	direction										
#	5	300-330	315										
#no.	class	wave	height										
#	1	0	0										
u	(m/s)	-0.05	0.14	0.32	0.28	0.18	0.12	0.01	-0.09	-0.18	-0.26	-0.24	-0.18
v	(m/s)	-0.14	0.13	0.49	0.59	0.48	0.33	0.12	-0.16	-0.41	-0.5	-0.47	-0.38
h	(m)	-0.39	-0.04	0.61	0.87	0.67	0.42	0.1	-0.2	-0.26	-0.28	-0.4	-0.44
#no.	class	wave	height										
#	2	.00-0.50	0.25										
u	(m/s)	-0.05	0.14	0.32	0.28	0.18	0.118	0.008	-0.09	-0.18	-0.26	-0.242	-0.18
v	(m/s)	-0.14	0.128	0.488	0.588	0.478	0.328	0.118	-0.164	-0.412	-0.502	-0.472	-0.38
h	(m)	-0.38	-0.03	0.622	0.882	0.682	0.43	0.11	-0.188	-0.248	-0.27	-0.39	-0.428
#no.	class	wave	height										
	3	.50-1-00	0.75										
u	(m/s)	-0.05	0.14	0.32	0.28	0.18	0.114	0.004	-0.09	-0.18	-0.26	-0.246	-0.18
v	(m/s)	-0.14	0.124	0.484	0.584	0.474	0.324	0.114	-0.172	-0.416	-0.506	-0.476	-0.38
h	(m)	-0.36	-0.01	0.646	0.906	0.706	0.45	0.13	-0.164	-0.224	-0.25	-0.37	-0.404
#no.	class	wave	height										
	4	1.00-1.50	1.25										
u	(m/s)	-0.05	0.14	0.32	0.28	0.18	0.11	0	-0.09	-0.18	-0.26	-0.25	-0.18

v	(m/s)	-0.14	0.12	0.48	0.58	0.47	0.32	0.11	-0.18	-0.42	-0.51	-0.48	-0.38
h	(m)	-0.34	0.01	0.67	0.93	0.73	0.47	0.15	-0.14	-0.2	-0.23	-0.35	-0.38
#no.	class	wave	height										
	5	1.50-2.00	1.75										
u	(m/s)	-0.05	0.133	0.317	0.277	0.177	0.11	0	-0.093	-0.183	-0.263	-0.25	-0.183
v	(m/s)	-0.147	0.11	0.47	0.573	0.463	0.317	0.107	-0.187	-0.427	-0.513	-0.483	-0.387
h	(m)	-0.3	0.047	0.71	0.967	0.767	0.51	0.19	-0.1	-0.16	-0.19	-0.31	-0.34
#no.	class	wave	height										
	6	2.00-2.50	2.25										
u	(m/s)	-0.05	0.127	0.313	0.273	0.173	0.11	0	-0.097	-0.187	-0.267	-0.25	-0.187
v	(m/s)	-0.153	0.1	0.46	0.567	0.457	0.313	0.103	-0.193	-0.433	-0.517	-0.487	-0.393
h	(m)	-0.26	0.083	0.75	1.003	0.803	0.55	0.23	-0.06	-0.12	-0.15	-0.27	-0.3
#no.	class	wave	height										
	7	2.50-3.00	2.75										
u	(m/s)	-0.05	0.12	0.31	0.27	0.17	0.11	0	-0.1	-0.19	-0.27	-0.25	-0.19
v	(m/s)	-0.16	0.09	0.45	0.56	0.45	0.31	0.1	-0.2	-0.44	-0.52	-0.49	-0.4
h	(m)	-0.22	0.12	0.79	1.04	0.84	0.59	0.27	-0.02	-0.08	-0.11	-0.23	-0.26
#no.	class	wave	height										
	8	3.00-3.50	3.25										
u	(m/s)	-0.053	0.117	0.307	0.27	0.17	0.107	-0.003	-0.103	-0.193	-0.273	-0.253	-0.19
v	(m/s)	-0.167	0.08	0.443	0.553	0.443	0.3	0.09	-0.21	-0.447	-0.527	-0.497	-0.407
h	(m)	-0.167	0.17	0.843	1.093	0.89	0.64	0.32	0.033	-0.03	-0.06	-0.177	-0.207
#no.	class	wave	height										
	9	3.50-4.00	3.75										
u	(m/s)	-0.057	0.113	0.303	0.27	0.17	0.103	-0.007	-0.107	-0.197	-0.277	-0.257	-0.19
v	(m/s)	-0.173	0.07	0.437	0.547	0.437	0.29	0.08	-0.22	-0.453	-0.533	-0.503	-0.413
h	(m)	-0.113	0.22	0.897	1.147	0.94	0.69	0.37	0.087	0.02	-0.01	-0.123	-0.153
#no.	class	wave	height										
	10	4.00-4.50	4.25										
u	(m/s)	-0.06	0.11	0.3	0.27	0.17	0.1	-0.01	-0.11	-0.2	-0.28	-0.26	-0.19
v	(m/s)	-0.18	0.06	0.43	0.54	0.43	0.28	0.07	-0.23	-0.46	-0.54	-0.51	-0.42
h	(m)	-0.06	0.27	0.95	1.2	0.99	0.74	0.42	0.14	0.07	0.04	-0.07	-0.1
#no.	class	wave	height										
	11	4.50-9.99	extr										
u	(m/s)	-0.06	0.11	0.3	0.27	0.17	0.1	-0.01	-0.11	-0.2	-0.28	-0.26	-0.19
v	(m/s)	-0.18	0.06	0.43	0.54	0.43	0.28	0.07	-0.23	-0.46	-0.54	-0.51	-0.42
h	(m)	-0.06	0.27	0.95	1.2	0.99	0.74	0.42	0.14	0.01	0.04	-0.07	-0.1
	wind	direction											
#	number	sector	direction										
#	6	330-360	345										
#no.	class	wave	height										
#	1	0	0										

u	(m/s)	-0.05	0.14	0.32	0.28	0.18	0.12	0.01	-0.09	-0.18	-0.26	-0.24	-0.18
v	(m/s)	-0.14	0.13	0.49	0.59	0.48	0.33	0.12	-0.16	-0.41	-0.5	-0.47	-0.38
h	(m)	-0.39	-0.04	0.61	0.87	0.67	0.42	0.1	-0.2	-0.26	-0.28	-0.4	-0.44
#no.	class	wave	height								
#	2	.00-0.50	0.25								
u	(m/s)	-0.05	0.138	0.318	0.28	0.18	0.118	0.008	-0.092	-0.182	-0.262	-0.242	-0.182
v	(m/s)	-0.142	0.124	0.486	0.586	0.476	0.328	0.118	-0.166	-0.414	-0.504	-0.472	-0.384
h	(m)	-0.382	-0.034	0.618	0.878	0.678	0.428	0.108	-0.192	-0.252	-0.272	-0.392	-0.432
#no.	class	wave	height								
#	3	.50-1.00	0.75								
u	(m/s)	-0.05	0.134	0.314	0.28	0.18	0.114	0.004	-0.096	-0.186	-0.266	-0.246	-0.186
v	(m/s)	-0.146	0.112	0.478	0.578	0.468	0.324	0.114	-0.178	-0.422	-0.512	-0.476	-0.392
h	(m)	-0.366	-0.022	0.634	0.894	0.694	0.444	0.124	-0.176	-0.236	-0.256	-0.376	-0.416
#no.	class	wave	height								
#	4	1.00-1.50	125								
u	(m/s)	-0.05	0.13	0.31	0.28	0.18	0.11	0	-0.1	-0.19	-0.27	-0.25	-0.19
v	(m/s)	-0.15	0.1	0.47	0.57	0.46	0.32	0.11	-0.19	-0.43	-0.52	-0.48	-0.4
h	(m)	-0.35	-0.01	0.65	0.91	0.71	0.46	0.14	-0.16	-0.22	-0.24	-0.36	-0.4
#no.	class	wave	height								
#	5	1.50-2.00	1.75								
u	(m/s)	-0.057	0.123	0.307	0.273	0.173	0.107	-0.003	-0.103	-0.197	-0.273	-0.253	-0.193
v	(m/s)	-0.16	0.09	0.457	0.56	0.453	0.31	0.097	-0.2	-0.437	-0.527	-0.49	-0.407
h	(m)	-0.33	0.01	0.673	0.93	0.73	0.477	0.157	-0.137	-0.197	-0.223	-0.343	-0.377
#no.	class	wave	height								
#	6	2.00-2.50	2.25								
u	(m/s)	-0.063	0.117	0.303	0.267	0.167	0.103	-0.007	-0.107	-0.203	-0.277	-0.257	-0.197
v	(m/s)	-0.17	0.08	0.443	0.55	0.447	0.3	0.083	-0.21	-0.443	-0.533	-0.5	-0.413
h	(m)	-0.31	0.03	0.697	0.95	0.75	0.493	0.173	-0.113	-0.173	-0.207	-0.327	-0.353
#no.	class	wave	height								
#	7	2.50-3.00	2.75								
u	(m/s)	-0.07	0.11	0.3	0.26	0.16	0.1	-0.01	-0.11	-0.21	-0.28	-0.26	-0.2
v	(m/s)	-0.18	0.07	0.43	0.54	0.44	0.29	0.07	-0.22	-0.45	-0.54	-0.51	-0.42
h	(m)	-0.29	0.05	0.72	0.97	0.77	0.51	0.19	-0.09	-0.15	-0.19	-0.31	-0.33
#no.	class	wave	height								
#	8	3.00-3.50	3.25								
u	(m/s)	-0.073	0.1	0.29	0.253	0.153	0.093	-0.017	-0.117	-0.22	-0.29	-0.267	-0.203
v	(m/s)	-0.19	0.053	0.417	0.527	0.427	0.277	0.057	-0.237	-0.47	-0.553	-0.52	-0.433
h	(m)	-0.253	0.077	0.75	1.003	0.8	0.54	0.217	-0.057	-0.117	-0.16	-0.28	-0.297
#no.	class	wave	height								
#	9	3.50-4.00	3.75								
u	(m/s)	-0.077	0.09	0.28	0.247	0.147	0.087	-0.023	-0.123	-0.23	-0.3	-0.273	-0.207
v	(m/s)	-0.2	0.037	0.403	0.513	0.413	0.263	0.043	-0.253	-0.49	-0.567	-0.53	-0.447
h	(m)	-0.217	0.103	0.78	1.037	0.83	0.57	0.243	-0.023	-0.083	-0.13	-0.25	-0.263

#no.	class	wave	height										
#	10	4.00-4.50	4.25										
u	(m/s)	-0.08	0.08	0.27	0.24	0.14	0.08	-0.03	-0.13	-0.24	-0.31	-0.28	-0.21
v	(m/s)	-0.21	0.02	0.39	0.5	0.4	0.25	0.03	-0.27	-0.51	-0.58	-0.54	-0.46
h	(m)	-0.18	0.13	0.81	1.07	0.86	0.6	0.27	0.01	-0.05	-0.1	-0.22	-0.23
#no.	class	wave	height										
#	11	4.50-9.99	extr										
u	(m/s)	-0.08	0.08	0.27	0.24	0.14	0.08	-0.03	-0.13	-0.24	-0.31	-0.28	-0.21
v	(m/s)	-0.21	0.02	0.39	0.5	0.4	0.25	0.03	-0.27	-0.51	-0.58	-0.54	-0.46
h	(m)	-0.18	0.13	0.81	1.07	0.86	0.6	0.27	0.01	-0.05	-0.1	-0.22	-0.23
#	wind	direction											
#	number	sector	direction										
#	7	0-30	15										
#no.	class	wave	height										
	1	0	0										
u	(m/s)	-0.05	0.14	0.32	0.28	0.18	0.12	0.01	-0.09	-0.18	-0.26	-0.24	-0.18
v	(m/s)	-0.14	0.13	0.49	0.59	0.48	0.33	0.12	-0.16	-0.41	-0.5	-0.47	-0.38
h	(m)	-0.39	-0.04	0.61	0.87	0.67	0.42	0.1	-0.2	-0.26	-0.28	-0.4	-0.44
#no.	class	wave	height										
	2	.00-0.50	0.25										
u	(m/s)	-0.052	0.136	0.316	0.278	0.178	0.116	0.006	-0.094	-0.184	-0.264	-0.244	-0.184
v	(m/s)	-0.146	0.122	0.482	0.582	0.474	0.324	0.114	-0.168	-0.418	-0.506	-0.476	-0.386
h	(m)	-0.388	-0.042	0.612	0.872	0.672	0.42	0.1	-0.198	-0.258	-0.28	-0.4	-0.438
#no.	class	wave	height										
	3	.50-1.00	0.75										
u	(m/s)	-0.056	0.128	0.308	0.274	0.174	0.108	-0.002	-0.102	-0.192	-0.272	-0.252	-0.192
v	(m/s)	-0.158	0.106	0.466	0.566	0.462	0.312	0.102	-0.184	-0.434	-0.518	-0.488	-0.398
h	(m)	-0.384	-0.046	0.616	0.876	0.676	0.42	0.1	-0.194	-0.254	-0.28	-0.4	-0.434
#no.	class	wave	height										
	4	1.00-1.50	1.25										
u	(m/s)	-0.06	0.12	0.3	0.27	0.17	0.1	-0.01	-0.11	-0.2	-0.28	-0.26	-0.2
v	(m/s)	-0.17	0.09	0.45	0.55	0.45	0.3	0.09	-0.2	-0.45	-0.53	-0.5	-0.41
h	(m)	-0.38	-0.05	0.62	0.88	0.68	0.42	0.1	-0.19	-0.25	-0.28	-0.4	-0.43
#no.	class	wave	height										
	5	1.50-2.00	1.75										
u	(m/s)	-0.067	0.113	0.297	0.263	0.163	0.097	-0.013	-0.113	-0.207	-0.287	-0.263	-0.2
v	(m/s)	-0.18	0.077	0.44	0.54	0.44	0.293	0.08	-0.213	-0.457	-0.54	-0.507	-0.417
h	(m)	-0.377	-0.05	0.623	0.883	0.68	0.42	0.097	-0.187	-0.243	-0.28	-0.4	-0.427
#no.	class	wave	height										
	6	2.00-2.50	2.25										
u	(m/s)	-0.073	0.107	0.293	0.257	0.157	0.093	-0.017	-0.117	-0.213	-0.293	-0.267	-0.2

v	(m/s)	-0.19	0.063	0.43	0.53	0.43	0.287	0.07	-0.227	-0.463	-0.55	-0.513	-0.423
h	(m)	-0.373	-0.05	0.627	0.887	0.68	0.42	0.093	-0.183	-0.237	-0.28	-0.4	-0.423
#no.	class	wave	height										
	7	2.50-3.00	2.75										
u	(m/s)	-0.08	0.1	0.29	0.25	0.15	0.09	-0.02	-0.12	-0.22	-0.3	-0.27	-0.2
v	(m/s)	-0.2	0.05	0.42	0.52	0.42	0.28	0.06	-0.24	-0.47	-0.56	-0.52	-0.43
h	(m)	-0.37	-0.05	0.63	0.89	0.68	0.42	0.09	-0.18	-0.23	-0.28	-0.4	-0.42
#no.	class	wave	height										
	8	3.00-3.50	3.25										
u	(m/s)	-0.087	0.087	0.28	0.24	0.14	0.08	-0.03	-0.133	-0.233	-0.307	-0.277	-0.207
v	(m/s)	-0.213	0.03	0.4	0.507	0.403	0.26	0.04	-0.263	-0.49	-0.573	-0.533	-0.447
h	(m)	-0.363	-0.05	0.633	0.893	0.683	0.42	0.087	-0.177	-0.223	-0.277	-0.403	-0.417
#no.	class	wave	height										
#	9	3.50-4.00	3.75										
u	(m/s)	-0.093	0.073	0.27	0.23	0.13	0.07	-0.04	-0.147	-0.247	-0.313	-0.283	-0.213
v	(m/s)	-0.227	0.01	0.38	0.493	0.387	0.24	0.02	-0.287	-0.51	-0.587	-0.547	-0.463
h	(m)	-0.357	-0.05	0.637	0.897	0.687	0.42	0.083	-0.173	-0.217	-0.273	-0.407	-0.413
#no.	class	wave	height										
#	10	4.00-4.50	4.25										
u	(m/s)	-0.1	0.06	0.26	0.22	0.12	0.06	-0.05	-0.16	-0.26	-0.32	-0.29	-0.22
v	(m/s)	-0.24	-0.01	0.36	0.48	0.37	0.22	0	-0.31	-0.53	-0.6	-0.56	-0.48
h	(m)	-0.35	-0.05	0.64	0.9	0.69	0.42	0.08	-0.17	-0.21	-0.27	-0.41	-0.41
#no.	class	wave	height										
#	11	4.50-9.99	extr										
u	(m/s)	-0.1	0.06	0.26	0.22	0.12	0.06	-0.05	-0.16	-0.26	-0.32	-0.29	-0.22
v	(m/s)	-0.24	-0.01	0.36	0.48	0.37	0.22	0	-0.31	-0.53	-0.6	-0.56	-0.48
h	(m)	-0.35	-0.05	0.64	0.9	0.69	0.42	0.08	-0.17	-0.21	-0.27	-0.41	-0.41
#	wind	direction											
#	number	sector	direction										
#	8	30-60	45										
#no.	class	wave	height										
#	1	0	0										
u	(m/s)	-0.05	0.14	0.32	0.28	0.18	0.12	0.01	-0.09	-0.18	-0.26	-0.24	-0.18
v	(m/s)	-0.14	0.13	0.49	0.59	0.48	0.33	0.12	-0.16	-0.41	-0.5	-0.47	-0.38
h	(m)	-0.39	-0.04	0.61	0.87	0.67	0.42	0.1	-0.2	-0.26	-0.28	-0.4	-0.44
#no.	class	wave	height										
#	2	.00-0.50	0.25										
u	(m/s)	-0.048	0.14	0.32	0.282	0.182	0.12	0.01	-0.088	-0.18	-0.26	-0.24	-0.18
v	(m/s)	-0.138	0.13	0.49	0.588	0.48	0.328	0.12	-0.16	-0.41	-0.5	-0.47	-0.38
h	(m)	-0.376	-0.028	0.624	0.884	0.684	0.434	0.114	-0.186	-0.246	-0.266	-0.386	-0.426
#no.	class	wave	height										
#	3	.50-1.00	0.75										
u	(m/s)	-0.044	0.14	0.32	0.286	0.186	0.12	0.01	-0.084	-0.18	-0.26	-0.24	-0.18

v	(m/s)	-0.134	0.13	0.49	0.584	0.48	0.324	0.12	-0.16	-0.41	-0.5	-0.47	-0.38
h	(m)	-0.348	-0.004	0.652	0.912	0.712	0.462	0.142	-0.158	-0.218	-0.238	-0.358	-0.398
#no.	class	wave	height										
#	4	1.00-1.50	1.25										
u	(m/s)	-0.04	0.14	0.32	0.29	0.19	0.12	0.01	-0.08	-0.18	-0.26	-0.24	-0.18
v	(m/s)	-0.13	0.13	0.49	0.58	0.48	0.32	0.12	-0.16	-0.41	-0.5	-0.47	-0.38
h	(m)	-0.32	0.02	0.68	0.94	0.74	0.49	0.17	-0.13	-0.19	-0.21	-0.33	-0.37
#no.	class	wave	height										
#	5	1.50-2.00	1.75										
u	(m/s)	-0.053	0.123	0.307	0.271	0.177	0.107	-0.003	-0.097	-0.197	-0.273	-0.253	-0.19
v	(m/s)	-0.153	0.103	0.467	0.563	0.46	0.303	0.1	-0.187	-0.433	-0.52	-0.487	-0.4
h	(m)	-0.377	-0.043	0.62	0.88	0.683	0.427	0.103	-0.187	-0.243	-0.273	-0.397	-0.43
#no.	class	wave	height										
#	6	2.00-2.50	2.25										
u	(m/s)	-0.067	0.107	0.293	0.263	0.163	0.093	-0.017	-0.113	-0.213	-0.287	-0.267	-0.2
v	(m/s)	-0.177	0.077	0.443	0.547	0.44	0.287	0.08	-0.213	-0.457	-0.54	-0.503	-0.42
h	Cm>	-0.433	-0.107	0.56	0.82	0.627	0.363	0.037	-0.243	-0.297	-0.337	-0.463	-0.49
#no.	class	wave	height										
#	7	2.50-3.00	2.75										
u	(m/s)	-0.08	0.09	0.28	0.25	0.15	0.08	-0.03	-0.13	-0.23	-0.3	-0.28	-0.21
v	(m/s)	-0.2	0.05	0.42	0.53	0.42	0.27	0.06	-0.24	-0.48	-0.56	-0.52	-0.44
h	(m)	-0.49	-0.17	0.5	0.76	0.57	0.3	-0.03	-0.3	-0.35	-0.4	-0.53	-0.55
#no.	class	wave	height										
#	8	3.00-3.50	3.25										
u	(m/s)	-0.09	0.08	0.27	0.24	0.14	0.07	-0.04	-0.14	-0.24	-0.31	-0.287	-0.213
v	(m/s)	-0.213	0.03	0.403	0.513	0.403	0.257	0.043	-0.257	-0.497	-0.573	-0.53	-0.453
h	(m)	-0.513	-0.203	0.473	0.737	0.543	0.27	-0.063	-0.327	-0.373	-0.427	-0.56	-0.577
#no.	class	wave	height										
#	9	3.50-4.00	3.75										
u	(m/s)	-0.1	0.07	0.26	0.23	0.13	0.06	-0.05	-0.15	-0.25	-0.32	-0.293	-0.217
v	(m/s)	-0.227	0.01	0.387	0.497	0.387	0.243	0.027	-0.273	-0.513	-0.587	-0.547	-0.467
h	(m)	-0.537	-0.237	0.447	0.713	0.517	0.24	-0.097	-0.353	-0.397	-0.453	-0.59	-0.603
#no.	class	wave	height										
#	10	4.00-4.50	4.25										
u	(m/s)	-0.11	0.06	0.25	0.22	0.12	0.05	-0.06	-0.16	-0.26	-0.33	-0.3	-0.22
v	(m/s)	-0.24	-0.01	0.37	0.48	0.37	0.23	0.01	-0.29	-0.53	-0.6	-0.56	-0.48
h	(m)	-0.56	-0.27	0.42	0.69	0.49	0.21	-0.13	-0.38	-0.42	-0.48	-0.62	-0.63
#no.	class	wave	height										
#	11	4.50-9.99	extr										
u	(m/s)	-0.11	0.06	0.25	0.22	0.12	0.05	-0.06	-0.16	-0.26	-0.33	-0.3	-0.22
v	(m/s)	-0.24	-0.01	0.37	0.48	0.37	0.23	0.01	-0.29	-0.53	-0.6	-0.56	-0.48
h	(m)	-0.56	-0.27	0.42	0.69	0.49	0.21	-0.13	-0.38	-0.42	-0.48	-0.62	-0.63

Table C: Current velocities and water levels of TRIWAQ-model per wind direction and wave height class at depth of 20m, profile 76. After Van Rijn (1995), Table 3.4.3A. See Section 4.3 of report.

(row 1: velocity x-direction (east) in m/s)
(row 2: velocity y-direction (north) in m/s)
(row 3: water levels to NAP in m)

WL | Delft Hydraulics

Rotterdamseweg 185
postbus 177
2600 MH Delft
telefoon 015 285 85 85
telefax 015 285 85 82
e-mail info@wldelft.nl
internet www.wldelft.nl

Rotterdamseweg 185
p.o. box 177
2600 MH Delft
The Netherlands
telephone +31 15 285 85 85
telefax +31 15 285 85 82
e-mail info@wldelft.nl
internet www.wldelft.nl